A Study of Non-Linear Thermochemical Wave Propagation in Fixed-bed Gas-Solid Reactors



Mohammed Allamin Daggash II

Lady Margaret Hall University of Oxford

A thesis submitted for the degree of

Doctor of Philosophy

Trinity Term 2018

A Study of Non-Linear Thermochemical Wave Propagation in Fixed-bed Gas-Solid Reactors

Mohammed Allamin Daggash
Lady Margaret Hall,
University of Oxford

Abstract

The flow of a reactive fluid in a fixed-bed reactor, where a fluid-solid reaction takes place, can be described as a progression of thermal and thermochemical fronts that have a wave-like character. These waves are characterised by their dynamics such as their spatio-temporal patterns, constant pattern behaviour, temperature plateaus, and wave velocities.

A wave model is developed for determining approximate thermal and material profiles in the reactor, which is significantly simpler and less time-consuming to compute than the integration of a complete set of highly stiff, non-linear partial differential equations. The wave model can only be applied when the waves become coherent. Guidelines to predict the transient time to coherence are outlined for the specific reacting systems in the thesis.

A full numerical model for irreversible, exothermic and endothermic, and reversible exothermic, gas-solid reactions has also been developed and applied to the decoking of fixed bed reactors, reduction of iron pyrite and oxidation of magnetite respectively. The results of the numerical model reveal that, regardless of the combination of kinetic and transport parameters, wave propagation eventually assumes a stable, constant pattern form independent of time. The wave model matches the numerical simulations reasonably well; in particular, the width and position of thermal and thermochemical wave fronts, and the temperature plateau in the bed, are accurately predicted.

The current work provides a simple and efficient tool essential to understanding, designing and controlling slowly reacting systems through non-linear wave theory and the theory of coherence. A new simple, mechanistic, and conceptually appealing way of looking at reactor dynamics in gas-solid reactions. The wave model is a powerful tool for pre-design problems and screening potential operating schemes/strategies. The reduced heating strategy developed using the wave model saves 36.6% of the energy required to heat the injected oxygen in the decoking process. Pre-heat strategy involves injecting concentrated hydrogen whilst still pre-heating the fixed bed of pyrite particles with nitrogen. The strategy saves 10.4% of the energy required to preheat the pyrite.

Acknowledgements

This thesis is the culmination of my journey of Higher Learning which was just like climbing a high peak step by step accompanied with encouragement, hardship, trust, and frustration. When I found myself at the top experiencing the feeling of fulfilment, I realized though only my name appears on the cover of this thesis, a great many people including my family members, well-wishers, my friends, colleagues and various institutions have contributed to accomplish this huge task.

I thank the Almighty, Allah, whose blessings have enabled me to accomplish my research work successfully. To my family, thank you for encouraging me in all of my pursuits and inspiring me to follow my dreams. I am especially grateful to my parents, who supported me emotionally and financially.

I am most grateful to the University of Oxford particularly the academic staff at Department of Engineering Science for the past 8 years of rigorous learning. I am thankful to the department for giving me the permission to use the computers which helped to carry out the numerical simulations in the software laboratory.

I am indebted to my research guide, Prof Nicholas Hankins, who accepted me as his DPhil student and offered me his mentorship, supervising and advising my work progress towards its completion over the past three and a half years. This work would not have been possible without his guidance and involvement, his support and encouragement from the start of the project till date. Under his guidance, I successfully overcame many difficulties and learnt a lot. His own zeal for perfection, passion, unflinching courage and conviction has always inspired me to do more. For all these, I thank him and will be truly indebted to him throughout my life time.

To my Father, who has provided and supported me throughout my life. He has consistently proven to be an exemplary figure. Enjoyed the thought-provoking conversations that expanded the horizon of my research. The older I get the more I realize how important it is to have a dad like you. You have provided stability in my life and the love and acceptance I needed. If not for you, I would not be where I am today. You have always carried me with care and supported me like a pillar. Thank you, Dad.

To my Mother, for your unconditional love, never-ending piety, and an unlimited supply of thoughtfulness and understanding, I will be forever grateful. Thank you for making me feel like the luckiest child in the world. I thank God so much that He made you my mother. I am very blessed to have a mother who is so loving and unselfish, and so patient and forgiving. No one can ever take your place, Mom, but you can easily take the place of so many others. Over the years you have fulfilled so many roles with ease and confidence. If I could just be half the person that you are, I will be very blessed. Thank you for all that you do for us, Mom. I love you very much. There are so many people that I'm grateful to have in my life. You top that list, Mom! I don't know what I would do without you. I am the person that I am
today because of your love and guidance.

To my brother Mustapha, Thanks for always being the perfect older brother who is protective without being suffocative, liberal without being careless and watchful without being stifling. Dear brother when even my friends betrayed me, you were there for me. Thanks for being my loyal friend who has supported me everywhere and every time. Spending childhood with an elder brother is the best practice you can get to master the sport called Life. Thanks brother.

To my sister Habiba, my sister is likely the most competitive relationship within the family, but once we are both grown, it becomes the strongest relationship. But when we stand shoulder to shoulder, with the will of God who stands a chance against us?

To my brothers Baba and Ahmad. My brothers are the most precious gift sent by Allah, thank you Allah. I am very proud of the young men you are becoming. And I hope for you to understand the importance of being there for one another. That dependence combined with diligence will thrive you to even greater heights than the one achieved here.

To my dearest Aunties; Aunt Debbie, Aunt Saratu, Aunt Suzie. Their constant care and prayers have guided me through this degree and would not be able to substitute them for anyone else. I truly appreciate the encouragement and the protection you provide. Special acknowledgment to Aunt Roni, who has been a wonderful guidance and thoughtful presence in my life.

To my friends, Jack Cottam, Tom Scott, Arend Versteegh, Frank Collings, Goziem Isichei, Suleiman Waziri. You provided me with sleepless nights and occasional laughs that made the past few years enjoyable.

To my parents and siblings

Surah 46 Al-Ahqaf, Ayat 15-15

"My Lord, dispose me that I may give thanks for the bounty that You have bestowed upon me and my parents, and dispose me that I may do righteous deeds that would please You, and also make my descendants righteous. and that I may do good deeds that will please You and grant me good children. Surely I turn to You in repentance and surely I am of those who are Muslims."

Nomenclature

Symbol	Definition	Units
a	Stoichiometric coefficient of fluid A	
$A(z)$	Cross-section area as a function of location perpendicular to flow	
b	Stoichiometric coefficient of solid B	
c	Stoichiometric coefficient of solid C	
c_f	Specific heat capacity of fluid at constant pressure	J/kgK
c_s	Specific heat capacity of solid at constant pressure	J/kgK
C_A	Concentration of reacting fluid component A	mol/dm^3
C_{Aeq}	Equilibrium concentration of reacting fluid component A	mol/dm^3
C_{AINT}	Concentration of reacting fluid component A in plateau zone	mol/dm^3
$\tilde{C}_i$	Total concentration of element *i* as function of time and distance	mol/dm^3
C_i	Total concentration of element *i* in the aqueous phase	mol/dm^3
C_{im}	Total concentration of element *i* in the flowing phase *m*	mol/dm^3
C_{is}	Total concentration of element *i* in the solid phase	mol/dm^3
C_j	Concentration of flowing phase species *j*	mol/dm^3
C_k	Concentration of flowing phase species *k*	mol/dm^3
$\tilde{C}_{ie}$	Total concentration of element *i* in the injected fluid	mol/dm^3
ΔH	Enthalpy of reaction	J/kmol
ΔT_C	Thermochemical temperature rise	K
ΔT_T	Temperature rise due to thermal wave	K
D_a	Damkohler number	
D_{ax}	Coefficient of axial dispersion of mass	m^2/s
D_E	Effective diffusion coefficient of fluid A	m^2/s
D_m	Diffusion coefficient in the solids-free fluid phase	m^2/s
d_p	Normal packing diameter	m
E_A	Activation energy related to surface reaction	J/Kmol
E_{DE}	Activation energy related to diffusion	J/Kmol
E_R	Activation energy related to reaction at the core	J/Kmol
f_m	Fractional flow of phase *m*	

F_i	Fractional flux of element *i*	
g_{ik}	Stoichiometric coefficient of element *i* in solid *k*	
h	Solid-Fluid heat transfer coefficient	W/mK
h_{ij}	Stoichiometric coefficient of element *i* in single flowing phase species *j*	
i	Number of chemical elements in flow systems	
j	Number of chemical elements in flowing phase	
K_{eq}	Equilibrium constant	
k'	Overall forward rate of reaction coefficient	m/s
k''	Overall reversible rate of reaction coefficient	m/s
k_o	Fluid to mass transfer coefficient	m/s
k_p	Ratio of the thermal conductivity of gas and solid phase	
k_T	First order surface rate constant	m/s
L	Length of reactor	m
M_B	Molecular mass of solid B	g/mol
m	Number of flowing phases	
N_p	Number of moles of B	
N	Number of nodes	
n_B	Mole fraction of B	
n_c	Mole fraction of C	
n_p	Number of particles reacting	
Pe_0	Peclet Number	
Q	Constant heat flux	W/m
$q(t)$	Variable volumetric flow rate	/s
$\dot{q}_Y$	Heat flux in a controlled volume	W/m
R	Universal rate constant	
R_1	Radius of reactor	M
R_s	Radius of particle	m/s
r_A'	Rate of reaction of fluid A per particle	kmol/s
r_B'	Rate of reaction of solid B per particle	kmol/s
r_C'	Rate of reaction of solid C per particle	kmol/s
T_f	Temperature of reacting fluid	K
$T_{plateau}$	Plateau temperature	K

T_s	Temperature of solid bed	K
T_w	Wall temperature	K
t	Time	s
t_D	Dimensionless time	
u	Superficial velocity	m/s
u_e	Interstitial velocity	m/s
v	Specific wave velocity	m/s
V_R	Reaction wave velocity	m/s
V_T	Thermal wave velocity	m/s
$V_{T/C}$	Thermochemical wave velocity	m/s
V_s	Volume of the flowing phase in the reactor	m^3
$\bar{X}$	Percentage of reacted bed	
X_B	Conversion of Bed	
X_{Beq}	Equilibrium conversion of reacting solid component B	
X_{BINT}	Conversion of reacting solid component B in plateau zone	
Z_T	Position of thermal wave	m
$Z_{T/C}$	Position of thermochemical wave	m
z	Distance from inlet of medium	m
z_D	Dimensionless distance	
z_{HTZ}	Width of heat transfer zone	m
z_{MTZ}	Width of reaction zone	m

Greek Letters

ε	Void fraction/Porosity	
Θ_n	Numerical truncation error	
λ	Thermal heat conduction	W/mK
ξ_i	Function describing change in $\widetilde{C}_{ie}$ with distance	
ρ_B	Density of solid B	kg/m^3
ϕ_{vl}	Van Leer flux limiter	
ψ_i	Function describing change in $\widetilde{C}_{ie}$ with time	

Mathematical operators

∂	Partial derivative of
d	Full derivative of
Δ	Total change of

Subscripts

ax	Axial
i	Index
inj	Injected
L	Final value at length
o	Initial Value
V	Volume
w	Reactor wall
Tot	Total

Table of Contents

1. Introduction 19

1.1. Background 19

1.1.1. Non-linear Wave Theory 19

1.1.2. Coherence 20

1.1.3. Reactive Flow in Fluid-Solid Systems 20

1.1.4. Fixed-Bed Reactors 21

1.2. Aims and Objectives of the Research 22

1.3. Physical Model of Gas-Solid Reacting Systems 26

1.4. Wave Model and Constant Pattern Model 28

2. Literature Survey 31

2.1. 'Coherence': Principle 31

2.2. Non-linear Wave Propagation 33

2.3. Decoking Fixed-Bed Reactors 39

2.4. Roasting of Pyrite 43

3. Theory of Non-Linear Wave Propagation 48

3.1. Definitions 48

3.2. Constant Pattern Attainment 53

3.3. Concept and Conditions for Coherence 55

3.4. Wave Model 56

3.4.1. Reaction Wave Velocity 58

3.4.2. Thermal Wave Velocity 59

3.4.3. Thermochemical Wave Velocity 60

3.4.4. Temperature of Plateau 61

3.4.5. Incomplete or Partial Reactions 63

3.4.6. Thermal Wave Velocity with Heat addition 65

3.4.7. Thermochemical Wave Velocity with Heat addition 66

3.4.8. Temperature of Plateau with Heat addition 68

3.5. Summary 69

4. Physical Model Development & Numerical Analysis 70

4.1. Shrinking Core Model 70

4.2. Material and Energy balances 74

4.2.1. Governing Equations 74

4.2.2. Scope and Assumptions 75

4.3. Extension of Numerical Model 76

4.3.1. Dispersive Reaction Fronts 77

4.3.2. Dispersive Thermal Fronts 78
4.3.3. Heat Flux 79
4.4. Method of Lines 82
4.4.1. Overview of Method of Lines 83
4.4.2. The Template of Information Flow 85
4.4.3. Flux Limiter 86
4.5. Evaluation of Numerical Model and Induced Dispersion 87
4.5.1. Convergence 88
4.5.2. Numerical Dispersion 88
4.6. Constant Pattern Solution 92
4.7. Summary and Limitations 97
5. Exothermic Fluid-Solid Reactions 99
5.1. Transient time before Coherence for Decoking system 99
5.2. Comparison between numerical simulations and wave model 110
5.2.1. Ignition Temperature 111
5.2.2. Approximation of Total Conversion in Reactor 111
5.2.3. Preheat Wave 112
5.2.4. Hot Spot 132
5.3. Results for Dilute case 114
5.3.1. Hot fluid into a Preheated bed 114
5.3.2. Hot fluid into a cold bed 116
5.3.3. Cold fluid into a Preheated bed 118
5.3.4. Hot fluid pulse into a Preheated bed 122
5.3.5. Reduced heat strategy 124
5.4. Results for Concentrated case 127
5.4.1. Hot fluid into a Preheated bed 128
5.4.2. Hot fluid into a cold bed 129
5.4.3. Cold fluid into a Preheated bed 130
5.4.4. Hot fluid pulse into a Preheated bed 134
5.4.5. Preheated Bed strategy 136
5.4.6. Hot Spot 139
5.5. Summary and Comparison with other works 141
6. Endothermic Fluid-Solid Reactions 145
6.1. Transient time before Coherence for Pyrite system 145
6.2. Comparison between numerical simulations and wave model 148
6.2.1. Ignition Temperature 148
6.2.2. Preheat Wave 149

6.3. Results for Dilute case 150
6.3.1. Hot fluid into a Preheated bed 151
6.3.2. Hot fluid into a cold bed 154
6.3.3. Cold fluid into a Preheated bed 155
6.3.4. Reduced heat strategy 159
6.4. Results for Concentrated case 161
6.4.1. Hot fluid into a Preheated bed 162
6.4.2. Hot fluid into a cold bed 164
6.4.3. Cold fluid into a Preheated bed 165
6.4.4. Preheated Bed strategy 167
6.4.5. Cold Spot 170
6.4.6. Effect of variation in h_w 174
6.5. Summary and Comparison with other works 177
7. Reversible Exothermic Fluid-Solid Reactions 181
7.1. Physical model for reversible exothermic fluid-solid reactions 182
7.1.1. Rate Equations 186
7.1.2. Material and Energy balances 187
7.1.3. Equilibrium Constant 189
7.1.4. Evaluation of Physical Model 190
7.1.5. Parameters of Reversible Exothermic Gas-solid system 191
7.2. Prediction of wave behaviour for reversible reactions 191
7.2.1. Dilute Fluid case 192
7.2.2. Concentrated Fluid case 193
7.2.3. Hot Spot case 194
7.3. Wave Model Simultaneous equations 195
7.4. Comparison between numerical simulations and wave model 197
7.4.1. Dilute Oxygen case 197
7.4.2. Concentrated Oxygen case 201
7.5. Summary 206
8. Conclusions 208
8.1. Summary 208
8.2. Future Work 211
References 213
Appendices 227
A. Prediction of Wave Behaviour for Exothermic System 227
A.1. Dilute Fluid Case 228
A.2. Concentrated Fluid Case 232

B. Prediction of Wave Behaviour for Endothermic System 238
B.1. Dilute Fluid Case 238
B.2. Concentrated Fluid Case 242
C. Flux Limiter 248

List of Figures

Figure 3-1: Composition Profile 41
Figure 3-2: Composition History 42
Figure 3-3: Sharpening behaviour of self-sharpening wave. Concentration profiles at two successive times, t_1 and t_2 42
Figure 3-4: Sharpening behaviour of non-sharpening wave. Concentration profiles at two successive times, t_1 and t_2 42
Figure 3-5: Sharpening behaviour of indifferent wave. Concentration profiles at two successive times, t_1 and t_2 43
Figure 3-6: Distance-time diagram for injection of reactive fluid (schematic) 45
Figure 3-7: Distance-time diagram for injection of reactive fluid (schematic) 47
Figure 3-8: Reaction wave.....51
Figure 3-9: Thermal wave.....52
Figure 3-10: Thermochemical wave……..…….53
Figure 3-11: Temperature plateau…….……..54
Figure 3-12: Reaction wave showing incomplete solid reaction (dilute fluid case)…….....55
Figure 3-13: Reaction wave showing incomplete fluid reaction (concentrated fluid case)…….56
Figure 3-14: Thermal wave velocity with heat addition……..57
Figure 3-15: Thermochemical wave velocity with heat addition…….58
Figure 3-16: Temperature plateau with heat addition……..……..59
Figure 4-1: Diagram of concentration profile for SCM.....62
Figure 4-2: Unit volume of reactor 64
Figure 4-3: The template (green) and corresponding MATLAB functions (blue) showing information flows 76
Figure 4-4: Constant pattern solution of dilute decoking system 85
Figure 4-5: Constant pattern solution of concentrated decoking system 85
Figure 4-6: Constant pattern solution of dilute pyrite system 86
Figure 4-7: Constant pattern solution of concentrated pyrite system 87
Figure 5-1: Temperature profile for hot fluid into a preheated bed (dilute) 91
Figure 5-2: Temperature profile for hot fluid into a cold bed (dilute) 91
Figure 5-3: Temperature profile for cold fluid into a preheated bed (high T_{inj}) (dilute) 92
Figure 5-4: Temperature profile for cold fluid into a preheated bed (low T_{inj}) (dilute) 92
Figure 5-5: Temperature profile for hot fluid pulse into a cold bed (dilute) with thermochemical wave (red).....94
Figure 5-6: Distance-time diagram for constant temperature (dilute) 95
Figure 5-7: Distance-time diagram for constant temperature dilute case with incomplete reaction..... 96
Figure 5-8: Distance-time diagram for hot fluid pulse into a hot bed (dilute) 96
Figure 5-9: Temperature profile for hot fluid into a hot bed (concentrated) 98
Figure 5-10: Temperature profile for hot fluid into a cold bed (high T_o) (concentrated).. 98
Figure 5-11: Temperature profile for hot fluid into a cold bed (low T_o) (concentrated)... 99
Figure 5-12: Temperature profile for cold fluid into a preheated bed (concentrated) 99
Figure 5-13: Temperature profile for hot fluid pulse into a cold bed (concentrated) 100
Figure 5-14: Distance-time diagram for constant temperature (concentrated) 100
Figure 5-15: Distance-time diagram for constant temperature incomplete reaction (dilute) 101
Figure 5-16: Distance-time diagram for hot fluid pulse (concentrated).....101
Figure 5-17: Wave model prediction of temperature plateau with varying inlet conc.....103
Figure 5-18: Total conversion of solid at $t_{elapsed}$ 105
Figure 5-19: Preheating reactor bed with nitrogen.....106

Figure 5-20: 3D plot of dependent variables with independent variables (dilute) 108
Figure 5-21: Composition profiles for hot fluid into a hot bed with Z_T (black dashed), $Z_{T/C}$ (purple dashed), $T_{plateau}$ (green dashed). $T_o = 898K$, $T_{inj} = 898K$ 109
Figure 5-22: Composition profiles for hot fluid into a cold bed with Z_T (black dashed), $Z_{T/C}$ (purple dashed), $T_{plateau}$ (green dashed). $T_o = 298K$, $T_{inj} = 898K$ 110
Figure 5-23: Distance-time diagram for complete reaction (dilute) with thermochemical wave (blue), thermal wave (red) 111
Figure 5-24: Temperature profiles for cold Fluid into hot bed (dilute) with T_{inj} reducing (a) T_{inj}, $T_o > T_{ign}$ (b) $T_{inj} < T_{ign}$, $T_o > T_{ign}$ 112
Figure 5-25: Concentration profiles for cold fluid into hot bed (dilute) with T_{inj} reducing (a) T_{inj}, $T_o > T_{ign}$ (b) $T_{inj} < T_{ign}$, $T_o > T_{ign}$ 112
Figure 5-26: Composition profiles for cold fluid into a hot bed with Z_{T1} (black dashed), $Z_{T/C}$ (purple dashed), $T_{plateau}$ (green dashed). $T_o = 898K$, $T_{inj} = 848K$ 113
Figure 5-27: Composition profiles for cold fluid into a hot bed with Z_{T1} (black dashed), $Z_{T/C}$ (purple dashed). $T_o = 898K$, $T_{inj} = 698K$ 114
Figure 5-28: Distance-time diagram for incomplete reaction (dilute) with thermochemical wave (blue), thermal wave (red) 115
Figure 5-29: Composition profiles for hot fluid pulse into a hot bed with Z_{T1} (black dashed), Z_{T2} (blue dashed), $Z_{T/C}$ (purple dashed), $T_{plateau}$ (green dashed), T_{fo} (grey dashed). $T_o = 898K$, $T_{inj} = \{898K,298K\}$ 116
Figure 5-30: Distance-time diagram for hot fluid pulse into a hot bed (dilute) with thermochemical wave (blue), thermal wave 1 (red) thermal wave 2 (green).....117
Figure 5-31: Distance-time diagram for post-heat strategy (dilute) 118
Figure 5-32: 3D plot of dependent variables with independent variables (dilute post-heat strategy).....118
Figure 5-33: Composition profiles for dilute post-heat strategy with Z_{T1} (black dashed), Z_{T2} (blue dashed), $Z_{T/C}$ (purple dashed), $T_{plateau}$ (green dashed), T_{fo} (grey dashed). $T_o = 898K$, $T_{inj} = \{898K,298K\}$ 119
Figure 5-34: Distance-time diagram for post-heat strategy (dilute) with thermochemical wave (blue), thermal wave 1 (red) thermal wave 2 (green) 120
Figure 5-35: 3D plot of dependent variables with independent variables (concentrated). 121
Figure 5-36: Composition profiles for hot fluid into a hot bed with Z_T (black dashed), $Z_{T/C}$ (purple dashed), $T_{plateau}$ (green dashed). $T_o = 898K$, $T_{inj} = 898K$ 121
Figure 5-37: Composition profiles for cold fluid into a hot bed with Z_{T1} (black dashed), $Z_{T/C}$ (purple dashed, $T_{plateau}$ (green dashed). $T_o = 898K$, $T_{inj} = 298K$ 122
Figure 5-38: Distance-time diagram with thermochemical wave (blue), thermal wave (red) for concentrated case 123
Figure 5-39: Temperature profiles for hot fluid into cold bed (concentrated) with T_o reducing (a) T_o, $T_{inj} > T_{ign}$ (b) $T_o < T_{ign}$, $T_{inj} > T_{ign}$.....124
Figure 5-40: Concentration profiles for hot fluid into cold bed (concentrated) with T_o reducing (a) T_o, $T_{inj} > T_{ign}$ (b) $T_o < T_{ign}$, $T_{inj} > T_{ign}$ 124
Figure 5-41: Composition profiles for hot fluid into a cold bed with Z_T (black dashed), $Z_{T/C}$ (purple dashed), $T_{plateau}$ (green dashed). $T_o = 798K$, $T_{inj} = 898K$ 125
Figure 5-42: Composition profiles for hot fluid into a cold bed with Z_T (black dashed). $T_o = 698K$, $T_{inj} = 898K$.....126
Figure 5-43: Distance-time diagram with thermochemical wave (blue), thermal wave (red) for concentrated case hot fluid into a cold bed 127
Figure 5-44: Composition profiles for hot fluid pulse into a hot bed with Z_{T1} (black dashed), Z_{T2} (blue dashed), $Z_{T/C}$ (purple dashed), $T_{plateau}$ (green dashed), T_{fo} (grey dashed). $T_o = 898K$, $T_{inj} = \{898K,298K\}$ 128
Figure 5-45: Distance-time diagram for hot fluid pulse into a hot bed (concentrated) with

thermochemical wave (blue), thermal wave 1 (red) thermal wave 2 (green).....129
Figure 5-46: Distance-time diagram for pre-heat strategy (concentrated) 130
Figure 5-47: 3D plot of dependent variables with independent variables for (concentrated pre-heat strategy) 130
Figure 5-48: Composition profiles with Z_{T1} (blue dashed), Z_{T2} (black dashed), $Z_{T/C}$ (purple dashed), $T_{plateau}$ (green dashed), T_{fo} (grey dashed) for concentrated pre-heat strategy 131
Figure 5-49: Distance-time diagram for pre-heat strategy (concentrated) with thermochemical wave (blue), thermal wave 1 (green) thermal wave 2 (red) 131
Figure 5-50: Composition profiles with $Z_{T/C}$ (purple dashed) for T_o = 698K, T_{inj} = 698K for hot spot 132
Figure 5-51: 3D plot of dependent variables with independent variables (hot spot) 133
Figure 5-52: Distance-time diagram for hot spot with thermochemical wave (blue) 134
Figure 6-1: Temperature profile for hot fluid into a hot bed (dilute) 138
Figure 6-2: Temperature profile for hot fluid into a cold bed (dilute).....138
Figure 6-3: Temperature profile for cold fluid into a hot bed (dilute).....139
Figure 6-4: Temperature profile for cold fluid into a hot bed (dilute).....139
Figure 6-5: Distance-time diagram for constant temperature (dilute).....140
Figure 6-6: Temperature profile for hot fluid into a hot bed (concentrated) 141
Figure 6-7: Temperature profile for cold fluid into a hot bed (concentrated) 141
Figure 6-8: Temperature profile for hot fluid into a cold bed (concentrated) 142
Figure 6-9: Distance-time diagram for constant temperature (concentrated) 142
Figure 6-10: Distance-time diagram for constant temperature with partial concentration (dilute) 143
Figure 6-11: Temperature profile for hot fluid into a preheated bed with h_w.....144
Figure 6-12: Wave model prediction of temperature plateau with varying inlet conc.....146
Figure 6-13: 3D plot of dependent variables with independent variables (dilute).....151
Figure 6-14: Composition profiles for hot fluid into a hot bed with Z_T (black dashed), $Z_{T/C}$ (purple dashed), $T_{plateau}$ (green dashed). T_o = 908K, T_{inj} = 908K 152
Figure 6-15: Composition profiles for hot fluid into a cold bed with Z_T (black dashed), $Z_{T/C}$ (purple dashed), $T_{plateau}$ (green dashed). T_o = 298K, T_{inj} = 908K 152
Figure 6-16: Distance-time diagram with thermochemical wave (blue), thermal wave (red) for dilute cases 153
Figure 6-17: Temperature profiles for cold fluid into a hot bed (dilute) with T_{inj} reducing (a) T_{inj}, $T_o > T_{ign}$ (b) $T_{inj} < T_{ign}$, $T_o > T_{ign}$ 155
Figure 6-18: Concentration profiles for cold fluid into a hot bed (dilute) with T_{inj} reducing (a) T_{inj}, $T_o > T_{ign}$ (b) $T_{inj} < T_{ign}$, $T_o > T_{ign}$ 155
Figure 6-19: Composition profiles for cold fluid into a hot bed with Z_{T1} (black dashed), $Z_{T/C}$ (purple dashed), $T_{plateau}$ (green dashed). T_o = 908K, T_{inj} = 908K 156
Figure 6-20: Composition profiles for cold fluid into a hot bed with Z_{T1} (black dashed), $Z_{T/C}$' (purple dashed), $T_{plateau}$' (grey dashed). T_o = 908K, T_{inj} = 298K.....157
Figure 6-21: Distance-time diagram for cold fluid (298K) into a hot bed with thermochemical wave (blue), thermal wave (red) (dilute).....158
Figure 6-22: Distance-time diagram for post-heat strategy (dilute).....159
Figure 6-23: 3D plot of dependent variables with independent variables (dilute post-heat strategy).....160
Figure 6-24: Composition profiles for dilute post-heat strategy with Z_{T1} (black dashed), Z_{T2} (blue dashed), $Z_{T/C}$ (purple dashed), $T_{plateau}$ (green dashed), T_{fo} (grey dashed) 160
Figure 6-25: Composition profiles for hot fluid into a hot bed with Z_T (black dashed), $Z_{T/C}$ (purple dashed), $T_{plateau}$ (green dashed). T_o = 1208K, T_{inj} = 1208K 162
Figure 6-26: 3D plot of dependent variables with independent variables (concentrated).163
Figure 6-27: Composition profiles for cold fluid into a hot bed with Z_{T1} (black dashed), $Z_{T/C}$

(purple dashed), $T_{plateau}$ (green dashed). T_o = 1208K, T_{inj} = 298K 164
Figure 6-28: Distance-time diagram (concentrated) with thermochemical wave (blue), thermal wave (red).....165
Figure 6-29: Composition profiles for hot fluid into a cold bed with Z_{T1} (black dashed), $Z_{T/C}$ (purple dashed), $T_{plateau}$' (grey dashed). T_o = 298K, T_{inj} = 1208K 166
Figure 6-30: Distance-time diagram hot fluid into a cold bed (298K) (concentrated) with thermochemical wave (blue), thermal wave (red).....167
Figure 6-31: Distance-time diagram for pre-heat strategy (concentrated) 168
Figure 6-32: 3D plot of dependent variables with independent variables (concentrated post-heat strategy) 169
Figure 6-33: Composition profiles for concentrated pre-heat strategy with Z_{T1} (blue dashed), Z_{T2} (black dashed), $Z_{T/C}$ (purple dashed), $T_{plateau}$ (green dashed), T_{fo} (grey dashed) 169
Figure 6-34: Distance-time diagram for pre-heat strategy (concentrated) with thermochemical wave (blue), thermal wave 1 (green) thermal wave 2 (red) 170
Figure 6-35: 3D plot of dependent variables with independent variables (cold spot).....171
Figure 6-36: Composition profiles for cold spot with $Z_{T/C1}$ (purple dashed), $Z_{T/C2}$ (green dashed), $T'_{plateau}$ (grey dashed). T_o = 908K, T_{inj} = 908K 171
Figure 6-37: Distance-time diagram with thermochemical wave1 (blue) thermochemical wave 2 (yellow) for cold spot (908K) 172
Figure 6-38: Composition profiles with Z_{T1} (black dashed), $Z_{T/C}$ (purple dashed), $T_{plateau}$ (green dashed) for dilute cold spot case (5008K).....173
Figure 6-39: Composition profiles for concentrated cold spot case (5008K) with Z_T (black dashed), $Z_{T/C}$ (purple dashed), $T_{plateau}$ (green dashed) 174
Figure 6-40: Comparison of positions of waves for dilute 175
Figure 6-41: Comparison of positions of waves for concentrated 176
Figure 7-1: Shrinking core model for reversible reactions 184
Figure 7-2: Activation energies for reversible reaction.....185
Figure 7-3: Temperature profile for hot fluid into a preheated bed (dilute).....189
Figure 7-4: Temperature profile for hot fluid into a preheated bed (concentrated) 190
Figure 7-5: Temperature profile for hot fluid into a preheated bed (hot spot) 191
Figure 7-6: Wave model temperature profile (concentrated) 192
Figure 7-7: Composition profile for hot fluid into a preheated bed (forward reaction).....194
Figure 7-8: Composition profile for hot fluid into a preheated bed (reversible reaction).....195
Figure 7-9: Composition profile for hot fluid into a preheated bed (reverse reaction).....196
Figure 7-10: Composition profile for hot fluid into a preheated bed (forward reaction).....198
Figure 7-11: Composition profile for hot fluid into a preheated bed (reversible reaction).....199
Figure 7-12: Rates of reaction for reversible reaction 200
Figure 7-13: Composition profile for hot fluid into a preheated bed (reverse reaction).....201
Figure 7-14: Effect of injected fluid temperature on X_B 202
Figure 7-15: Schematic diagram for multiple reactor design.....202

List of Tables

Table 2-1: Decoking procedures from various authors 34
Table 5-1: Decoking system parameters 102
Table 5-2: Comparison of distance travelled by thermal, thermochemical waves & plateau temperature for complete reaction (dilute) 109
Table 5-3: Comparison of distance travelled by thermal, thermochemical waves & plateau

temperature for dilute case cold fluid (698K) into a hot bed 114
Table 5-4: Comparison of distance travelled by thermal, thermochemical waves & plateau temperature for hot fluid pulse into a hot bed (dilute) 116
Table 5-5: Comparison of distance travelled by thermal, thermochemical waves & plateau temperature for dilute post-heat strategy 119
Table 5-6: Comparison of distance travelled by thermal, thermochemical waves & plateau temperature for concentrated cases 122
Table 5-7: Comparison of distance travelled by thermal, thermochemical waves & plateau temperature for concentrated case hot fluid into a cold bed (698K) 126
Table 5-8: Comparison of distance travelled by thermal, thermochemical waves & plateau temperature for concentrated case hot fluid pulse into a hot bed 128
Table 5-9: Comparison of distance travelled by thermal, thermochemical waves & plateau temperature for concentrated pre-heat strategy 131
Table 5-10: Comparison of distance travelled by thermal, thermochemical waves & plateau temperature for concentrated case hot spot 133
Table 6-1: Pyrite reduction parameters 145
Table 6-2: Comparison of distance travelled by thermal, thermochemical waves & plateau temperature for dilute cases 153
Table 6-3: Comparison of distance travelled by thermal, thermochemical waves & plateau temperature for dilute case cold fluid (298K) into a hot bed 155
Table 6-4: Comparison of distance travelled by thermal, thermochemical waves & plateau temperature for dilute post-heat strategy 161
Table 6-5: Comparison of distance travelled by thermal, thermochemical waves & plateau temperature for concentrated cases 164
Table 6-6: Comparison of distance travelled by thermal, thermochemical waves & plateau temperature for concentrated case hot fluid into a cold bed (298K) 166
Table 6-7: Comparison of distance travelled by thermal, thermochemical waves & plateau temperature for concentrated pre-heat strategy 169
Table 6-8: Comparison of distance travelled by thermochemical waves & plateau temperature for cold spot case (908K) 172
Table 6-9: Comparison of distance travelled by thermal, thermochemical waves & plateau temperature for dilute cold spot case 173
Table 6-10: Comparison of distance travelled by thermal, thermochemical waves & plateau temperature for concentrated cold spot case 174
Table 6-11: Comparison of distance travelled by thermal, thermochemical waves & plateau temperature for concentrated cold spot case……..……..175
Table 6-12: Comparison of distance travelled by thermal, thermochemical waves & plateau temperature for concentrated cold spot case……..……176
Table 7-1: Comparison of distance travelled by thermal, thermochemical waves & plateau temperature for dilute case k” = 0.1k’……193
Table 7-2: Comparison of distance travelled by thermal, thermochemical waves & plateau temperature for dilute case k” = k’……..……195
Table 7-3: Comparison of distance travelled by thermal, thermochemical waves & plateau temperature for dilute case k” = 10k’……..……..196
Table 7-4: Comparison of distance travelled by thermal, thermochemical waves & plateau temperature for conc. case k” = 0.1k’……..……198
Table 7-5: Comparison of distance travelled by thermal, thermochemical waves & plateau temperature for conc. case k” = 0.1k’……..…198
Table A4-1: Errors and convergence rates and various meshes for Test (a), (b) and (c)……227
Table A4-2: Errors and convergence rates and various meshes for ϕ Albada and ϕ (van Leer) ……..……228

Chapter 1

Introduction

This chapter introduces the general key ideas in the thesis. Clear aims and objectives are stated along with summaries and contributions of each chapter.

1.1 Background

1.1.1 Non-linear Wave Theory

The overall context of non-linear wave propagation theory was originally developed in 1963 to allow a conceptual and quantitative understanding of multicomponent, ion exchange and adsorption processes (Helfferich 1967, 1968). Major extensions were later made to encompass multiphase, multicomponent systems in chromatography. The concept of coherence embodied within the wave propagation theory was refined to include reversible reactions, such as precipitation – dissolution reactions (Walsh et al., 1984; Helfferich, 1989; Araque-Martinez and Lake, 2000). In more recent years, there has been application to reaction-separation processes (Tartakovsky 2007). This research was extended further to complex foam enhanced oil recovery displacements and the simulators that represent them (Zanganeh et al., 2011). The wave theory has also been used to design and control reactive distillation columns in the production of terephthalic acid (Kim et al., 2010).

The two central facets of the wave theory are a description in terms of waves, that is, concentration or other dependent variable variations traveling through the system e.g. a fixed bed reactor, and the concept of coherence. The focus on waves rather than on heat and mass transfer of molecules leads to a clearer picture of the phenomena and an insight to reactive flow system in terms of cause and effect. This is particularly true for complex

initial and feed conditions which give rise to phenomena best understood as propagation of wave.

1.1.2 Coherence

The utility of the theory of coherence lies in the fact that it identifies a particular type of physical behaviour and develops this into a concept which helps us understand the aforementioned wave propagation phenomena in terms of cause and effect. In particular, it enables us to predict what will happen but with a greatly reduced need for intensive calculation; as such, it is related to the ideas of equilibrium and steady state. Both are states to which a system settles down if not disturbed further; so is the state of coherence. But while equilibrium is restricted to a closed system and steady state is restricted to open systems with fixed boundaries and constant boundary conditions, coherence is not so restricted. In fact, it includes the latter two as special cases, but also covers deviations from those cases – typically the propagation of perturbations through systems otherwise regarded as at equilibrium or steady state. Coherence theory addresses itself to general, arbitrary wave propagation problems containing two or more dependent variables (such as concentration or temperature) related by partial differential equations to two or more independent variables such as distances and time). The concept identifies the state which such a dynamic, multicomponent system strives to attain.

1.1.3 Reactive Flow in Fluid-Solid Systems

Flow accompanied by chemical reactions and mass transfer is central to a wider range of applications. The flow of a reactive fluid through a chemically reactive medium is an example of those applications (Dria, 1995). Flow through porous media is central to processes ranging from geological scales (Lake, 2002) (e.g., ground-water transport or

enhanced oil recovery) to refinery-scale processes (e.g., fixed-bed chemical reactors), to small-scale processes such as in fuel-cell or battery electrodes. Most catalytic refining and petrochemical reactions are operated with fixed-bed reactors. Due to its fairly simple construction, stability, and controllability, this reactor type retains its favoured position in industrial practice over other more advanced and sophisticated reactors.

Reactive flow through a fixed bed reactor gives rise to complex behaviour, which can be attributed to the non- linearity of the systems. The important phenomena typically associated with the behaviour observed is sensitivity with respect to the initial state of the system and the operating conditions. This may lead to sudden changes in qualitative and quantitative behaviour of the system. Since these reactions provide us with an inherent non-linearity, simple linear analysis fails, and a deeper understanding of the underlying phenomena is acquired using non-linear wave theory tools.

1.1.4 Fixed-Bed Reactors

The fixed-bed reactor is historically one of the oldest reactor configurations for performing fluid-solid reactions. A fixed bed reactor is an assembly of usually uniformly sized catalytic particles, which are randomly arranged and firmly held in position within a vessel or tube. The reactions considered here are the fluid-solid reactions in the pores of the catalyst. The bulk fluid flows through the voids of the bed. The reactants are transported firstly from the bulk of the fluid to the catalyst surface, then through catalyst pores, where the reactant fluid reacts with the reactive solid on the surface of the pores and then undergo chemical transformation. Convection of the bulk fluid is tied in with heat and mass dispersion. Dispersion effects are largely caused by the complex flow patterns in the reactor induced by the presence of the packing. In most cases, chemical reactions are accompanied with heat generation or consumption. In the case of pronounced heat effects,

the heat is removed or supplied through the tube wall (Behroozi et al., 2010). It should be noted that in industrial cooled or heated fixed bed reactors, a bundle of tubes filled with the particles in the catalyst is usually arranged within a large reactor shell.

1.2 Aims and Objectives of the Research

The aim of this work is to apply the wave theory to non-isothermal, gaseous-solid reactive systems with finite rates of reaction, and specifically, where the reaction and transport processes are slow so that local equilibrium does not apply. To do so is intuitively appealing, as it allows us to picture more readily comprehend reactor dynamics in terms of cause and effect. The overall goal of this research is to understand the nature of reactive flow in fixed-bed reactors, in terms of non-linear wave dynamics to study the properties of waves in the presence of non-equilibrium and slow rate-controlled reactions. We present several extensions and advancements in theory, building from the fundamental theory developed by Helfferich and Peterson, 1963, Lake, 1984, Bryant, 1986.

The objectives of this research can be summarised:

- Develop a wave theory for irreversible and reversible fluid-solid reactions.
- Develop a numerical model to describe mass and heat transfer in convective reactive flow for irreversible and reversible fluid-solid reactions.
- Mathematically define a coherent pattern in this context and demonstrate the approach to coherence in the reactive systems examined.
- Test different operating strategies with varying inlet concentrations and temperatures and compare the numerical model with predictions from the wave model.
- Examine critical parameters which lead to hot spots (exothermic reaction) and cold spots (endothermic reactions) in irreversible reactions.
- Examine the effects of adiabatic wall heating on wave behaviour.

- Evolve the shrinking core model to account for reversible reactions and investigate the formation of double thermochemical waves.

Chapter 2 reviews the literature of all relevant studies on non-linear wave propagation, coherence, reactive flow in a timeline, highlighting milestones in the theoretical approach. A literature review of the industrial application of the research was also provided and work performed by researchers from companies and other universities. A discussion of local equilibrium follows and its validity in the current work.

Chapter 3 is the theoretical part of the thesis. The chapter starts by presenting some basic definitions related to the non-linear wave theory. The concept of coherence is defined qualitatively and quantitatively for fluid-solid reactions in fixed bed reactors. A wave model including heat and reaction zones width in the equations for wave velocities and the effect of additional heat on the propagation of the thermal and thermochemical waves is developed. A model which incorporates this allows for the accurate prediction of thermal and thermochemical waves with adiabatic heating, which consequently allows the amount of heat required to avoid cold spots in endothermic reactions to be calculated.

Chapter 4 is a complete description of the numerical modelling of the non-isothermal flow in a fixed bed reactor. This chapter also provides equations representing the material and thermal balances across the reactor. The numerical model is based on the Method of Lines and is applied to the set of stiff hyperbolic PDEs to handle a wide range of reaction conditions. This allows the model to be useful in evaluation and testing up to a full-scale operation. The accuracy and flexibility of the developed code is tested and a comprehensive examination of parameters influencing the reaction is also provided. A novel flux limiter is included in the developed code to reduce oscillations in the results shown in the following chapters. A mathematical explanation of the approach to a constant fixed width of thermochemical waves is explained and calculated for the reaction systems in this thesis.

Chapter 5 comprises of wave model predictions using the wave model equations in Chapter 4 and the numerical simulation described in Chapter 4 to model an exothermic gas-solid system; decoking catalysts in a fixed bed reactor. The wave model and the numerical simulations demonstrate a dilute injected oxygen feed into a bed of solids produces a slow coherent thermochemical wave and a faster thermal wave travelling ahead of it with a temperature plateau formed between the two waves.

Firstly, it is shown that if the injected fluid is dilute and above ignition temperature, the thermochemical wave where the reaction takes place moves into a hot enough region and the reaction profile propagates in a stable manner with a constant width as calculated in Chapter 4. The wave model was used to develop a reduced heat injection strategy, reducing the requirement of constant heating of the injected fluid.

Secondly, it is shown that if the injected fluid is concentrated, the thermochemical wave travels ahead of the thermal wave and can only propagate if the thermochemical wave is moving to a bed set above ignition temperature. The critical concentration where the temperature becomes a delta function was examined resulting in a hot spot. The wave model predicts no separation of the thermal and thermochemical waves in the absence of dispersion. This was confirmed by running a numerical simulation at the critical concentration.

Chapter 6 investigates different temperature and concentration strategies for an endothermic gas-solid system; reduction of iron pyrite by hydrogen. Injection strategies included in this chapter involved injection of fluids which are colder, warmer and at the same temperature as the initial bed temperature. The positions of the thermochemical and thermal waves are also shown to travel with a constant width with a temperature drop between the thermal and thermochemical waves. The pre-heat and reduced heat strategies are shown to also be energy saving in the endothermic system as well.

An interesting observation was made when the injected fluid was set to a critical concentration, producing a cold spot. This cold spot causes a new phenomenon which splits the thermochemical waves across the cold spot region, thereby having two different reaction zones travelling at different velocities. Further analysis into the rates of reaction during the simulation showed two peaks propagating through the reactor bed, which match up to the positions of the splitting thermochemical waves. The wave model showed is value here by accurately predicting the positions of the two thermochemical waves. Adiabatic heating from the reactor wall is shown to reduce the cold region, whilst not distorting the coherent thermochemical wave in both the dilute and concentrated cases within a range of wall temperatures and heat transfer coefficients.

Chapter 7 presents a numerical model based on a modified shrinking core model and is implemented in the material balances with an alteration of the rate equation in the PDEs for the oxidation of magnetite to hematite. Wave model predictions are made for a dilute and concentrated cases with different reversible rates and are compared with the numerical simulations. The wave model predicts a trailing thermochemical wave in the dilute case and two reaction zones (double thermochemical waves) in the concentrated case.

The contribution in this chapter is the analysis of an exothermic gas-solid reaction system with even slower reacting non-equilibrium systems than in the irreversible case. The injected fluid temperature is shown to be important and a temperature rise or drop causes a change in the equilibrium concentration and conversion at the inlet. Each concentration change is associated with a temperature drop/rise from the plateau temperature to the injected fluid temperature, which favours (temperature drop) or opposes (temperature rise) the conversion of magnetite (the forward reaction). However, there is a

limit to the temperature drop as the reaction extinguishes itself below the ignition temperature.

Varied temperature conditions existed for the reverse element of the reaction to occur in the upstream part of the bed where the rate of overall conversion is increased. The wave model predictions were shown to be useful in designing a system involving multiple fixed reactor beds. This showed the simplicity and usefulness in applying the wave model to designing fixed bed reactors for reversible exothermic gas-solid reactions.

Chapter 8 summarises the conclusions of the thesis and the avenues of future work.

1.3 Physical Model of Gas-Solid reacting systems

The physical model is a mathematical description of a chemical reaction occurring in a fixed bed of solids. The model is based on a system of PDEs presented in Chapter 4 representing the dynamic process of a heterogeneous gas-solid chemical reaction based on the shrinking core model (Bischoff 1963, 1965). A gaseous reactant is injected over the fixed bed of solids, where the reacting gases diffuses through the external-film and shell to the "core surface" of the solid spherical particles. At first, the reaction takes place at the outside surface of the particle, but as the reaction proceeds, the surface of the reaction will move to the interior of the solid leaving behind a porous solid product. During this process, the reaction surface moves inward forming an unreacted core which shrinks with time. Assumptions of the physical model are:

(1) Gas flow in the reactor is characteristic of plug flow.

(2) Chemical reaction is irreversible

(3) The particle temperature and the reactor temperature are constant and the same

throughout. Superficial linear gas velocity is constant throughout the reactor during the course of the reaction.

(4) Axial gas dispersion is negligible.

(5) The reacting fluid is incompressible (no change in density with temperature)

(6) The particles are spherical, and their properties do not change as the reaction proceeds. Reaction rate is first order with respect to the concentration of the reacting gas.

A typical result of the numerical simulation of the physical model within a technical fixed bed reactor is shown in Fig 1-1. The data presented shows the concentration of the injected gas (C_A (mol/dm³)), conversion of a fixed bed of solid particles (X_B), temperature of the injected fluid (T_f (K)) and temperature of the solid particles (T_s (K)) as a function of distance from the reactor inlet (z (m)) as shown in Fig 1-1. These are known as profiles. X_B is the amount of solid reacted as a fraction of the original amount of solid. The concentration of the gas is normalised by dividing C_A by C_{AO} (the injected reacting gas concentration) to form a basis of comparison with X_B.

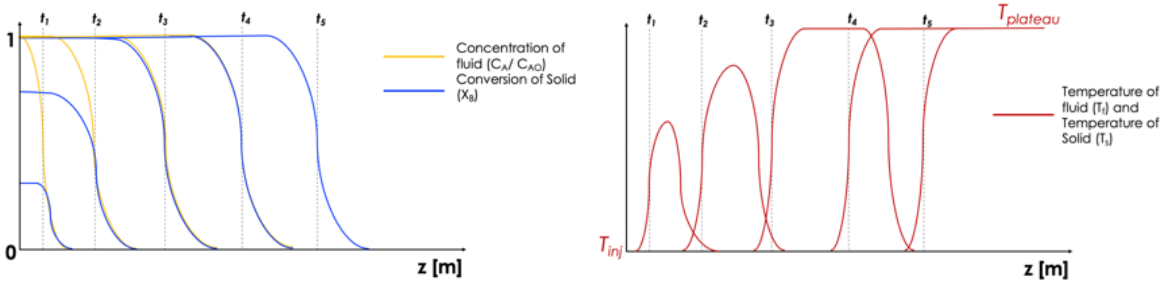

Figure 1-1: Schematic profiles of numerical simulation of Physical Model

Depending on the velocity of the injected gas and the kinetics of the reaction, a part of the solid bed reacts with the injected gas (Muller et al., 2010) giving a certain length of the reactor bed. The injected gas enters the reactor across a length Δz within the time interval Δt, reacting with the fixed bed of solids and ahead of the wave an unreacted bed (Kern and Jess, 2005). In the general case, after a transient period, C_A and X_B become coherent, that is they travel together jointly without separation. This is collectively known as a reaction

wave (Fig 1-2(a)). There is a transient period before a constant pattern is reached. A reaction wave consists of a synchronous C_A and X_B waves at constant pattern. A constant pattern is defined as a wave travelling fixed width and at a constant velocity (from t_3 onwards in Fig 1-1). In a non-isothermal case, the reaction wave has an associated temperature change from the heat of the reaction. The reaction wave and the temperature change associated with it is known as a thermochemical wave (ΔT_C). The C_A and X_B wave are coherent with the tail end of the T_s and T_f waves. When thermochemical wave has passed through the reactor, the reaction is complete. A heat front also moves through the bed, which heats up the reactor bed ahead of the moving thermochemical wave from the plateau temperature $T_{plateau}$ (reached after coherence and a constant pattern thermochemical wave are attained) to the initial temperature of the bed T_O. This is known as the thermal wave. The numerical simulation of the physical model does not make any assumptions about the solution beyond the physical parameters and assumptions mentioned. The physical model does not give an insight to the results of the beforehand and cannot be used as an efficient design and optimisation tool.

A description of a wave in a wave model is the constant pattern model, but the waves in the constant pattern model have a fixed width and shape instead of a sharp interface. The width of the constant pattern model is measured from 1% to 96% when comparing with the physical model (Fig 1-3).

1.4 Wave Model and Constant Pattern Model

The rate of reaction and heat transfer constants play a part in the dispersive shape of the waves in the simulation of the physical model. In the limiting case where all the kinetic and heat transfer rates are infinitely fast, the waves reduce to infinitely thin moving interfaces. The wave model uses a material and energy balance to predict the velocity of the reaction

(V_R), thermal (V_T) and thermochemical ($V_{T/C}$) waves as well as the temperature of the plateau ($T_o + \Delta T_C$ or $T_{inj} + \Delta T_C$). The wave model assumes the velocities (see Fig 1-2(a) and (b)) of these waves are constant. The wave model also assumes that the temperature is high enough for the reaction to progress.

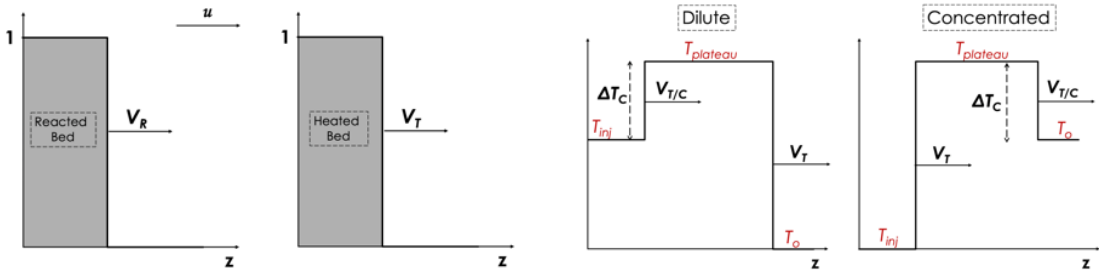

Figure 1-2(a): Reaction and Thermal waves (iso) Figure 1-2(b): Profiles of T_s and T_f (non-iso)

The velocities of the reaction, thermal and thermochemical waves are constant and have been derived in Daggash, 2019. In addition to assumption 1-8 of the physical model, the wave model assumes:

(7) The reactor is uniformly packed with a uniform cross-sectional area

(8) Kinetic and heat transfer rates of reaction are infinite

(9) Diffusion, conductivity and radiation are neglected

Fig 1-2(b) shows the wave model prediction of T_s and T_f for a low (dilute) and high (concentrated) concentration of reacting fluid. According to the wave model equation for $V_{T/C}$, an injection of a dilute gas gives $V_{T/C} < V_T$. Conversely, for a concentrated gas injection $V_{T/C} > V_T$. The definition of a dilute or concentrated injected gas depends on the order of the thermal and thermochemical waves. A slow thermochemical wave arises when there is a low concentration of injected reacting fluid (dilute). Conversely, a highly concentrated injection feed leads to a fast thermochemical wave which travels ahead of the thermal wave.

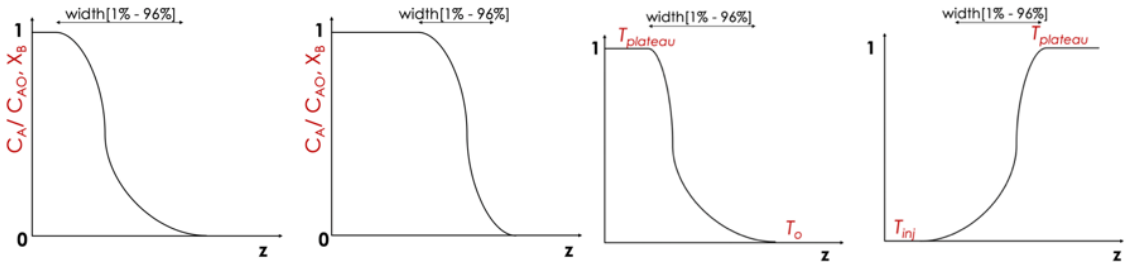

Figure 1-3: Solution to Constant Pattern Model

The constant pattern model assumes that if the traveling wave is observed with a moving point of reference which is stationary with respect to the wave, the wave shape is not changing. The constant pattern model assumes steady state and there is no accumulation. The constant pattern solution presumes a reaction front propagating with a constant velocity in an infinitely large domain. When this is presumed, the physical model consisting of 4 simultaneous PDEs simplify is simplified to a set of simple ODEs, reducing the computational effort significantly. The constant pattern model can be used to measure the fixed width of the thermochemical waves and the temperature of the plateau, giving a more complete description of reaction dynamics. Furthermore, the width of the wave becomes essential when developing reactor wall heating strategies for endothermic reactions.

Chapter 2

Literature Survey

Presented below is a review of past works. The chapter is divided into theoretical and practical aspects of the thesis. The former reviews work in the field of non-linear wave propagation, reactive flow and coherence. The latter discusses the industrial applications of the work particularly decoking of fixed bed reactors and reduction of pyrite and magnetite oxidation. Thermodynamic and kinetic data are also discussed in the later sections.

2.1 'Coherence': Principle

Although the fundamental ideas embodied within the concept of coherence are simple, the concept is nevertheless an abstract and unfamiliar one, which is difficult to grasp; because of this a full introduction of coherence is warranted. The concept of "coherence" Helfferich (1967, 1968, 1984; Helfferich and Klein, 1970) was originally developed to facilitate qualitative understanding and quantitative calculation of multicomponent chromatography, particularly under arbitrary initial and feed conditions. Beyond chromatography it has since been used in multicomponent, multiphase flow in porous media (Helfferich, 1981b) and multicomponent distillation (Nandakumar and Andres, 1981) and seems widely applicable to dynamics of multicomponent systems.

In general terms, the systems of interest here are given by simultaneous, nonlinear, partial differential equations relating two or more dependent variables (concentrations of reacting fluid or solid) to two or more independent variables (distance and time); the dependent variables are coupled so the behaviour of the system cannot be calculated by additive superposition of solutions of single differential equations, one for each dependent variable

separately. Any non-equilibrium in a starting condition of such a system generates a complex response described in this thesis in terms of wave propagation , a "wave" being defined here as a variation of the values of the dependent variables (Aris and Amundson, 1973; Jeffrey, 1976; Helfferich, 1984).

The coherence concept identifies a state which such a system will strive to attain, much as a closed system will approach equilibrium and an open system with fixed boundaries and constant boundary values will approach a steady state (with exceptions in all cases). In fact, coherence can be so defined that it will contain equilibrium and steady state as special cases but is more broadly applicable in that it includes arbitrary propagation problems in open systems (Helfferich and Klein, 1970). As discussed in some detail in the quoted earlier publications, coherence can be defined as a state in which the variations of all dependent variables move in a synchronized fashion, that is, without shift of their profiles relative to one another. In the language of mathematics of waves and of the method of characteristics, such behaviour is known as that of a "simple wave" (Aris and Amundson, 1973; Jeffrey, 1976). Thus, simple waves are coherent by definition, and the coherence principle expresses that an arbitrary perturbation will be resolved into simple waves. More specifically and in the language of the method of characteristics: an arbitrary starting variation, if embedded between sufficiently large regions of constant state, is resolved into simple waves, which become separated by new regions of constant state. It is surprising that this simple principle with inestimable predictive value was not formulated explicitly much earlier. Once a wave has become coherent it will remain so until disturbed. The wave may sharpen or spread but will retain coherence. Not being restricted by operating conditions, coherence is a state which, given enough time and reactor length is attained from any arbitrary initial conditions for undisturbed development.

2.2 Non-Linear Wave Propagation

Convective transport phenomena can be viewed as propagation of waves. For such a purpose, a wave is defined as a variation of the values of dependent variables, usually concentrations, temperature, pressure, etc. This introductory chapter reviews the principles and illustrates the application of non-linear wave theory with several applications in chemical engineering listed below in a timeline.

Isothermal Systems

Precipitation/Dissolution Reactions

Walsh (1983) investigated reactive flow of a single phase with constant initial and boundary conditions. A finite difference model based on Newton-Raphson scheme was developed. General observations were found, and a simple algebraic scheme developed for very simple reactive flow problems. Walsh also studied precipitation/dissolution reactions incorporating redox reactions. Walsh found that metals in various oxidation states could exist in adjacent regions and that certain forms could be more easily dissolved and mobilized.

Redox Reactions

Bryant (1986) took a more theoretical approach to elucidate the wave movements in permeable media. Bryant together Walsh discovered the 'downstream local equilibrium' principle to be applied in various forms to reactive flow problems for their solution. This enabled the algebraic solution to be theorized: if the sequence of minerals were known, then the aqueous solution in equilibrium with these regions as well as solid amounts and wave velocities could be calculated algebraically using the downstream local equilibrium condition. A general solution procedure was postulated. Bryant incorporated ion exchange for the model Walsh developed and applied this new model to alkaline flooding for the

prediction of alkaline loss during enhanced oil recovery. This wave behaviour was not simply additive, but instead caused an entirely different sequence of waves.

Alkaline Flooding

Helfferich and Lake (1978) showed the wave theory was applied to a set of reactions and a theoretical understanding of precipitation/dissolution waves indicated what to expect when a high-pH solution is injected into sandstone: a quartz dissolution wave. The features of this wave provide some insight into alkaline flooding. Local equilibrium approximation was applied and in the absence of any interactions involving hydrogen, the hydrogen cation concentration was shown to be the same upstream and downstream of the dissolution wave.

Thus, the local equilibrium condition provides a simple relationship between the inlet composition and the composition downstream of the dissolution wave. The reactions were considered isothermal, an assumption relaxed in later work by Lake (1995).

Acidising Wells

Walsh et al. (1982) showed the theory of precipitation/dissolution waves provides useful insights into acid treatments. Important trends were identified, which are confirmed by studies that relax the local equilibrium assumption (LEA) (Quinn et al., 2000; Sevougian et al., 1995; Lund and Fogler, 1976). A key treatment design objective of the work is the depth of stimulation, the distance into the formation within which formation damage has been removed. Precipitating a mineral within the formation can reduce the permeability, which is exactly contrary to the effect desired from the treatment. These precipitates ultimately get dissolved by fresh (undersaturated) incoming fluid, but this occurs in dissolution waves which necessarily propagate even slower than the wave that originally precipitated the mineral. Thus, zones containing precipitated minerals propagated into the medium. The wave model was used to determine the permeability reduction associated with these zones

is in the worst possible position (for radial flow profiles) near a wellbore.

Non-isothermal Systems

Precipitation-Dissolution Reactions

Dria, Schechter, Lake (1995) examined temperature effects on wave velocities and mineral sequences during reactive flow with precipitation/dissolution. The term 'thermochemical wave' was used to describe a change in chemical composition including changes in temperature. The waves treated in the paper were shock waves. Material balances assuming local phase equilibrium was used to derive specific velocity of reactive components. Coherence conditions introduced by Helfferich and Klein (1970) was used to reduce the problem of solving for concentrations at all positions to either side of the wave.

The concepts of coherence were applied to a geochemical system involving aqueous solutions of H^+ and CO_3^{2-} ions and precipitates $CaCO_3$ and $BaSO_4$ to name a few. With heterogeneous reactions occurring at different rates. The main contribution of this research was the expansion of the coherence condition to include propagating temperature changes. It was illustrated that thermochemical effects can cause portions of the medium to be at a temperature different from the initial temperature, showing a promise in future application. The effect of temperature was modest, this did not lead to interesting effects of temperature on the system. The assumption of local equilibrium is a simplification for the system. In the current work, it is shown this local phase and thermal equilibrium can be relaxed. The assumption of the physical system was grossly simplified to exclude dissipative effects, diffusion, thermal conductivity and variation of initial and injection conditions.

Non-equilibrium Seawater Injection

Araque-Martinez (2001) investigated seawater injection into oil fields, showing it may account for the largest volume of reactive transport occurring in oil exploration and

production activities. Seawater contains relatively large concentrations of cations and anions, along with significant concentrations of dissolved oxygen and carbon dioxide. Results were based on local equilibrium. Large fluid velocities (usually the largest seen in a field) makes LEA a poor approximation near the well. Furthermore, supersaturation of secondary minerals (those responsible for potential damage) was neglected. The method of characteristics (MOC) solution, with the new dimensionless variables, made it possible to investigate well damage without these restrictions.

Reactive distillation columns and chromatographic reactors

Gruner (2004) provided a general framework for analysing and understanding the dynamics of reactive separation processes. The theory assumes simultaneous phase equilibrium.

Operating conditions whereby these nonlinear wave propagation phenomena occur were investigated. For ideal and moderately non-ideal mixtures, the concentration fronts are of the constant pattern type, i.e. after a disturbance some of these fronts—depending on the sign and magnitude of the disturbance—travel through the column with initially constant shape and velocity. For non-ideal mixtures, the so-called combined waves showed only a part of the wave front represents a constant pattern wave, whereas the other part has a variable shape. The constant pattern solution was not formulated, a powerful tool effective in distillation column design. A constant pattern solution is modelled and shown to propagate through the bed at a constant velocity in the current work. An addition to the non-linear wave model, which is paramount when including non-adiabatic heating.

Hankins (2007) extended a non-linear wave model for dynamic behaviour and wave propagation in non-isothermal distillation columns. The wave model assumed local phase and thermal equilibrium. The results showed validated the wave model, in both qualitative and quantitative description. Specifically, composition, temperature and molar flows

moving in a synchronised fashion. Constant pattern behaviour was also observed. The simplicity and predictive power of the non-linear wave theory was shown to be valuable in designing and control of high purity distillation columns.

Propagation of Non-Linear Waves in Fixed-Bed Reactors

Reactive isothermal flow of a single fluid phase with constant initial and boundary conditions was first investigated for exothermic liquid-solid reactions. The wave model accurately predicted the trajectories of the reaction wave for a reaction between magnesium carbonate and nitric acid. The numerical simulation and wave model were extended to include non-isothermal exothermic reactions. This included both the magnesium carbonate system and the single irreversible reaction between carbon and oxygen.

The calculations established the nature of the wave propagation and its development into a stable, constant pattern form involving a synchronized variation of the temperature, concentration and conversion. This was satisfactory and allows a simple modelling framework through non-linear wave theory. The main contribution of the research was to demonstrate the concentration and conversion wave profiles overlapped (coherent) and attained a constant pattern.

Individually summarised past studies in the application of a wave model approach to industrial processes as well as the theoretical development of the physical model used are given in Table 2-1. The wave model assumptions in Helfferich and Klein, 1970 and Bryant, 1986 was simplified by excluding thermal effects. Dria et al., 1995 and Araque-Martinez, 2001 included thermal effects but were unable to use the wave model approach to investigate operational strategies to optimise in precipitation/dissolution system and mineral precipitation respectively. The current work highlights a new approach of using the wave model, specifically show how the wave model can be used to test out different

operating strategies quickly and effectively in decoking fixed bed reactors and roasting of pyrite particles. The physical model also includes thermal effects neglected in Helfferich and Klein, 1970 and Bryant, 1986. Araque-Martinez, 2001 did not include heat transfer in the precipitation/dissolution mass-balance equations. Araque-Martinez, 2001 used the method of characteristics to solve the mass-balance equations but had issues with rising thermal effects which could have been solved using a flux limiter. The van leer flux limiter was included in solving the mass and energy balances in Chapter 4.

	Helfferich and Klein, 1970	**Bryant, 1986**	**Dria et al., 1995**	**Araque-Martinez, 2001**
Research focus	Helfferich, 1970 investigated the Interference of sorbable species in multicomponent chromatography. Particularly operations such as elution development with a displacement development and frontal analysis.	Bryant, 1986 incorporated ion exchange for the model. The results elucidate the wave movements in permeable media.	Dria, et al., 1995 examined temperature effects on wave velocities and mineral sequences during reactive flow with precipitation/ dissolution. The term 'thermochemical wave' was used to describe a change in chemical composition including changes in temperature. The waves treated in the paper were shock waves.	Araque-Martinez, 2001 investigated mineral precipitation in geochemical modelling. The effect of dissolution and precipitation on injection wells was studied using a wave model approach.
Wave Model assumptions	Applied to arbitrary operating conditions, comprising the standard modes of chromatographic operation as well as other phenomena with multicomponent flow through porous solvents.	Conditions of local equilibrium apply, and the dissolution and precipitation processes exhibited a wave−type behaviour reminiscent of chromatographic fronts.	Material balances assuming local phase equilibrium was used to derive specific velocity of reactive components. Coherence conditions introduced by Helfferich and Klein, 1970 was used to reduce the problem of solving for concentrations at all positions to either side of the wave.	The model used was based on local thermodynamic equilibrium. Large fluid velocities make the LEA a poor approximation near the well.

Theoretical development of Physical Model	Isothermal conditions with a constant feed into a chromatographic column. Development of shock fronts representing concentrations of sorbable species across the column.	A finite difference scheme which uses a combination of graph theory and heuristics to minimise trials and compared to time−sequencing solutions of the set of partial differential equations governing the reactive flow behaviour.	The assumption of the physical system was grossly simplified to exclude dissipative effects, diffusion, thermal conductivity and variation of initial and injection conditions.	The transport of fluids is modelled with kinetic reactions in partial differential equations. The mass-balance equations for each component flowing in the medium is solved using the method of characteristics (MOC).

Table 2-1: Wave Model application by various authors

2.3 Decoking Fixed-Bed Reactors

A description of the decoking process is explained here with references to common industrial practice. This is necessary to find thermodynamic data to run the numerical simulations as well as to test out different approaches to decoking reactors and explain some of the phenomena observed in experimental studies using the wave model.

Catalytic Naphtha Reforming

George J. Antos and Abdullah M. Aitini (1995) studied catalyst regeneration to restore the catalyst to its fresh activity state. To regenerate the catalyst, the coke is burned off in a controlled manner. Carbonaceous material or coke is deposited on the catalyst as an undesirable by-product of the naphtha reforming Catalytic activity and selectivity performance usually deteriorate as the platinum and acid sites become covered with coke. In fixed-bed reactors, reactor temperatures are either increased to compensate for the catalyst deactivation or more frequent regenerations are effected.

Decoking of Fixed-Bed Catalytic Reactors

K. Roel Westerterp (1988) studied a catalytic hydrocarbon conversion processes and

stated the catalyst must be periodically regenerated. This is carried out by shutting the reactor down, removing the reaction mixture by purging with an inert gas and, if necessary, partly cooling down the catalyst bed and then passing an oxygenic gas through the reactor in order to burn off the coke. He showed a non-steady state, exothermic process occurs in the fixed bed reactor: a reaction zone migrates through the bed, the heat generated being transported by the gas and temporarily retained by the catalyst. He concluded in order to prevent deterioration of the catalyst, it is of the utmost importance that the temperature in the bed should not exceed a certain maximum permissible level.

Formation of coke deposits and coke inhibition methods

Boris Jambor (2018) researched steam cracking as a thermal process accompanied by secondary reactions. The main secondary process is coke formation. The coke formation in the steam cracking has negative impact on the economy of the process. Coke formed caused pressure drop increase, heat transfer reduction, hot spots and corrosion by carbonization.

Direct detection of coking and regeneration of single particles and fixed bed reactors by electrical sensors

Kern and Jess (2004) used empirical methods to study fixed bed catalysts used in refinery processes particularly the processes converting crude oil fractions and organic intermediates into required products. The catalysts deactivate by coke formation. To restore the activity of the catalyst, regeneration was conducted by burning off the coke with small amounts of oxygen in an inert gas stream. The regeneration involved both chemical reaction and transport processes, since oxygen must be transported by external mass transfer and by pore diffusion from the bulk phase to the internal coked surface.

For a strong limitation by pore diffusion, the particle was divided into two distinct zones, a carbon-free outer shell and a core rich in carbon (shrinking core model). During decoking, the zone that divides these two regions moves towards the centre of the particle (shrinking particle model). The reactor bed with fresh pellets was maintained at 550°C. The regeneration of the coked fixed bed is carried out with a mixture of N_2 and O_2 (4vol%) at 1 bar at NTP.

Mathematical modelling and study of a dehydrogenation catalyst decoking process

Rahimi et al. (2010) simulated coke combustion and compared the results to experimental data. The coke was reacted through diluted oxygen in a fixed bed reactor. Through this process, the catalyst was exposed to a very hot inert gas stream containing a certain percentage of oxygen. The effects of factors such as diffusion rate, reaction rate, and catalyst structure on regeneration conditions were evaluated. Both homogeneous or heterogeneous models were used. The heterogeneous models are developed based on grain model and shrinking core model. In the shrinking core model, in addition to the reactant diffusion and reaction resistances, two other resistances related to the remaining ash and gas film were considered. Since oxidative reactions, such as coke burning, are usually carried out at higher temperatures, and due to their inherent rapid nature, the shrinking core model was adopted.

Development of a control concept for catalyst regeneration by coke combustion

R. Kelling, G. Kolios (2002) simulated a characteristic regeneration behaviour with a fixed bed uniformly preheated with a varied amount of coke loaded. To start coke combustion, the catalyst bed was preheated above ignition temperature of combustion

(580°C). The initial and feed temperatures are chosen to be equal. After starting the reaction, the addition of a relatively small amount of oxygen to the inert gas feed, caused the temperature to rise immediately. Two propagating fronts develop. Under the considered oxygen-limited conditions, the thermal front was much faster than the reaction front. Sufficiently high inlet temperatures were used in order to ensure the ignition of coke combustion. A summary of the decoking procedures is summarized in Table 2-1. The procedure used in the reviewed papers show the results in Chapter 5 agree with current industrial procedures. Table 2-2 shows some of the parameters used and the procedure for decking fixed bed reactors simulated in Chapter 5.

	Kolios (2002)	**Kern and Jess (2004)**	**Westerterp (1988)**	**Rahimi et al. (2010)**
Purging method	Nitrogen was partially mixed with the gas to be purged out. The mixture exits through the outlet.	A slow flow rate of nitrogen was used to displace the unwanted residues in the reactor.	Pure nitrogen was used at a raised temperature of 150°C to purge residual gases.	Nitrogen was used to purge residual gases. After that, very high-pressure steam at 400°C and 104 bar was used.
Preheating method	The reactor bed was heated in nitrogen to a target temperature of 398°C and maintained there.	Hot nitrogen was used to increase the catalyst bed temperature to 380°C.	The reactor bed was heated with nitrogen at a rate of 30°C per hour to a target temperature of 398°C.	Electrical heating wass used to heat the reactor bed to 400°C. This heats up the jacket around the reactor.
Parameter	Air was used as an oxygen source. Oxygen concentration was maintained at 2% in nitrogen. Temperatures were carefully maintained at 575°C to prevent a runaway exothermic reaction.	3% oxygen mixed with nitrogen enters the reactor and the decoking process begins with a Superficial velocity of O_2 at 0.24 m/s. Temperatures was kept less than 580 ^{o}C.	3% oxygen was mixed with air. Large injected amounts of oxygen were limited to prevent sintering of the catalyst.	A stream mixture of steam and air was introduced. The air concentration is raised from 0.1% to 1%. The temperature should not exceed 550°C.

Table 2-2: Decoking procedures from various authors

2.4 Roasting of Pyrite

The roasting of pyrite and magnetite by hydrogen (irreversible endothermic) and oxygen (reversible exothermic) have been discussed by many researchers. The methods explained here form the basis of the data required to run the irreversible endothermic and reversible exothermic cases.

The kinetics and mechanism of the pyrite-to-pyrrhotite transformation

The thermal decomposition of pyrite was investigated by many researchers such as Lambert (1998) Janzen et al. (2000), Laurent (2010). The apparent activation energy of the reaction were reported to be in the range of 70 to 200 kJ/mol. It was concluded that the rate is controlled by the diffusion of sulphur in the pyrite lattice and by the availability of hydrogen to remove sulphur from the pyrite surface. According to the accepted phase equilibria of iron sulphides, pyrite decomposes to pyrrhotite in the temperature range of 523K to 1016K. The system was first operated by evacuating the contents of the vessel with a mechanical roughing pump and then pressurising the system to the desired level using Nitrogen. The reaction rate is assumed to be first order. Pyrite decomposition appeared to commence on the exterior of the surface and progresses inwardly. Therefore, the reaction could best be described by the shrinking core model. The diffusion of pyrite through pyrrhotite appears to be the rate controlling step. At the exterior of the shrinking core, a pyrrhotite layer forms. In 4 hours reaction time, only 10% of the initial weight was lost.

Kinetics and mechanisms of iron sulphide reduction in hydrogen and carbon monoxide

Laurent (2010) studied the reduction of iron sulphide by hydrogen using plug flow. The reactions were studied in the 523K - 723K temperature range and were found to be first order processes. The research was in support of a project which seeks to develop a coal

desulphurisation process. Laurent (2010) suggested that the rate determining step in this process is the diffusion of sulphur in the solid pyrite. In the case of reduction by hydrogen, results indicated a complex mechanism in which both surface reaction and solid diffusion appear to contribute. Normally, samples are preheated in helium at the reaction temperature to obtain a constant weight. The reduction of the sample was initiated by adding hydrogen at a temperature between 653K - 693K. Reactions were found to be very sensitive to the pyrite pre-treatment. In the experiments, pyrite samples were heated under dry, flowing, oxygen-free helium for 24 hr before the reductions were begun. Heating pyrite under flowing helium increases the surface area of pyrite and increases the reaction rates of hydrogen. The kinetic and thermal parameters in this paper was implemented in the numerical simulations presented in Chapter 6.

Kinetics of pyrite to pyrrhotite reduction by hydrogen in calcite buffered solutions between 90 and 180 °C: Implications for nuclear waste disposal

Pyrite thermal degradation into pyrrhotite induced by hydrogen has been investigated using thermogravimetric analysis over a temperature range of 350–700 °C (Wiltowski et al., 1987; Lambert et al., 1998). In aqueous media, the reverse reaction of pyrite with oxygen has been more extensively studied within the framework of the global geochemical iron–sulphur cycles (Graham and Ohmoto, 1994; Benning et al., 2000; Butler and Rickard, 2000).

Lambert (1998) addressed the rate and mechanism of pyrite reduction by hydrogen under conditions similar to those predicted for the nuclear waste storage assessment. For safety reasons, 10% H_2 in Ar (grade 5.0) was used rather than pure H_2 as the source of hydrogen in the system. In the reaction of pyrite reduction into pyrrhotite by H_2, three critical steps were suggested to control the pyrite reduction kinetics: (i) diffusion of $H_{2(aq)}$ and $H_2S_{(aq)}$

between the reaction front and the bulk solution through the porous pyrrhotite microstructure, (ii) surface reaction of pyrite dissolution, and (iii) surface reaction of pyrrhotite precipitation. Under conditions far from equilibrium, the observed decreasing rate of H_2S production as a function of time suggests that the pyrite reduction may be controlled by a diffusion process. It was considered that values of activation energy below 20 kJ mol indicate a diffusion- controlled kinetic regime, while values between 70– 100 kJ mol indicate that the kinetic regime is controlled by a mix of surface reactions and diffusion. This range is in agreement with the kinetic parameters estimated by Laurent (2010).

Thermal Decomposition of Iron Sulphide (Pyrite) – Shrinking Model

J. L. F. Monteiro et al. (2010) carried a study to investigate thermal decomposition of pyrite in a silica batch fluidized bed reactor using a temperature of 594 – 625˚ K. When pyrite was decomposed, pyrrhotites and lower contents of sulphides were obtained (Cyprès, Ghodsi, & Stocq, (1981)). In his study, particles were sampled in different each reaction run and those which had partially reacted, portrayed a sharp reaction front. Equilibrium is established between reacted pyrite and pyrrhotites until the primary core of iron sulphide disappears.

Research by Yamazaki et al. (2008), indicated during the reaction, mass and/or heat transfer is controlled. They proposed the use of shrinking core model as controller of heat transfer. Shrinking core model is used to assess conditions which pyrite particles are consumed by the reaction (Rickard & Luther, 2007). This model is useful because it helps control the heat transfer used in the reaction. Other authors who have conducted similar reaction to this, use thermal balance to control the reaction. Guillaume, & Giffaut (2010) were among researchers who studied the kinetics of thermal decomposition of iron

sulphide. The research gave much attention to reversibility of the reaction when discussing and analysing the results of the reaction.

Reaction of Magnetite

Schwab and Philinis (1957) carried out a study on the decomposition of magnetite in hydrogen using plug flow method. Subsequently, they examined air oxidation behaviour of iron sulphide. In this study, it was found the reaction of magnetite with oxygen can be considered to be first order. Obtained activation energy around 126 kJ/mole at a range of 693 – 823˚ K. The air oxidation of magnetite to hematite and the air oxidation of ferrous sulphide was investigated kinetically by measuring continuously the weight losses of the solids during the course of the reaction. The course of the air-oxidation reactions was further followed by measurements of the sulphur dioxide produced. The rate of reduction of pyrite by oxygen is proportional to the fraction of pyrite remaining to be reduced. The kinetic and thermal parameters in this paper were used to plot the variation of conversion of magnetite with time. The result showed the data can be deemed suitable for the numerical simulations of the reversible exothermic reactions presented in Chapter 7.

Table 2-3 is a comparison of authors that have developed a physical model to describe the roasting of pyrite process. Schwab and Philinis, 1947 provided the parameters for the rate expression. Hong and Fegley, 1997, Lambert, 1998 and Laurent, 2010 investigated the roasting of pyrite with hydrogen gas. The activation energy, concentration of H_2 gas and temperature of the injected gas were of similar order of magnitude. These parameters were used and applied in Chapter 6. Different operational strategies used in their individual processes. The physical model was simulated to replicate the strategies adopted by Lambert, 1998 and Laurent, 2010 and used to compare their energy requirement to a pre-heat strategy developed by the wave model in Chapter 6.

	Hong and Fegley, 1997	Lambert, 1998	Laurent, 2010
Industrial process applied to	Hong and Fegley, 1997 passed hydrogen at high flow rates at atmospheric pressure through beds of FeS_2 particles.	Lambert, 1998 investigates the kinetics and mechanism of the pyrite-to-pyrrhotite transformation of a pyrite particle.	Laurent, 2010 studied the reduction of iron sulphide by hydrogen using plug flow. The research was in support of a project which seeks to develop a coal desulphurisation process.
Inlet temperature conditions	Measurements were made at 773K, 808K and 840K, and an activation energy of 3.0 x 10^7 J/ kmol was proposed. A shrinking core model is assumed. The diffusion of hydrogen through a pyrite ash layer appears to be the rate controlling step.	According to the accepted phase equilibria of iron sulphides, pyrite decomposes to pyrrhotite in the temperature range of 523K to 1016K. The apparent activation energy of the reaction was reported to be in the range of 70 to 200 kJ/ mol.	The reactions were studied in the 623K - 823K temperature range and were found to be first order processes. The diffusion rate activation energy of the reaction was found to be 200 kJ/ mol.
Preparation method and composition of injection feed	H_2S-H_2 gas mixtures were used as the injection feed. Hydrogen concentration was maintained at 4% in H_2S.	The system was first operated by evacuating the contents of the vessel with a mechanical roughing pump and then pressurising the system to the desired level (4%) using Nitrogen. Pyrite decomposition appeared to commence on the exterior of the surface and progresses inwardly.	Samples are preheated in helium at the reaction temperature to obtain a constant weight. The reduction of the sample was initiated by adding hydrogen at 3% concentration in H_2S. Reactions were found to be very sensitive to the pyrite pre-treatment. In the experiments, pyrite samples were heated under dry, flowing, oxygen-free helium for 24 hr before the reductions were begun.
Rate constant determination	The results indicated a first order (with respect to hydrogen) reaction. The rate constants were determined from the weight loss and the thickness change of pyrite in reacted samples. The temperature dependent composition of the product was measured by electron microprobe analysis and X−ray diffraction.	It was concluded that the rate is controlled by the diffusion of sulphur in the pyrite lattice and by the availability of hydrogen to remove sulphur from the pyrite surface. The reaction rate is assumed to be first order.	Laurent, 2010 suggested that the rate determining step in this process is the diffusion of sulphur in the solid pyrite. In the case of reduction by hydrogen, results indicated a complex mechanism in which both surface reaction and solid diffusion appear to contribute.

Table 2-3: Physical Model of Roasting of Pyrite by various authors

Chapter 3

Non-Linear Wave Theory, Wave and Constant Pattern Model

The main purpose of this chapter is to provide a theoretical basis of the non-linear wave theory, to define terms used in the current work and to define the tools of the research. The derivations of the wave velocities are also explained in this chapter. Several improvements of the wave model originally proposed by Helfferich (1967), Lake (1995) are provided to account for mass and heat transfer zones, as well as adiabatic wall heating.

3.1. Definitions

Wave:

A wave is defined here as any spatial or temporal variation of dependent composition variables. In the present case, the dependent variables used here are the concentration of the reacting fluid component, the conversion of reacting solid and the temperatures of the solid and fluid in the reactor. Independent variables are distance and time. These waves display non-linear wave propagation behaviour, because their response behaviour is related in a non-linear way to the changes which cause them.

Concentration:

The concentration of a reacting species is usually defined as the amount (number of moles) of the reacting species per unit volume of the respective solid or fluid phase. For the solid phase, conversion of solid is the fraction of original reacting solid that has reacted. The concentration velocity is defined as the velocity at which a given concentration C_i of the

overall concentration of a component *i* is propagated in the direction of flow.

$$v_{C_i} \equiv \left(\frac{\partial z}{\partial t}\right)_{C_i} \tag{3.1}$$

Profiles and Histories:

It is convenient to describe reactor behaviour in terms of concentration profiles or histories. A concentration profile shows the concentration of the reacting species as a function of the distance from the reactor inlet at a fixed, specified time. A concentration history shows the concentration as a function of time at a fixed, specified distance from the reactor inlet. A set of synchronous concentration profiles of all reacting species (fluid and solid) constitutes a composition profile. Similarly, a set of synoptic concentration histories of all species constitutes a composition history. A profile referring to zero time is called initial profile.

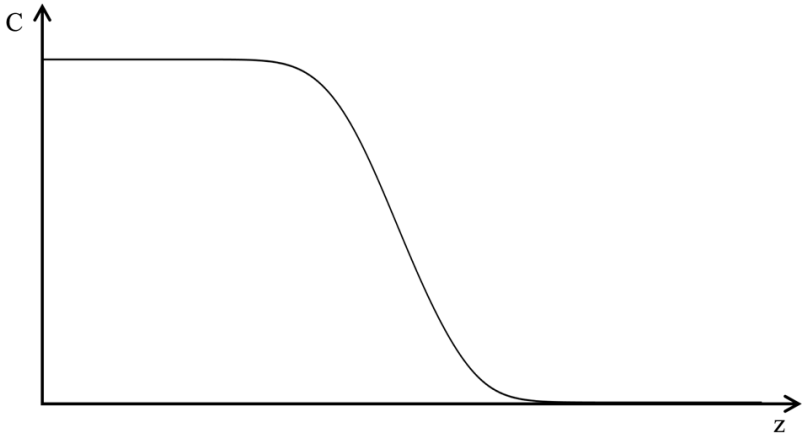

Figure 3-1: Composition Profile

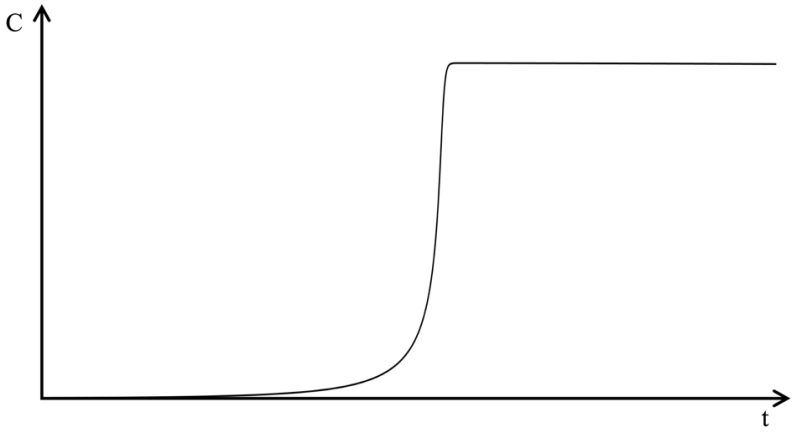

Figure 3-2: Composition History

Self-sharpening wave and Non-sharpening wave:

A self-sharpening wave becomes or remains a shock wave in the absence of dissipation; in real systems dissipation lets the shock attain a constant pattern, that is, an abrupt but continuous variation that travels without further sharpening or spreading and thus of constant shape.

Self-sharpening waves in the presence of dispersion tend to an asymptotic limit in which the wave travels in pure translation. The terms 'self-sharpening' and 'non-sharpening' are used to describe a trait rather than behaviour. Thus, a boundary, which has become ideally sharp or has attained its constant pattern, is still called self-sharpening, although it does not sharpen any further. A self-sharpening wave, which is initially diffuse sharpens into a shock in the absence of fluid dynamic dispersion. In our research, a constant pattern is attained instead.

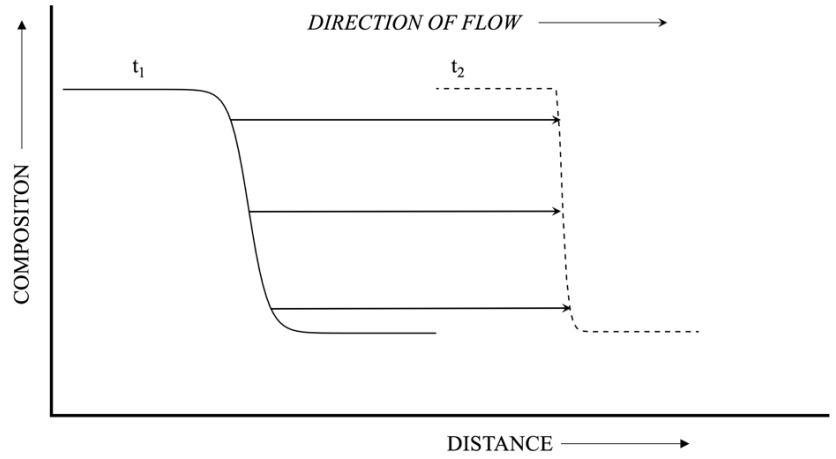

Figure 3-3: Sharpening behaviour of self-sharpening wave. Concentration profiles at two successive times, t_1 and t_2

A non-sharpening wave spreads regardless of dissipation and initial condition and retains or approaches a proportionate pattern in which its diffuseness increases in proportion to the distance travelled. For a non-sharpening wave, the compositions in the leading portions tend to advance faster than do those in the trailing portions, and the wave accordingly spreads on propagation in proportion to the distance travelled (proportionate pattern).

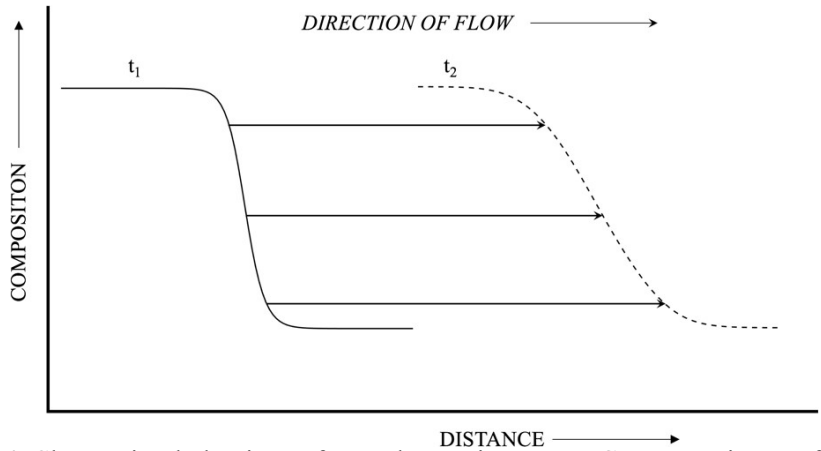

Figure 3-4: Sharpening behaviour of non-sharpening wave. Concentration profiles at two successive times, t_1 and t_2

Indifferent wave:

An indifferent wave in the absence of dissipation travels without change in sharpness; in real systems, dissipation makes it spread in proportion to the square root of distance travelled. There is no tendency for any composition to move faster than the other compositions as shown below.

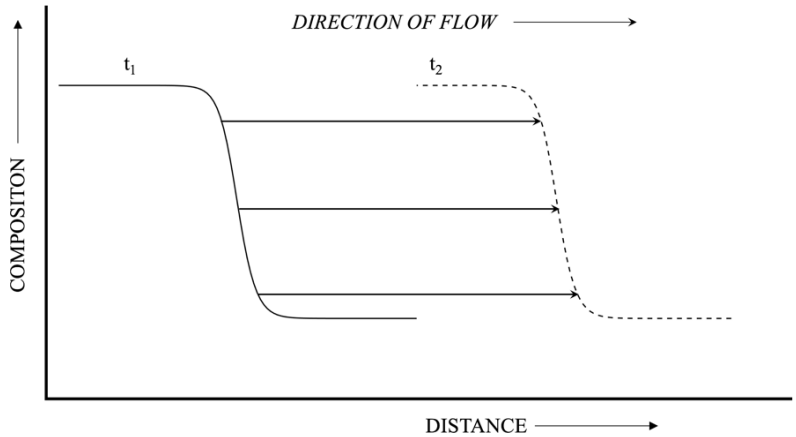

Figure 3-5: Sharpening behaviour of indifferent wave. Concentration profiles at two successive times, t_1 and t_2

Dispersion:

The significant attributes of dispersion are the following:

1. Dispersion causes spreading as quantified by a zone length (the distance over which concentration changes between pre-set limits).

2. Wave velocities are unaffected by dispersion. We will see that this will be a feature of the wave velocity equations.

3. The spreading caused by dispersion is irreversible.

Composition routes:

Composition routes can be defined as the sequence of compositions in a composition profile or history that can be mapped out in a composition space (Concentration/ Temperature of reacting species as the y-axis and distance or time as the x-axis). A distinction may be made between history routes (for a fixed location) and profile routes (at a fixed time). The resulting curve is called a composition route.

The composition route may be in terms of the fluid phase or solid phase. The composition route is completely covered by an infinite number of curves.

Distance-Time Diagrams:

Distance-time diagrams are valuable tools for depicting wave propagation. In such a diagram, fixed values of composition variables are tracked as curves or lines in a co-ordinate system. Hence, we would like a solution representation method that does not depend on the transform variable. The representations are discussed in the following paragraph and also are treated by Helfferich and Klein (1970).

- A plot of z versus t at fixed concentration is called a time-distance diagram. These diagrams are among the most counter-intuitive of the representations but, once understood, they offer excellent visualization of the solutions and the wave trajectories.

The advantage over a representation in terms of profiles or histories is that the entire response can be shown in a single diagram. Distance-time diagrams are also known as wave trajectories. These plots are concise and still remain quantitative.

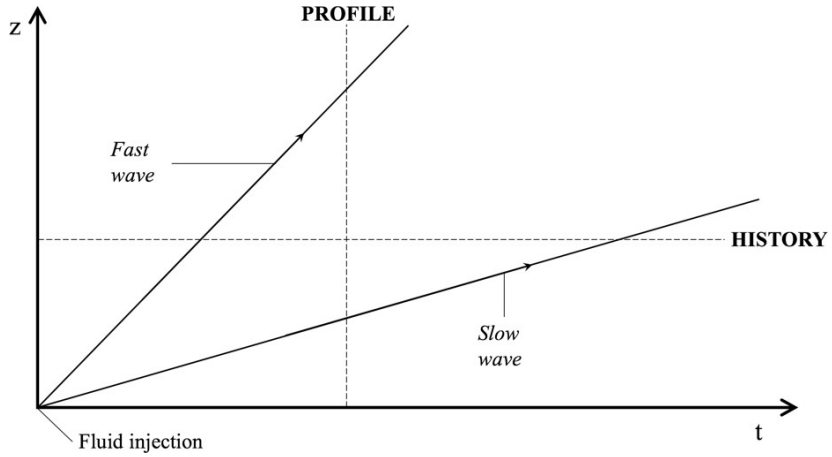

Figure 3-6: Distance-time diagram for injection of reactive fluid (schematic)

Riemann problems:

A Riemann problem is one having special boundary and initial conditions as follows: a permeable medium having initially the same phases and phase compositions at all points is disturbed by the injection of a fluid of constant composition. The entry of reactive fluid into a bed of initially unreacted solid is typical of this type of problem. This special functional relationship depends on the following assumptions:

(a) initial conditions that do not depend on x and boundary conditions that do not depend on t, yielding a discontinuity at the inlet (x = 0) at time t = 0, the so-called "step change" at the origin;

(b) chemical reactions are not at local equilibrium; this includes the reaction time scale from the problem,

(c) The medium is one-dimensional in the direction of flow;

The resulting Riemann problems are quasilinear systems of partial differential equations of the first order.

3.2 Constant Pattern Attainment

A constant pattern state of a wave/front can emerge in a sufficiently long spatial domain, in

which the wave/front travels self-preserving without losing shape. Constant pattern profile is a typical regime arising from gas-solid systems.

A reaction profile propagates downstream and reacts with the solid material on the reactor bed. This reaction profile reaches a fixed width. At the outset, the profile starts very sharp, which then spreads out. Eventually, the reaction profile does not change its shape. In other words, it is a constant pattern. A constant pattern guarantees coherence.

A constant pattern state of a wave/front can emerge in a sufficiently long spatial domain, in which the wave/front travels self-preserving without losing shape. Constant pattern profile is a typical regime arising from gas-solid systems.

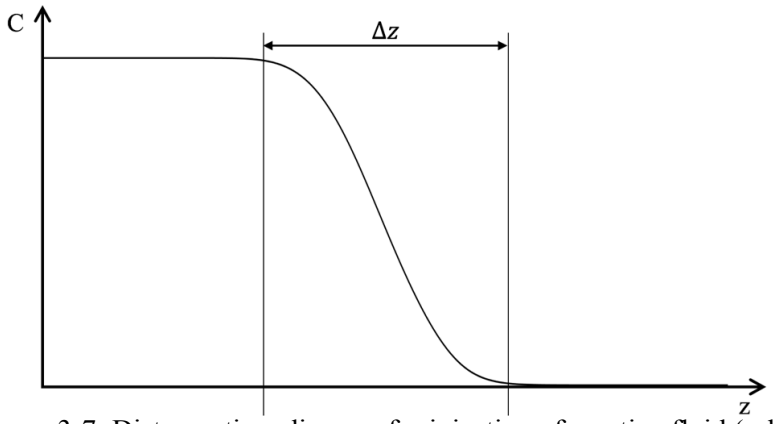

Figure 3-7: Distance-time diagram for injection of reactive fluid (schematic)

The proof of this would be to measure the reaction profile width by numerical simulations and show it does not change with time.

If the reaction wave travels at constant velocity, then the wave trajectory of the reaction wave should be a straight line. The numerical calculations with the numerical model have revealed the existence of constant pattern profiles. The reaction profile reaches a fixed reaction width and travels at constant velocity across the reactor bed. This fixed width of the reaction profile can actually be predicted directly with the wave model. The objective is to carry out a very simple one-off calculation which is only based on boundary conditions to define the reaction wave profile. If a constant pattern is formed and the limiting boundary conditions are known, the wave model can be used to predict the reaction wave profile

shape, width and speed.

3.3 Concept and Conditions for Coherence

A key concept of the multiple component coherence theory is that of ‘coherence’ itself. Coherence refers to stability in dynamic, transient phenomena.

Coherence is characterised by the fact that, at any given point and time in the reactor, the dependent variable (i.e. concentration and temperature) velocities of all species are equal. In the examples that will follow, only two species (one fluid and one solid) are used. The full power of coherence is more apparent with multiple species, but this study is a stepping-stone to multiple component systems. Coherence is an ideal concept to gain a qualitative understanding of systems having variable initial or feed conditions.

Coherence theory addresses itself to general, arbitrary wave propagation problems containing two or more dependent variables (such as concentration or temperature) related by partial differential equations to two or more independent variables (such as distances and time). The concept identifies the state which such a dynamic, multicomponent system strives to attain. A sufficient and necessary condition for a wave to be coherent is now defined

- For a wave to be coherent, the local, momentary wave velocities of all components present must be equal. This is the fundamental coherence condition and is sufficient and necessary for coherence. The equality of velocities in the coherence condition refers to wave velocities, not particle velocities.

Coherence may be viewed as an extension and generalisation of equilibrium and steady state. In equilibrium and steady state, no value of a dependent variable changes its position in space with time, so that sets of values automatically remain conserved. In contrast, coherence under non-steady state conditions allows values of dependent variables to change their positions in space with time, but they must do so jointly, that is, all values of a

set at one point in space and time must move in the same direction and with the same velocity, so that they will remain in each other's company. For a fluid-solid reacting system with dependent variables C_i (concentrations of fluid reactant component i), X_i (conversion of solid reactant component i) and distance z and time t independent variables, coherence requires at any point in time and space.

$$v_{C_i} = v_{X_i} = v \tag{3.2}$$

$$v_{C_i} \equiv \left(\frac{\partial z}{\partial t}\right)_{C_i} and\ v_{X_i} \equiv \left(\frac{\partial z}{\partial t}\right)_{X_i} \tag{3.3}$$

$$\left(\frac{\partial C_i}{\partial C}\right)_{z,t} = \left(\frac{\partial X_i}{\partial X}\right)_{z,t} \qquad i = A, B, C \tag{3.4}$$

where v is the composition velocity common to all reacting components. C is total concentration of fluid reactants and X is the total conversion of solid reactants. This is the differential coherence condition.

3.4 Wave Model

The wave model uses local phase equilibrium to predict the velocities of the reaction, thermal and thermochemical waves as well as the plateau temperature reached. In all of the cases considered in the thesis, the wave fronts are self-sharpening and assume a constant pattern. This is confined in chapters 5, 6 and 7. Because of this they can be replaced by a sharp moving front of negligible thickness and unique velocity. Before the velocities are derived, it is important to state the underlying assumptions and provide a graphical idea of what the waves resemble.

The principal assumptions in the wave model:

- The reactor is uniformly packed, to have uniform cross-section, and to exhibit ideal plug flow.
- Solid is in thermal equilibrium with the fluid but non-isothermal.
- The reaction between the fluid and the solid is fast and complete.
- The fluid is incompressible (no change in density with temperature).
- The rate of equilibration of the solid with respect to the fluid is high enough between the two reacting species to enable reactive equilibrium everywhere in the reactor.
- Diffusion, conductivity and radiation are neglected.

Imagine a reacting fluid at constant concentration being injected into a fixed bed reactor initially free of the reacting fluid and (at this stage) assume isothermal behaviour for now. The fluid reacts with the first reacting zones of the bed. Additional fluid passes through these reacted zones without change in composition, and instead reacts with solid zones further down the reactor. At any time, the bed can be viewed as consisting of two distinct zones; one of reacted and one of still unreacted solid, with a sharp transition in between them. This transition, traveling through the bed, will be called a "reaction wave" (see Fig. 3-8).

The isothermal condition is now relaxed and the case of a thermal wave traveling through a bed in which no reaction occurs is tackled. It is assumed that a fluid of higher temperature enters a bed initially at ambient temperature. At any time, the bed consists of two zones, of higher and initial reactor bed temperatures respectively, separated by a traveling "thermal wave" (see Fig. 3-9); the latter is, a temperature variation advancing in the direction of flow. As in the case of the reaction wave, the mechanism of retardation is the erosion of the advancing front, in this case by removal of heat from the fluid. The behaviour of the fixed bed reactor under non-isothermal conditions can now be fully

tackled. Now consider a bed at ambient temperature, receiving a fluid of constant composition and initial temperature, and reacting with solid exothermically. There will again be a reaction wave, but this wave will now also act as a traveling source of heat energy and releases the heat of reaction into each zone of the bed as that zone reacts. This is called a "thermochemical wave" (see Fig. 3-10), following Lake (1995).

As stated earlier, at any point in time, the reactor bed can be viewed as having two distinct zones; one of heated fluid and reacted solid, and one of unheated and unreacted solid. Similarly, the reactor bed can be viewed as having two distinct zones; one of heated fluid (T_f) or solid (T_s) and one of unheated fluid or solid. Coherence reduces the problem of solving for each concentration at all positions and times to one of solving for the concentrations on either side of the waves, a tremendous reduction in effort.

3.4.1 Reaction Wave Velocity

The derivation is based on a material balance argument, namely, that the change in content of a volume element must equal the difference between the amounts entering and leaving. Based on the description of reaction waves above, the two distinct waves (C_A and X_B) travel and remain together relative to each other in a synchronized fashion. The synchronized wave is known as the reaction wave. In this case, the reaction wave front assumes a constant pattern form. A frame of reference moving at the wave velocity will observe a steady state, for which there is no accumulation term. Let the reaction wave velocity be V_R. The reaction wave moves a distance $V_R \Delta t$ down the bed in time Δt, taking in unreacted solid at the front and rejecting the completely reacted solid at the rear. In a unit cross-section of reactor bed, in the moving frame of reference, the reaction wave velocity is given via a steady state material balance;

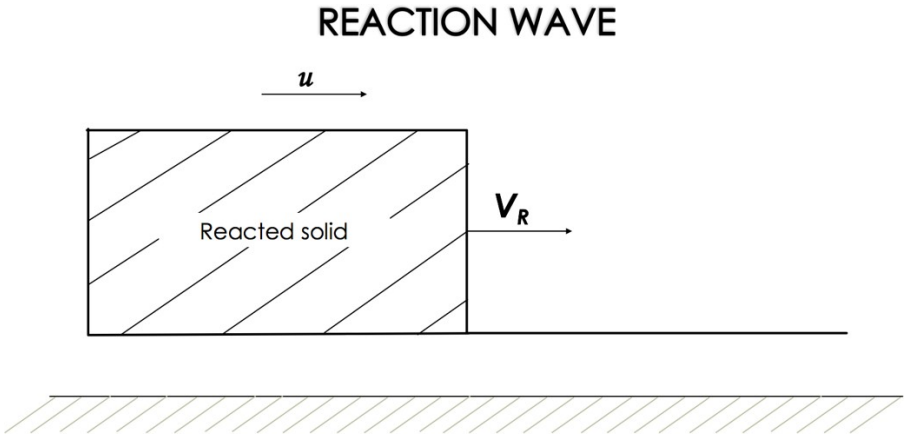

Figure 3-8: Reaction wave

Molar balance at the front:

Rate of convection of A/a = rate of consumption of A/a = rate of consumption of B/b

$$\left(u - V_R\right) . \varepsilon . C_{AO} = V_R . (1 - \varepsilon) . \rho_B . \frac{a}{b}$$

$$V_R = \frac{u \varepsilon C_{AO}}{\varepsilon C_{AO} + (1 - \varepsilon)\rho_B \frac{a}{b}}$$

$$V_R = \frac{u / \varepsilon}{1 + \frac{(1-\varepsilon)}{\varepsilon} \frac{\rho_B}{M_B} \frac{a}{b} \frac{1}{C_{AO}}} \qquad (3.5)$$

3.4.2 Thermal Wave Velocity

Let the thermal wave velocity be V_T. Heat is transported through the bed by the fluid; therefore, by analogy to the derivation of the reaction wave velocity in a unit cross-section of reactor bed;

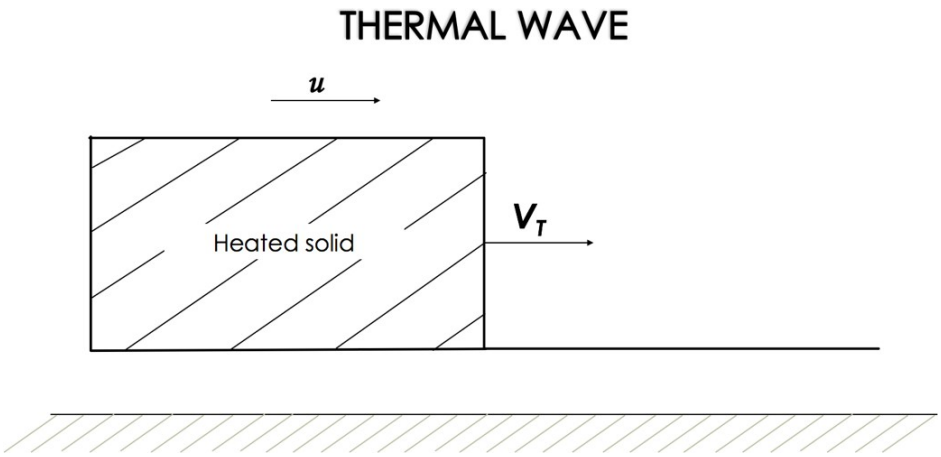

Figure 3-9: Thermal wave

Heat balance at the front:

Rate of heat convection in by the fluid = Rate of heat convection out by the solid

Thus, the heat balance for a constant pattern wave is

$$\varepsilon \,.\, \left(u - V_T\right) \,.\, c_{pf} \,.\, T_1 - \varepsilon \,.\, \left(u - V_T\right) \,.\, c_{pf} \,.\, T_2 = \; (1-\varepsilon) \,.\, V_T \,.\, c_{ps} \,.\, T_1 - (1-\varepsilon) \,.\, V_T \,.\, c_{ps} \,.\, T_2$$

$$V_T\Big(\varepsilon \,.\, c_{pf} \,.\, \left(T_1 - T_2\right) + (1-\varepsilon) \,.\, c_{pf} \,.\, \left(T_1 - T_2\right)\Big) = \; u \,.\, \varepsilon \,.\, c_{pf} \,.\, \left(T_1 - T_2\right)$$

$$V_T = \frac{u \varepsilon c_{pf}\left(T_1 - T_2\right)}{\varepsilon c_{pf}\left(T_1 - T_2\right) + (1-\varepsilon) c_{ps}\left(T_1 - T_2\right)} \tag{3.6}$$

$$V_T = \frac{u/\varepsilon}{1 + \frac{(1-\varepsilon)}{\varepsilon}\frac{c_{ps}}{c_{pf}}} \tag{3.7}$$

3.4.3 Thermochemical Wave Velocity

Thermochemical waves are waves where there is a coherent change in both chemical composition and temperature. In an isothermal system, the synchronised C_A and X_B waves are known as reaction waves but in a non-isothermal system, where there is a heat of reaction, the wave is referred to as a thermochemical wave. Combining Fig. 3-8 and 3-9:

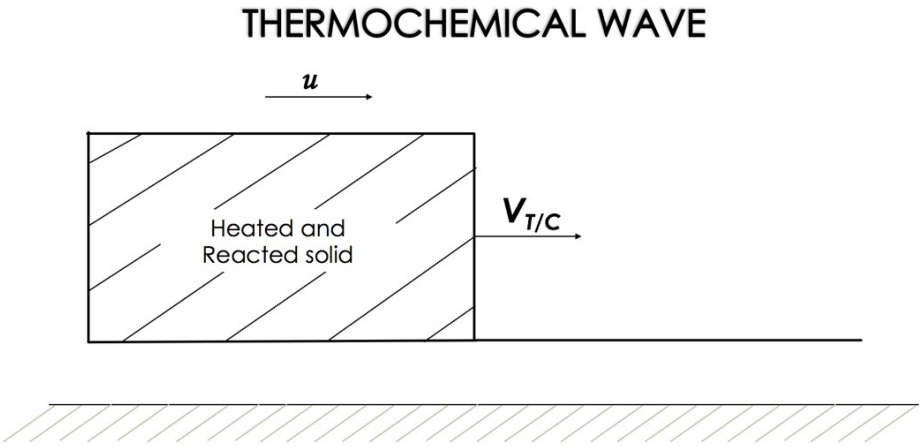

Figure 3-10: Thermochemical wave

Rate of heat convection in by fluid + Rate of heat generation = Rate of heat convection out by solid. The total heat balance for a constant pattern thermochemical wave is then:

$$\varepsilon . \left(u - V_{\frac{T}{C}} \right) . c_{pf} . T_1 - \varepsilon . \left(u - V_{\frac{T}{C}} \right) . c_{pf} . T_2 + V_{\frac{T}{C}} . \frac{\rho_B}{M_B} . (1 - \varepsilon) . \frac{a}{b} . (- \Delta H) =$$

$$(1 - \varepsilon) . V_{\frac{T}{C}} . c_{ps} . T_1 - V_{\frac{T}{C}} . (1 - \varepsilon) . c_{ps} . T_1$$

$$V_{\frac{T}{C}} . \left(\varepsilon . c_{pf} . (T_2 - T_1) + (1 - \varepsilon) . c_{ps} . (T_2 - T_1) + (1 - \varepsilon) . \frac{\rho_B}{M_B} . \frac{a}{b} . (- \Delta H) \right) = u . \varepsilon . c_{pf} . (T_2 - T_1)$$

$$V_{T/C} = \frac{u c_{pf} (T_2 - T_1)}{(1 - \varepsilon) \left\{ c_{ps} (T_2 - T_1) + \frac{\rho_B}{M_B} \frac{a}{b} (- \Delta H) \right\} + \varepsilon c_{pf} (T_2 - T_1)} \qquad (3.8)$$

The second term in the denominator then represents the contribution of heat of reaction to the thermochemical wave velocity. T_1 can be less than or greater than T_2, depending on the relative position of the thermal wave. The thermochemical wave may be either slower or faster than the thermal wave, depending on the concentration of the fluid. If the thermal wave is slower than the thermochemical wave, the thermochemical wave drops from T_1 to T_2 ($T_1 > T_2$) as in Fig 3-10. If the thermal wave is faster than the thermochemical wave, the thermochemical wave rises from T_1 to T_2 ($T_1 < T_2$)

3.4.4 Temperature of Plateau

The flat region of the temperature profile between the thermal and thermochemical wave is known as the temperature plateau and is where the heat of reaction accumulates.

The temperatures on the left and right of the temperature plateau do not have to be equal; the values depend on the temperature of the injected fluid and initial state of the solid bed.

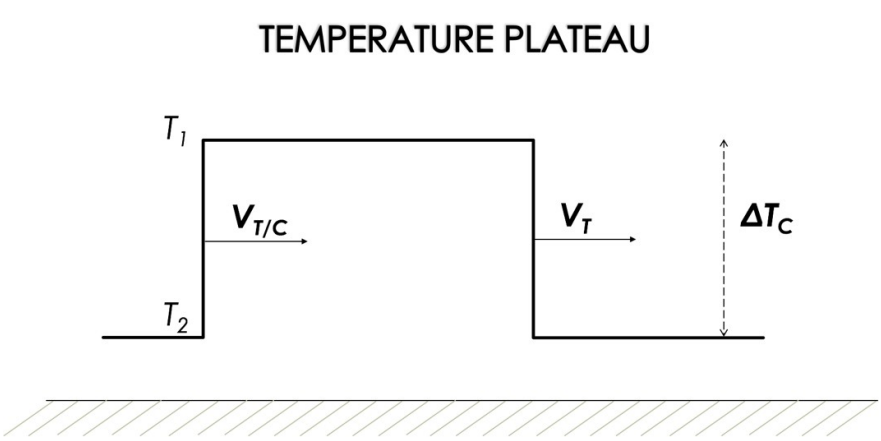

Figure 3-11: Temperature plateau

The second term in the denominators of T_1 and T_2 represent the contribution of the heats of reaction to these velocities. Since the thermochemical wave is coherent with respect to temperature and composition, the temperature rise can be derived by equating the two wave velocities equation (3.5) and (3.7):

$$\frac{(1-\varepsilon)}{\varepsilon}\frac{c_{ps}}{c_{pf}} + \frac{(1-\varepsilon)}{\varepsilon}\frac{\rho_B}{M_B}\frac{a}{b}\frac{(-\Delta H)}{c_{pf}(T_1-T_2)} = \frac{(1-\varepsilon)}{\varepsilon}\frac{\rho_B}{M_B C_{AO}}\frac{a}{b}$$

$$\frac{c_{pf}}{C_{AO}\Delta H} - \frac{c_{ps}}{c_{pf}}\frac{c_{pf}}{\rho_B}\frac{M_B b}{a(-\Delta H)} = \frac{1}{(T_1-T_2)}$$

$$\frac{1}{(-\Delta H)}\left(\frac{c_{pf}}{C_{AO}} - \frac{c_{ps}}{\rho_B}\frac{M_B b}{a}\right) = \frac{1}{\Delta T}$$

$$\Delta T = \frac{(-\Delta H)}{\left(c_{pf}\frac{1}{C_{AO}} - c_{ps}\frac{M_B}{\rho_B}\frac{b}{a}\right)} \qquad (3.9)$$

For the dilute case $\Delta T = T_1 - T_2$. For the concentrated case $\Delta T = T_2 - T_1$

The narrower the "accumulation zone" in which the heat is stored, the greater is the temperature change caused by that heat. A rearrangement of the wave velocities gives:

$$V_R = \frac{u/\varepsilon}{1 + \frac{(1-\varepsilon)}{\varepsilon}\frac{X}{C}} \qquad (3.10)$$

$$V_T = \frac{u/\varepsilon}{1 + \frac{(1-\varepsilon)}{\varepsilon}\frac{c_s}{c_f}} \qquad (3.11)$$

$$V_{T/C} = \frac{u}{1 + \frac{(1-\varepsilon)}{\varepsilon}\left(\frac{c_s}{c_f} + \frac{X(-\Delta H)}{c_f(T_2 - T_1)}\right)} \tag{3.12}$$

$$where\ C = C_{A0}\ and\ X = \frac{\rho_B}{M_B}\frac{a}{b}$$

ΔC and ΔX are the concentration differences between the upstream and downstream sides of step. Therefore, for a complete reaction, the wave velocities at a given flow rate u, thus are exclusively determined by the distribution ratios ΔX and ΔC, which are composition-dependent equilibrium properties. The velocities are determined by thermodynamic properties independent of operating conditions. ($v = u/\varepsilon$). By inspection of Fig 3-11, a hot spot will arise when the thermal and the reaction wave approach each other. When $V_R = V_T = V_{T/C}$, the denominator of eq. (3.12) is zero.

3.4.5 Incomplete or Partial Reactions

In a non-isothermal system, a cold dilute fluid injected into a hot bed leads to a partial conversion of solid ($X_{partial}$) wave in the fixed bed. Conversely, a hot concentrated fluid injected into a cold bed leads to a partial concentration ($C_{partial}$) wave. The wave model cannot predict the values of $X_{partial}$ and $C_{partial}$. However, the results show that if the values were known a priori, the wave model can predict the wave velocities accurately, as well as the new temperature rise.

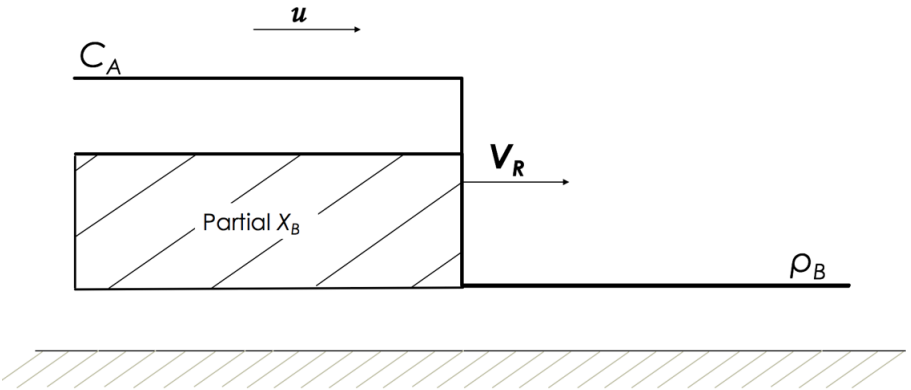

Figure 3-12: Reaction wave showing incomplete solid reaction (dilute fluid case)

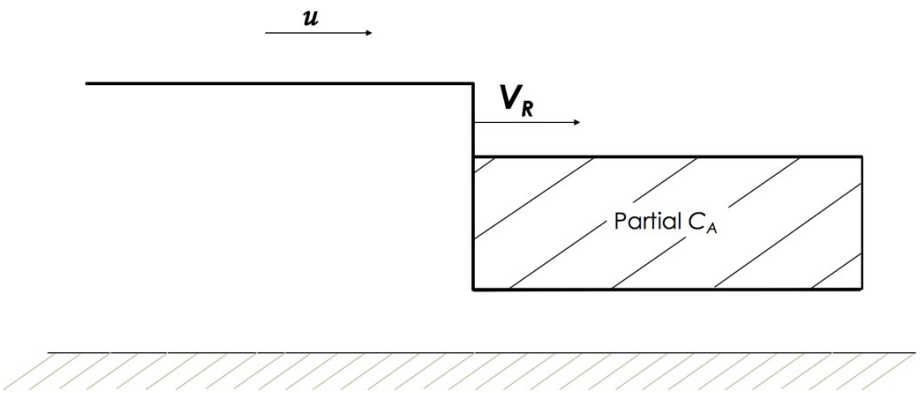

Figure 3-13: Reaction wave showing incomplete fluid reaction (concentrated fluid case)

If there is a fractional amount of either fluid or solid reacting, then then $C_{partial}$ or $X_{partial}$ would replace C_{AO}or $\frac{\rho_B}{M_B}\frac{a}{b}$ respectively in equation (3.10). The velocity of the reaction wave would be given by:

$$V_R{}' = \frac{u/\varepsilon}{1 + \frac{(1-\varepsilon)}{\varepsilon}\frac{X_{partial}\frac{\rho_B}{M_B}\frac{a}{b}}{C_{AO}}} \tag{3.13}$$

In Fig. 3-13, let $C_{partial}$ be the percentage of the reacting fluid, which remains. The velocity of the reaction wave would be given by:

$$V_R{}' = \frac{u/\varepsilon}{1 + \frac{(1-\varepsilon)}{\varepsilon}\frac{\frac{\rho_B}{M_B}\frac{a}{b}}{(C_{AO} - C_{partial})}} \tag{3.14}$$

Thus, when there is a partial solids conversion, $V_R{}'$ is larger than V_R as $X_{partial} < 1$; hence, the reaction wave travels faster when there is a partially converted bed than in a fully converted bed. Similarly, $V_R{}'$ is smaller than V_R if there is a partially reacted fluid ($C_{partial} > 0$). The temperature plateau reached is calculated by equating the reaction wave and thermochemical wave velocities. The temperature rises to the plateau when there is a

partial solid or fluid reaction is given by:

$$\Delta T' = \frac{(-\Delta H)}{\left(\frac{c_{pf}}{C_{AO}} - \frac{c_{ps}}{X_{partial}\frac{M_B}{\rho_B}\frac{b}{a}}\right)} \quad (3.15) \qquad \Delta T' = \frac{(-\Delta H)}{\left(\frac{c_{pf}}{(C_{AO} - C_{partial})} - \frac{c_{ps}}{\frac{M_B}{\rho_B}\frac{b}{a}}\right)} \quad (3.16)$$

In the previous cases, the wave derivations were based on assuming a sharp front separating the reacted bed and unreacted bed (reaction wave) or a sharp front separating the heated and unreacted bed (thermal wave).

If the wave model assumes a sharp transition between the regions previously mentioned, the wave model cannot predict the effect of heat addition. This assumption is relaxed, and a spreading zone is included in the wave model equations (3.10), (3.11), and (3.12).

Newly Developed wave model

The wave model previously discussed in Section 3.4 does not include reaction and heat transfer zones which is useful when heat addition is included in the reacting systems. This gives an accurate predicting the velocities of the reaction, thermal and thermochemical waves as well as the temperature of the plateau.

3.4.6 Thermal Wave Velocity with Heat addition

The sharp front is replaced by a wider heat transfer zone (z_{HTZ}). The heat transfer zone has a finite width. There is a finite amount of heat being transferred to the wave. Assuming there is an amount Q of heat transferred to the wave, per wall area. Q needs to be multiplied by the length of the transfer zone and pi times the diameter of the fixed bed reactor tube. Remember the heat balance below is written per unit cross-sectional area of the bed. Therefore, the amount of heat also needs to be divided by the area of the tube ($\frac{\pi D^2}{4}$). In this Chapter only two cases are analysed. Either the reactor is adiabatic (Q = 0) or the wall temperature is constant. In this last case Q (heat transfer added) is given by:

$$Q = \frac{2}{R_1} h_w (T_w - T_s) \tag{3.17}$$

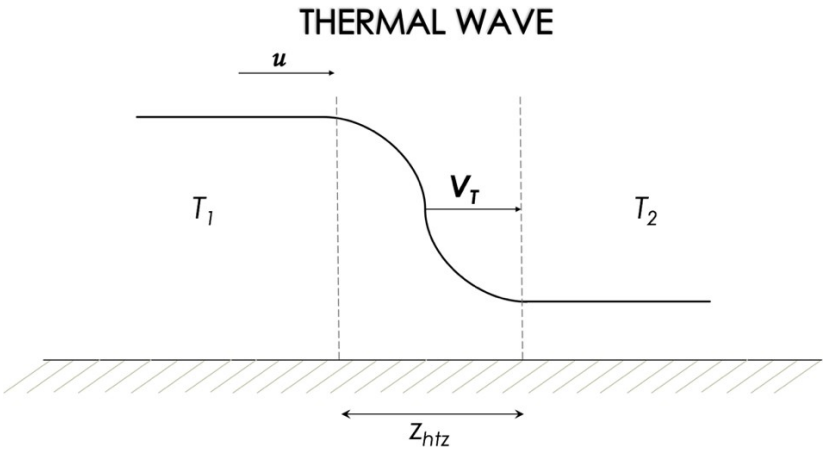

Figure 3-14: Thermal wave velocity with heat addition

Heat balance for the thermal wave is now: Heat in = Heat out

$$\varepsilon \,.\, \left(u - V_T\right) \,.\, c_{pf} \,.\, T_1 - \varepsilon \,.\, \left(u - V_T\right) \,.\, c_{pf} \,.\, T_2 + Q \,.\, z_{HTZ} \,.\, \frac{\pi D}{\frac{\pi D^2}{4}} = (1-\varepsilon) \,.\, V_T \,.\, c_{ps} \,.\, T_1 - (1-\varepsilon) \,.\, V_T \,.\, c_{ps} \,.\, T_2$$

$$V_T\Big(\varepsilon \,.\, c_{pf} \,.\, \left(T_1 - T_2\right) + (1-\varepsilon) \,.\, c_{pf} \,.\, \left(T_1 - T_2\right)\Big) = u \,.\, \varepsilon \,.\, c_{pf} \,.\, \left(T_1 - T_2\right) + Q \,.\, z_{HTZ} \,.\, \frac{2}{R}$$

$$V_T = \frac{u \varepsilon c_{pf}\left(T_1 - T_2\right)}{\varepsilon c_{pf}\left(T_1 - T_2\right) + (1-\varepsilon) c_{ps}\left(T_1 - T_2\right)} + \frac{Q z_{HTZ} \frac{2}{R}}{\varepsilon c_{pf}\left(T_1 - T_2\right) + (1-\varepsilon) c_{ps}\left(T_1 - T_2\right)}$$

$$V_T = \frac{u/\varepsilon}{1 + \frac{(1-\varepsilon)}{\varepsilon} \frac{c_{ps}}{c_{pf}}} + \frac{Q z_{HTZ} \frac{2}{R}}{\varepsilon c_{pf}\left(T_1 - T_2\right)\left\{1 + \frac{(1-\varepsilon)}{\varepsilon} \frac{c_{ps}}{c_{pf}}\right\}} \tag{3.18}$$

In the case of dilute endothermic reactions, the plateau temperature (T_1) is lower than the bed temperature (T_2). Q has to be positive, so in the dilute case, the thermal wave will be retarded by the heat addition. For concentrated cases, the thermal wave is accelerated.

3.4.7 Thermochemical Wave Velocity with Heat addition

For the thermochemical wave, a finite width is expected over which there is a reaction zone

(z_{MTZ}). This wave has a constant fixed pattern. The thermal is an indifferent wave. The thermochemical wave does not spread, and the width is fixed by thermodynamic data and the fluid injection velocity of the fluid (u). The higher the velocity, the more spread out the thermochemical wave is. The equations below show the energy and mass balance across the wave.

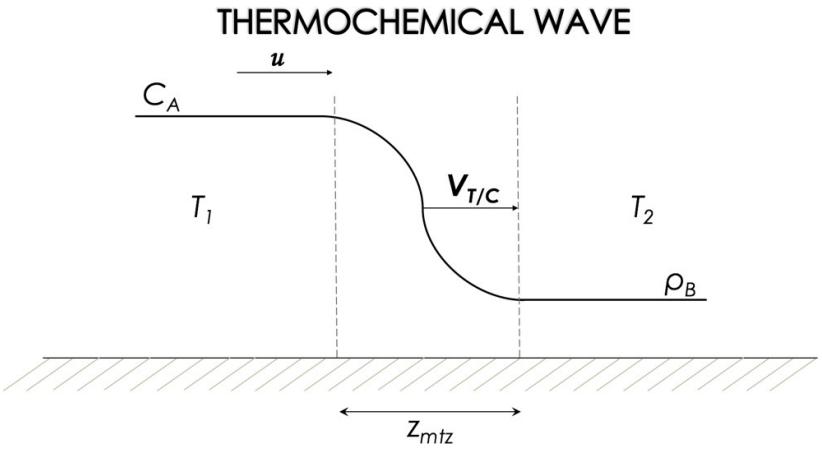

Figure 3-15: Thermochemical wave velocity with heat addition

$$\varepsilon . \left(u - V_{\frac{T}{C}}\right) . c_{pf} . T_1 - \varepsilon . \left(u - V_{\frac{T}{C}}\right) . c_{pf} . T_2 + V_{\frac{T}{C}} . \frac{\rho_B}{M_B} . (1-\varepsilon) . \frac{a}{b} . (\Delta H) + Q . z_{MTZ} . \frac{2}{R} =$$

$$(1-\varepsilon) . V_{\frac{T}{C}} . T_1 . c_{ps} - (1-\varepsilon) . V_{\frac{T}{C}} . T_2 . c_{ps}$$

$$V_{\frac{T}{C}} . \left((1-\varepsilon) . c_{ps} . (T_2 - T_1) + \varepsilon . c_{pf} . (T_2 - T_1) + (1-\varepsilon) . \frac{\rho_B}{M_B} . \frac{a}{b} . (\Delta H)\right) =$$

$$u . \varepsilon . c_{pf} . (T_2 - T_1) - Q z_{MTZ} \frac{2}{R}$$

$$V_{\frac{T}{C}} = \frac{u \varepsilon c_{pf} (T_2 - T_1) - Q z_{MTZ} \frac{2}{R}}{(1-\varepsilon)\left\{ c_{ps} (T_2 - T_1) + \frac{\rho_B}{M_B} \frac{a}{b} (\Delta H) \right\} + \varepsilon c_{pf} (T_2 - T_1)} \qquad (3.19)$$

Heat addition has the opposite effect on the velocity of the thermochemical wave. For the dilute cases, Q increases the velocity of the thermochemical wave. For the concentrated case, the opposite occurs. The modified thermochemical wave velocity, the thermal wave velocity, have been derived. The temperature of the plateau can now also be derived

3.4.8 Temperature of Plateau with Heat addition

The flat region of the temperature profile between the thermal and thermochemical wave is where the heat of reaction accumulates. Unlike in the exothermic case, there is a temperature drop rather than a rise as heat is absorbed in the endothermic reactions.

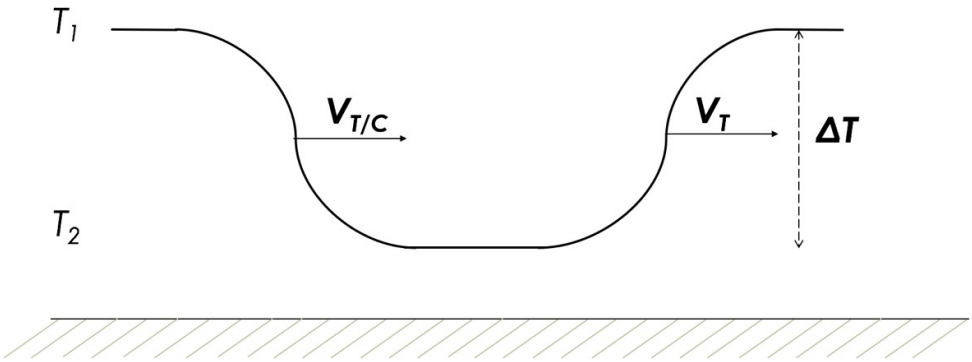

Figure 3-16: Temperature plateau with heat addition

The plateau temperature, T_2 can be written as $(T_1 - \Delta T)$. The equations for ΔT is derived below. At coherence,

$$V_{T/C} = \frac{u\varepsilon c_{pf}(T_2 - T_1) - Qz_{MTZ}\frac{2}{R}}{(1-\varepsilon)\left\{c_{ps}(T_2 - T_1) + \frac{\rho_B}{M_B}\frac{a}{b}(\Delta H)\right\} + \varepsilon c_{pf}(T_2 - T_1)} = V_R$$

$$(T_2 - T_1)\left(u\varepsilon c_{pf} - \varepsilon c_{pf}V_R - (1-\varepsilon)c_{ps}V_R\right) = (1-\varepsilon)\frac{\rho_B}{M_B}\frac{a}{b}(\Delta H)V_R + Qz_{MTZ}\frac{2}{R}$$

$$T_2 - T_1 = \frac{(\Delta H) + Qz_{MTZ}\frac{2}{R}\left(\frac{1}{V_R}\cdot\frac{1}{(1-\varepsilon)}\right)}{c_{ps}\frac{M_B}{\rho_B}\frac{b}{a} - c_{pf}\frac{1}{C_A}}$$

For the dilute case $\Delta T = T_2 - T_1$. For the concentrated case $\Delta T = T_1 - T_2$

$$\Delta T = \frac{(\Delta H) + Qz_{MTZ}\frac{2}{R}\frac{1}{u}\left(\frac{1}{\varepsilon}\frac{1}{C_A} + \frac{1}{(1-\varepsilon)}\frac{M_B b}{\rho_B a}\right)}{c_{pf}\frac{1}{C_A} - c_{ps}\frac{M_B}{\rho_B}\frac{b}{a}} \tag{3.20}$$

The narrower the "accumulation zone" in which the 'colder' heat is stored, the greater is the temperature drop caused. The addition of Q makes the temperature drop smaller. The

full effects of Q will now be explained on the temperature profiles in the dilute case.

3.5 Summary

In this chapter, the basic concepts, terms and descriptive tools used in the present approach to fluid-solid reactive systems have been defined and explained. Although some of the variables and diagrammatic representations are not commonly used to describe reactor dynamics, the concepts are not new but are required to be translated into a form which the reader may get acquainted. Extension to the fundamental wave theory by Hellferich (1986) and Lake (1999) for multicomponent reacting systems were extended to include non-equilibrium effects, heat and reaction zones. Increasing the complexity of the wave model equation but still showing its simplicity. These equations provide a general understanding of reactor behaviour in terms of varying conditions. The equations derived in this chapter are used to predict the velocities of thermal and thermochemical waves, and the plateau temperature in chapters 5 ,6 and 7.

Chapter 4

Physical Model Development & Numerical Analysis

A fixed bed reactor is an assembly of usually uniformly sized catalytic particles, which are randomly arranged and firmly held in position within a vessel or tube. The reactants are supplied to the reactor with the bulk of the fluid flowing through the packed bed. Contacting reactive fluid with the particles in the pores of the catalyst, the reactants undergo chemical transformations, which are usually accompanied with heat release or heat consumption. A physical model is explained based on the shrinking core model originally derived by Yagi and Kunii (1955,1957) and fully developed by Levenspiel (1999). The chapter addresses the rate equations required for the material and energy balances. The Method of Lines was used to solve the PDEs from the balances and extensions to the numerical model was investigated. This numerical model is required to simulate the reaction systems in chapters 5, 6 and 7. Axial mass and thermal dispersion effects on the wave shape and velocity are assessed.

4.1 Shrinking Core Model

The shrinking core model was first developed by Yagi and Kunii (1955,1957), Levenspiel (1999) who visualised the three steps occurring in sequence during reaction.

Step 1: Diffusion of A through the film surrounding the particle to the surface of the solid.

Step 2: Penetration of A through the blanket of ash to the surface of the unreacted core.

Step 3: Reaction of A with solid at this reaction surface.

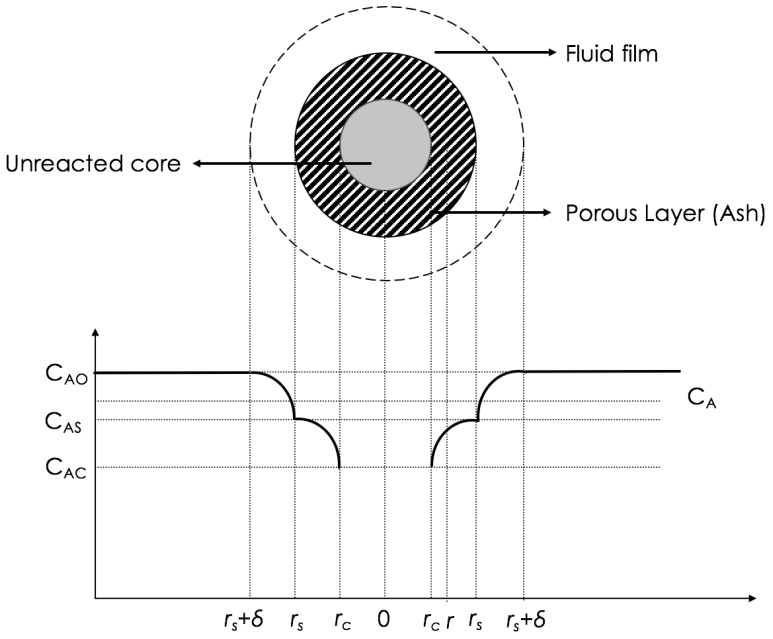

Figure 4-1: Diagram of concentration profile for SCM

Referring to Fig. 4-1, symbols appearing as C_{AO}, C_{AS} and C_{AC} $(kmol/m^3)$ are the concentrations of fluid reactant A in the bulk of the fluid stream, at the surface of the particle and at the surface of the core, respectively. R_s, r_c and r (m) are the radius of the particle, the radius of the unreacted core and the radius at any point from the centre of the particle, respectively. The shrinking core model is an unsteady state problem with moving boundaries (as the core radius is shrinking). A pseudo-steady state is assumed, in which the rates of diffusion through the fluid film and ash layer and the rate of reaction at the core surface are all equal and equal to the overall rate. The pseudo-steady state solution is a good approximation for most fluid-solid reaction systems, except for systems with extremely high pressures and low fluid reactant concentrations. For a single, irreversible fluid-solid reaction, the chemical reaction may be written as:

$$a\ A(fluid) + b\ B(solid) \rightarrow c\ C(product) \tag{4.1}$$

If the rate of reaction per pellet is written as $-r'_A$ $(kmol/s)$ then:

Film:

$$-r'_A = k_T 4\pi R_s^2 \left(C_A - C_{AS}\right) \tag{4.2}$$

Ash Layer:

$$-r'_A = D_e \frac{4\pi}{\frac{1}{r_c} - \frac{1}{R_s}} \left(C_{AS} - C_{AC}\right) \tag{4.3}$$

Core:

$$-r'_A = k 4\pi r_c^2 C_{AC} \tag{4.4}$$

where k_T (*m/s*) is the fluid to solid mass transfer coefficient, D_{EO} (m^2/s) is the effective diffusion coefficient of A in the porous ash, and k (*m/s*) is the first order surface rate constant.

Rearranging (4.3) gives

$$C_{AC} = \frac{-r'_A}{k 4\pi r_c^2} \tag{4.5}$$

Substituting (4.4) into (4.2) gives

$$C_{AS} = -r'_A \left(\frac{\frac{1}{r_c} - \frac{1}{R_s}}{4\pi D_e} + \frac{1}{k 4\pi r_c^2} \right) \tag{4.6}$$

Substituting (4.5) into (4.1) gives

$$C_A = -r'_A \left(\frac{1}{k_T} \frac{1}{4\pi R_s^2} + \frac{1}{D_e} \frac{\frac{1}{r_c} - \frac{1}{R_s}}{4\pi} + \frac{1}{k} \frac{1}{4\pi r_c^2} \right) \tag{4.7}$$

Eq. (4.6) may be written in terms of the core surface as

Therefore,

$$\frac{1}{k'} = \frac{1}{k_T} \left(\frac{r_c}{R_s} \right)^2 + \frac{1}{D_e} \frac{r_c}{R_s} \left(R_s - r_c\right) + \frac{1}{k} \tag{4.8}$$

Where k'(m/s) is the overall rate constant. The ratio of the volume of the core and the initial volume of the core can be written as

$$\left(\frac{r_c}{R_s} \right)^3 = 1 - X_B \tag{4.9}$$

Where X_B is the conversion of solid B. The overall rate constant can now be defined

replacing (4.9) in (4.8) giving:

$$k' = \frac{\left(1 - X_B\right)^{\frac{2}{3}}}{\frac{1}{k_{TO}} e^{\frac{E_R}{RT_f}} + \frac{R_s}{D_{EO}} e^{\frac{E_{de}}{RT_f}} \left(\left(1 - X_B\right)^{-\frac{1}{3}} - 1\right) + \frac{1}{k_O} e^{\frac{E_A}{RT_s}} \left(1 - X_B\right)^{-\frac{2}{3}}} \tag{4.10}$$

where the rate constants are written in Arrhenius form.

The number of moles of B in the core is given by:

$$N_B = \frac{4}{3} \pi {r_c}^3 \frac{\rho_B}{M_B} \tag{4.11}$$

where ρ_B is the concentration of B in the core (equal to the density if the core is pure B) and M_B is the relative molecular mass of B. The stoichiometry of the chemical balance gives:

$$\frac{-r_a'}{a} = \frac{-r_b'}{b} = -\frac{1}{b} \frac{dN_B}{dt} = -\frac{4\pi {r_c}^2 \rho_B}{bM_B} \frac{dr_c}{dt} \tag{4.12}$$

Combining (4.11) and (4.12)

$$\frac{dr_c}{dt} = \frac{-bM_B}{a\rho_B} k' C_A \tag{4.13}$$

The analysis above is needed to find the overall reaction rate, which will be required in the material balance equations (4.21) and (4.22). The assumptions stated above are for a single particle, but for a complete description of a reaction process in a fixed bed reactor, other assumptions need to be made about the flow of the fluid through the reactor.

The number of particles suspended in a unit volume of reactor (n_P) is calculated using a unit volume section of the reactor.

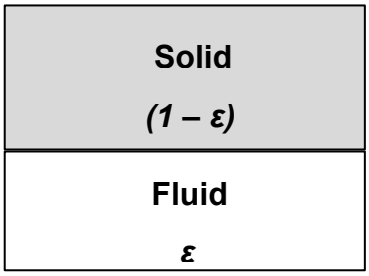

Figure 4-2: Unit volume of reactor

Volume of one solid pellet is

$$V_S = \frac{4}{3}\pi R_s^{\,3} \tag{4.14}$$

Volume of all particles in the unit volume is

$$V_{Total} = n_P \,.\, \frac{4}{3}\pi R_s^{\,3} \tag{4.15}$$

The volume of all the particles in the unit volume of reactor has to equal $(1 - \varepsilon)$, therefore

$$n_P = \frac{3}{4\pi R_s^{\,3}} . (1 - \varepsilon) \tag{4.16}$$

The analysis above is needed to find the overall reaction rate, which is required in the material and energy balance equations. The assumptions stated are for a single particle, other assumptions are made about the flow of reactive fluid through the reactor in the following sections.

4.2 Material and Energy balances

4.2.1 Governing Equations

Systems of coupled, first-order, nonlinear hyperbolic partial differential equations (PDEs) govern the dynamic process in a fixed bed reactor. The governing PDEs are derived from a mass and thermal balance of the fluid and solid reacting. The fluid component material balance for a reacting fluid in plug flow through a fixed bed of reacting solids (Iodarnidis (2002)) is given by:

$$r_a' n_P = \varepsilon \left(\frac{\partial C_A}{\partial t} \right)_z + u \left(\frac{\partial C_A}{\partial z} \right)_t \tag{4.17}$$

Since the solids do not move, but the solid conversion varies along the bed, the solid material balance becomes:

$$r_b' = - \frac{4\pi R_s^{\,3} \rho_B}{3 M_B} \left(\frac{\partial X_B}{\partial t} \right)_z \tag{4.18}$$

The energy balance for a fluid through a fixed bed reactor is given by:

$$A_s \frac{h(T_s - T_f)}{c_f} n_P = \varepsilon \left(\frac{\partial T_f}{\partial t} \right)_z + u \left(\frac{\partial T_f}{\partial z} \right)_t \tag{4.19}$$

When the reaction rate through the solid particle is uniform, we can write the following equation for the temperature of the solid particle in the fixed bed:

$$-\frac{3}{R_s} h\left(T_s - T_f\right) + \frac{r_a' n_P \Delta H}{(1 - \varepsilon)} = c_s \frac{\partial T_s}{\partial t} \tag{4.20}$$

It follows that four differential equations are used:

$$\varepsilon \frac{\partial C_A}{\partial t} + u \frac{\partial C_A}{\partial z} = -4\pi {R_s}^2 k' \left(1 - X_B\right)^{\frac{2}{3}} C_A n_P \tag{4.21}$$

$$\frac{\partial X_B}{\partial t} = k' \left(1 - X_B\right)^{\frac{2}{3}} C_A \frac{3 M_B b}{R_s \rho_B a} \tag{4.22}$$

$$\varepsilon c_f \frac{\partial T_f}{\partial t} + u c_f \frac{\partial T_f}{\partial z} = h\left(T_s - T_f\right) 4\pi {R_s}^2 n_P \tag{4.23}$$

$$c_s \frac{\partial T_s}{\partial t} = -\frac{3}{R_s} \left(h\left(T_s - T_f\right) - k' \left(1 - X_B\right)^{\frac{2}{3}} \Delta H C_A \right) \tag{4.24}$$

These stiff hyperbolic PDEs are solved using the Method of Lines, as explained in Section 4.4. To be able to solve the system of equations (4.21 – 4.24), initial and boundary conditions for the dependent variables are required:

$C_A = C_{AO}$ at $z = 0$ *for* $t > 0$ $X_{BO} = 0$ at $t = 0$ for $z > 0$

$T_s = T_f = T_{inj}$ at $z = 0$ for $t > 0$ $T_s = T_f = T_o$ at $t = 0$ for $z > 0$

The conditions given are for constant injection strategies, but these can also be varied.

4.2.2 Scope and Assumptions

The assumptions stated here are not just for a single reacting particle but for a process in a reactor; assumptions need to be made about the flow of the fluid through the reactor for a

tractable material and energy balance. When fluids pass through the fixed bed solid-fluid reactor, the compositions of each change during fluid passage. The solids do not move, but the solid conversion varies along the bed. The most important assumptions are as follows:

- The reactor is one dimensional in plug flow.
- Heat transfer coefficient, density (no change of pressure with time) and specific heat of the gas and solid reactants remain invariant during the reaction.
- Axial diffusion is neglected.
- Particle-particle heat conduction and heat transfer by radiation are negligible. The latter could be important if the temperature rise of the particles becomes very large.
- The reactant is not accompanied by sintering effects and the porosity of the solid remains unchanged during the reaction.
- The reactor is assumed to have a constant cross-sectional area.

4.3 Extension of Numerical Model

The lack of inclusion of axial dispersion is inadequate for a number of problems and the necessity for a heat flux term is paramount to further research into endothermic reactions. The effects of constant wall temperature and constant wall heat flux is added to both the physical and wave model. Considerable numerical and experimental studies on the effective thermal conductivity in axial and transverse directions in various packed beds are reported in the literature. In the most of these researches, the effective thermal conductivity ratio which is the ratio of the effective thermal conductivity of the porous continuum domain to the fluid thermal conductivity has been determined. Most of the obtained relations depend on two parameters as particle Reynolds and Peclet numbers. Experimental studies of heat flux into packed beds are less reported. A brief background on axial

diffusion and heat flux is now presented.

4.3.1 Dispersive Reaction Fronts

The coefficient D_{ax} for axial dispersion of mass can be calculated for random beds made of identical spherical particles according to the equation (4.25) – (4.27). Effective axial dispersion can be described by the following relating assuming averaged and space independent values of the molecular dispersion of the species present in the gas phase and of the gas velocity:

$$\frac{D_{ax}}{D_m} = \frac{D_{bed}}{D_m} + \frac{Pe_0}{K_{ax}} \tag{4.25}$$

In the equation above, the first term on the RHS accounts for the situation stagnant conditions, which can be obtained from the porosity of the fixed-bed and the molecular diffusion:

$$\frac{D_{bed}}{D_m} = 1 - \sqrt{1-\varepsilon} \tag{4.26}$$

In the second term of equation (4.26), Pe_0 is the mass Peclet number defined by:

$$Pe_0 = \frac{u_0 d_p}{D_m} \tag{4.27}$$

For $Pe_0 \rightarrow 0$, $D_{ax} = D_{bed}$ is obtained, which means that axial dispersion is due to diffusion. The ratio $\frac{D_{bed}}{D_m}$ (D_m: diffusion coefficient in the solids-free fluid phase) depends on porosity and can be calculated according to equation (4.26). On the contrary, when $Pe_0 \rightarrow \infty$. At this limit the bed behaves as a cascade of ideally mixed compartments and axial dispersion is caused by mixing of the fluid in the voids of the packing.

Axial mass dispersion in packed beds is determined by several factors. Under stagnant

conditions the dispersion takes place in the gas phase by molecular diffusion of the individual species. Under flow the molecular dispersion is superimposed by local velocity distribution consisting of eddy dispersion and transversal mixing and flow through bypasses. Moreover, the correlations are actually valid only for the steady state simulations and being applied in within the standard model. For industrial applications, however the axial mass dispersion is often neglected in one dimensional models.

Effective axial diffusivity, D_{ax} is still considered in the material balance:

$$\varepsilon \frac{\partial C_A}{\partial t} + u \frac{\partial C_A}{\partial z} = -4\pi {R_s}^2 k' \left(1 - X_B\right)^{\frac{2}{3}} C_A n_P + D_{ax} \frac{\partial^2 C_A}{\partial z^2} \tag{4.28}$$

See Appendix 2 for effects of mass and thermal dispersion.

4.3.2 Dispersive Thermal Fronts

Additional consideration of the fixed-bed heat conduction, λ, in the energy balances yields a dispersive model for the energy transport:

$$\varepsilon c_f \frac{\partial T_f}{\partial t} + u c_f \frac{\partial T_f}{\partial z} = h\left(T_s - T_f\right) 4\pi {R_s}^2 n_p + \lambda \frac{\partial^2 T_f}{\partial^2 z} \tag{4.29}$$

Such dispersive fronts are characterised by a permanent reduction of the maximum temperature due to the smearing of the temperature profiles, albeit the mean velocity corresponds to that of the thermal front presuming typical values of fixed-bed heat conduction. An analytic solution is available for an open-open system analogous to the axial dispersion model.

For the modelling of the decoking case in an adiabatic technical fixed bed reactor, a so-called one-dimensional pseudo-homogeneous reactor model with axial mixing is developed. Due to the high ratio of the reactor to particle diameter in case of a technical fixed bed (100), radial gradients of the O_2-content and temperature are neglected. Axial dispersion of heat and mass

transfer is considered by the use of an effective dispersion and heat conduction coefficient, $D_{ax,eff}$ and $\lambda_{ax,eff}$. This relaxes assumptions made in our earlier work. The effective dispersion coefficients of heat and mass ($\lambda_{ax,eff}$, $D_{ax,eff}$) in the fixed bed were calculated based on literature correlations (Davis, Mark E., and Robert J. Davis, 2002):

$$D_{ax,eff} = D_{fb} + \frac{u_e d_p}{2} \tag{4.30}$$

$$\lambda_{ax,eff} = \lambda_{fb} + \frac{u_e \rho_g c_{pg} d_p}{2} \tag{4.31}$$

λ_{fb} and D_{fb} represent the minimal values of $\lambda_{ax,eff}$ and $D_{ax,eff}$ without gas flow:

$$D_{fb} = D_{O_2,mol}\left(1 - \sqrt{1-\varepsilon}\right) \tag{4.32}$$

$$\lambda_{fb} = \lambda_G K \tag{4.33}$$

Based on literature correlations (Davis, Mark E., and Robert J. Davis, 2002), the factor K is given here for a void fraction of the fixed bed of 0.4 – 0.6 by

$$K = \frac{11k_P + 4}{2k_P + 13} \tag{4.34}$$

The above equation is only valid for $K < 20$.

For a typical value of the thermal conductivity λ_S of fixed bed reactor of 0.2 W/mK

k_P can be estimated here by:

$$k_P = \frac{\lambda_S}{\lambda_G(500°\mathrm{C})} = \frac{0.2\ (\mathrm{W/mK})}{0.05\ (\mathrm{W/mK})} = 4. \tag{4.35}$$

For the given reaction conditions, the value of K is about 2.3.

4.3.3 Heat Flux

Heat generation and losses are important to analyse because of heat generation in certain

reactions. There are different approaches to model heat flux in packed beds. The chosen method of heating is the uniform inlet temperature approach based on its simplicity. This approach was mostly used in the early studies of heat transfer in porous media. In this method, radially uniform temperature change can be obtained by a heated jacket around the wall of the packed bed. Heat can also be applied using a heated fluid at the inlet.

A pulse heat input variation in time can be achieved with an injected fluid. For a step change, a sudden temperature change is applied at the inlet boundary and then the temperature remains constant. The measurements are made for upstream and downstream temperature change as the difference in the concentration of fluid and conversion of solid waves is negligible (Appendix A.3). Hence only the temperature response to inlet temperature disturbances was investigated.

1) At the inlet boundary, time varying form of the temperature is used, e.g. a temperature pulse with constant amplitude.
2) Initially constant temperature is assumed within the bed.
3) Constant temperature boundary is also used at the outlet.

The heating method uses a set-up of an electrical heater array at the inlet of test section and the temperature of the bed increases at the inlet boundary of the bed. In some cases, the heat step input is provided by pumping unreactive fluid from the inlet and outlet at the different temperatures. The lateral boundary of the bed is insulated. The methods used for the heat addition at the inlet/outlet boundaries are explained below. Simulations were conducted by using radially uniform temperature at the inlet of the packed bed.

Considering the assumptions above and incorporating the heat flux is related to $\dot{q}_v$, the heat flux in a controlled volume as defined by a specific heat transfer area, $a^1{}_v$. The energy balance with the addition of heat flux and axial dispersion is

$$\varepsilon c_f \frac{\partial T_f}{\partial t} + u c_f \frac{\partial T_f}{\partial z} = h(T_s - T_f) 4\pi {R_s}^2 n_p + \lambda_{ax,eff} \frac{\partial^2 T_f}{\partial^2 z} + \dot{q}_v \quad (4.36)$$

where $\dot{q}_v = \dot{q}_A {a^1}_v$

The area can be derived from the control volume:

$$a^1{}_v = \frac{\Delta A}{\Delta V} = \frac{P \Delta z}{A_q \Delta z} = \frac{2\pi R_1}{\pi (R_1)^2} = \frac{2}{R_1} \quad (4.37)$$

Assuming a linear driving force for the heat flux between the solid temperature, T_s and its wall temperature T_w yields the balance:

$$\varepsilon c_f \frac{\partial T_f}{\partial t} + u c_f \frac{\partial T_f}{\partial z} = h\left(T_s - T_f\right) 4\pi {R_s}^2 n_P + \frac{2}{R_1} \overline{h}_w (T_w - T_s) \quad (4.38)$$

4.4 Method of Lines

A popular method for solving evolutionary PDEs is the method of lines, which proceeds in two basic steps (space and time are two independent variables under consideration):

I. Spatial derivatives are first approximated using finite difference methods.

II. The resulting system of semi-discrete (discrete in space and continuous in time) equations is then integrated in time.

In this work, the material and energy balances are solved using the Numerical Method of Lines. Spatial derivatives are evaluated using a 4th order finite difference approximation and then temporal derivatives ($\frac{\partial T_s}{\partial t}$, $\frac{\partial T_f}{\partial t}$, $\frac{\partial X_B}{\partial t}$ and $\frac{\partial C_A}{\partial t}$) are evaluated by from the discretized spatial derivatives using the ode15s solver (Schiesser and Griffiths, 2009).

The success of the MOL is in the availability of efficient time integrators for solving a wide range of mathematical equations, including ordinary differential equations (ODEs). Due to the highly stiff nature of the PDEs here, ode15s is the solver used. Even with the use of this solver, spurious oscillations still arise due to the sharp concentration and temperature fronts,

which are seen in the wave profiles. Approximation techniques ensuring reduced oscillation in the numerical solution, are used to handle problems that develop sharp spatial gradients such as concentration or temperature fronts.

MATLAB is now widely used in academia and industry and provides a very convenient basis for the development of MOL algorithms. Most of the spatial approximation techniques because they are linear operators, can be implemented using the concept of differentiation matrices i.e. spatial derivatives of a dependent variable can easily be obtained through a matrix multiplication.

4.4.1 Overview of Method of Lines

The method of lines involves discretising the spatial domain and thus replacing the PDE with a vector system of ordinary differential equations (ODEs), for which efficient and effective integrating packages have been developed (Schiesser, 1991). This method is used to solve the system of simultaneous Eqs. (4.21 – 4.24).

Consider the length domain (along the reactor length):

$$z_i = z_o + \Delta z \qquad where\ i = 0,1,2\ldots n\,. \tag{4.39}$$

where Δz is fixed, z_o is some arbitrary starting point, i is a counter, and the domain has n + 1 nodes. Also, consider a differentiable function $f(z)$ and note that finite difference approximations to any finite order can be estimated for $f'(z_i)$. The errors in these approximations become smaller as the order of approximation increases. In applying the method of lines, the fourth order formulae to approximate the first $f'(z_i)$ can be used, and these formulae are represented in the matrix (Schiesser, 1991) below:

$$M = \frac{1}{24\,\Delta z}\begin{bmatrix} -50 & 96 & -72 & 32 & -6 \\ -6 & -20 & 36 & -12 & 2 \\ 2 & -16 & 0 & 16 & -2 \\ -2 & 12 & -36 & 20 & 6 \\ 6 & -32 & 72 & -96 & 50 \end{bmatrix} \tag{4.40}$$

The middle row of M represents the fourth-order central, or symmetric, finite-difference representation of $f'(z)$ while the first and second rows of M represent backward-difference representations. The fourth and fifth rows represent the corresponding forward-difference representations. The rows of M are used to obtain derivative representations of $f'(z)$ on the domain. The fourth order central-difference representation of $\frac{df'(z_i)}{dz}$, is given by.

$$\frac{df(z_i)}{dz} = \frac{1}{24\,\Delta z}[-6 \quad -20 \quad 36 \quad -12 \quad 2] \bigotimes \begin{bmatrix} f_{i-2} \\ f_{i-1} \\ f_i \\ f_{i+1} \\ f_{i+2} \end{bmatrix} \tag{4.41}$$

where $\otimes$ is the mathematical dot or scalar product and uses the third row of M. The first upwind finite-difference representation involves the second row of M, and

$$\frac{df(z_i)}{dz} = \frac{1}{24\,\Delta z}[-6 \quad -20 \quad 36 \quad -12 \quad 2] \bigotimes \begin{bmatrix} f_{i-3} \\ f_{i-2} \\ f_{i-1} \\ f_i \\ f_{i+1} \end{bmatrix} \tag{4.42}$$

Notice the displacement of the counter i on the vector of $f(z)$ values being used. Finite-difference representations of f' to any order can be written in similar form (Wilson and Turcotte, 2002). Consider Eq. (4.40) on the domain and define $\mathbf{C_A}$ as the vector of values of $C_A\,(z, t)$ at the nodal points. Then the derivatives $\frac{\partial C_A}{\partial z}$ at the nodes can be calculated using the derivative representations in Eq. (4.41). The concentration terms are discretised using central-difference representations or the middle row in the matrix M (van de Wouwer et al., 2001). The forward or backward representations are used near the ends of the lattice so as to avoid the use of bogus points (Schiesser, 1991). The same method is used to discretize T_f

and T_s in the spatial domain. The same method can be used for fourth order spatial differentiation; the method is not discussed here for the sake of conciseness but is illustrated in Schiesser, 1991.

MOL has two major steps.

At 1st step, the spatial derivatives of equation are approximated by finite difference.

At 2nd step, the resulting system of ordinary differential equations is integrated in time.

1st order spatial derivatives are approximated by upwind scheme and 2nd order derivatives are approximated by 2nd order central difference scheme.

$$\frac{\partial C_A}{\partial z} = \frac{C_i - C_{i-1}}{2h} + O(h^2) \tag{4.43}$$

$$\frac{\partial^2 C_A}{\partial z^2} = \frac{-C_{i+2} + 8C_i - 8C_{i-1} + C_{i-2}}{2h} + O(h^6) \tag{4.44}$$

$$\frac{\partial T_f}{\partial z} = \frac{T_i - T_{i-1}}{2h} + O(h^2) \tag{4.45}$$

$$\frac{\partial^2 T_s}{\partial z^2} = \frac{-T_{i+2} + 8T_i - 8T_{i-1} + T_{i-2}}{2h} + O(h^6) \tag{4.46}$$

We use subscript i for z. Δz is the spatial length scale. $h = \Delta z$ denotes constant spatial length scale. $z_i = z_L + i\,\Delta\,\mathrm{z}$, i = 0, 1, 2...N, where z_i is the left boundary. $z_R = z_N$ is the right boundary. $cell_\mathrm{i} = [z_{i-1}, z_i]$.

The finite difference approximations are substituted in Eqs. (4.43 – 4.46) yielding 4 x n coupled ordinary differential equations, which may then be integrated simultaneously.

4.4.2 The Template of Information Flow

The functionality and matrix-based capabilities of MATLAB are exploited to solve Eqs. (4.21 – 4.24). The conceptual steps are in green as shown Fig. 4-3, the blue boxes show the corresponding subroutine structure and pathways of information for the MATLAB code implementation. The conceptual steps of initialising parameters, setting up the initial profile and the output steps are common features of any numerical solution.

The initialisation step defines the necessary parameters for the computational model. For example, the 'Initialise' routine will define the physical parameters as in Table 1. Also, the routine will initialise geometric parameters i.e. the total length in the *z*-direction and the number of nodes over this length. The 'Domain' routine generates the spatial domain, the indexing of these nodes and the housekeeping vectors, which identify the nodes associated with the boundaries of the physical domain. The 'Initial' routine sets up the initial values of C_A, T_s, X_B, T_f on the domain. Note that the matrix-based structure of MATLAB enables mathematical formulae to be expressed directly into the code (Leea, 2003).

The 'FODM' (fourth-order differentiation matrix) routine receives information on the structure and indexing of the grid, including the location of boundaries, to generate the matrix M for C_A, T_s, and T_f. The differential matrices are then passed to the RHS routine, which generates the right-hand side of Eqs. (4.22 – 4.25) (the LHS contains only derivatives in time). Values of $\mathbf{C_A}$, $\mathbf{T_f}$, $\mathbf{X_B}$, $\mathbf{T_s}$ are passed from the 'ODE15s' routine to the 'RHS' routine to calculate the right-hand side of PDEs to give an approximation for $\frac{\partial \boldsymbol{T_s}}{\partial t}$, $\frac{\partial \boldsymbol{T_f}}{\partial t}$, $\frac{\partial \boldsymbol{X_B}}{\partial t}$ and $\frac{\partial \boldsymbol{C_A}}{\partial t}$. The $\frac{\partial \boldsymbol{C_A}}{\partial t}$ vector is then returned to the ODE solver calculating $\mathbf{C_A}$ at the next time step. The routine is repeated for $\mathbf{T_f}$ and $\mathbf{T_s}$ (X_B does not vary in the z direction). In general, 'ODE15s' from the MATLAB library is used as a variable order ODE solver in the template, which is used to solve highly stiff equations.

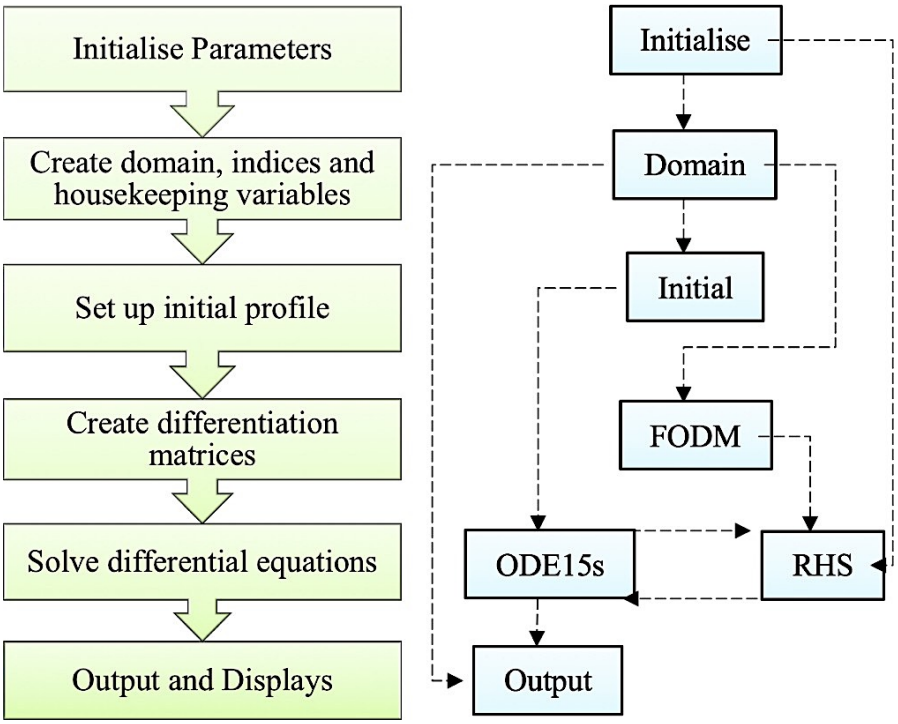

Figure 4-3: The template (green) and corresponding MATLAB functions (blue) showing information flows

4.4.3 Flux Limiter

A problem addressed in this chapter is the stiffness of the source terms. The stiffness of chemical systems is caused by extreme differences in time scales of different reactions. To be capable of dealing with stiff differential equation systems, a numerical method must incorporate an automatic control of the integration step size. Step size adjustment not only optimizes the integration step sizes, but also guaranties a certain predetermined accuracy of the solution. One way of handling the stiffness of PDEs is the use of flux limiters. Flux limiters are used in high resolution schemes to avoid undesirable oscillations in the solution profiles of a system of PDEs particularly stiff hyperbolic equations with sharp fronts in the solution. It is generally necessary to resort to flux limiters to avoid numerical diffusion of solutions. Numerical diffusion is not substantially reduced by reducing spatial and time steps, therefore, schemes such as flux limiters and upwind finite differences are sought to reduce the oscillations but not necessarily eliminate them.

The main idea behind flux limiter schemes is to limit the spatial derivatives to realistic

values. Consider the 1D semi-discrete scheme below,

$$\frac{df_i}{dt} = \frac{1}{\Delta z_i}\left[f\left(z_{i+\frac{1}{2}}\right) - f\left(z_{i-\frac{1}{2}}\right)\right] \qquad where\ i = 0,1,2,\ldots n\,. \tag{4.47}$$

where, $f\left(z_{i+\frac{1}{2}}\right)$ and $f\left(z_{i-\frac{1}{2}}\right)$ represent boundary fluxes for the ith cell. If these boundary fluxes can be represented by low and high-resolution schemes, then a flux limiter can switch between these schemes depending upon the gradients close to the particular cell (Wesseling, 2001), as follow,

$$f\left(z_{i+\frac{1}{2}}\right) = f_{i+\frac{1}{2}}{}^{low} - \phi(r_i)(f_{i+\frac{1}{2}}{}^{low} - f_{i+\frac{1}{2}}{}^{high}) \tag{4.48}$$

$$f\left(z_{i-\frac{1}{2}}\right) = f_{i-\frac{1}{2}}{}^{low} - \phi(r_{i-1})(f_{i+\frac{1}{2}}{}^{low} - f_{i+\frac{1}{2}}{}^{high}) \tag{4.49}$$

where f^{low} = low-resolution flux, f^{high}= high-resolution flux, $\phi(r)$ = flux limiter function, and r represents the ratio of successive gradients on the solution grid,

$$r_i = \frac{z_i - z_{i-1}}{z_{i+1} - z_i} \tag{4.50}$$

The flux limiter function is constrained to be greater than or equal to zero. Therefore, when the limiter is equal to zero (sharp gradient or zero gradient), the flux is represented by a low-resolution scheme. Similarly, when the limiter is equal to 1 (smooth solution), it is represented by a high-resolution scheme (Wesseling, 2001).

The limiter used in this study is the van leer flux limiter which has a flux limiter function, as below,

$$\phi_{vl}(r) = \frac{r + |r|}{1 + |r|}; \qquad \lim_{r\to\infty} \phi_{vl}(r) = 2 \tag{4.51}$$

All the necessary algorithms needed to perform the numerical solution of the material and energy balances have been defined. It should be noted flux limiters do not eliminate

oscillations around the true value but instead reduce these oscillations to a minimum. The enhanced van Leer limiter function and the van Albada limiter was compared in the Appendix. The results that the van Leer limiter satisfies sufficient conditions for a limiter function to lead to a formally second-order accurate, TVD (Total Variation Diminishing) stable, and symmetry-preserving results. Their numerical performances are assessed by solving the highly stiff system of simultaneous PDE.

4.5 Evaluation of Numerical Model and Induced Dispersion

4.5.1 Convergence

This problem can be considered dominant convection. These kinds of problems are very unstable and it is not able to overcome by usual finite difference method. The typical finite difference method to solve dominant convection problem is upwind method. This method overcomes instability using forward or backward difference against convection speed u. We have to consider of Courant–Friedrichs–Lewy (CFL) condition.

$$\left| u \frac{\Delta t}{\Delta z} \right| < 1 \tag{4.52}$$

When CFL condition is satisfied, approximating of solution of evolution equation is stable and convergence. To solve this ODE system by ode15s, we use a time step that satisfied CFL condition.

4.5.2 Numerical Dispersion

It is important to briefly discuss numerical dispersion. It needs to be clear the differences in results due to a change in any of the mentioned parameters is not due to numerical dispersion in the chosen method of solving the numerical model. The packed bed model is based on approximating spatial gradients by finite differences. In order to quantify the difference

between numerical dispersion and axial dispersion. It is important to approximate the order of numerical error. At first, the energy balance mentioned above is evaluated. Errors induced by the transport terms are of interest. It is noteworthy to mention that boundary conditions can have a large influence on the solution of dispersive models, particularly when dispersion becomes dominating. The analysis is performed for the balance using simple up-wind approximation for the first order spatial gradients and central scheme for the dispersive transport. First, the spatial domain is discretized in N_p nodes with finite increments $\Delta z = \frac{L}{Np-1}$ to solve:

$$\varepsilon c_f \frac{\partial T_f}{\partial t} + u c_f \frac{\partial T_f}{\partial z} = h\left(T_s - T_f\right) 4\pi {R_s}^2 n_P + \lambda \frac{\partial^2 T_s}{\partial z^2} \tag{4.53}$$

assuming the temperatures of the solid and fluid are the same. This assumption is valid as clearly seen in results shown after a very short period of time.

$$\varepsilon c_f \frac{\partial T}{\partial t} \approx - u c_f \frac{T_n - T_{n-1}}{\Delta z} + \lambda \frac{T_{n+1} - 2T_n + T_{n-1}}{\Delta z^2} \tag{4.54}$$

If we define a numerical or grid Peclet number Pe_n as:

$$Pe_n = \frac{u c_f \Delta z}{\lambda} \tag{4.55}$$

and expansion of the equation (4.55) with yields a differential equation, in which the left-hand side is abbreviated by f_D in the equation below:

$$f_D = - Pe_n \Delta z \frac{\partial T}{\partial z} + \Delta z^2 \frac{\partial^2 T_s}{\partial z^2} \tag{4.56}$$

And from the difference equation (4.56) above, one obtains the difference equation of the numerical scheme, abbreviated by f_n:

$$f_n = T_{n+1} + \left(-2 - Pe_n\right) T_n + \left(Pe_n + 1\right) T_{n-1} \tag{4.57}$$

In the next step, the temperatures of the grid, T_{n+1} and T_{n-1}, are replaced by the corresponding Taylor series defined as:

$$T_{n+1} \approx T_n + \left.\frac{\partial T}{\partial z}\right|_n \frac{\Delta z}{1!} + \left.\frac{\partial^2 T}{\partial z^2}\right|_n \frac{\Delta z^2}{2!} + \left.\frac{\partial^3 T}{\partial z^3}\right|_n \frac{\Delta z^3}{3!} + \cdots + O(\Delta z^4) \quad (4.58)$$

$$T_{n-1} \approx T_n - \left.\frac{\partial T}{\partial z}\right|_n \frac{\Delta z}{1!} + \left.\frac{\partial^2 T}{\partial z^2}\right|_n \frac{\Delta z^2}{2!} - \left.\frac{\partial^3 T}{\partial z^3}\right|_n \frac{\Delta z^3}{3!} + \cdots + O(\Delta z^4) \quad (4.59)$$

Below is a simplified notation is used, in which ∇ represents the first order derivative in the space, and ∇^n for the n-th order derivatives with respect to the spatial coordinate. Replacing in the difference formula the variables T_{n+1} and T_{n-1} by the corresponding Taylor series yields the following expression:

$$f_n = -Pe_n \nabla T \Delta z + (2 + Pe_n) \nabla^2 T \frac{\Delta z^2}{2} - Pe_n \nabla^3 T \frac{\Delta z^3}{6} + (2 + Pe_n) \nabla^4 T \frac{\Delta z^4}{24} + \ldots + O(\Delta z^5) \quad (4.60)$$

The higher order terms ($O(\Delta z^5)$) have been ignored. Subtraction of the original differential equation from the expanded difference equation leads to the following expression, in which the first order derivative has dropped out.

$$f_n - f_D = \frac{Pe_n \Delta z^2}{2} \nabla^2 T - Pe_n \frac{\Delta z^3}{6} \nabla^3 T + (2 + Pe_n) \frac{\Delta z^4}{24} \nabla^4 T + \ldots + O(\Delta z^5) \quad (4.61)$$

The truncation error of up-winding combined with central difference scheme is proportional to Δz in the first instance, while higher order terms are of order 2 ($O(\Delta z^2)$), or in short:

$$\Theta_n = u c_f \frac{\Delta z}{2} \nabla^2 T + \ldots + O(\Delta z^2) \quad (4.62)$$

The numerical error can be implemented in the original differential equation to obtain

$$\varepsilon c_f \frac{\partial T_f}{\partial t} + u c_f \frac{\partial T_f}{\partial z} = h\left(T_s - T_f\right) 4\pi R_s^2 n_P + \left(\lambda + \frac{u c_f \Delta z}{2}\right) \frac{\partial^2 T_s}{\partial z^2} + \ldots + O(\Delta z^2) \quad (4.63)$$

4.5.3 Effect of Heat Conduction

This analysis reveals that the simulated heat conduction, λ_{sim}, is proportional to the space increment Δz and the physical convection of the gas phase with the velocity u. The simulated heat conduction can be expressed in the following way:

$$\lambda_{sim} = \lambda + u c_f \frac{\Delta z}{2} = \lambda + u c_f \frac{L_R}{2\left(N_p - 1\right)} \tag{4.64}$$

Thereby a fraction of 'numerical' heat conduction defined by can be considered.

With the Peclet number for heat transport defined as:

$$Pe_h = \frac{u \rho c_f L_R}{\lambda} \tag{4.65}$$

a relation between numerical Peclet number and physical Peclet number can be specified according to:

$$Pe_h = \left(N_p - 1\right) Pe_n = \frac{L_R}{\Delta z} Pe_n \tag{4.66}$$

It is further instructive to relate the simulated heat conduction to the real physical heat conduction λ,

$$\frac{\lambda_{sim}}{\lambda} = 1 + \frac{Pe_n}{2} = 1 + \frac{Pe_h}{2\left(N_p - 1\right)} = 1 + \frac{Pe_h}{2} \frac{\Delta z}{L_R} \tag{4.67}$$

Physical and simulated heat conduction are identical if Δz tends to zero. And, what is more important, for a rather convective transport (large Pe_n), it becomes increasingly difficult to represent realistic heat conduction with the uniform scheme used. For that reason, it is known that convective dominated systems can only be well approximated with very small Δz.

Below the Peclet number Pe_n of 2, it is possible to exactly simulate any physical dispersion

$$\frac{\lambda^*}{\lambda} = \frac{Pe_n}{2} \qquad or \qquad \frac{\lambda_{mod}}{\lambda} = 1 - \frac{Pe_n}{2} \tag{4.68}$$

Thereby the physical dispersion λ needs a correction by a portion λ^* yielding a modified

value λ_{sim} to be implemented in the model. It holds for the correction $\lambda_{sim} - \lambda^* = \lambda$ and for the modified value $\lambda_{mod} = \lambda - \lambda^*$:

As long as $Pe_n < 2$ is ensured. The main results of this approach are:

- The suggested scheme is first order accurate and the numerical dispersion is proportional to the grid Peclet number Pe_n.
- There exists a critical Peclet number $Pe_n = 2$, above which the simulated dispersion is always composed of physical and numerical dispersion.
- Below $Pe_n = 2$ it is possible to accurately simulate the physical dispersion.

  Note: $\lambda_{sim} = \lambda + \lambda_n = 2\lambda$ thus $2 = 1 + 1/2Pe_n$ yielding $4 = 2 + Pe_n$, which is $Pe_n = 2$.

In summary, with our chosen very small Δz and the inclusion of a flux limiter. The numerical dispersion is kept to a minimum and the results discussed in the sections to follow will have the axial diffusions as the only visible change in the wave shape and position.

4.6 Constant Pattern Solution

The description of the constant pattern solution presumes a reaction front propagating with a constant velocity V_R on an infinitely large spatial domain. To formulate the equations to calculate the width of the reaction profile, we must first define mathematically a substantial derivative. A substantial derivative is a derivative taken with respect to a moving coordinate system. Imagine a point on top of the reaction wave. Let us call the velocity that the point is moving along the fixed bed is V_i. That is the reaction wave velocity, and that means the point is moving at the same speed as the wave.

$$\frac{\partial C_A}{\partial t} = - V_i \frac{\partial C_A}{\partial z} \tag{4.69}$$

$$\frac{\partial X_B}{\partial t} = - V_i \frac{\partial X_B}{\partial z} \tag{4.70}$$

Recall, the partial differential equations for the material balance:

$$\varepsilon \frac{\partial C_A}{\partial t} + u \frac{\partial C_A}{\partial z} = - 4\pi {R_s}^2 k' \left(1 - X_B\right)^{\frac{2}{3}} C_A n_P \tag{4.71}$$

$$\frac{\partial X_B}{\partial t} = k' \left(1 - X_B\right)^{\frac{2}{3}} C_A \frac{3 M_B b}{R_s \rho_B a} \tag{4.72}$$

Substituting equation (4.70) in (4.72) and (4.71) in (4.73) gives (4.75) and (4.76).

$$\varepsilon c_f \frac{\partial T_f}{\partial t} + u c_f \frac{\partial T_f}{\partial z} = h\left(T_s - T_f\right) 4\pi {R_s}^2 n_P \tag{4.73}$$

$$c_s \frac{\partial T_s}{\partial t} = - \frac{3}{R_s} h\left(T_s - T_f\right) - \frac{3}{R_s} k' \left(1 - X_B\right)^{\frac{2}{3}} \Delta H C_A \tag{4.74}$$

For an observer watching the point on the wave, the wave itself is not changing its shape in time. If the point on the wave is moving at the same speed as the wave, there will be no time derivative term. Therefore, for a constant pattern, it is assumed that all the time-dependent terms are zero. By transformation into a moving coordinate system, the system of partial differential equations is reduced to a system of ordinary equations. In other words,

$$\therefore \quad \left(\frac{u}{\varepsilon} - V_R\right) \frac{dC_A}{dz} = \frac{-4\pi {R_s}^2 k' \left(1 - X_B\right)^{\frac{2}{3}} C_A n_P}{\varepsilon} \tag{4.75}$$

$$- V_i \frac{dX_B}{dz} = k' \left(1 - X_B\right)^{\frac{2}{3}} C_A \frac{3 M_B b}{R_s \rho_B a} \tag{4.76}$$

Similarly, for a thermal balance across the wave,

$$\varepsilon c_f \frac{\partial T_f}{\partial t} + u c_f \frac{\partial T_f}{\partial z} = h\left(T_s - T_f\right) 4\pi {R_s}^2 n_P \tag{4.77}$$

$$c_s \frac{\partial T_s}{\partial t} = - \frac{3}{R_s} h\left(T_s - T_f\right) - \frac{3}{R_s} k' \left(1 - X_B\right)^{\frac{2}{3}} \Delta H C_A \tag{4.78}$$

At constant pattern:

$$\frac{\partial T_f}{\partial t} = - V_i \frac{\partial T_f}{\partial z} \tag{4.79}$$

$$\frac{\partial T_s}{\partial t} = - V_i \frac{\partial T_s}{\partial z} \tag{4.80}$$

$$\therefore \quad \left(\frac{u}{\varepsilon} - V_R \right) \frac{dT_f}{dz} = \frac{h\left(T_s - T_f \right) 4\pi R_s{}^2 n_P}{\varepsilon c_f} \tag{4.81}$$

$$V_i \frac{dT_s}{dz} = \frac{\frac{3}{R_s} h\left(T_s - T_f \right) + \frac{3}{R_s} k' \left(1 - X_B \right)^{\frac{2}{3}} \Delta H C_A}{c_s} \tag{4.82}$$

The boundary conditions are $C_A = C_{AO}$ at $z = 0$ *for* $t > 0$, $X_B = 0$ at $t = 0$ for $z > 0$

The initial conditions are $T_s = T_{so}$, $T_f = T_{fo}$ at $z = 0$ for $t > 0$, $T_s = T_{so}$, $T_f = T_{fo}$ at $t = 0$ for $z > 0$

V_R is treated as a variable and therefore implemented in the equation system using an additional equation, C_A (z = 0) = 0.5C_{AO}, fixing the front in the origin. Additionally, a large but finite spatial domain must be provided to find a numerical solution. After discretization of the spatial coordinate, the large nonlinear system of equations can be solved with Newton- type solvers.

There is a large sensitivity towards the initial values. The approach taken was to generate initial values based on the solution of the corresponding dynamic problem. Then, by starting from a single constant pattern solution it is straight forward to study ranges of parameters of interest, though existence of the constant pattern is not guaranteed for all parameter sets. The representation of the front properties is also restricted to isolated fronts without interaction with boundaries. Solution of the time-dependent full set of PDEs and inspection of the fronts provides proof of a constant pattern.

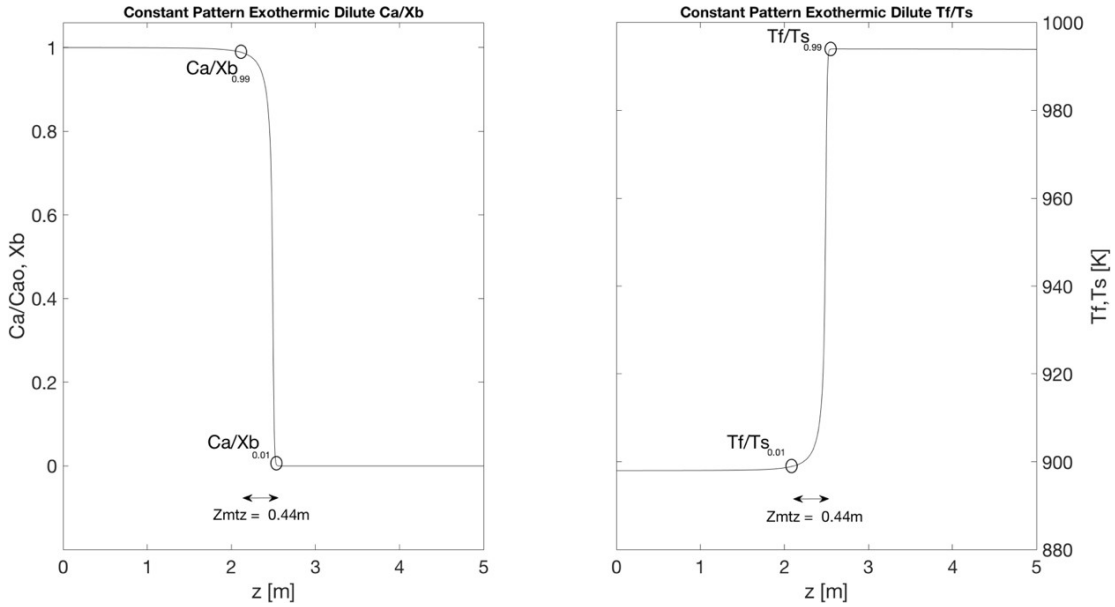

Figure 4-4: Constant pattern solution of dilute decoking system

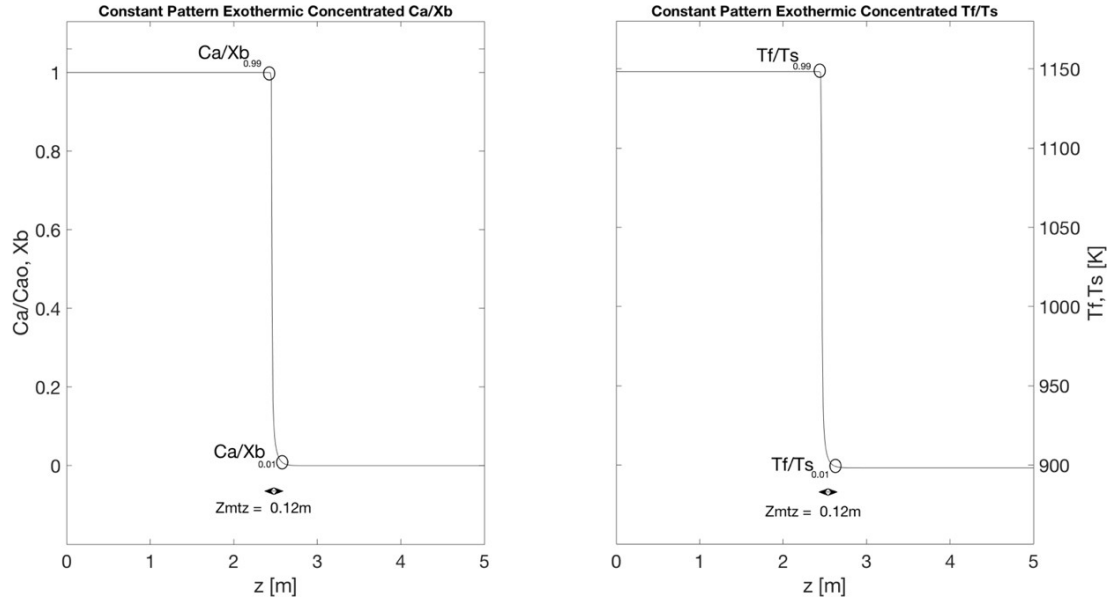

Figure 4-5: Constant pattern solution of concentrated decoking system

The analysis of the constant pattern solution has shown a self-sharpening character of the reaction fronts. In a dilute system, the thermal wave travels ahead of the thermochemical wave. Therefore, the temperature rise is from the initial fluid temperature to the plateau temperature as shown in Fig. 4-4. In a concentrated system, the thermal wave lags behind thermochemical wave. The thermochemical wave has a temperature drop from the plateau temperature to the bed temperature. The reaction zone width is defined as the reactor bed length from the location where 99% of the solid material has reacted to that where just the

first percent of the solid has reacted. Fig.4-4 shows the reaction zone width is larger in a dilute system as the temperature reached is moderate. In a concentrated system, the temperature of the plateau is higher, which gives a smaller reaction width as shown in Fig. 4-5. This means the concentrated case is closer to equilibrium than the dilute case.

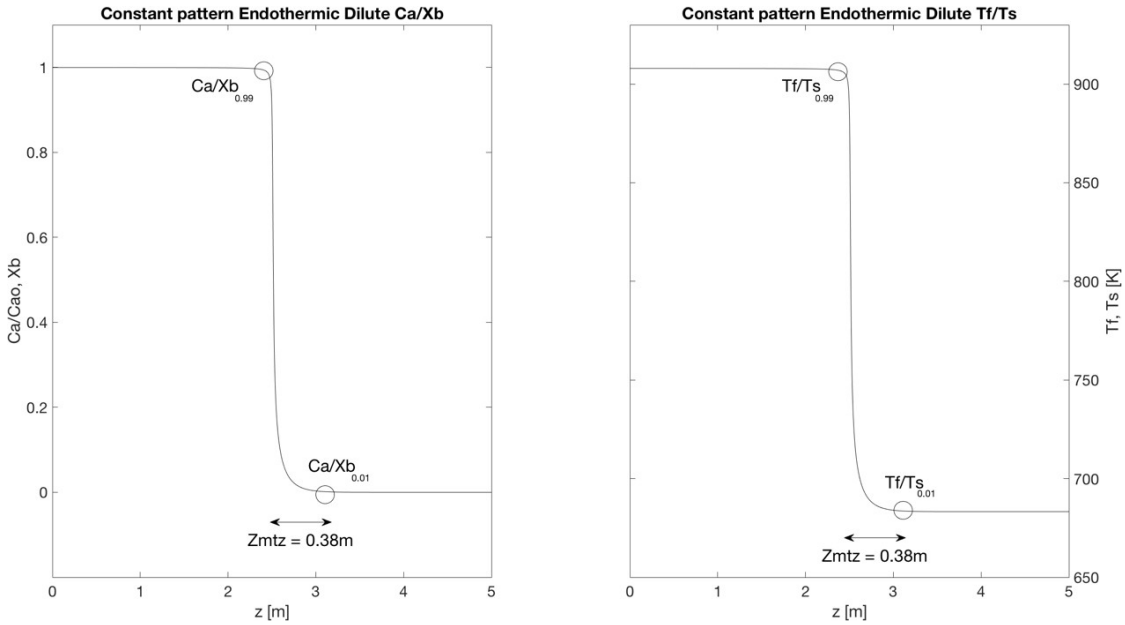

Figure 4-6: Constant pattern solution of dilute pyrite system

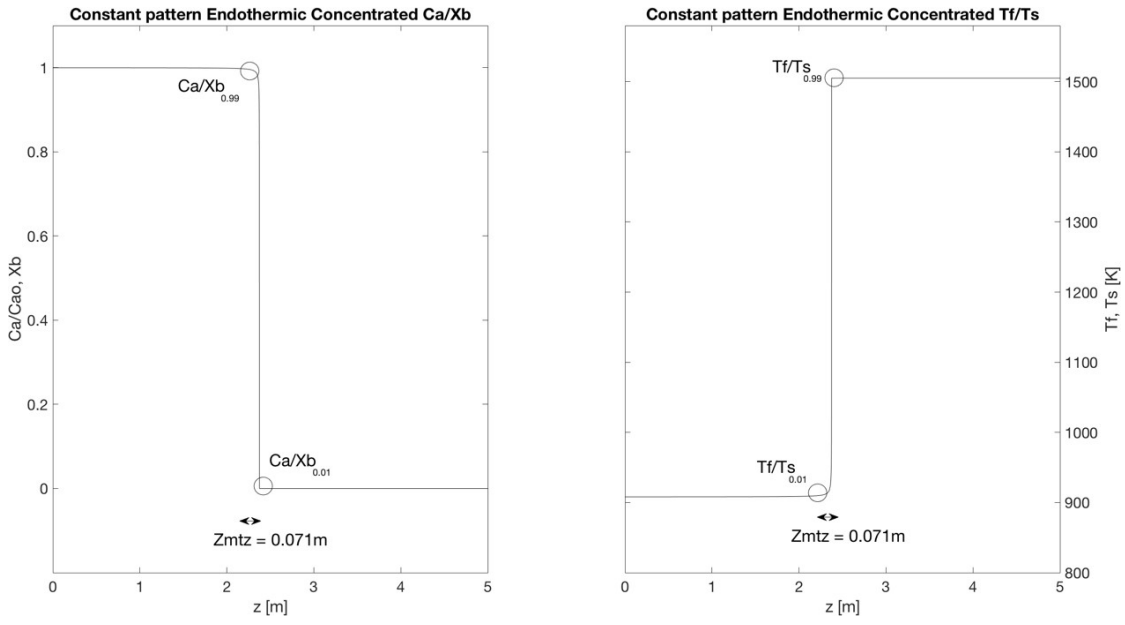

Figure 4-7: Constant pattern solution of concentrated pyrite system

In general, thermochemical waves are non-coherent unless dispersive effects of non-equilibrium and axial diffusion have become negligible but, in this research, it is shown that the general assumption is not strictly true. Until a constant pattern is reached. In self-

sharpening thermochemical waves, the extent of deviations from local equilibrium depends on reaction rates and mass transfer. The wave sharpens or spreads until the constant pattern is attained. Axial diffusion impairs coherence through its effect on the concentration velocities.

4.7 Summary and Limitations

A complete description of the shrinking core model developed by Levenspiel (1999) was provided and forms the basis of the rate expressions to be used in the material and energy balance of the physical model of the fluid-solid reacting system. The material and energy balances are solved by a well-developed numerical method of lines. The results from the solution of these material and energy balances form the basis of comparison with the wave model. The concept of a constant pattern solution was presented. This resulted in an estimation of the width of the heat and reaction zones for the endothermic and exothermic systems considered. A constant mass and heat transfer zone matching the constant pattern is a proof of coherence. Evaluation of numerical dispersion in the MOL was also discussed and the implementation of van leer flux limiter.

The assumptions made for the shrinking core model can lead to some limitations of applicability of the model, which must be carefully considered before using it. In particular, the following issues must be pointed out:

- The reaction located on a surface is the most important assumption of the model. This is not always physically correct. In particular, if the particle is initially porous, it doesn't behave like a shrinking core, unless the controlling regime is diffusion. If the reaction is very fast if compared to diffusion, the gas diffuses in region where the solid reactant has already been consumed.
- On the contrary, if kinetic is controlling over intra particle diffusion, a porous particle will react homogeneously, because the gas composition is always radially

uniform. Therefore, the shrinking core model is applicable in the case of kinetic regime only if the particle is initially not porous.

- ➢ Thermal homogeneity of the particle must be evaluated. This is usually a correct assumption for small particles, but this is also related to the value of heat of reaction.

MOL solutions on the thermal response of the bed were discussed by Amiri et al. (1995). Jiang et al. (1996) used constant wall heat flux boundary conditions to investigate the effects of the local thermal non-equilibrium, the thermal conductivity of the solid particles and the particle diameter on the convection heat transfer.

Other design models have been used to describe fluid-solid reactions. Amiri et al. (1995) and Jiang et al. (1996, 1999a) found that the numerical results from a convection-diffusion problem assuming that the heat flux transferred by solid particles was equal to that transferred by the fluid on the wall for the constant wall heat flux boundary conditions agreed well with experimental data. The numerical results agree well with the experimental data for the longitudinal dispersion coefficients in packed beds. The results showed that the longitudinal dispersion is higher than the transverse dispersion. Similar models for transverse thermal dispersion were presented in Iordanidi (2002) and Koning et al. (2006). The coefficients presented in these models, however, vary by as much as thirty folds. The convection heat transfer coefficients in porous media predicted using the thermal non-equilibrium model with the ideal constant wall heat flux boundary condition presented by From the micropoint of view, the fluid velocity in the voids between the particles of porous media is not uniform and a discontinuity exists in the velocity and temperature fields because of solid particles. Although microscopic analysis of heat and mass flow has been reported in the literature, most of the researchers prefer to employ macroscopic approach.

Chapter 5

Exothermic Fluid-Solid Reactions

The exothermic fluid-solid reaction to be discussed in this chapter is the decoking of fixed bed reactors. Wave model predictions based on the equations derived in chapter 3 are compared with the numerical simulation of the physical model in chapter 4. The results show the wave model is in good agreement with the numerical simulations. The thermochemical wave shows self-sharpening behaviour reaching a fixed shape, the width of which is accurately predicted in Chapter 4, showing a constant pattern assumption is valid. This shows the applicability of the wave model in slow non-equilibrium exothermic reactions.

The wave model can be used to predict in a rapid and straightforward fashion, the result of different injection strategies adopted in common industrial practice during the operation of fixed-bed non-catalytic reactions. The coke combustion reaction may be written as (Rahimi et al., 2010)):

$$CH_n + \left(1 + \frac{p}{4}\right) O_2 \rightarrow CO_2 + \frac{p}{2} H_2O \; where \; n = p = 0.5$$

5.1 Transient time before coherence for decoking system

The wave model does not account for the transient time before the thermochemical wave approaches a constant pattern. The constant pattern model can accurately predict the reaction zone width (shown in Fig A.3) and the wave model accurately predicts the velocity of the coherent thermochemical wave, but this is limited by the transient time to approach this constant pattern. The time taken for the thermochemical wave to reach a constant pattern is dominated by the physical parameters of the reacting solid, kinetic parameters of

the reaction as well as the gas flow velocity. The gas flow velocity is an adjustable parameter but depending on the rate of reaction, a constant pattern may not be achieved. Qualitatively, it is important be able to predict the transient time using the wave model, but this is beyond the scope of this research topic. However, guidelines are necessary for when the wave model can be used and approximately what time a constant pattern is achieved using the physical model simulations.

To make the problem simple, initially the reaction is assumed to be isothermal, by setting the heat of reaction (ΔH) to 0. In Gas-Solid reactions, there are competing effects of convection of incoming reactive gas in plug flow and reaction in the perpendicular direction into the particle, where there is external mass transport, diffusion into the particle, reaction at the surface. The approach to a constant pattern is dominated by the aforementioned parameters. The more concentrated the reactive gas, the faster the constant pattern is approached. Physical model simulations where concentrated reactive gases are used for the decoking and pyrite processes show that the transient time is <5% of the total reaction time. The following analysis is based on a dilute injected reactive gas.

r_c(m) and R_S (m) are the radii of the shrinking core and the particle. Equation (5.1) represents the rate of reaction per particle ($-r'_A$ (mol/s)), which depends on the overall rate constant (k' (m/s)); a composite equation (5.2) of the surface rate coefficient (k_O (m/s)), mass transfer coefficient which depends on velocity but assumed constant (k_{TO} (m/s)) and diffusion coefficient (D_{EO} (m^2/s)) for the ash layer as well as the concentration of the reactive fluid, C_A (mol/dm^3). These steps take place consecutively and the slowest becomes the rate controlling step. However, many reactions are influenced simultaneously by more than one step.

$$-r'_A = k4\pi r_c^2 C_{AC} \tag{5.1}$$

$$k' = \frac{\left(1 - X_B\right)^{\frac{2}{3}}}{\frac{1}{k_{TO}} e^{\frac{E_R}{RT_f}} + \frac{R_s}{D_{EO}} e^{\frac{E_{de}}{RT_f}} \left(\left(1 - X_B\right)^{-\frac{1}{3}} - 1\right) + \frac{1}{k_O} e^{\frac{E_A}{RT_s}} \left(1 - X_B\right)^{-\frac{2}{3}}} \tag{5.2}$$

Since the three rate processes occur in series, their rates must be equal at the steady state. The resulting relation may then be solved to give the gaseous reactant concentration at the particle interface in terms of known quantities. Each of these kinetic parameters is exponentially dependent on the heat of reaction. It is important to find which of these parameters affects the propagation of the waves in terms of time it takes to approach a constant pattern and the width of the wave. A reaction wave is said to have approached constant pattern if the reaction wave width (z_R) remains constant before wave leaves the reactor bed. The numerical simulation is run with dimensionless time (t_D) and distance (z_D) to give a general basis depending on the length of the reactor (L (m)) or superficial gas flow velocity (u (m/s)) which linearly affects the time it takes for the reaction to be complete (T (s)). k_O (m/s), k_{TO} (m/s) and D_{EO} (m^2/s) and physical parameters listed in the appendix are experimental data extracted from Kern and Jess, 2005 and Muller et al., 2010 for the decoking process. Both authors used the SCM model and the same chemical reaction. D_{EO} and k_{TO} are varied individually by orders of magnitude. A snapshot of the simulations of the physical model at $t_D = 0.5$ is shown in Fig. 5.1 and Fig. 5.2 chosen which guarantees a constant pattern, and the reaction wave width can be easily measured.

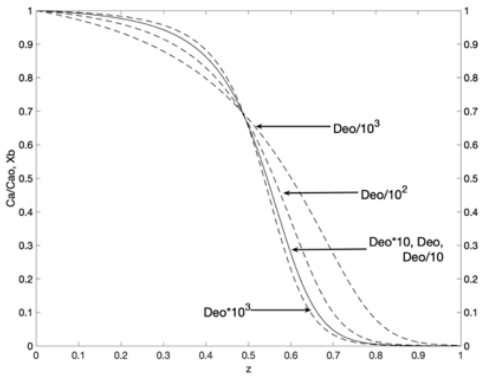

Figure 5-1: Variation of D_{EO} at $t_D = 0.5$

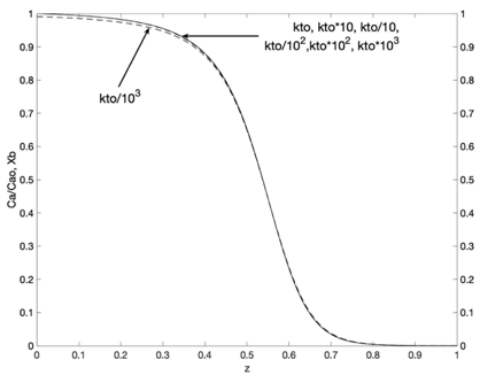

Figure 5-2: Variation of k_{TO} at $t_D = 0.5$

Fig. 5-2 shows mass transfer has little to no effect on the time it takes for the constant pattern to be reached or the reaction wave width. The physical and constant model simulations are practically the same within six orders of magnitude. However, correlations of mass transfer in packed show mass transfer has a larger effect at higher velocities (Cussler, 1984). D_{EO} has a more significant effect on constant pattern formation when reduced by more than two orders of magnitude (Fig. 5-1). The width of the reaction wave increases from 0.58 to 0.81 ($/10^2$) and 0.90 ($/10^3$) giving a 33% and 51% error between the physical and constant pattern model. In the latter case, a constant pattern is not reached by $t_D = 0.5$. However, in practice gases tend to have the same order of magnitude D_{EO}. It can be concluded that the rate limiting step is the reaction at the core surface (k_o). This means if experimentally if the diffusion and fluid to mass transfer coefficient are of the right order, the simulation of the physical model provides simply the same results. To confirm this k' is monitored during the simulations and is shown to vary almost linearly with k_o. More importantly, this means the reaction for the decoking process is not controlled by mass transfer and diffusion, it is controlled by the reaction on the surface. The mass transfer and diffusion coefficient are related by the Sherwood number (Ahn, and Sangmini, 2017), which can also be used to investigate the two rates further.

The simulation is run isothermally, the temperature of the coked bed (Ts (K)) and temperature of the oxygen (Tf (K)) are chosen to be the ignition temperature. The ignition temperature is the lowest temperature at which the reaction can be completed without additional external heat supply during the reaction. Therefore, the approach to constant pattern gives a worst-case scenario because and increase during the reaction which means a constant pattern can be approached even sooner if the starting temperatures are higher than the ignition temperature.

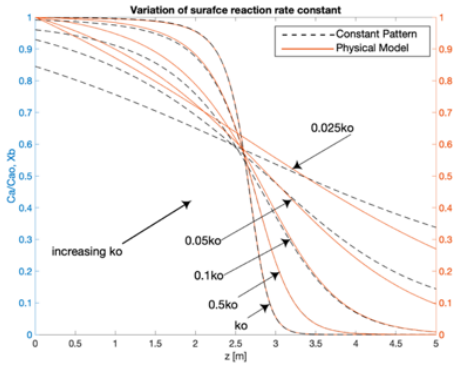

Figure 5-3: Variation of ko at t_D = 0.5.

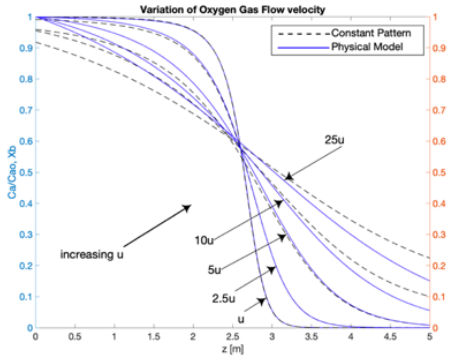

Figure 5-4: Variation of u at t_D = 0.5

k_O, is very sensitive to temperature because it has a much higher activation rate (E_A). The effect of k_O is significant on the reaction wave width shown in Fig. 5-3. One order of magnitude higher and the width of the wave doubles and a constant pattern is not reached at t_d = 0.5. k_O clearly has the largest effect on the overall rate constant, k'. As k_O increases, the match to a constant pattern prediction becomes more exact. The gas flow velocity also strongly affects the development of the reaction. The larger the u, the more spread the width of the reaction wave as shown in Fig. 5-3. Clearly, the rate of approach to constant pattern depends completely on the rate of reaction (particularly k_o) and the gas flow velocity in the physical model with the other physical parameters kept constant. Fig. 5-3 and 5-4 show at that fixed time, there is perfect coherence if the rate is fast (large k_o) and/or a slow injection of gas (low u).

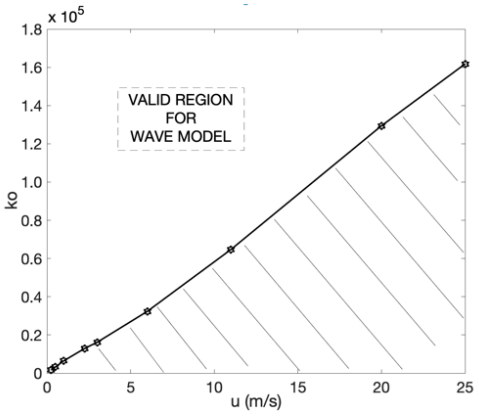

Figure 5-5: Variation of u, k_o at $t_D = 0.5$

For any value of k_O and consequently k' there is a value of u which would guarantee coherence at $t_D = 0.5$. Simulations were run for different values of k_O and the corresponding maximum gas flow velocity that would guarantee coherence at $t_d = 0.5$. ko and u are set to their experimental values and u is increased until a constant pattern is just reached. These values of k_O against u are plotted in Fig. 5-5. It just so happens conveniently that u and k_O have the same units. Therefore, a dimensionless group k_O/u, which represents the gradient is assumed to be the controlling factor. The gradient of the graph (k_O/u) is approximately 7.11×10^3. It can be concluded if k_O/u is larger than 7.11×10^3 then a constant pattern is achieved before $t_D = 0.5$ (valid region shown in Fig. 5-5). Above these values with all the other parameters kept constant, the wave and constant pattern model can be applied successfully at $t_D = 0.5$. To give a complete description, a dynamic plot is required at different values of t_D to approximate when a constant pattern is reached for varied values of k_O and u. The dynamic plot shown in Figs. 5-6 and 5-7 shows both the simulation of the physical model and the constant pattern model of the reaction wave in dimensionless distance and time. The width of the reaction zone is taken as the distance between 96% to 1% of the coherent solid conversion and fluid concentration waves. The distance between these two points is the point of comparison of both models. If the distance between those two points as it moves through the bed is fixed, then a

constant pattern has been reached. The dashed lines are only shown when the constant pattern prediction of the reaction wave width matches the physical simulation to a 95% accuracy. The simulations shown are for ratios of the simulated to the experimental values from the physical model of k_O and u ($k_{o\ sim}/k_{o\ exp.}$ and $u_{sim.}/u_{exp.}$) with all the other variables set to their experimental values. Fig. 5-5 shows the dimensionless time when constant is reached. Similarly, Fig. 5-6 shows the simulations with varied factors of u and the corresponding transient time to guarantee a constant pattern.

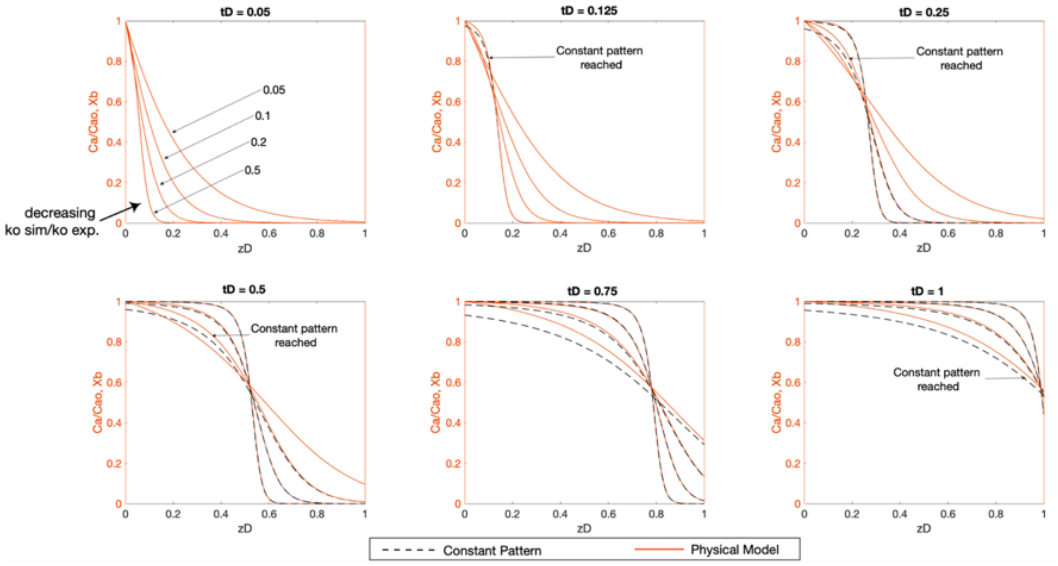

Figure 5-6: Variation of k_o for (z_D, t_D)

Using the values of $k_{o\ sim}$ in table 1, k' is calculated using the experimental values of k_{TO} and $D_{EO.}$ k'.n_p is the overall rate constant for all the particles in the reaction, where n_p is the number of particles in the reaction.

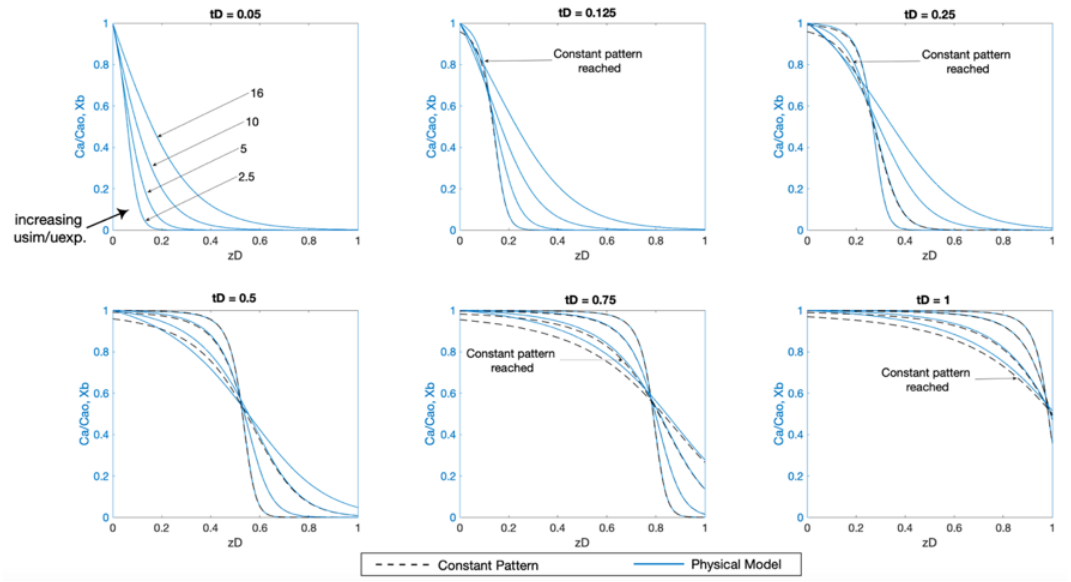

Figure 5-7: Variation of u for (z_D, t_D)

As an example, an engineer has the value of k'/u = 3.0 x 10^5 for a decoking process (all other parameters assumed the same), then the transient time before constant pattern is reached is t_D 0.25. Depending on the length of the reactor and the time taken for the reaction to complete, the engineer can estimate the reaction wave width (in m) and the transient time (in s) for constant pattern to be reached. Hence, the wave model is applicable from that transient time onwards.

ko sim/ko exp.	**z_R**	**usim/uexp.**	**z_R**
0.5	0.33	2.5	0.33
0.2	0.50	5	0.51
0.1	0.87	10	0.83
0.05	1.21	16	1.08
k_o variation	u variation		
Transient time	**k'/u**	**Transient time**	**k'/u**
$0 < t_D < 0.1$	1.45 x 10^6	$0 < t_D < 0.1$	1.75 x 10^6
$0 < t_D < 0.125$	7.25 x 10^5	$0.1 < t_D < 0.125$	6.25 x 10^5
$0 < t_D < 0.25$	2.91 x 10^5	$0.125 < t_D < 0.25$	2.81 x 10^5
$0 < t_D < 0.5$	1.45 x 10^5	$0.25 < t_D < 0.5$	1.44 x 10^5
$t_D = 1$	7.95 x 10^4	$0.85 < t_D < 1$	8.05 x 10^4

Table 5-1: Reaction wave width and Transient times for k'/u for Decoking process (z_D, t_D)

If the physical model simulation and the constant pattern approximation match up, point for point from 1% to 96% giving a maximum error of 5% then all of the assumptions that made for the constant pattern and the wave model are correct. Fig. 5-5 shows the range of values of k_o and u which will guarantee a constant pattern. This diagram gives a rule of thumb for the chemical engineer to ascertain the transient time to reach a constant pattern; and hence when the wave model assumption is valid for use in the decoking process. In the non-isothermal case, the temperature will have a huge effect on the rate, but it will mainly affect the surface reaction. It will not affect the mass transfer or diffusion through the ash layer, because the activation energies are lower.

Several figures have been presented, not so much because of the significance of any one but, rather, to illustrate a range of variables that might be interest. There is a larger uncertainty in the measurements when t_D is close to 0 as the C_A and X_B waves have not risen to 96%, so it would be impossible to compare with the constant pattern model. Table 5-1 shows in the same transient time, k'/u are roughly the same when varying k_o with a fixed u and vice versa. Thereby, confirming the protocol for transient time to constant pattern in the decoking process.

A further extension would be to plot 1/k', u and different C_A, T_s and T_f values to further isolate and develop a wave model to calculate this transient time more directly at different concentrations of oxygen and starting temperatures. This would change the dimensionless terms as temperature would be included. I would suggest normalising the temperature as well. An important condition to change is the constant gas phase velocity (u). Especially when high temperatures are reached, the density of the gas changes and therefore the velocity will change. A velocity equation as a function of density can be incorporated in both the physical, wave and constant pattern model.

Several workers have simulated the decoking process and compared their simulations with experimental values. Rahimpour et al., 2010, Dehghani, 2013 and Toghyani et al., 2015 investigated the experimental study for the process of decoking in the hydrogenation catalyst Pt/Al_2O_3. The results were compared to a first order reaction model which is different from the shrinking core model (SCM) adopted in the physical model. The shrinking core model adopted by Toghyani et al., 2015 uses rate expressions per unit area of catalyst whilst the rate expression used in the paper is per unit mass of catalyst. Furthermore, the model in the paper does not have a mass transfer model. The objective is to compare the experimental results from Toghyani et al., 2015 with the wave model and the physical model.

Parameter	Definition	Decoking	Units
a	Stoichiometric coefficient of fluid	1	-
b	Stoichiometric coefficient of solid	1.125	-
C_A	Reactive fluid concentration		$kmol/m^3$
C_{AO}	Injected fluid concentration	2.03×10^{-4}	$kmol/m^3$
c_f	Specific heat capacity of fluid	1.3×10^3	J/kmolK
c_s	Specific heat capacity of solid	3.5×10^6	J/kmolK
D_{EO}	Diffusion constant through ash layer	3.0×10^{-6}	m^2/s
E_A	Activation energy for surface rate of reaction	2.1×10^8	J/kmol
E_{DE}	Activation energy for diffusivity	1.4×10^7	J/kmol
E_k	Activation energy for fluid to mass transfer	1.4×10^7	J/kmol
h	heat transfer coefficient between solid and fluid	300	W/mK
k'	Composite overall rate constant	-	m/s
k_O	Surface rate constant	1.68×10^8	m/s
k_{TO}	Mass to fluid mass transfer coefficient	1.96×10^3	m/s
L	Length of reactor bed	5	m
M_B	Molecular mass	12.5	g/mol
n	Number of nodes in numerical simulation	1000	-
n_p	Number of particles per unit volume	1.49×10^9	-
P	Pressure of injected fluid	4.3×10^5	Pa

R	Universal gas rate constant	8314	J/kmolK
r_b	mass of coke per volume of catalyst	22	kg/m^3
r_c	Radius of shrinking core		m
R_s	Radius of particle	0.6 x 10^{-3}	m
t_D	Dimensionless time		-
T	Time to complete reaction	38000	s
T_f	Temperature of reacting fluid	898	K
T_s	Temperature of reacting solid	898	K
u	Superficial gas velocity in the direction of flow	0.5	m/s
V	Volume of injected fluid		m^3
V_R	Velocity of reaction wave	Varies	m/s
V_T	Velocity of thermal wave	Varies	m/s
$V_{T/C}$	Velocity of thermochemical wave	Varies	m/s
X	Fraction of reacting solid	0.022	-
X	Average conversion of reacted bed		-
X_B	Reacting solid conversion		-
X_{O2}	Fraction of injected O_2 in air		%
z_D	Dimensionless distance		-
Z	Distance travelled after time t		-
ΔH	Enthalpy of reaction	-400 x 10^6	J/kmolK
ΔT_C	Temperature rise associated with chemical reaction	91	K
ε	Porosity of fixed bed	0.4	-

Table 5-2: Parameters for decoking and pyrite case.

Fig. 5-3 shows the variation of temperature rise associated with the thermochemical wave (ΔT_c) with inlet fluid concentration. The graph was plotted by using the parameters in Table 5-3 and the wave model equation (3.9) for the thermochemical temperature rise. In the dilute case, the minimum temperature rise is much lower than that in the concentrated case. If a larger range on the x-axis was used, the temperature rise reaches at high concentration reaches a limit of ~250K. This shows that, for the concentrated case, the temperature rise will always be very large.

A critical concentration exists for which the denominator of the temperature rise equation tends to zero. This leads to a “hot spot” and will be discussed further in later sections.

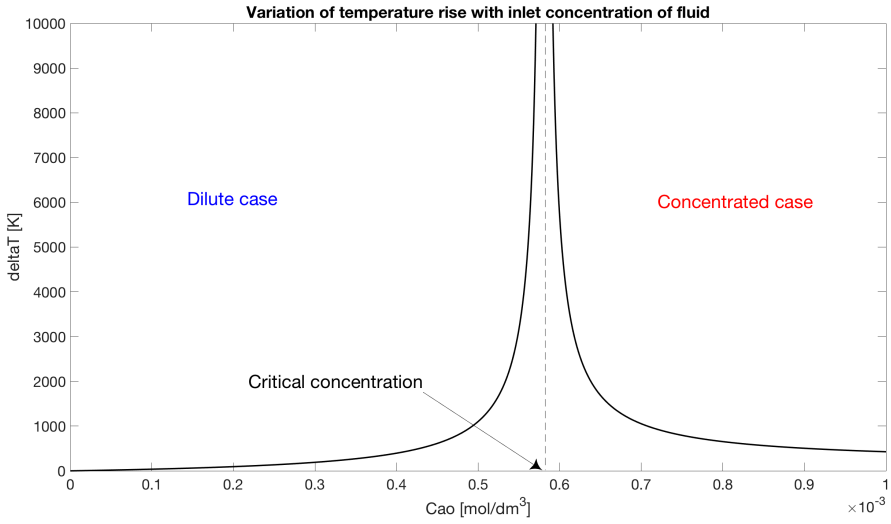

Figure 5-8: Wave model prediction of temperature plateau variation with inlet concentration

5.2 Comparison between numerical simulations and wave model

The values of the thermochemical and thermal wave velocities, and the temperature of the plateau, are calculated from the wave model equations. Using the wave model, predictions were made for different strategies of the decoking process. These predictions are now compared with those obtained by numerical integration of the complete set of PDEs, which represent the energy and material balances of the system.

The wave model is compared with the numerical simulations by analysing snapshots of the chemical process for various operation strategies. The position of the waves at certain times are represented as vertical dashed lines and the plateau temperature is represented as a horizontal dashed line in the figures. The values for the thermochemical and thermal wave velocities are used to calculate the distance travelled by the waves, and compared to the numerical simulations in a summarised table format.

5.2.1 Ignition Temperature

A specific focus is set on the temperature which is required to initiate exothermic reaction fronts. In particular, this level should exceed a specific ignition temperature. Coke particles can be ignited heterogeneously, by direct contact of oxygen on the whole coke particles. The ignition temperature is taken as the Common values of the ignition temperature of coke range from 833K to 918K depending on the composition of the coke.

In the current study, an estimation of the ignition temperature was found by trial and error. The trial and error process was carried out by running the numerical simulation at low initial and inlet temperatures of the fluid and solid to 298K with 10K increment until the reaction occurs completely. The temperature at which the decoking process runs into full completion is known as the ignition temperature. Below this temperature, the reaction may still occur but only partially. The ignition temperature (T_{ign}) was found to be approximately 898K.

Above this bed or fluid temperature (depending on the operation scheme), the reaction can keep going without external heat supply. Further tests were carried out to verify the ignition temperature; it was observed the oxygen concentration and flow rate, size of coked particles and bed porosity had little effect on ignition temperature, although more analysis would be required to make a definitive conclusion.

5.2.2 Approximation of Total Conversion in Reactor

The total conversion of coke in the reactor bed can be calculated from the simulation results. The area under the X_B curve is the total percentage of carbon converted as shown in the Fig. 5-9. In mathematical terms,

$$\bar{X}_{simulation} = \frac{\int X_B dz}{z_{bed}} \tag{5.3}$$

The wave model predicts the amount of converted solid to be

$$\bar{X}_{wave\ model} = \frac{V_{T/C} \times t_{elapsed}}{L} \tag{5.4}$$

Intuitively, $\overline{X}_{partial}$ = 1 is when the thermochemical wave has passed through the reactor. Fig. 5-9 is for illustration purposes, the values in the equation (5.3) would depend on the parameters of the decoking process.

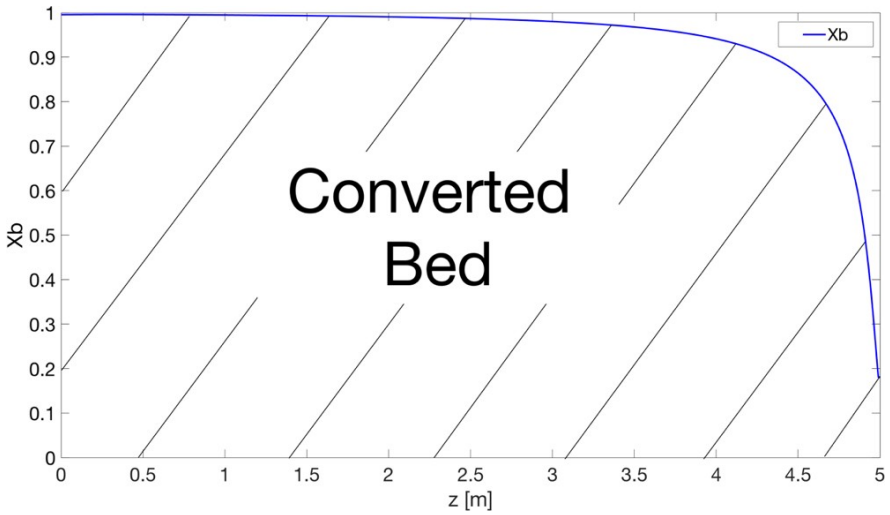

Figure 5-9: Total conversion of solid at t

5.2.3 Preheat Wave

There are different ways to heat the bed prior to injecting reactive fluid. In the decoking process, where the required temperatures are high. There are a variety of methods for heating fixed bed reactors. Preheating with nitrogen is more cost effective and is chosen as the primary method of heating the fixed bed in our study. Fig. 5-10 shows a numerical simulation of a hot nitrogen stream heating a reactor bed. Preheating the bed with nitrogen produces a pure thermal wave only as there is no reaction occurring. The concentration of the fluid (O_2) remains zero and is of no importance at this stage. Therefore, no concentration of fluid and conversion of solid waves are shown in the Fig 5-10. The temperature of the fluid and solid match up almost immediately and their waves travel together jointly through the reactor. The reason for this is due to the high transfer heat

coefficient between the solid (catalyst particle) and the fluid (nitrogen). The velocity of the thermal waves from the simulation is compared with the approximation from the wave model. The dashed lines represent the wave model approximation. It is clear that the simulation and the wave model below show good agreement.

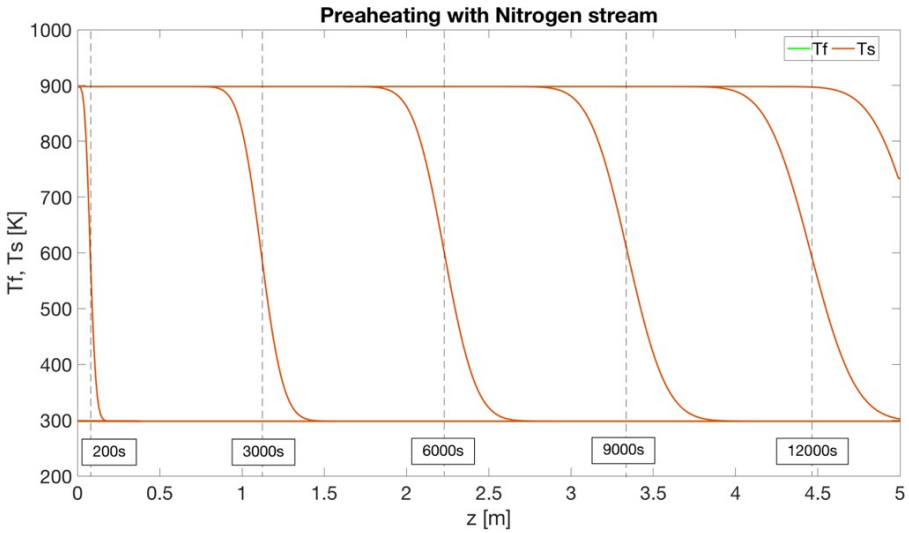

Figure 5-10: Preheating reactor bed with nitrogen

Decoking of reactors is a very important reaction process is CRE. Removal of coke from the reactor bed is crucial for hydrocarbon processes. As mentioned earlier, there are different "possible" strategies used to remove coke from the surface of catalyst in reactors.

It should be noted that the maximum permissible temperature allowed in the reactor is ~1000K. Above this temperature, the catalyst sinters, which is undesirable. In the strategies to be analysed, it should be realised when a hot bed is used, nitrogen has already been used to heat the bed up to the required temperature and will not be shown in the diagrams, instead the bed will already be uniformly heated to the required temperature. In the injection strategies to be analysed, it should be noted that nitrogen has already been used to heat the bed up uniformly to the required temperature when a hot bed is used.

For all the injection strategies considered, the reacting fluid (oxygen mixed with inert nitrogen) is injected into an unreacted bed (catalyst particles coated with coke). The effect of preheating both the fluid and the bed is investigated, both dilute and concentrated feed

oxygen are considered.

The numerical simulations show the composition profiles of selected strategies. Comparisons are carried out both graphically and in a tabulated manner. The simulations can only be shown at certain times (snapshots) for the sake of clarity. These times along with the calculated wave model equations are used to predict the distance travelled by each wave. Of course, this comparison assumes the velocity of the wave to be constant. The wave trajectories confirm in a concise manner, the validity of constant wave velocity assumption.

5.3 Results for Dilute Oxygen Case

The concentration of oxygen for the dilute cases is 2.03×10^{-4} mol/dm^3 (3 mol% O_2 in N_2 at STP). The wave model predictions are then $V_{T/C} = 1.297 \times 10^{-4}$ m/s, $V_T = 3.713 \times 10^{-4}$ m/s, $\Delta T_c = 95.8$K. The temperature of the fluid and solid waves become completely coherent after approximately 100s. Hence, the two temperature waves are superimposed on each other in the bed profiles.

5.3.1 Hot Fluid into a Preheated Bed

The temperature of the fluid (T_{inj}) and solid (T_o) are set to the ignition temperature, a travelling hot zone is generated ahead of the reaction. The concentration of the fluid and conversion of the solid become coherent and travel jointly with the tail end of the temperature wave. Hence, the attainment of a trailing coherent thermochemical wave and a leading thermal wave is achieved.

The sets of values of dependent variables remain conserved, that is, the values of different variables do not move relative to one another in space with time. The requirement for coherence is that all values of a set of variables at one point in space and time must

move in the same direction and with the same velocity, so that they will remain in each other's company. This is shown in Fig. 5-11. The average conversion according to the numerical simulation, $X = 97\%$.

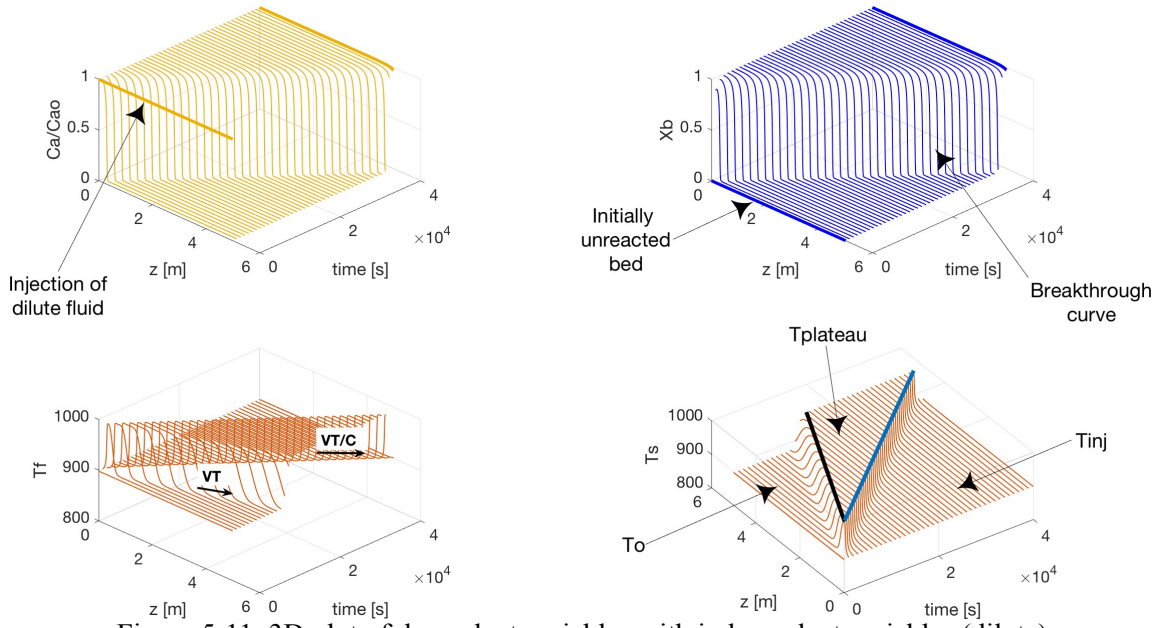

Figure 5-11: 3D plot of dependent variables with independent variables (dilute)

The wave model prediction of the thermochemical wave velocity, thermal wave velocity and temperature rise are used to calculate distance travelled in Table 5-3 and compared with the predictions of the numerical simulation at time periods shown in Fig. 5-12.

Agreement is within a few %, notwithstanding the difficulty in locating the position of a steep, constant pattern.

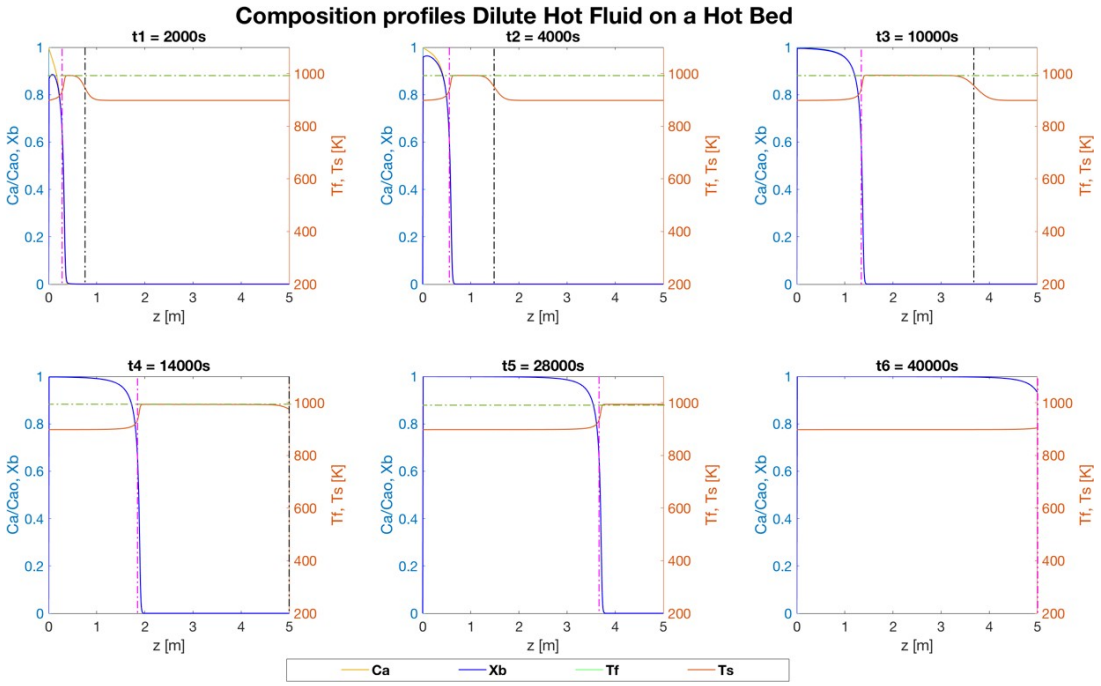

Figure 5-12: Composition profiles for hot dilute fluid into a preheated bed with Z_T (black dashed), $Z_{T/C}$ (purple dashed), $T_{plateau}$ (green dashed). T_o = 898K, T_{inj} = 898K

Time (s)	Wave Model			Simulation Results		
t	$Z_{T/C}$	Z_{T1}	ΔT_c (K)	$Z_{T/C}$	Z_{T1}	ΔT_c (K)
2.0 x 10^3	0.26	0.74	95.8	0.2	0.7	96
4.0 x 10^3	0.52	1.49	95.8	0.5	1.5	96
1.0 x 10^4	1.30	3.71	95.8	1.2	3.7	96
1.4 x 10^4	1.82	-	95.8	1.9	-	96
2.8 x 10^4	3.63	-	95.8	3.6	-	96
4.0 x 10^4	5.1	-	95.8	5.0	-	96

Table 5-3: Comparison of distance travelled by thermal and thermochemical waves & plateau temperature for dilute fluid cases

5.3.2 Hot Fluid into a Cold Bed

The fluid is injected at a high enough temperature to ensure complete regeneration of the bed while the temperature of the bed starts at 298K. It should be noted that the length of the reactor bed was chosen to represent a large-scale industrial fixed bed reactor. Therefore, a longer time period is required for complete regeneration than common convention.

Fig. 5-13 shows the time evolution of the fluid and solid temperature. At 4000s, the

profiles again obtain a practically constant shape. As the profile approaches the exit, the reaction is nearly completed, and the reaction zone is eventually swept out. The wave model is in good agreement with the numerical simulation. In this scenario, the trailing thermochemical wave guarantees that the reaction zone enters a region preheated by the leading thermal wave. The latter is associated with a large temperature drop to the cold bed. The width of the thermochemical wave in the numerical simulation shows excellent agreement with the constant pattern solution in section 4.6 (z_{mtz} = 0.44m). Showing that constant pattern assumption is indeed valid (see wave trajectories in Fig. 5-14).

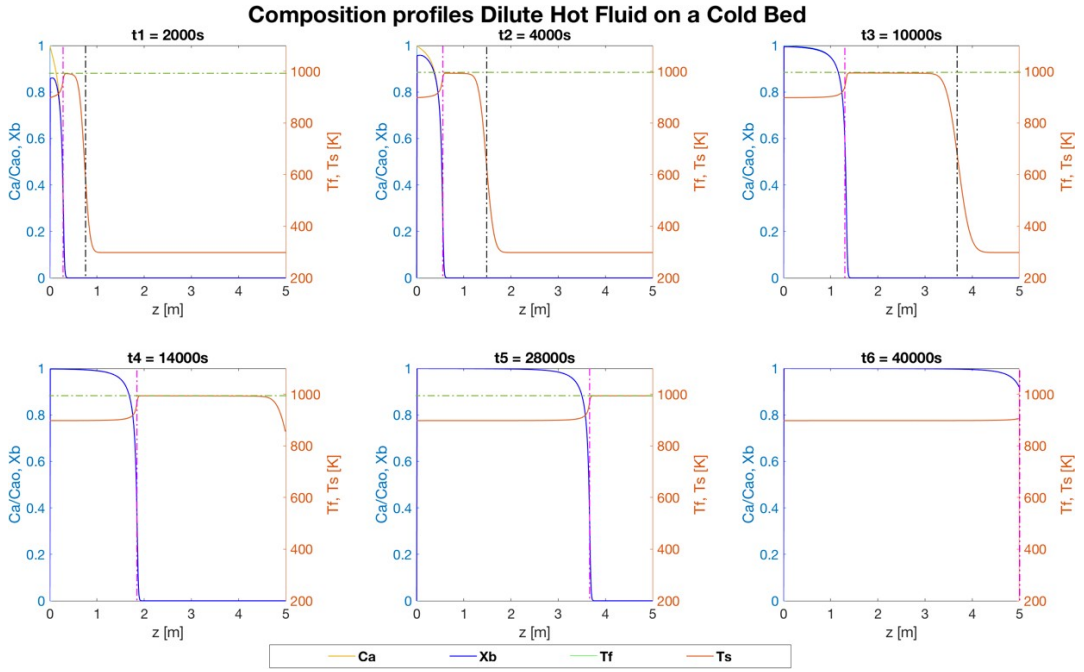

Figure 5-13: Composition profiles for hot fluid into a cold bed with Z_T (black dashed), $Z_{T/C}$ (purple dashed), $T_{plateau}$ (green dashed). T_o = 298K, T_{inj} = 898K

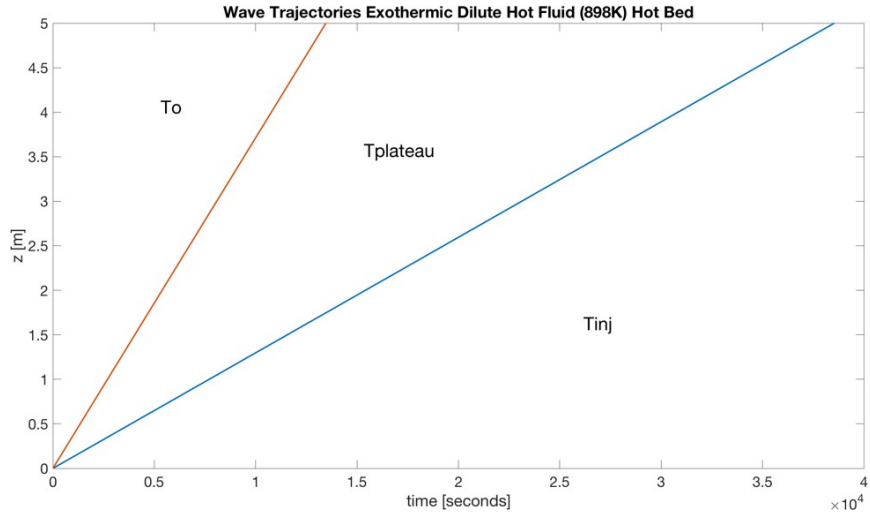

Figure 5-14: Distance-time diagram for complete reaction (dilute) with thermochemical wave (blue), thermal wave (red) for dilute cases (constant T_{inj})

5.3.3 *Cold Fluid into a Hot bed*

The third scenario simulated is the case where a cold fluid is injected into a heated bed. Full conversion along the reactor bed is not achieved giving an incomplete reaction. Cold fluid is pumped continuously into a hot bed and there is an uncharacteristic temperature rise. The C_A and X_B waves are still coherent but the X_B wave has risen to a lower value. The part of the reactor nearer to the inlet does not react. Depending on the temperature of the injected fluid, there may be an incomplete reaction for this scenario. There are two cases are to be considered:

- T_{inj} and T_o are both above the ignition temperature giving a complete reaction.
- T_{inj} is below ignition temperature but T_o is above ignition temperature, resulting in partial conversion of the fixed bed.

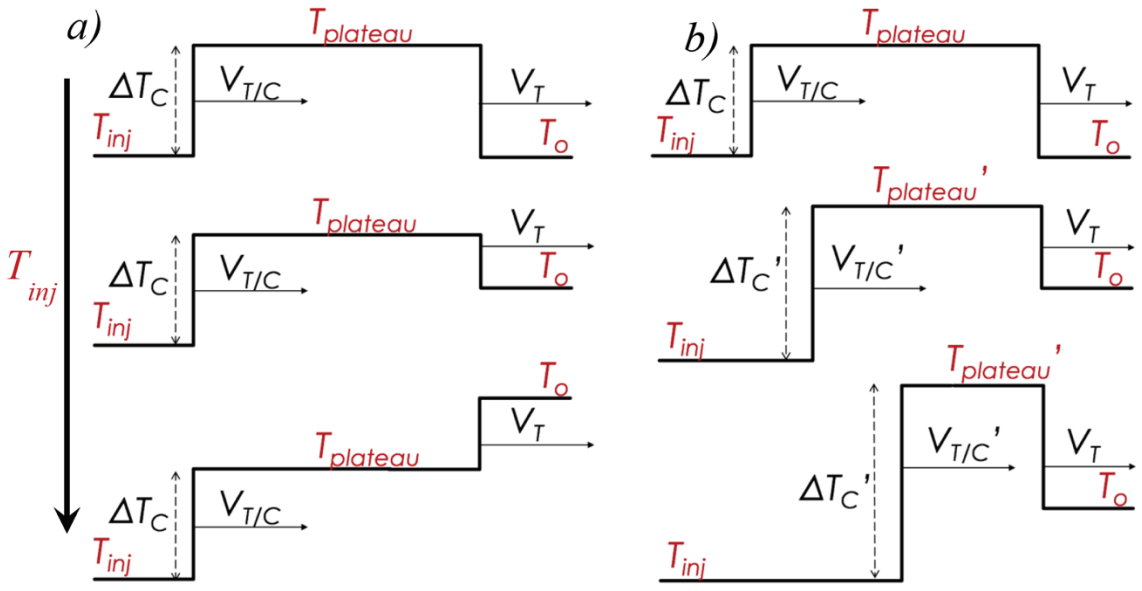

Figure 5-15: Temperature profiles for cold Fluid into hot bed (dilute) with T_{inj} reducing (a) T_{inj}, $T_o > T_{ign}$ (b) $T_{inj} < T_{ign}$, $T_o > T_{ign}$

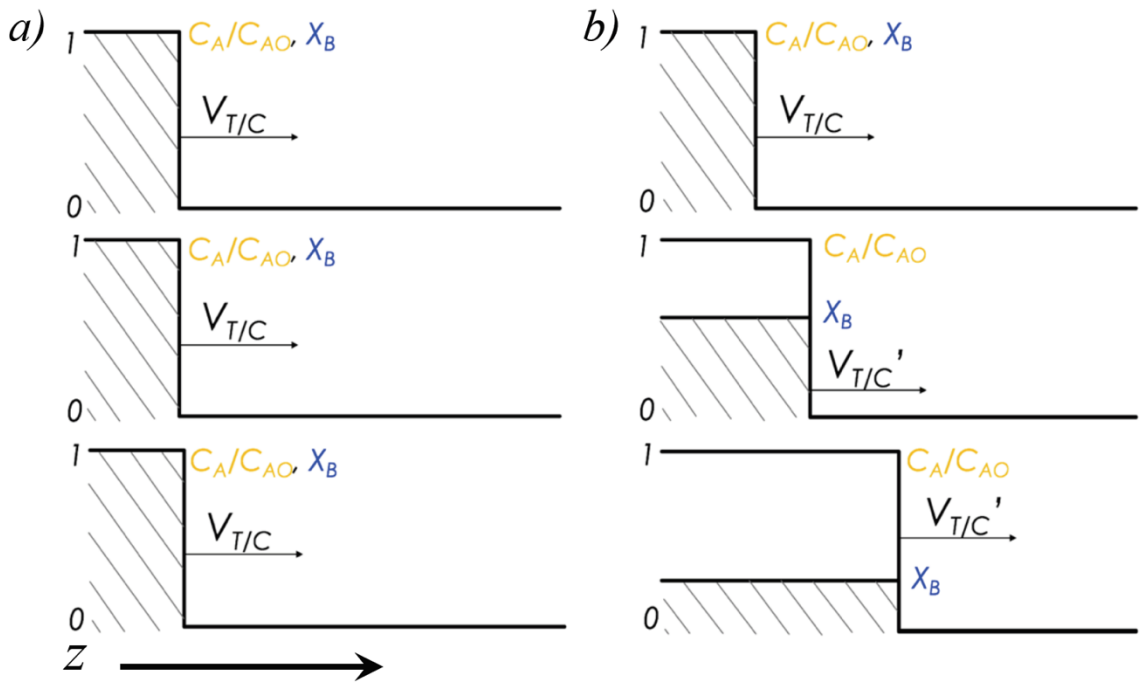

Figure 5-16: Concentration profiles for cold fluid into hot bed (dilute) with T_{inj} reducing (a) T_{inj}, $T_o > T_{ign}$ (b) $T_{inj} < T_{ign}$, $T_o > T_{ign}$

Reacted solid

Case (a): Both the injected fluid temperature and the bed temperature are always above ignition temperature. As T_{inj} is reduced, the thermochemical temperature rise does not change leading to the profiles in Fig 5-15 and Fig 5-16.

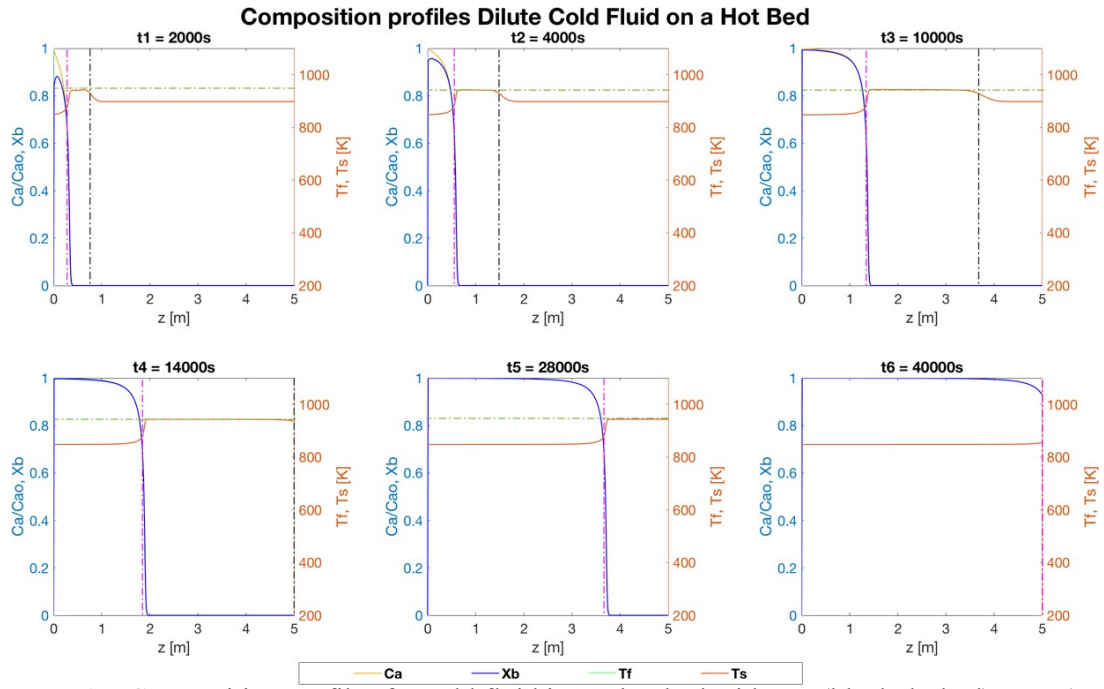

Figure 5-17: Composition profiles for cold fluid into a hot bed with Z_{T1} (black dashed), $Z_{T/C}$ (purple dashed), $T_{plateau}$ (green dashed). T_o = 898K, T_{inj} = 848K

T_{inj} is always assumed to be above ignition temperature, complete conversion is expected. An interesting case is when T_{inj} is chosen to be $T_o - \Delta T_C$ then the thermal wave would be unidentifiable, and a pure thermochemical wave would pass through the reactor.

Case (b): The injected fluid temperature and the bed temperature are initially set to ignition temperature. If T_{inj} is set below the ignition temperature, only part of the coke reacts. Essentially, the dilute oxygen is only reacting partly with the carbon, as a consequence the thermochemical wave (where the reaction occurs) travels faster. There is an uncharacteristic temperature rise associated with the thermochemical wave, this is attributed to increased reactant concentration in the hot downstream section of the fixed bed. Essentially, the dilute oxygen is only reacting partly with the carbon, wave model cannot predict what the partial conversion would be but if the conversion was known, the wave model can accurately predict the velocity of the thermochemical wave, and consequently the temperature rise due to the faster thermochemical wave.

$\bar{X}$ was found to be 43%. Using the equation (3.22), $V_{T/C}$ = 3.242 x 10^{-4} m/s and the temperature rise is 3 times larger than in the previous cases. The lower the injected fluid temperature, lower the conversion and higher temperature rises are expected as shown in Figs. 5-15 and 5-16. The temperature rise can be very high due to lower conversions, a temperature plateau may not be reached in the reactor. But if the reactor bed was infinitely long, a temperature plateau will always be reached except in the case of a hot spot.

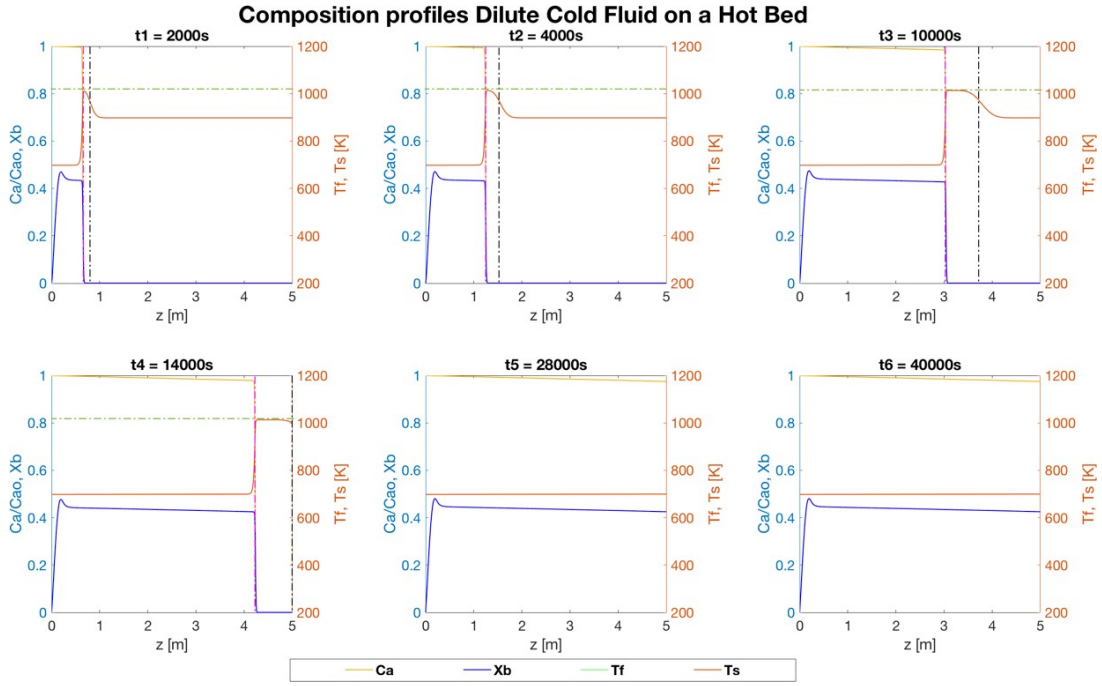

Figure 5-18: Composition profiles for cold fluid into a hot bed with Z_{T1} (black dashed), $Z_{T/C}$ (purple dashed). T_o = 898K, T_{inj} = 698K

Time (s)	Wave Model			Simulation Results		
t	$Z_{T/C}$'	Z_{T1}	ΔT_c' (K)	$Z_{T/C}$'	Z_{T1}	ΔT_c' (K)
2.0 x 10^3	0.64	0.74	315.2	0.7	0.75	310
4.0 x 10^3	1.29	1.49	315.2	1.3	1.5	310
1.0 x 10^4	3.24	3.71	315.2	3.2	3.7	310
1.4 x 10^4	4.3	-	315.2	4.2	-	310
2.8 x 10^4	-	-	315.2	-	-	310
4.0 x 10^4	-	-	315.2	-	-	310

Table 5-4: Comparison of distance travelled by thermal, thermochemical waves & plateau temperature for dilute case cold fluid (698K) into a hot bed

For this partial conversion case, the thermochemical wave travels at a correctly predicted faster velocity by equations (3.22) and a new temperature rise is reached. For the other cases, the velocities of the thermal and thermochemical waves are the same as there is no change in any parameter except temperature, which does not affect the velocities of the wave model. The wave trajectory is drawn by tracking the mid-point of the waves in the numerical solution at different time periods.

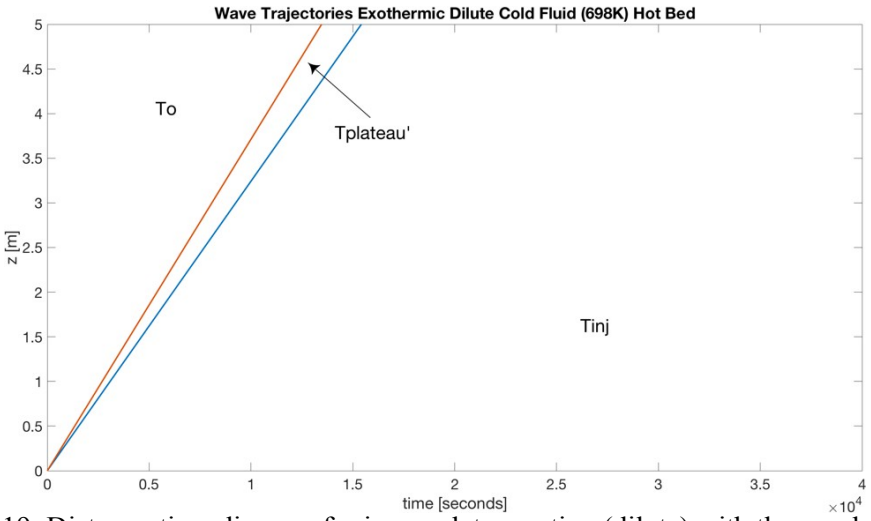

Figure 5-19: Distance-time diagram for incomplete reaction (dilute) with thermochemical wave (blue), thermal wave (red)

5.3.4 Hot Fluid Pulse into a Preheated Bed

In this operating strategy, the injected fluid is heated for a finite time only to save energy (a 'pulse'). A hot fluid pulse is defined as an injected fluid which is initially heated to 898K and then cooled to 298K after 10000s. As before, the wave model predicts a thermal wave (thermal wave 1) travelling with velocity V_T and a trailing thermochemical wave at $V_{T/C}$. As $V_T > V_{T/C}$, the second cold thermal wave 2 is introduced at the end of the pulse and catches up with the thermochemical wave at $\mathbf{t_3}$, a small temperature peak is generated as seen in Fig. 5-20 from t_3 to t_4. The second cold thermal wave (thermal wave 2) then overtakes the thermochemical wave (t_3 onwards).

This front quench the reaction at the trailing edge of the reaction and causes a faster thermochemical wave, due to the partially reacted bed and the thermochemical temperature rise is higher

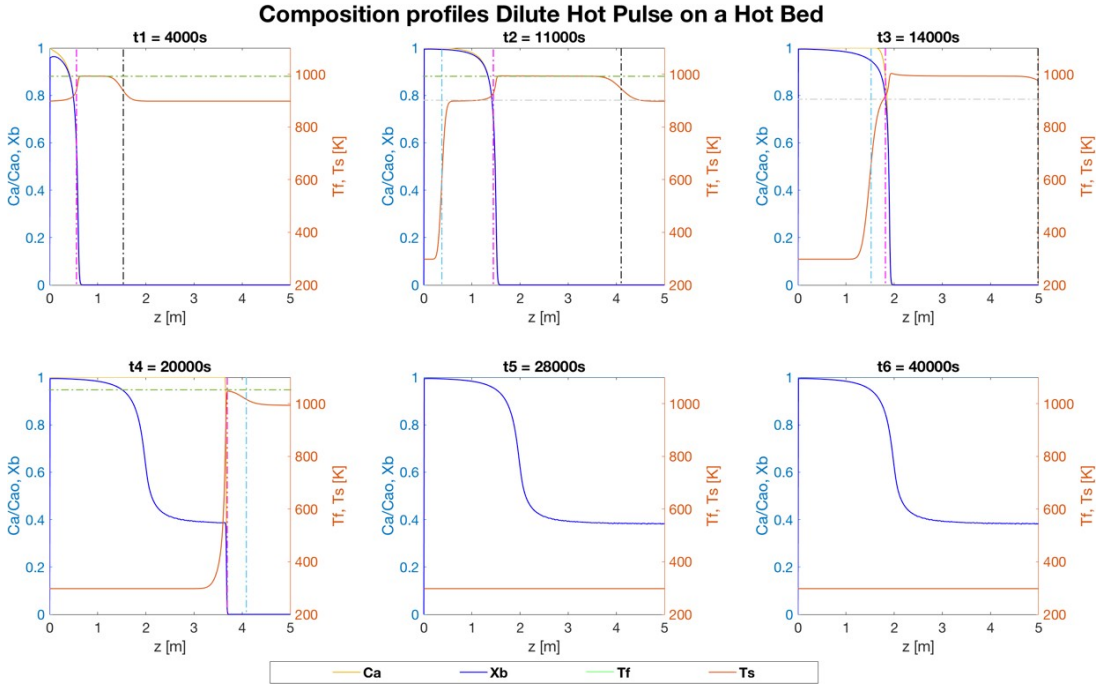

Figure 5-20: Composition profiles for hot fluid pulse into a hot bed with Z_{T1} (black dashed), Z_{T2} (blue dashed), $Z_{T/C}$ (purple dashed), $T_{plateau}$ (green dashed), T_{fo} (grey dashed). T_o = 898K, T_{inj} ={898K,298K}

Time (s)	Wave Model				Simulation Results			
t	$Z_{T/C}$	Z_{T1}	Z_{T2}	ΔT_c (K)	$Z_{T/C}$	Z_{T1}	Z_{T2}	ΔT_c (K)
4.0 x 10^3	0.52	1.49	-	95.8	0.5	1.5	-	96
1.1 x 10^4	1.43	4.08	0.37	95.8	1.4	4.1	0.35	96
1.4 x 10^4	1.82	5.1	1.48	-	1.9	5	1.5	-
2.0 x 10^4	3.5	-	3.71	82.6	3.6	-	3.75	84
2.8 x 10^4	-	-	-	-	-	-	-	-
4.0 x 10^4	-	-	-	-	-	-	-	-

Table 5-5: Comparison of distance travelled by thermal, thermochemical waves & plateau temperature for hot fluid pulse into a hot bed (dilute)

The leading thermal wave and the trailing thermal wave travel at the same speed (V_{T1} = V_{T2} = V_T). Therefore, the distance between thermal wave 1 and thermal wave 2 is kept constant as the pulse travels across the reactor. Table 5-4 shows the distance the waves have travelled as predicted by the wave model at the time periods shown in Fig. 5-20.

The distance-time diagram in Fig. 5-21 show the waves are travelling at a constant velocity until the trailing cold thermal wave 2 meets the thermochemical wave. The thermochemical wave then travels much faster but remains behind cold thermal wave 2. Since the temperature at the trailing edge of the thermochemical wave is now much lower, the reaction here is quenched.

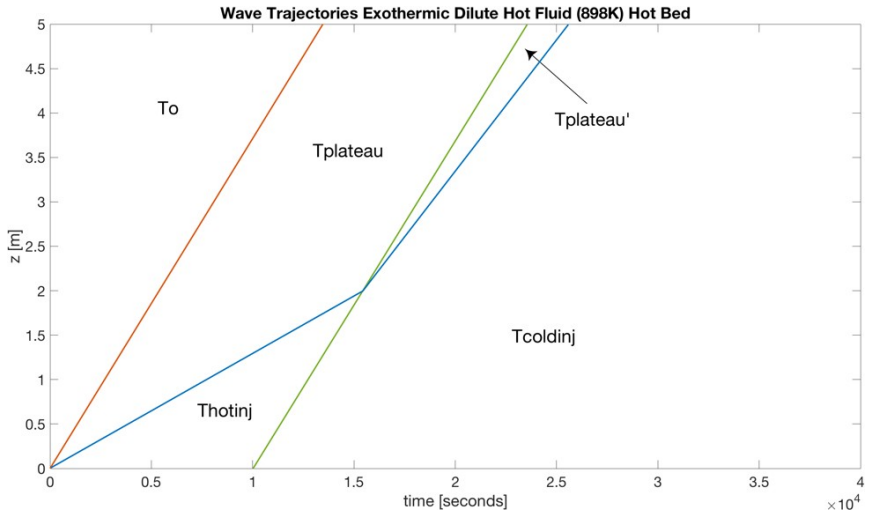

Figure 5-21: Distance-time diagram for hot fluid pulse into a hot bed (dilute) with thermochemical wave (blue), thermal wave 1 (red) thermal wave 2 (green)

Comparing the dilute cases, it requires much more energy to heat both the fluid and solid up than just the fluid. Initially the idea of a temperature pulse may seem prudent, but the results show otherwise as the cold fluid has not been delayed enough. The strategy where a cold dilute fluid delayed sufficiently is now tackled.

5.3.5 Reduced Heat strategy

A first observation from the numerical simulations is that the reactor bed does not have to be pre-heated for full conversion. A second improvement to the strategy is to inject cold dilute oxygen after a period of time. A reduced heat strategy involves delaying the cold dilute fluid long enough so that the trailing cold thermal wave meets the thermochemical wave at the end of the reactor bed. This avoids the switchover of the trailing cold thermal wave and the thermochemical wave inside the reactor. This avoids the quench observed in

Fig. 5-20.

The wave model was used to calculate the time it takes a pure thermal wave to travel through the reactor (t_T) and time it takes a thermochemical wave to travel through the reactor ($t_{T/C}$); the cold thermal wave (pulse end) is therefore delayed until:

$$t_{delayed} = t_{T/C} - t_T \tag{5.3}$$

where $t_T = 14000s$ and $t_{T/C} = 40000s$. Therefore, the time to inject cold dilute fluid, $t_{inj,fluid} = 26000s$. The diagram below can explain the reaction simply:

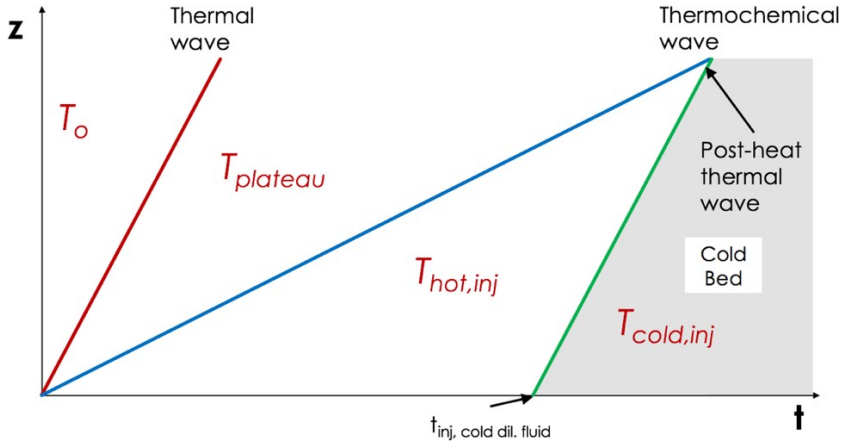

Figure 5-22: Distance-time diagram for reduced heat strategy (dilute)

The cold fluid is injected at 298K and it produces a cold thermal wave. This is represented as the post-heat thermal wave above. The gradient of the post-heat thermal wave is the same as the leading thermal wave, because both waves travel at the same velocity (V_T)

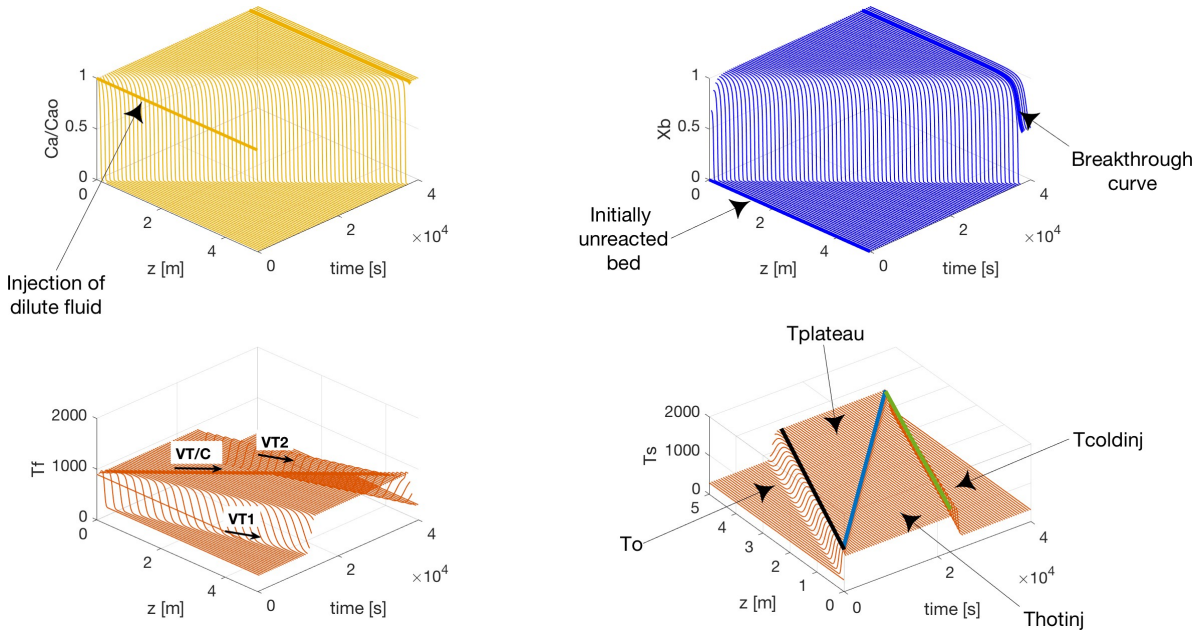

Figure 5-23: 3D plot of dependent variables with independent variables (dilute reduced heat strategy)

The post-heat thermal wave leaves a cold bed behind. This strategy leads to 35% less energy use than in any of the previous heating strategies, whilst decoking and regenerating the bed completely. Fig. 5-23 and Fig. 5-24 show the evolution of the temperature and concentration profiles.

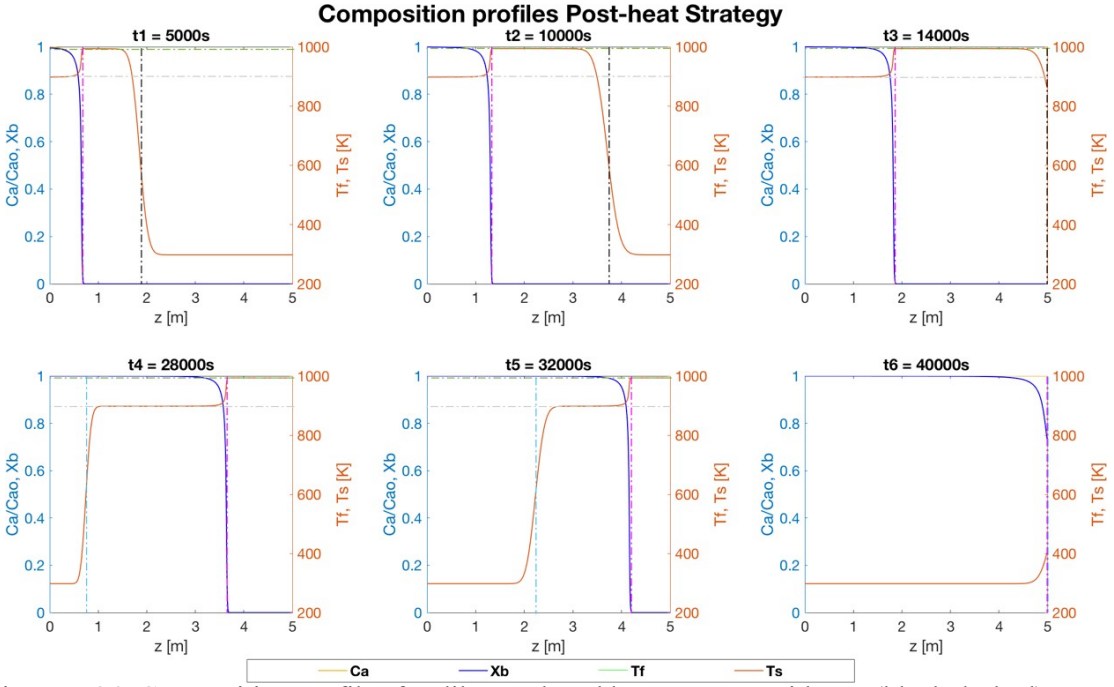

Figure 5-24: Composition profiles for dilute reduced heat strategy with Z_{T1} (black dashed), Z_{T2} (blue dashed), $Z_{T/C}$ (purple dashed), $T_{plateau}$ (green dashed), T_{fo} (grey dashed). T_o = 898K, T_{inj} = {898K,298K}

Time (s)	Wave Model				Simulation Results			
t	$Z_{T/C}$	Z_{T1}	Z_{T2}	ΔT_c (K)	$Z_{T/C}$	Z_{T1}	Z_{T2}	ΔT_c (K)
5.0 x 10^3	0.52	1.49	-	95.8	0.6	1.7	-	96
1.0 x 10^4	1.41	4.08	0.78	95.8	1.3	3.8	0.8	96
1.4 x 10^4	1.82	5.12	2.16	95.8	1.8	5	2.2	96
2.8 x 10^4	3.51	-	5.01	95.8	3.6	-	5.0	96
3.2 x 10^4	4.18	-	-	95.8	4.2	-	-	96
4.0 x 10^4	5.09	-	-	-	5.0	-	-	-

Table 5-6: Comparison of distance travelled by thermal and thermochemical waves & plateau temperature for dilute reduced heat strategy

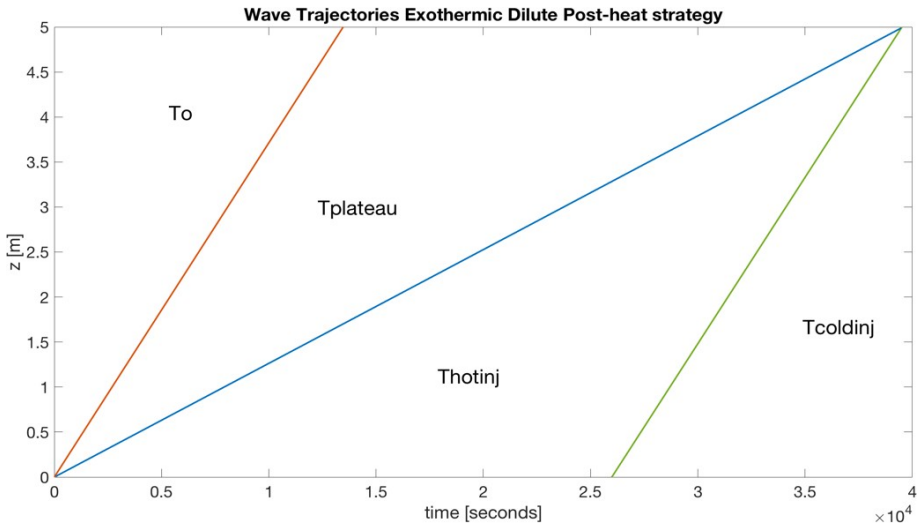

Figure 5-25: Distance-time diagram for reduced heat strategy (dilute) with thermochemical wave (blue), thermal wave 1 (red) thermal wave 2 (green)

The numerical simulation confirms the reduced heat strategy introduces a cold thermal wave (as seen at t_4), meeting the thermochemical wave at the exit of the reactor at time t_6. The distance- time diagram matches the distance-time diagram from the numerical simulation. The simple diagram describes the essential features of the reactor dynamics behaviour completely, saving time and effort. This shows the simplicity, predictive power and intuitive appeal of the wave model.

5.4 Results for Concentrated Oxygen Case

When the oxygen concentration is high, the leading thermochemical wave moves faster than the trailing thermal wave. This means that the bed is no longer preheated by the reaction but instead the heat generated is retained in the bed behind the reaction front. It can be expected that a bed preheat rather than a heated injection strategy will be preferable

The inlet fluid concentration is increased to 2×10^{-3} mol/dm^3 (30 mol% in N_2 at STP). The wave model predicts that the thermochemical wave will be faster than the thermal wave in this case; $V_{T/C} = 1.615 \times 10^{-3}$, $V_T = 4.651 \times 10^{-4}$ & $\Delta T_c = 250.6$K.

5.4.1 *Hot Fluid into a Preheated Bed*

The composition profiles in Fig. 5-27 for the concentrated case show that the thermochemical waves are sharper than in the dilute case. The thermochemical waves are more closely related to the "ideal case" in the wave model. This means the system is closer to equilibrium since higher temperatures are reached. However, the thermal wave preserves its shape as there is no reaction associated with the thermal wave. It can further be observed that the thermal wave spreads slightly, the result of numerical dispersion.

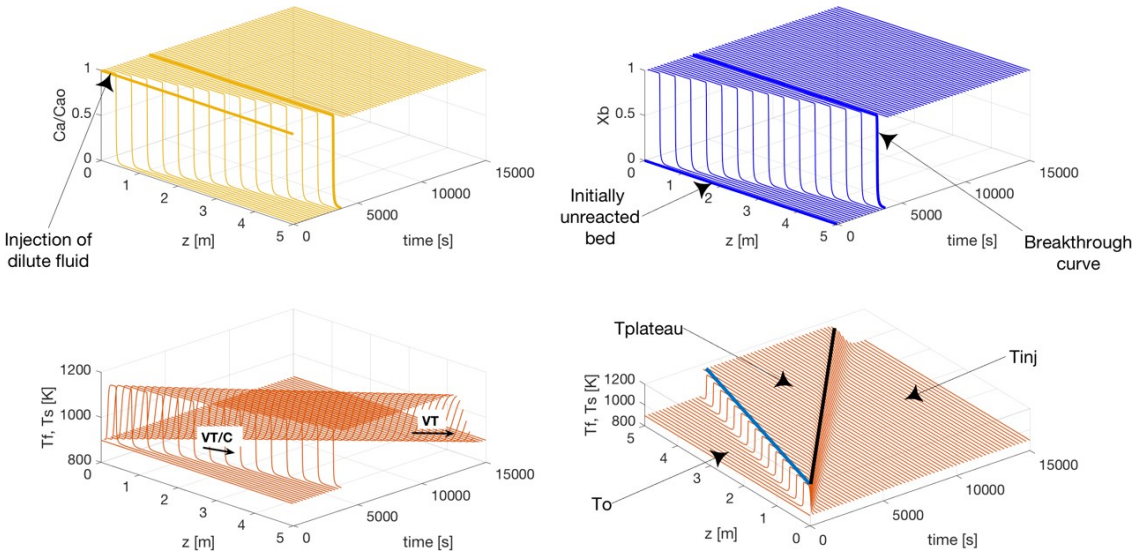

Figure 5-26: 3D plot of dependent variables with independent variables (concentrated)

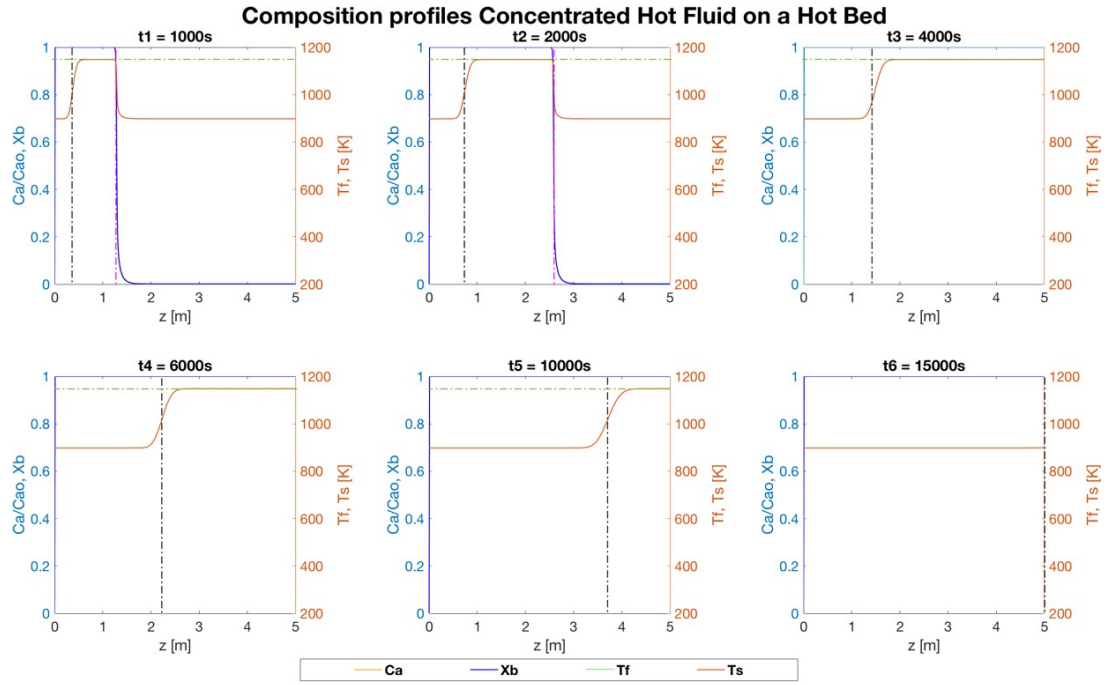

Figure 5-27: Composition profiles for hot fluid into a hot bed with Z_T (black dashed), $Z_{T/C}$ (purple dashed), $T_{plateau}$ (green dashed). T_o = 898K, T_{inj} = 898K

5.4.2 *Cold Fluid into a Preheated Bed*

In this scenario, the thermochemical wave moves ahead of the thermal wave into a hot unreacted bed, Fig. 5-28. The trailing cold thermal wave displays a much bigger temperature drop because it goes from the cold injection temperature to the plateau temperature. The reaction is very stable since it runs at a relatively temperature.

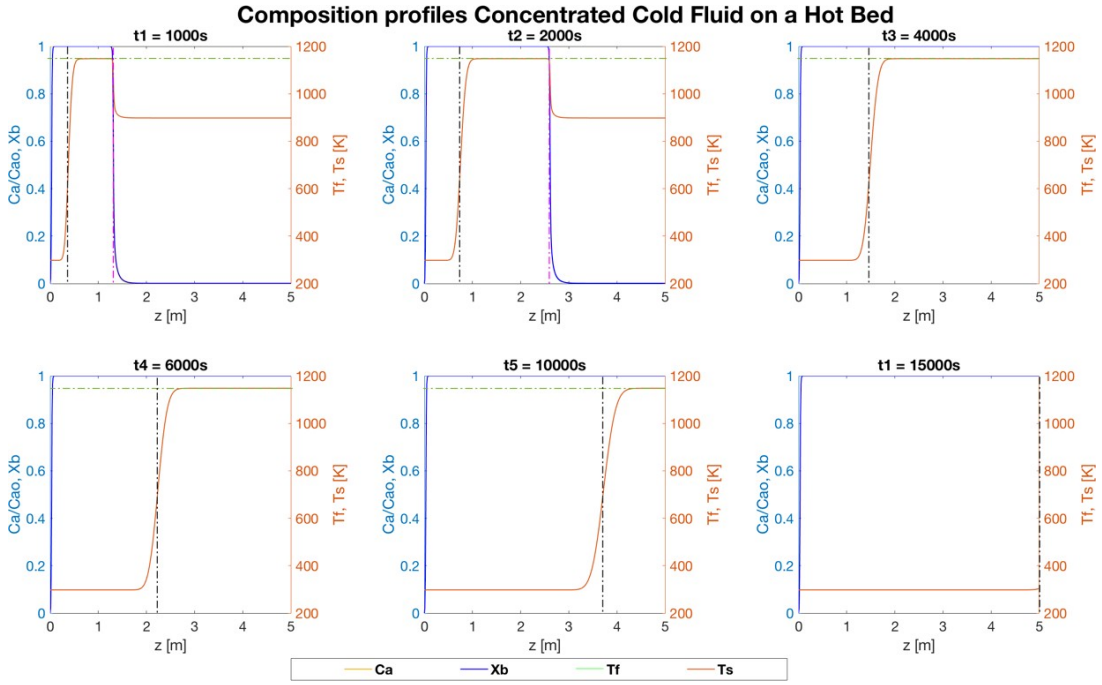

Figure 5-28: Composition profiles for cold fluid into a hot bed with Z_{T1} (black dashed), $Z_{T/C}$ (purple dashed, $T_{plateau}$ (green dashed). T_o = 898K, T_{inj} = 298K

Time (s)	Wave Model			Simulation Results		
t	Z_{T1}	Z_{T1}	ΔT_c **(K)**	$Z_{T/C}$	Z_{T1}	ΔT_c **(K)**
1.0 x 10^3	1.29	0.37	250.6	1.3	0.35	250
2.0 x 10^3	3.23	0.93	250.6	3.3	0.95	250
4.0 x 10^3	5.1	1.49	250.6	5	1.5	250
6.0 x 10^3	-	2.28	250.6	-	2.2	250
1.0 x 10^4	-	3.7	250.6	-	3.7	250
1.5 x 10^4	-	-	250.6	-	-	250

Table 5-7: Comparison of distances travelled by thermal and thermochemical waves & plateau temperature for concentrated cases

The numerical simulations are in good agreement with the wave model predictions as shown in Figure 5-28 and Table 5-7.

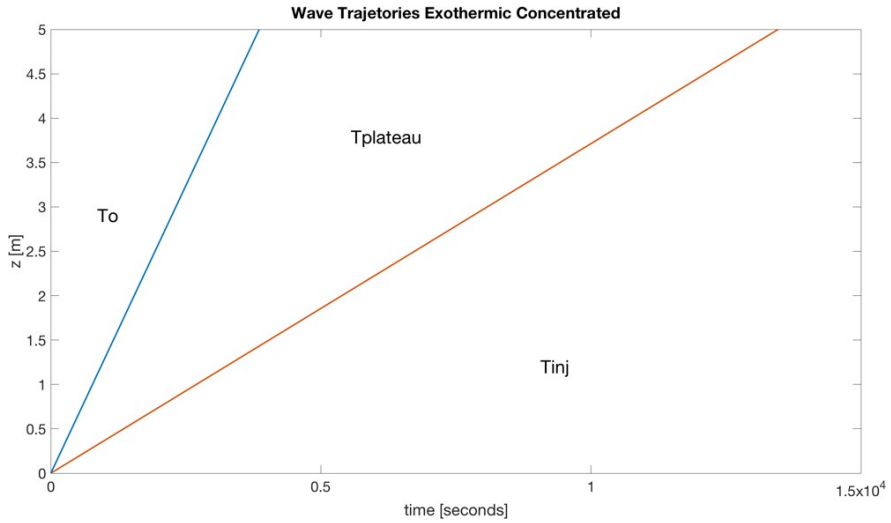

Figure 5-29: Distance-time diagram with thermochemical wave (blue), thermal wave (red) for concentrated case

5.4.3 Hot Fluid into a Cold Bed

The two cases to be examined; T_o above ignition temperature and T_o far below the ignition temperature. If the bed temperature is above to the ignition temperature, the thermochemical wave is running into a sufficiently hot region to guarantee reaction. The reaction is then expected to be stable, as shown in Fig. 5-28. On the other hand, if the bed temperature is low, the fluid does not react completely with the solid and passes through the bed more rapidly, giving a partial reaction (Figs. 5-30 and 5-31). The reaction starts to occur in the early parts of the bed when the hot fluid is injected. The thermochemical wave is retarded due to the partial reaction, which gives rise to a higher plateau temperature. In the region where the temperature is low, the reaction rate is low, and the reactant concentration is correspondingly high. Due to heat released locally by the incomplete reaction, the temperature in the reaction zone grows well beyond the predicted temperature rise for a complete reaction, but the actual thermochemical wave velocity and the thermochemical temperature rise are adequately predicted by equation (3.24) respectively (See Table 5-8).

Two cases to be analysed for partial concentration:

- T_{inj} and T_o are both above ignition temperature.
- T_o is below ignition temperature but injected fluid temperature (T_{inj}) is above ignition temperature, which results in partial concentration of the fixed bed.

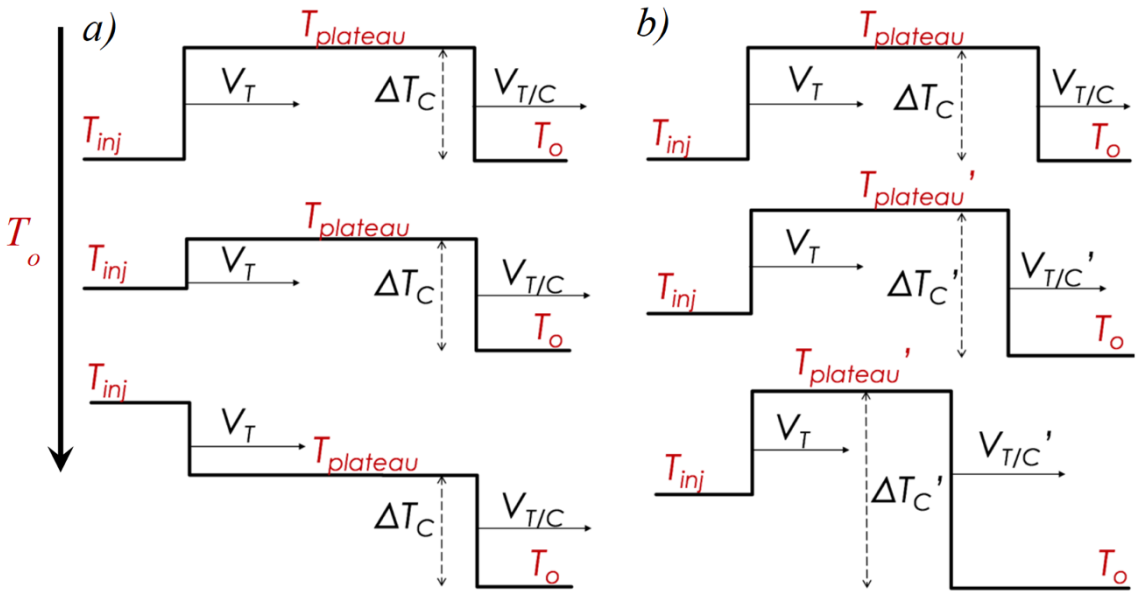

Figure 5-30: Temperature profiles for hot fluid into cold bed (concentrated) with T_o reducing (a) T_o, $T_{inj} > T_{ign}$ (b) $T_o < T_{ign}$, $T_{inj} > T_{ign}$

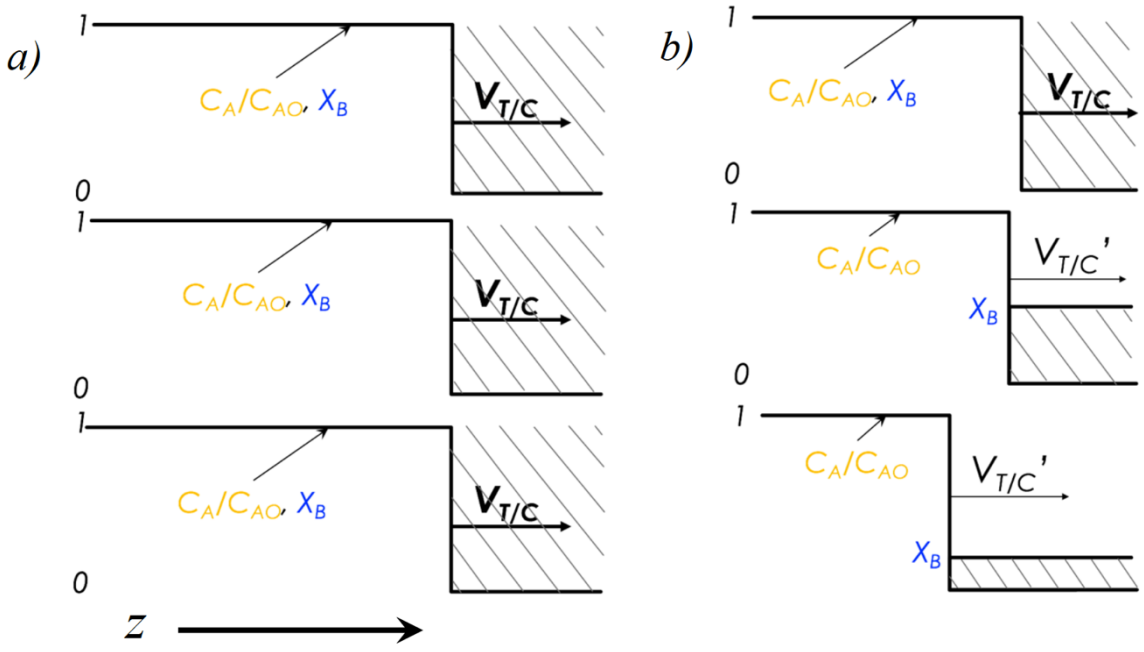

Figure 5-31: Concentration profiles for hot fluid into cold bed (concentrated) with T_o reducing (a) T_o, $T_{inj} > T_{ign}$ (b) $T_o < T_{ign}$, $T_{inj} > T_{ign}$

Reacted fluid

Case (a): Both the injected fluid temperature and the bed temperature are always above ignition temperature. The first diagrams describe the concentration and temperature profile of a heated fluid injected into a hot bed. If T_{inj} is kept constant and the bed temperature is lowered, the thermochemical temperature rise does not change leading to the concentration profiles in Figure 5-31(b) and 5-32(b). These profiles are only expected if both the reduced bed temperature and injected fluid temperature are above the ignition temperature. Fig. 5-30(a) shows the associated concentration profiles. T_{inj} is always assumed to be above ignition temperature, complete concentration and conversion is expected. Fig. 5-32 shows the numerical simulation of case (a).

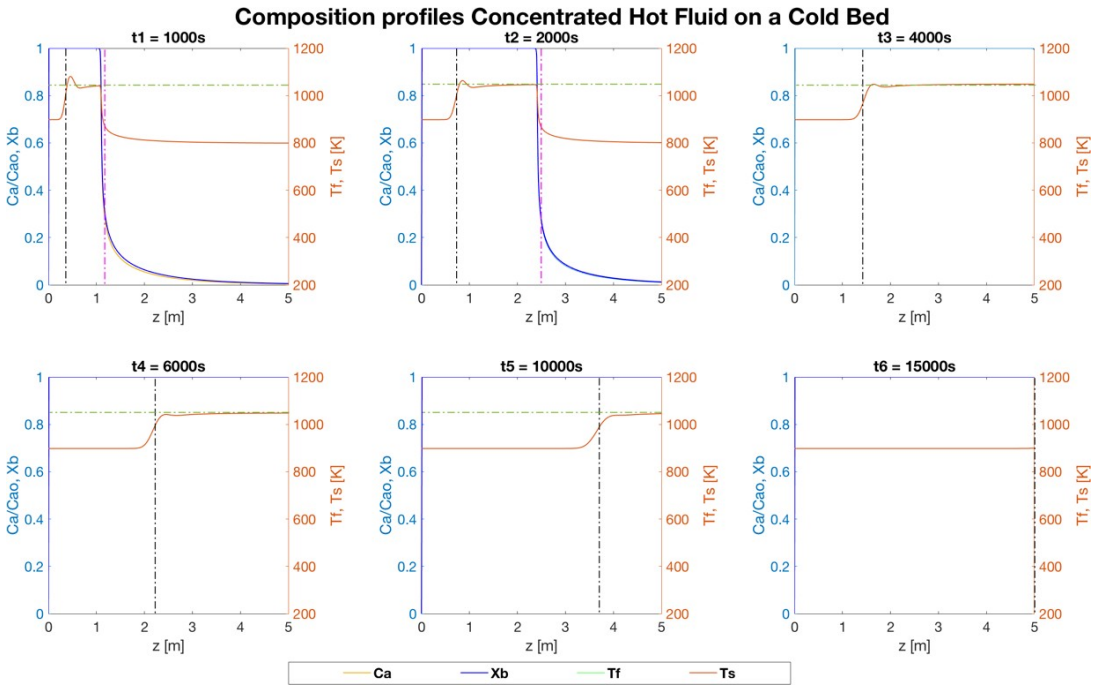

Figure 5-32: Composition profiles for hot fluid into a cold bed with Z_T (black dashed), $Z_{T/C}$ (purple dashed), $T_{plateau}$ (green dashed). For concentrated hot fluid into a cold bed

Case (b): The injected fluid temperature and the bed temperature are initially set to ignition temperature. If T_{inj} is kept constant (above the ignition temperature) and T_o is lowered below ignition temperature, only part of the concentrated oxygen is reacting with the carbon, as a consequence the thermochemical wave (where the reaction occurs) travels slower.

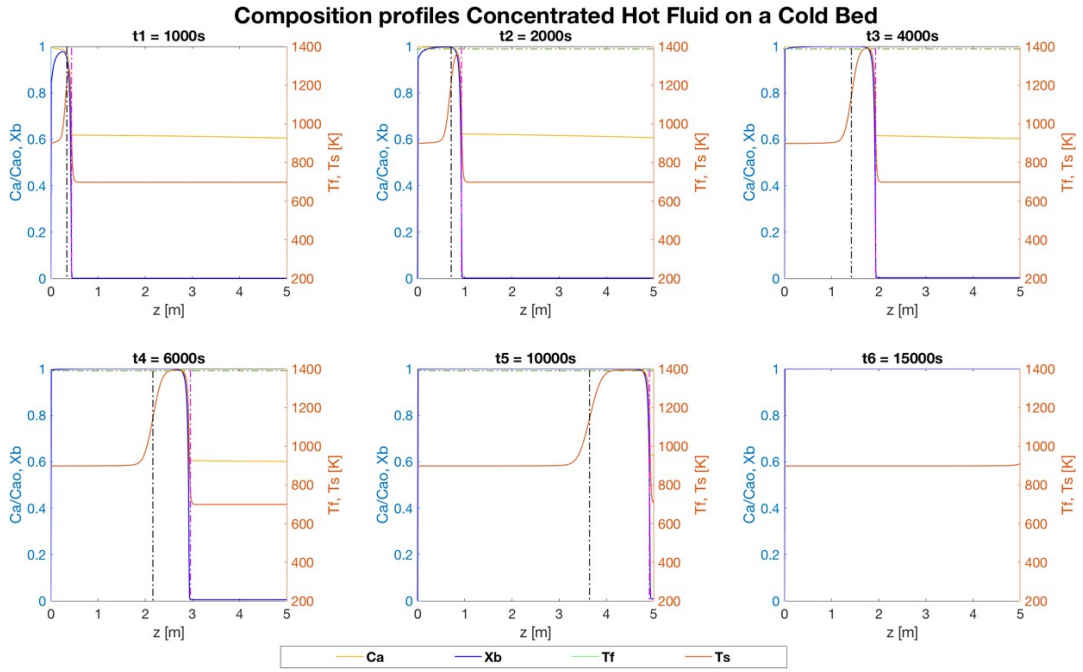

Figure 5-33: Composition profiles for concentrated hot fluid into a cold bed with Z_T (black dashed). T_o = 698K, T_{inj} = 898K

Time (s)	Wave Model			Simulation Results		
t	$Z_{T/C}$'	Z_{TI}	ΔT_c (K)	$Z_{T/C}$	Z_{TI}	ΔT_c' (K)
1.0 x 10^3	0.49	0.37	-	0.5	0.35	-
2.0 x 10^3	0.99	0.93	701.5	0.9	0.95	690
4.0 x 10^3	1.97	1.49	701.5	1.9	1.5	700
6.0 x 10^3	2.95	2.28	701.5	3.0	2.2	700
1.0 x 10^4	4.93	3.7	701.5	4.9	3.6	700
1.5 x 10^4	-	-	701.5	-	-	700

Table 5-8: Comparison of distance travelled by thermal, thermochemical waves & plateau temperature for concentrated case hot fluid into a cold bed (698K)

Similar to the dilute case, there is an uncharacteristic temperature rise associated with the thermochemical wave. This behaviour is shown in Figure 5-33. The partial concentration, $\bar{C}$ was found to be 58%, giving a new thermochemical wave velocity $V_{T/C}$ = 5.01 x 10^{-4} m/s and ΔT_c'= 700K. The lower the bed temperature, lower the concentration and higher temperature rises are expected as shown in Figure 5-30(b) and Figure 5-31(b). Table 5-7 compares the wave model predictions to the measured values from the numerical simulation.

The wave trajectories for the concentrated cases mentioned are shown in Fig. 5-34 is the same except for the hot fluid into a cold bed case ($T_o < T_{inj}$) where there is a partial concentration. For the other cases, the velocities of the thermal and thermochemical waves are the same, there is a faster thermochemical wave passing through the reactor shown as a steep straight line in Figure 5-34 and a less steep thermal wave. The diagram summarises in a succinct way, the full development of the waves. The wave model accurately predicts the wave trajectories for the concentrated cases. The partial concentration case gives a slower thermochemical wave, which is represented as a flatter line on the distance-time diagram in Figure 5-29. The thermal wave velocity does not change. The narrow region between the two waves is the new plateau temperature is also shown.

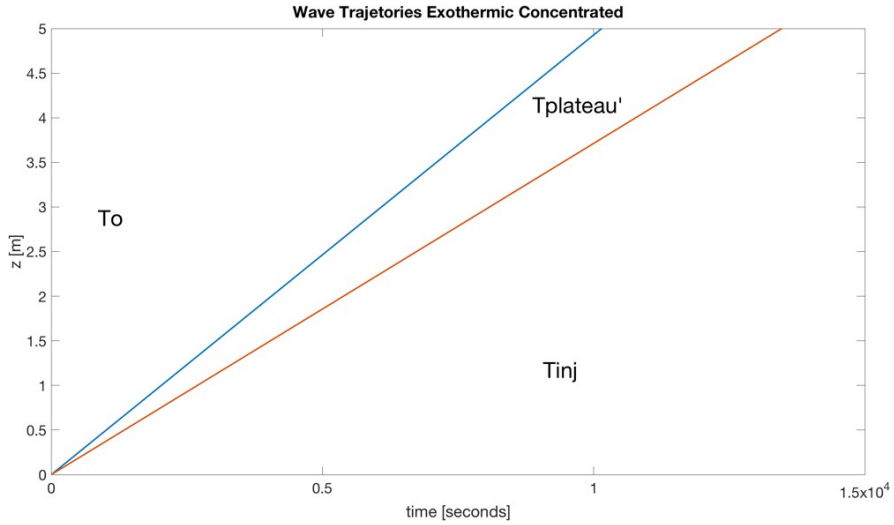

Figure 5-34: Distance-time diagram with thermochemical wave (blue), thermal wave (red) for concentrated hot fluid into a cold bed case

5.4.4 Hot Fluid Pulse into a Preheated Bed

The final scenario is the injection of a hot fluid pulse into a hot reactor bed. The temperature of injection is reduced from 898K to 298K after 0.6h. Therefore, a trailing cold thermal wave arises. The wave model predicts that the two thermal waves will not meet and both will travel at the same velocity V_T behind the thermochemical wave (Fig. 5-35).. The trailing thermal waves have no effect on the faster thermochemical wave ahead.

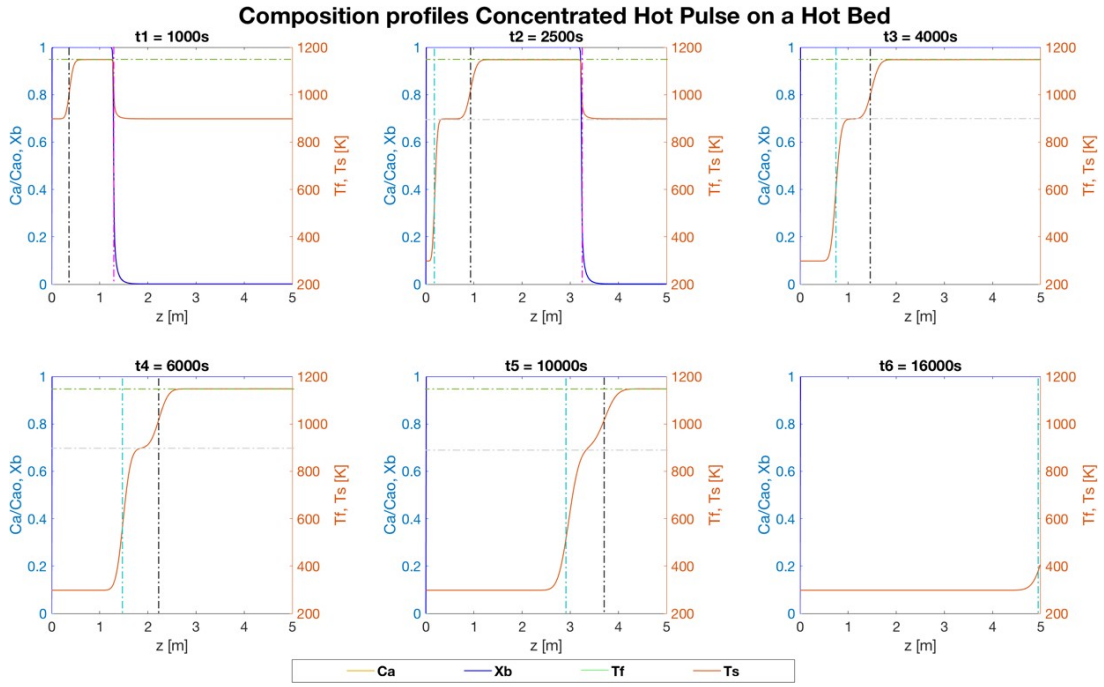

Figure 5-35: Composition profiles for hot fluid pulse into a hot bed with Z_{T1} (black dashed), Z_{T2} (blue dashed), $Z_{T/C}$ (purple dashed), $T_{plateau}$ (green dashed), T_{fo} (grey dashed). T_o = 898K, T_{inj} = {898K,298K}

Time (s)	**Wave Model**				**Simulation Results**			
t	$Z_{T/C}$	Z_{T1}	Z_{T2}	ΔT_c ***(K)***	$Z_{T/C}$	Z_{T1}	Z_{T2}	ΔT_c ***(K)***
1.0 x 10^3	1.29	0.37	-	250.6	1.3	0.35	-	250
2.5 x 10^3	3.23	0.93	0.18	250.6	3.3	0.95	0.2	250
4.0 x 10^3	5.1	1.49	0.74	250.6	5	1.5	0.75	250
6.0 x 10^3	-	2.28	1.49	250.6	-	2.2	1.5	250
1.0 x 10^4	-	3.7	2.97	250.6	-	3.7	3	250
1.6 x 10^4	-	-	5.1	250.6	-	-	5	250

Table 5-9: Comparison of distance travelled by thermal and thermochemical waves & plateau temperature for concentrated hot fluid pulse into a preheated bed

This confirms that a heated pulse or indeed heated injection strategy in general confers no benefit, it is the preheat of the bed that is important. The thermal wave is not self-sharpening as it spreads while travelling across the reactor bed, due to dispersive effects. Table 5-9 shows good agreement despite the spreading of the trailing cold thermal wave as the mid-point of the wave is tracked, which is unaffected by dispersion.

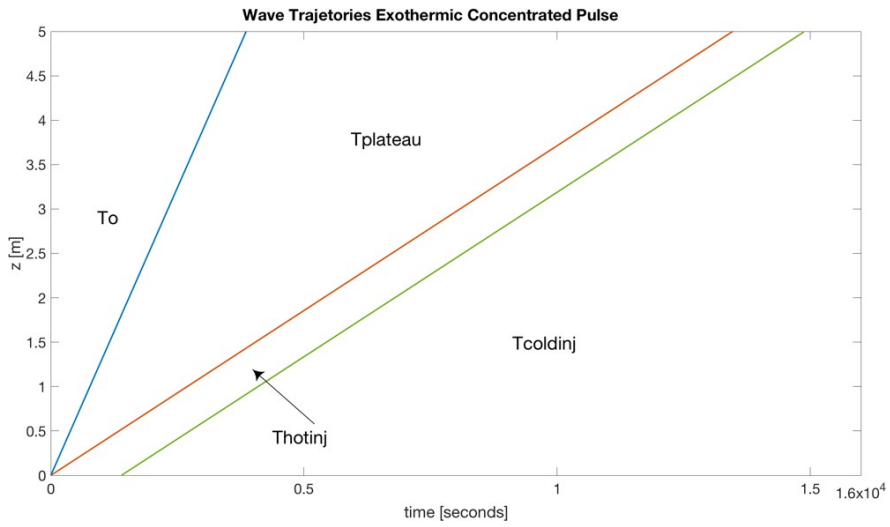

Figure 5-36: Distance-time diagram for hot fluid pulse into a hot bed (concentrated) with thermochemical wave (blue), thermal wave 1 (red) thermal wave 2 (green)

5.4.5 Pre-heated Bed strategy

In the cases where a preheated reactor bed is used, the bed is heated with a nitrogen stream before the reactive fluid is injected. The Pre-heated bed strategy involves injecting concentrated cold fluid before the leading thermal wave associated with the pre-heat nitrogen stream leaves the reactor bed. The resulting thermochemical wave is now faster than the thermal wave. The optimum strategy is to inject the concentrated fluid at just the right time that the thermochemical wave meets the leading thermal wave at the reactor exit. The wave model was used to calculate the correct time to inject the concentrated cold fluid:

$$t_{injection} = t_T - t_{T/C} \tag{5.5}$$

where $t_T = 14000s$ and $t_{T/C} = 2600s$.

Therefore, the time to inject cold dilute fluid, $t_T = 11400s$.

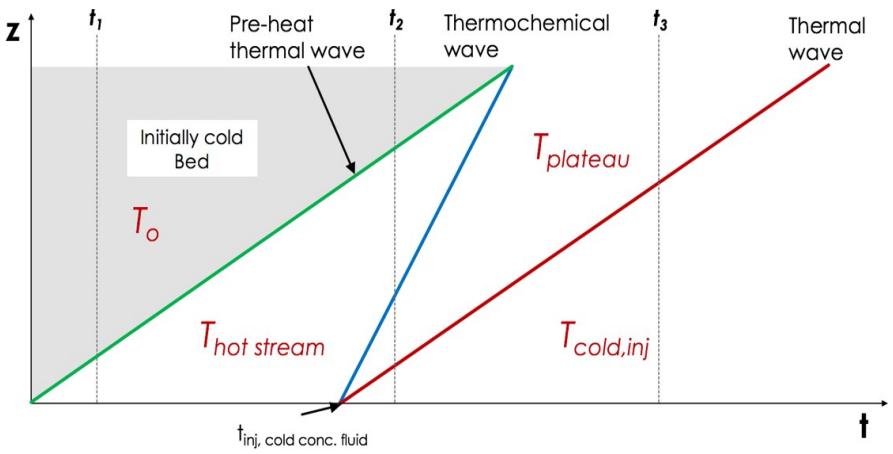

Figure 5-37: Distance-time diagram for pre-heated bed strategy (concentrated)

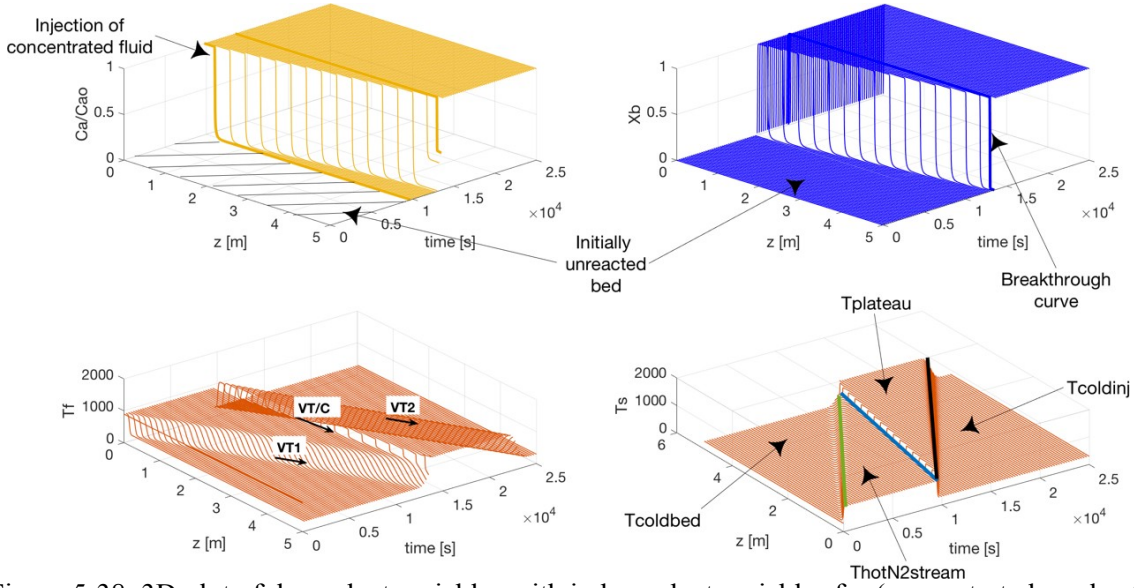

Figure 5-38: 3D plot of dependent variables with independent variables for (concentrated pre-heat strategy)

The nitrogen stream is represented as a pre-heat thermal wave in Fig. 5-37. Figs. 5-38 and 5-34 shows a simulation with the injection of cold concentrated fluid at $t_{injection}$. This leads to 0.83h less heating of nitrogen than in the previous heating strategy, in which the bed is completely preheated first whilst decoking and regenerating the bed completely. Table 5-10 shows the wave model gives accurate predictions to the numerical simulations. Again, this shows the usefulness of the wave approach as an initial design tool to screen potential operating schemes.

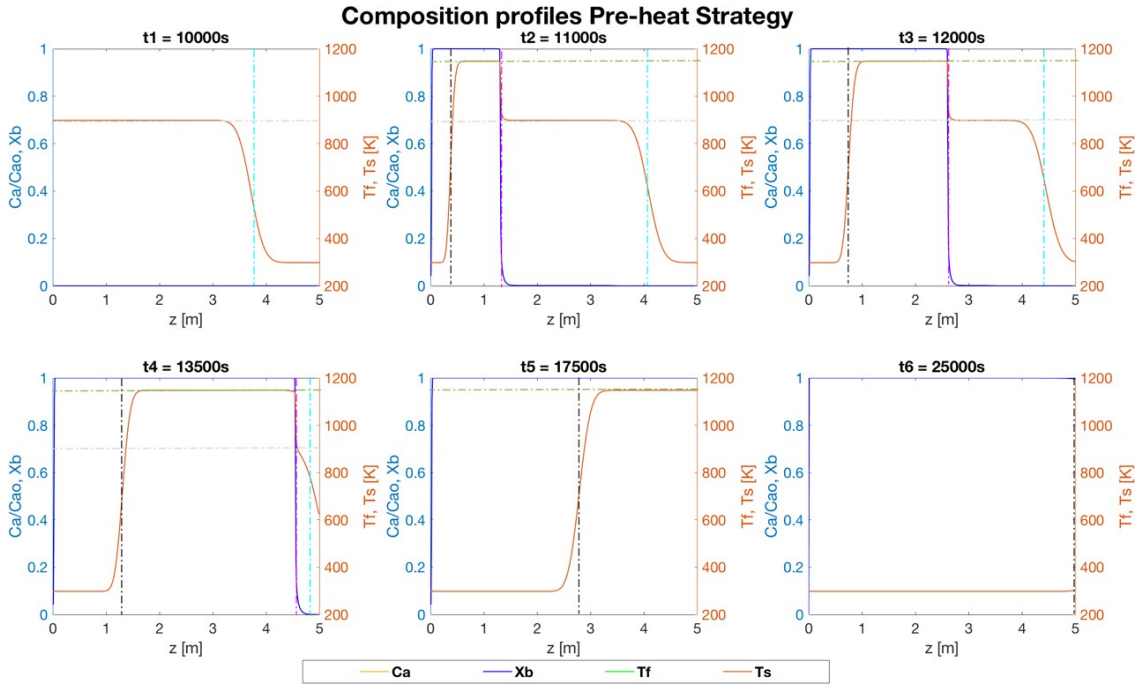

Figure 5-39: Composition profiles with Z_{T1} (blue dashed), Z_{T2} (black dashed), $Z_{T/C}$ (purple dashed), $T_{plateau}$ (green dashed), T_{fo} (grey dashed) for concentrated pre-heated bed strategy

Time (s)	Wave Model				Simulation Results			
t	$Z_{T/C}$	Z_{T1}	Z_{T2}	ΔT_c (K)	$Z_{T/C}$	Z_{T1}	Z_{T2}	ΔT_c (K)
1.0 x 10^4	-	3.71	-	250.6	-	3.8	-	250
1.1 x 10^4	1.29	4.08	0.37	250.6	1.2	4.1	0.3	250
1.2 x 10^4	2.59	4.46	0.74	250.6	2.6	4.4	0.7	250
1.35 x 10^4	4.54	5.00	1.29	250.6	4.5	4.9	1.2	250
1.75 x 10^4	-	-	2.78	250.6	-	-	2.8	250
2.5 x 10^4	-	-	-	-	-	-	-	-

Table 5-10: Comparison of distance travelled by thermal and thermochemical waves & plateau temperature for concentrated pre-heated bed strategy

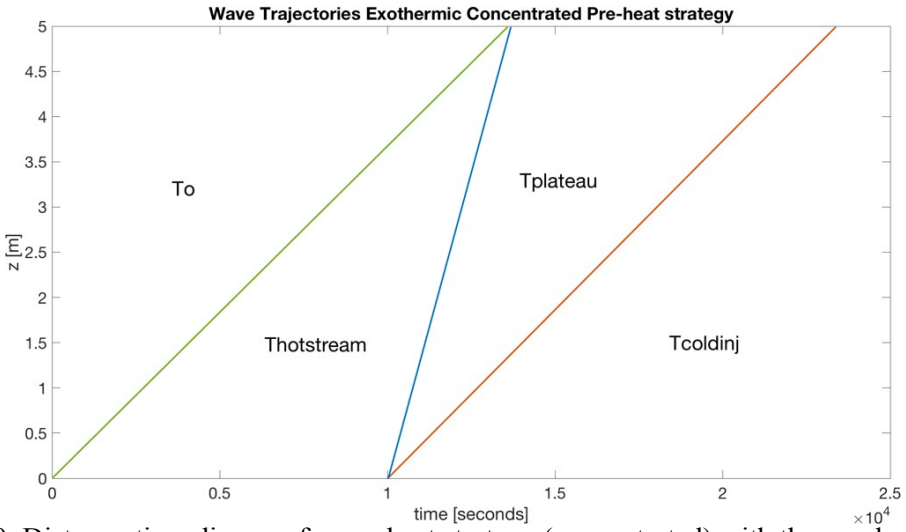

Figure 5-40: Distance-time diagram for pre-heat strategy (concentrated) with thermochemical wave (blue), thermal wave 1 (green) thermal wave 2 (red) for concentrated pre-heated bed strategy

5.4.6 *Hot Spot*

The case for which $V_T = V_{T/C}$ was investigated. This occurs at a particular value of inlet fluid concentration, for which the denominator in equation (3.23) in zero. In the decoking case, $C_{AO} = 5.74 \times 10^{-4}$ mol/dm^3 is the critical concentration, as shown in Fig. 5-3 For this value ΔT_C tends to keep increasing as shown in Fig. 5-41.

It is clear that the temperature rise due to the heat generated by the thermochemical wave depends on the difference between V_T and $V_{T/C}$: if the difference is large, the heat liberated by the reaction is distributed over an increasing portion of the bed, leading to a moderate temperature increase. Conversely, if $V_{T/C}$ approaches V_T, the heat liberated accumulates in a small portion of the bed, leading to high temperature increase, the heat liberated accumulates in a very narrow zone, with excessively high peak temperatures.

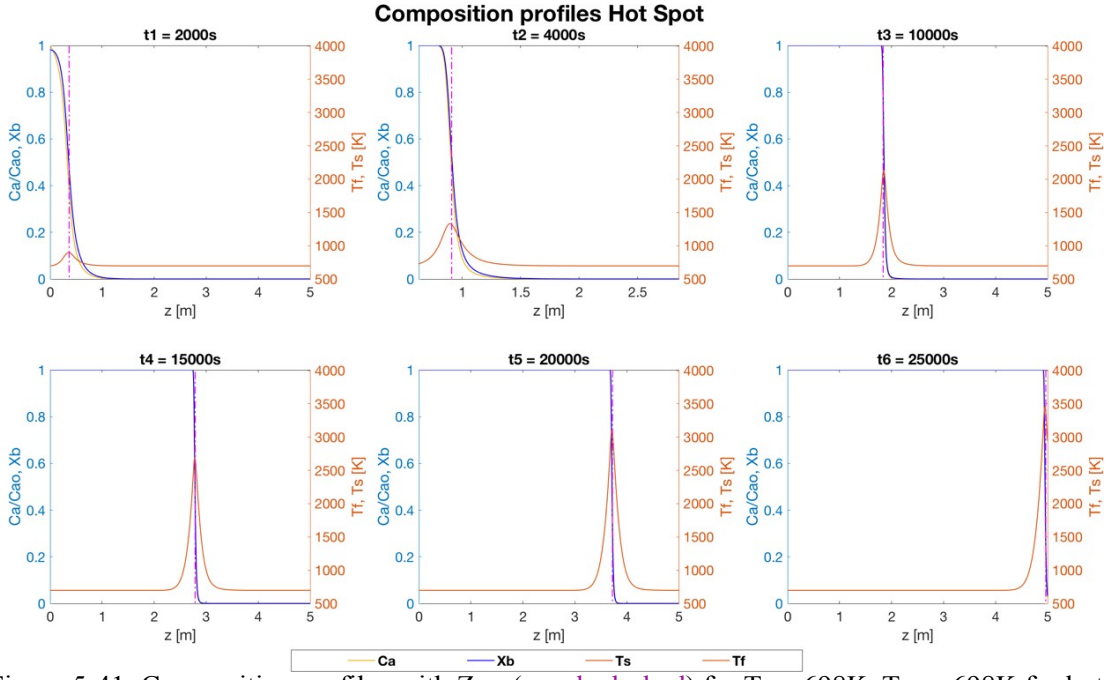

Figure 5-41: Composition profiles with $Z_{T/C}$ (purple dashed) for T_o = 698K, T_{inj} = 698K for hot spot

Time (s)	Wave Model	Simulation Results
t	$Z_{T/C}$	$Z_{T/C}$
2.0 x 10^3	0.39	0.4
4.0 x 10^3	0.77	0.8
1.0 x 10^4	1.84	1.8
1.5 x 10^4	2.81	2.8
2.0 x 10^4	3.78	3.7
2.5 x 10^4	4.81	4.9

Table 5-11: Comparison of distance travelled by thermal, thermochemical waves & plateau temperature for concentrated case hot spot

When the concentration of the fluid is set to the critical concentration, The wave model predicts a delta function in temperature, no plateau will be formed.

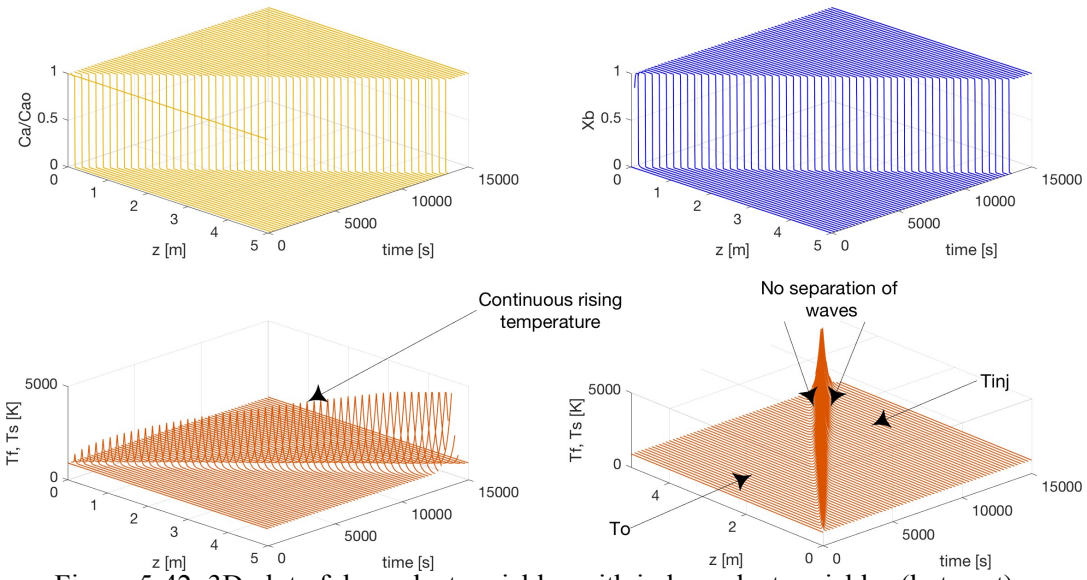

Figure 5-42: 3D plot of dependent variables with independent variables (hot spot)

The thermochemical and thermal waves travel together through the reactor with no separation as shown in Fig 5-42 and Fig 5-43. Thus, the distance-time diagram shows the thermochemical wave superimposed on the thermal wave, as they are travelling at the same velocity. Due to heat dispersion, there is however a constant spread of the travelling thermal and thermochemical waves. So that a true delta function is not achieved.

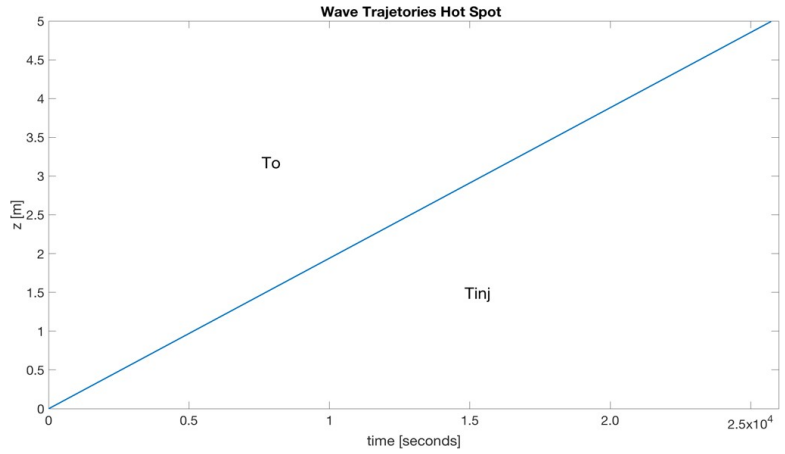

Figure 5-43: Distance-time diagram for hot spot with thermal & thermochemical wave (blue)

5.5 Summary and comparison with other works

A non-linear wave propagation model has been developed which can be used to predict the dynamic behaviour of fixed bed systems during fluid-solid reactions. The wave model predicts the full numerical simulations well in terms of the position of thermal and reactive wave fronts, and the maximum temperature in the bed. It also provides an initial design and operational tool using concentration of reacting fluid, injection and initial bed temperatures as adjustable parameters and reduced strategy when required. A coherent thermochemical wave was attained, travelling at a constant velocity. It is also shown that under certain scenarios: the reaction fails to occur completely. Nevertheless, in these cases, the wave model still has value. The wave model is used to minimise the energy requirements for the decoking process. Coke combustion with a large gas flow rate suggested by Behroozi et al., 2012 will increase the rate of catalyst generation, but at the cost of large flow resistance and low outlet temperature, which consumes energy on the one hand and lowers the energy of the coke combustion heat. The results from the physical model show that the heating of the catalyst bed to ignition temperature is not necessary. The heat generated from the reaction heats the bed ahead of the reaction. Therefore, a cold reactor bed can be used. This

saves the unnecessary energy used in heating of the reactor bed. Saving 65 mins of catalyst bed heating employed in Toghyani et al., 2015. A spiral tube heater was used to heat the raise the catalyst bed to the ignition temperature. The danger of low bed temperature is the large temperature drop from the plateau temperature to the bed temperature (Daggash, 2019). This could lead to radiative effects as well as a large change in the density of the oxygen pumped. Zhang at al., 2010 used a moderately high reactor bed and the oxygen pumped still needs to be heated to the ignition temperature regardless for the decoking process to occur. The current thesis shows the continuous heating of a diluted oxygen feed is not necessary for complete regeneration.

Modelling of decoking in packed bed reactors has been investigated by various authors in recent years. Kern and Jess (2004) studied the effect of changing parameters on the regeneration of a packed bed. Kern and Jess successfully modelled the coke burn off process and derived the wave velocities and adiabatic temperature rise in the packed bed but failed to use the wave model as a tool, rather a computer software was used. The advantage of the wave model is the simplicity of it rather than blow-by-blow numerical simulations whilst still giving an insight into cause and effect. Xinping (2010) used concentration of oxygen and inlet temperature, and initial temperature as controlled parameters to ensure safe regeneration of the fixed bed by numerical interpolation and compared the results with experimental values. Again, this was not time and cost effective and gave no insight into reactor dynamics.

It was also shown under certain scenarios; the reaction will fail to occur completely but in these cases the wave model still has value. This incomplete reaction leads to a temperature rise within the reactor across the thermochemical wave. This phenomenon has been observed by many researchers namely Levenspiel (1999), Jaree (2001), Eigenberger (2000), Eigenberger, Kolios (2004). Levenspiel proposed coupling exothermic and

endothermic reactions termed the RE-GAS process for coal gasification.

The idea was taken up by Kulkarni and Dudukovic (1996, 1998) and Eigenberger, Kolios (1999), but similar problems with excessive peak temperatures and a narrow reaction zone was encountered. The results show that the wave model can accurately predict the temperature rise in the fixed bed reactor as well as the position of the temperature rise. The responses to the cold injection of dilute reactive fluid showed the temperature increases in a narrowly sharp zone, where the reactant is consumed. Conversely, during the injection of concentrated reactive fluid into a cold reactor bed gives an incomplete reaction and the same temperature rise problem. The positions of the temperature rise due to the incomplete reaction is coherent with the thermochemical wave allowing a simple material balance across the wave. A major contribution of the research was the use of the wave model to explain and accurately predict the temperature rise due to incomplete reactions in finite rate-controlled fluid-solid reactions in fixed bed reactors. This shows promise in the use of the wave model design and control exothermic fluid-solid systems in fixed bed reactors.

The current strategies aim to make regeneration time should be as short as possible, because the decoking process is capital intensive in terms of running cost. This requires continuous heating of the injected oxygen, which is energy intensive. Moreover, a long period of regeneration time is not economically desirable. The coke removal from the catalyst particle should be done so that the catalyst could recover its original performance completely (Mehraban and Shahraki, 2019). The proposed reduced heating strategy constitutes heating the injected dilute oxygen for a period of time before injecting cold dilute oxygen. The strategy constitutes delaying the cold dilute fluid long enough so that the trailing cold thermal wave meets the thermochemical wave at the end of the reactor bed. When the cold dilute oxygen is injected, a thermal wave is generated which travels faster than the thermochemical wave. The key to this strategy is the time when the cold

oxygen is injected into the reactor bed to avoid the cold injected fluid thermal wave from overtaking the thermochemical wave. If the trailing thermal wave overtakes the thermochemical wave, there is a risk of overheating the reactor and an incompletely regenerated bed. The wave model equations in Daggash, 2019 are used to calculate the time it takes a pure thermal wave (t_T) and the thermochemical wave ($t_{T/C}$) to travel through the reactor. The cold oxygen is injected at $t_{T/C} - t_T$. This will guarantee the thermal wave to meet the thermochemical wave at the reactor bed exit. Daggash, 2019 shows the numerical simulation of the reduced heating strategy. In the case of the decoking process, t_T = 14200s which is fixed by the thermal capacities of the coke present in the catalyst and the injected oxygen. The regeneration time for the process is $t_{T/C}$ = 38850s. Therefore, cold dilute oxygen should be injected at 24650s, saving 14200s of heating time of the injected oxygen. This ultimately saves 36.6% of the energy required to heat the injected oxygen. To calculate the amount of energy saved, the mass flow rate (m) can be calculated using the density (ρ), specific heat capacity (cp) of the oxygen and superficial gas flow velocity (u). The cross-sectional area (A) is based on a circular cross-section with a 0.5 m radius.

$$E = m.cp.\Delta T$$

$$\text{Where } m = \rho.u.A = 7.9 \text{ kg/s}$$

$$E = 5.05 \text{ MW}$$

If the thermochemical wave approaches the speed of the thermal wave, the reduced heating strategy becomes even more useful as the cold oxygen can be injected even earlier. Therefore, even more energy saving. A safety procedure needs to be in place when the temperature of the injected oxygen is reduced giving a large temperature drop. This could cause both radiative effects and even heat flow in the opposite direction due to the steep temperature gradient. A possible solution to this is step-wise reduction in the injected oxygen temperature over a short period of time. The same strategy is applied to the pyrite hydrogenation process.

Chapter 6

Endothermic Gas-Solid Reactions

Chapter 6 investigates different injection strategies for an endothermic gas-solid system; reduction of iron pyrite by hydrogen. Injection strategies included in this chapter involved injection of fluids which are colder, warmer and at the same temperature as the initial bed temperature. The thermochemical waves are also shown to travel with a constant width predicted in Chapter 4 except when cold spot temperatures are reached. When the temperature approaches very cold temperatures, the thermochemical waves split across the temperature plateau. The pre-heat strategy is shown to also be energy saving in the endothermic system as well.

6.1 Transient time before coherence for pyrite reduction

The same analysis was conducted for the reduction of pyrite process. There are a couple of differences in the reduction of pyrite process, namely, the endothermic nature of the process which limits the reaction progressing based on the temperature of the hydrogen injected to the fixed bed of solids and the diffusion through the ash layer of he pyrite is also significant on the overall reaction rate. The injected temperature also fixes the concentration of the injected hydrogen. The concentration of hydrogen is chosen to be as high as possible (0.0018 mol/dm^3) whilst still limiting the temperature of the pyrite to at least 600K. Below this temperature, the fixed bed of pyrite does not react completely. Using the experimental values in the appendix, Table 6-1 is extracted from the physical model simulations. The table serves as the protocol to estimate the transient time for the k'/ u values given. If a lower concentration or higher temperature is used, the lowest temperature of the pyrite and hydrogen is even higher. Constant pattern is approached even

(5.6)

faster. Therefore, Table 6-1 is a worst-case scenario for the pyrite process with all other physical parameters given in Table 6-2.

ko sim/ko exp.	z_R	DEO sim/ DEO exp.	z_R	usim/uexp.	z_R
1.0	0.19	1.0	0.19	1.0	0.19
0.5	0.47	0.5	0.21	2.5	0.45
0.2	0.88	0.1	0.52	5	0.81
0.1	1.18	0.05	0.87	10	1.22
0.05	1.71	0.01	1.23	20	1.08
0.01	3.80	0.005	1.75	50	3.54

Constant pattern	k'/u	Constant pattern	k'/u
$0 < t_D < 0.1$	9.47×10^9	$0 < t_D < 0.1$	7.47×10^9
$0 < t_D < 0.125$	5.23×10^8	$0.1 < t_D < 0.125$	4.43×10^8
$0 < t_D < 0.25$	3.01×10^8	$0.125 < t_D < 0.25$	2.77×10^8
$0 < t_D < 0.5$	9.47×10^7	$0.25 < t_D < 0.5$	9.34×10^7
$t_D = 1$	1.85×10^7	$t_D = 1$	1.80×10^7

Table 6-1: Reaction wave width and Transient times for k'/u for Pyrite reduction (z_D, t_D)

After proper model validation, the same parameters reported in Table 6-1 were used to evaluate the dynamic behaviour of the pyrite reduction of a fixed bed of solids (Philinis, 1957). Below are the parameters of the system as given in the literature review. Units are given in the beginning of the thesis.

Parameter	Definition	Pyrite	Units
a	Stoichiometric coefficient of fluid	1	-
b	Stoichiometric coefficient of solid	1	-
C_A	Reactive fluid concentration		$kmol/m^3$
C_{AO}	Injected fluid concentration	2.0×10^{-3}	$kmol/m^3$
c_f	Specific heat capacity of fluid	5.0×10^2	J/kmolK
c_s	Specific heat capacity of solid	3.0×10^6	J/kmolK
D_{EO}	Diffusion constant through ash layer	2.1×10^{-8}	m^2/s

E_A	Activation energy for surface rate of reaction	1.3×10^8	J/kmol
E_{DE}	Activation energy for diffusivity	3.4×10^7	J/kmol
E_k	Activation energy for fluid to mass transfer	1.0×10^7	J/kmol
h	heat transfer coefficient between solid and fluid	3000	W/mK
k'	Composite overall rate constant	-	m/s
k_O	Surface rate constant	1.50×10^4	m/s
k_{TO}	Mass to fluid mass transfer coefficient	56.61	m/s
L	Length of reactor bed	5	m
M_B	Molecular mass	120	g/mol
n	Number of nodes in numerical simulation	1000	-
n_p	Number of particles per unit volume	6.11×10^{12}	-
P	Pressure of injected fluid		Pa
R	Universal gas rate constant	8314	J/kmolK
r_b	mass of coke per volume of catalyst	5000	kg/m^3
r_c	Radius of shrinking core		m
R_s	Radius of particle	2.5×10^{-4}	m
t_D	Dimensionless time		-
T	Time to complete reaction		s
T_f	Temperature of reacting fluid	908	K
T_s	Temperature of reacting solid	908	K
u	Superficial gas velocity in the direction of flow	1.0	m/s
V	Volume of injected fluid		m^3
V_R	Velocity of reaction wave		m/s
V_T	Velocity of thermal wave		m/s
$V_{T/C}$	Velocity of thermochemical wave		m/s
X	Fraction of reacting solid	41.7	-
X	Average conversion of reacted bed		-
X_B	Reacting solid conversion		-
X_{O2}	Fraction of injected O_2 in air		%
z_D	Dimensionless distance		-
Z	Distance travelled after time t		-
ΔH	Enthalpy of reaction	38×10^6	J/kmolK
ΔT_C	Temperature rise associated with chemical reaction	-298	K

ε	Porosity of fixed bed	0.27	-

Table 6-2: Parameters for decoking and pyrite case.

FiIn the dilute case, the temperature drop is much lower than in the concentrated case. As the inlet concentration approaches 0.0064 mol/dm^3 the temperature drop is extremely. The temperature drop reaches a limit of ~750K for the concentrated case but reaches 0 in the other end for the dilute case. Another interesting point to be discussed is the critical concentration where the denominator of the temperature drop equation tends to rise to very high values. This is known as a cold spot and will be discussed further in the later sections.

6.2 Comparison between numerical simulations and wave model

The values of the thermochemical and thermal wave velocities, and the temperature of the plateau, are calculated from the wave model equations. Using the derived wave model equations, predictions were made for different strategies of reducing pyrite with hydrogen. These predictions are now compared with those obtained by numerical integration of the complete set of PDEs, which represent energy and material balances of the system.

The wave model is compared with the numerical simulations by analysing snapshots of the chemical process for various possible strategies. The values for the thermochemical and thermal wave velocities are used to calculate the distance travelled by the waves, and consequently the plateau temperature, which are compared to the numerical simulations in a summarised table format. The position of the waves at certain times are represented as vertical dashed lines and the plateau temperature is represented as a horizontal dashed line in the results.

6.2.1 Ignition Temperature

A specific focus is set on the temperature which is required to initiate reaction fronts. In

the pyrite case, the particles are solid particles. We are assuming that we have 100% pure pyrite. For any mineral including pyrite, gangue must be accounted for, which is irreducible. A shrinking particle cannot be assumed, because in fact there will be an ash layer, which is the gangue, and that gangue could be as much as 50%. Gangue is accounted for in the density of the pyrite.

Common values of the ignition temperature of pyrite range from 872K to 938K depending on the composition of the pyrite. In the current study, an estimation of the ignition temperature was found by trial and error. The trial and error process is carried out by running the numerical simulation at low initial and inlet temperatures of the fluid and solid to 298K with 10K increment until the reaction occurs completely. The ignition temperature (T_{ign}) was found to be approximately 908K. Unlike in the decoking case, the pyrite particles are not sitting on a catalyst. The process is not limited to a certain temperature range. For endothermic reactions, there is a temperature drop which represents heat being absorbed during the reaction. There is a minimum temperature below which the reaction does not occur called the cold spot. Above this temperature, the reaction can keep going without external heat supply. Reduction of pyrite can be carried out with oxygen as well. Oxidation of pyrite can be reversible, which is not the focus of this study. The irreversible reduction of pyrite with hydrogen is the main contribution of this chapter.

6.2.2 Preheat Wave

There are different ways to heat the bed prior to injecting reactive fluid. In the reduction of pyrite process, where the required temperatures are high. There are a variety of methods for heating fixed bed reactors. Preheating with nitrogen is more cost effective and is chosen as the primary method of heating the fixed bed in this study. Preheating the bed with nitrogen produces a pure thermal wave as there is no reaction occurring. The concentration of the fluid (H_2) remains zero and is of no importance at this stage. There is a constant

velocity of the thermal waves. The temperature of the fluid and solid match up almost immediately and travel together jointly through the reactor. The reason for this, is due to the high transfer heat coefficient between the solid (pyrite) and the fluid (nitrogen). The velocity of the thermal waves from the simulation is compared with the approximation from the wave model. The dashed lines represent the wave model approximation. It is clear that the simulation and the wave model are in good agreement. Iron pyrite is a fairly common mineral and is mined or extracted globally for its many industrial uses, such as extraction of the sulphur for sulphur dioxide or sulphuric acid, and also as an ore for iron. It oxidises readily, making it easy to extract the component minerals, but care must be taken as this also makes it quite combustible. There are different "possible" strategies used to reduce pyrite. Eight possible temperature strategies will be examined. Four cases where the hydrogen feed is diluted and the other four cases where the hydrogen feed is concentrated. Energy saving strategies will also be suggested for both the dilute and concentrated cases. The injection temperature of the hydrogen and bed temperature are varied, and the numerical simulations of these strategies are compared with the wave model predictions for the dilute and concentrated cases. It should be noted that the maximum permissible temperature allowed in the reactor is ~550-600K.

6.3 Results for Dilute case

The numerical simulations show the composition profiles of selected strategies. Comparisons are carried out both graphically and in a tabulated manner. The simulations can only be shown at certain times (snapshots) for the sake of clarity. These times along with the calculated wave model equations are used to predict the distance travelled by each wave. Of course, this comparison assumes the velocity of the wave to be constant. The wave trajectories confirm in a concise manner, the validity of constant wave velocity assumption.

The concentration of hydrogen for the dilute cases is 0.002 mol/dm^3. The wave model predictions are $\boldsymbol{V_{T/C}}$ = 7.997 x 10^{-6} m/s, $\boldsymbol{V_T}$ = 2.775 x 10^{-5} m/s, $\boldsymbol{\Delta T_c}$ = 224.7K. The value of the internal heat transfer coefficient is high, T_s and T_f are rarely any different.

6.3.1 Hot fluid into a Preheated bed

Where dilute hydrogen is used, we have a very slow thermochemical wave and the temperature just beyond the thermochemical wave matters. The temperature of the plateau must be above a certain temperature for the reaction to be stable. The thermal and thermochemical waves are far apart, and the temperature drop is small. This minimum temperature is known as the cold spot. In a very short space of time, there is a massive drop in temperature. In reality, it would take some time for that to happen because we have ignored the conductive effects and the heat transfer effects, which would change the spreading of the thermochemical wave.

The dashed lines and Table 6-2 show the wave model predictions are in good agreement with the simulations. The sets of values of dependent variables remain conserved, that is, the values of different variables do not move relative to one another in space with time. The conversion of solid wave travels jointly with the concentration of fluid wave at a particular velocity. This shows the two waves are indeed coherent. There is also a change in temperature across this wave, which is attributed to heat from the reaction. These waves travelling jointly are collectively known as the thermochemical wave. The thermal wave has a much higher velocity and travels ahead of the thermochemical waves because the fluid concentration is low. The requirement for coherence is that all values of a set of variables at one point in space and time must move in the same direction and with the same velocity, so that they will remain in each other's company. The average conversion according to the numerical simulation, $\bar{X}$ = 98%.

Table 6-2 compares the wave model prediction and the simulation results. The wave model predictions of the thermochemical wave velocity, thermal wave velocity and temperature rise are also given. The table shows the distance the waves have travelled as predicted by the wave model at the time periods shown in Fig. 6-3. The table also shows the distance the waves have travelled according to the numerical simulation.

Fig. 6-4 shows the wave trajectories, which describes the process fully. To show the significance of wave trajectories, a 3-dimensional diagram describing the hot fluid into a hot bed case is shown in Fig. 6-1.

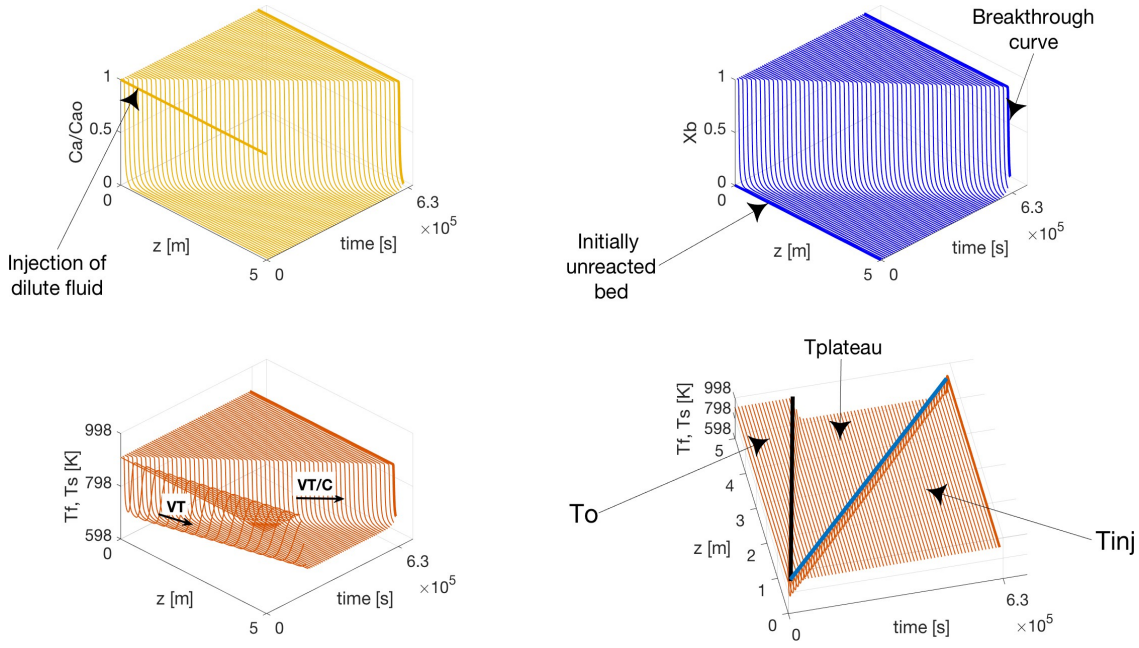

Figure 6-1: 3D plot of dependent variables with independent variables (dilute)

The lines in bold, show the initial (reactor entry) and final (reactor exit) values of the dependent variable. This is very time intensive. As stated earlier, the temperatures of the fluid and solid are practically the same and are superimposed on each other in Fig. 6-1. Viewing the 3-dimensional temperature diagram from the top is just simply the distance-time diagram. As shown in the fourth diagram, the thermal and thermochemical velocities are indeed constant.

It should also be noted Fig. 6-2 shows the composition profiles at selected times to show the coherent behaviour of the system, but Figure 6-1 shows both the composition profiles and histories for a larger range of time and distance, giving a more complete description of the process.

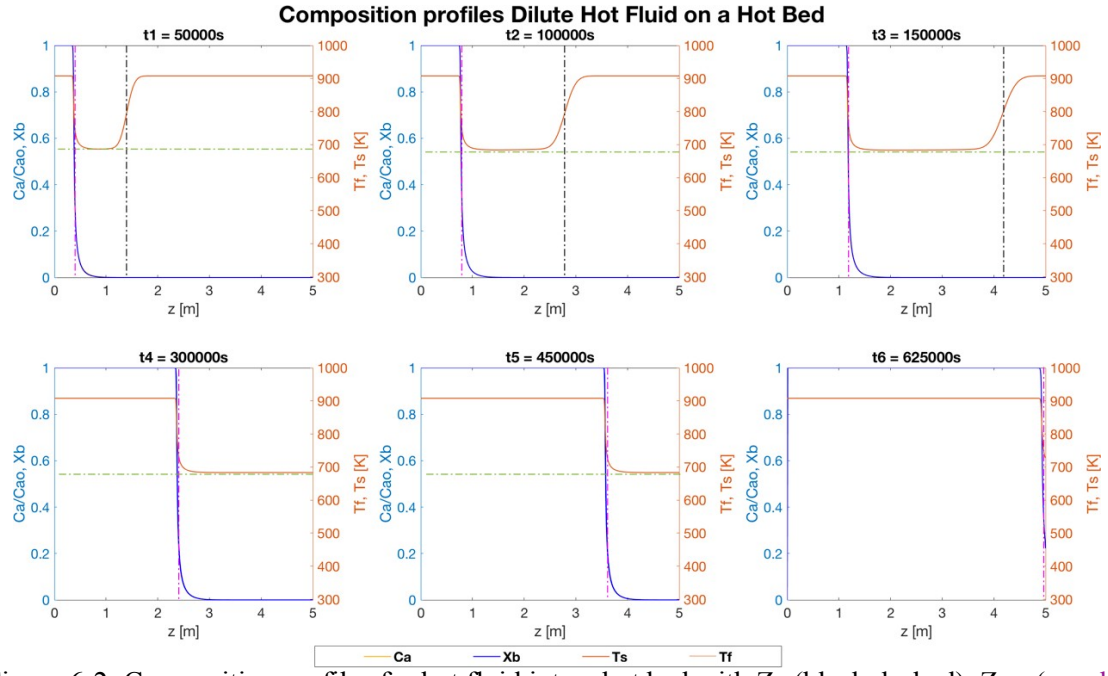

Figure 6-2: Composition profiles for hot fluid into a hot bed with Z_T (black dashed), $Z_{T/C}$ (purple dashed), $T_{plateau}$ (green dashed). T_o = 908K, T_{inj} = 908K

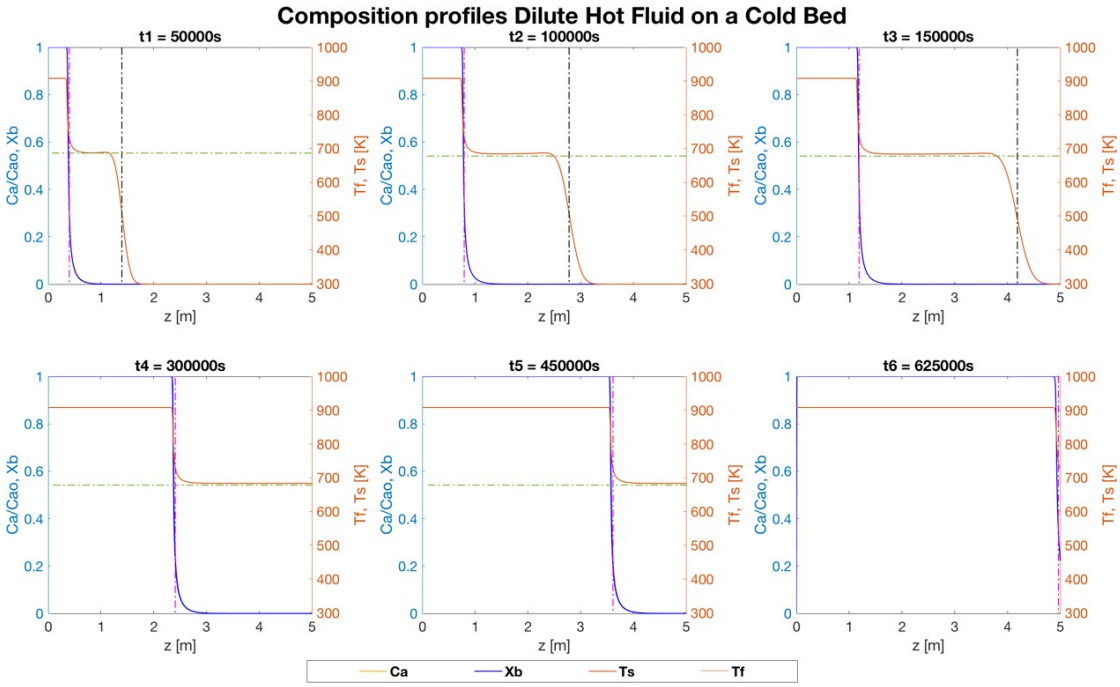

Figure 6-3: Composition profiles for hot fluid into a cold bed with Z_T (black dashed), $Z_{T/C}$ (purple dashed), $T_{plateau}$ (green dashed). T_o = 298K, T_{inj} = 908K

Time (s)	Wave Model	Simulation Results

t	$Z_{T/C}$	Z_{T1}	$T_{plateau}$ (K)	$Z_{T/C}$	Z_{T1}	$T_{plateau}$ (K)
5.0 x 10^4	0.4	1.39	683.3	0.3	1.35	686
1.0 x 10^5	0.8	2.78	683.3	0.8	2.8	686
1.5 x 10^5	1.2	4.17	683.3	1.1	4.1	686
3.0 x 10^5	2.39	-	683.3	2.4	-	686
4.5 x 10^5	3.58	-	683.3	3.6	-	686
6.5 x 10^5	5.0	-	683.3	4.9	-	686

Table 6-2: Comparison of distance travelled by thermal, thermochemical waves & plateau temperature for dilute cases

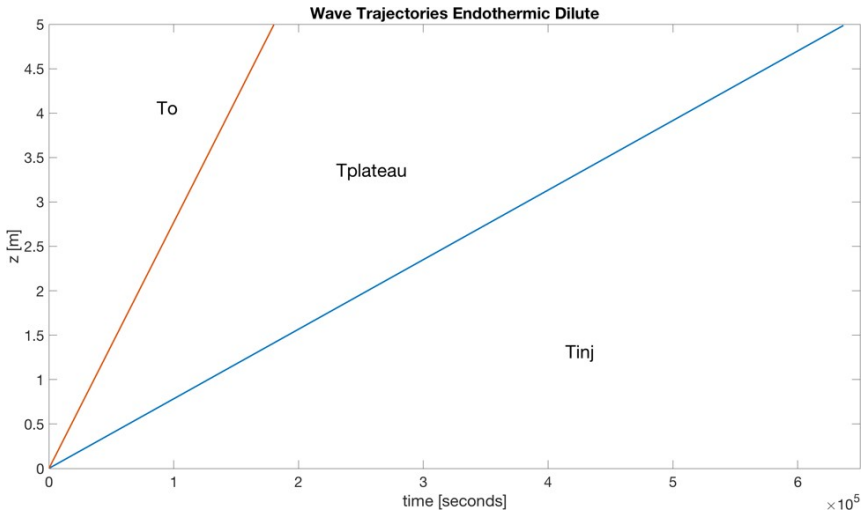

Figure 6-4: Distance-time diagram with thermochemical wave (blue), thermal wave (red) for dilute cases

6.3.2 *Hot fluid into a cold bed*

The thermochemical wave is moving into a region hot enough for the reaction to be stable. If the temperature of the fluid injected is high enough, and the temperature drop is above the critical temperature (cold spot) then the reaction is stable. A low fluid injection fluid is used, the thermochemical wave is sharp and the concentration of fluid wave (C_A) and conversion of solid (X_B) wave are coherent before t_1 in Fig. 6-3. The wave model is in good agreement with the numerical simulation. The thermal waves in the simulation results show the waves spread out. The wave model tells us the important temperature is the temperature just ahead of the thermochemical wave.

The temperature of the bed does not affect the reaction. The overall conversion of the total solid in the reactor bed in this case is 98% according to the numerical simulation. The wave model predicts a 100% conversion after 173.6h. It should be noted that the length of the reactor bed was chosen to compare the exothermic and endothermic reactions and does not represent the common length of fixed bed of pyrite particles.

6.3.3 Cold fluid into a hot bed

The third scenario simulated is the case where a cold fluid is injected into a heated bed. The initial temperature of the bed is set to the bed temperature whilst keeping the fluid temperature at 808K. Fig. 6-7 shows a stable reaction. The colder the fluid, the lower the conversion of the pyrite. The concentration of the fluid and conversion of the solid are coherent but are starting to separate. Full conversion along the reactor bed is still achieved. Due to the partial reaction, the plateau temperature is lower in this scenario than in the previous cases. In the exothermic case, there is an uncharacteristic temperature rise. However, in the endothermic case, there is an uncharacteristic temperature drop which increases with lower T_{inj}. Fig. 6-8 shows the composition profiles when the injected fluid temperature is 298K. There is a much smaller conversion of about 20%. The wave model cannot predict this conversion as the amount of reacted pyrite is dependent on the kinetics of the system. Two cases are to be analysed:

- Injected fluid temperature (T_{inj}) and bed temperature (T_o) are both above ignition temperature giving complete conversion.
- Injected fluid temperature (T_{inj}) is below ignition temperature but bed temperature (T_o) is above ignition temperature, which results in partial conversion of pyrite.

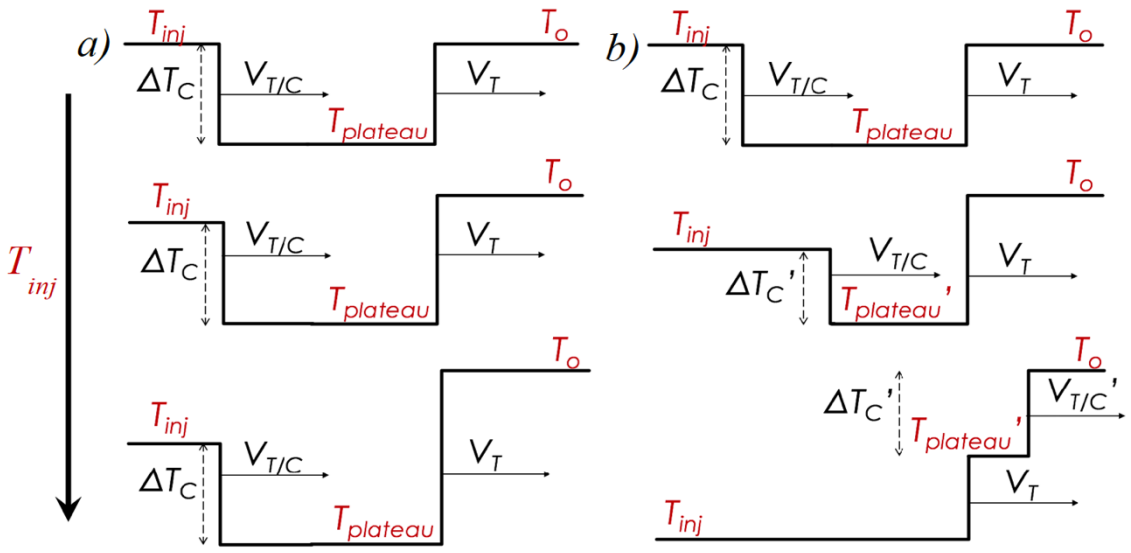

Figure 6-5: Temperature profiles for cold fluid into a hotbed (dilute) with T_{inj} reducing (a) T_{inj}, $T_o > T_{ign}$ (b) $T_{inj} < T_{ign}$, $T_o > T_{ign}$

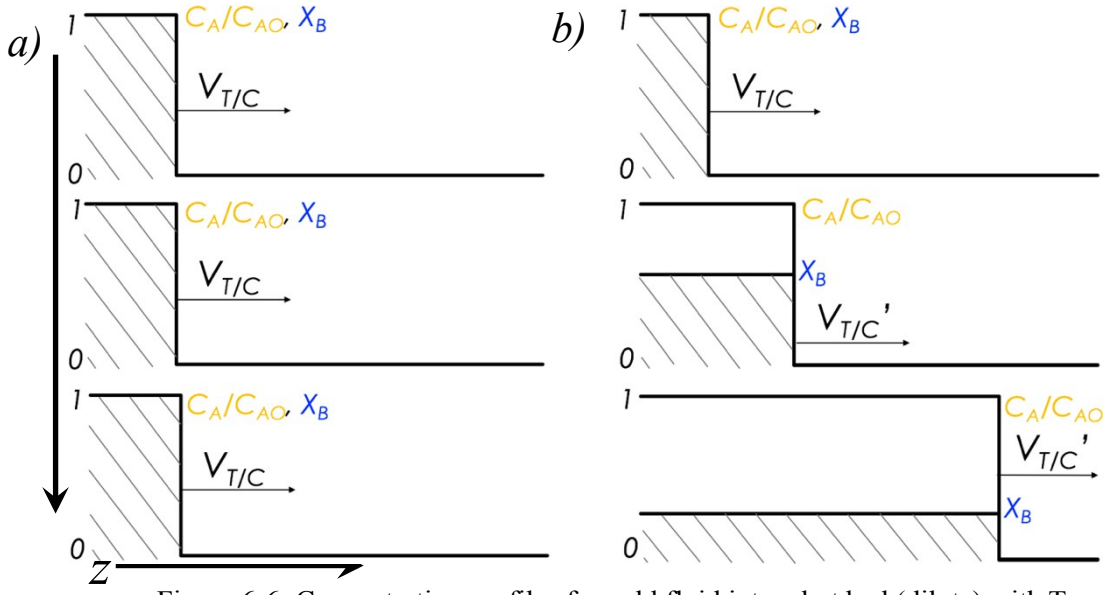

Figure 6-6: Concentration profiles for cold fluid into a hot bed (dilute) with T_{inj} reducing (a) T_{inj}, $T_o > T_{ign}$ (b) $T_{inj} < T_{ign}$, $T_o > T_{ign}$

Reacted solid

Case (a): Both the injected fluid temperature and the bed temperature are always above ignition temperature. The first diagram describes the concentration and temperature profile of a hot fluid injected into a hot bed. As T_{inj} is reduced, the thermochemical temperature rise does not change leading to the profiles in Fig. 6-5(a). This assumes that the plateau temperature is above the cold spot so there is no partial reaction. Fig. 6-6(a) shows the associated concentration profiles (both C_A and X_B). To confirm this, a numerical simulation

of case (a) is shown in Fig. 6-8. T_{inj} - ΔT_c has to be higher than the cold spot.

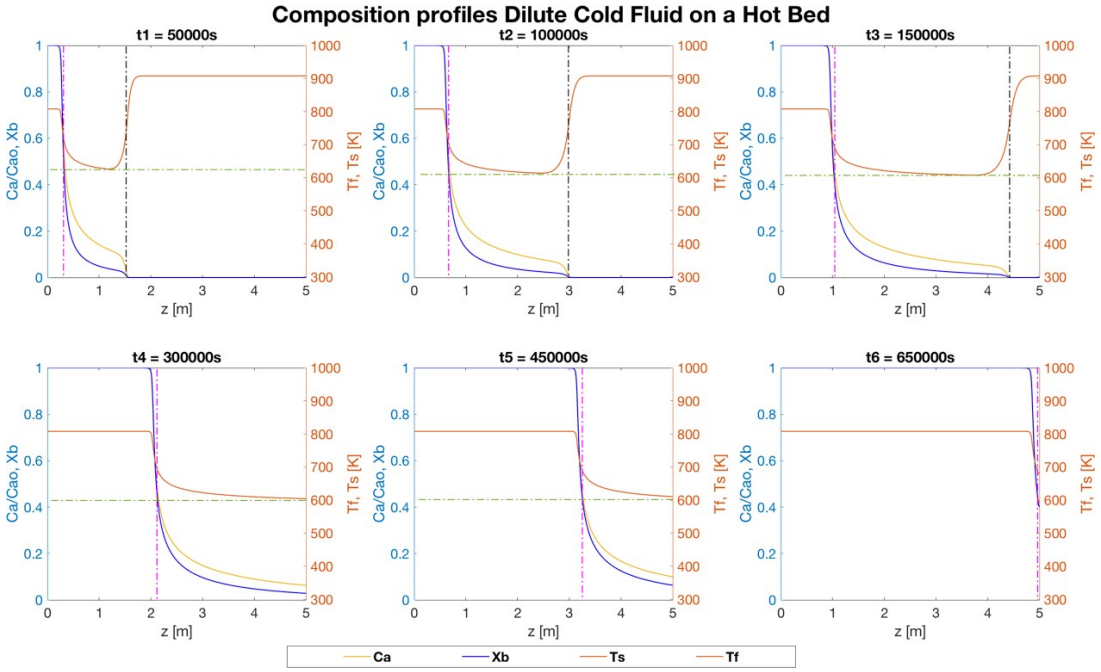

Figure 6-7: Composition profiles for cold fluid into a hot bed with Z_{T1} (black dashed), $Z_{T/C}$ (purple dashed), $T_{plateau}$ (green dashed). T_o = 908K, T_{inj} = 908K

Case (b): The injected fluid temperature and the bed temperature are initially set to ignition temperature. If T_{inj} is set below the ignition temperature, only part of the pyrite reacts. Due to the partial conversion, the thermochemical wave travels faster but the thermal wave velocity does not change. The smaller the distance between the two waves, the larger the temperature drop. However, there is a minimum temperature where the reaction does not occur below that of 575K. If $T_{inj} - \Delta T_C$ is lower than the cold spot temperature, the plateau temperature remains at this cold spot temperature. Therefore, lowering the injected fluid temperature has no effect on the plateau temperature when this limit is reached. The wave model cannot predict what the partial conversion ($X_{partial}$) would be but if the conversion was known, the wave model can accurately predict the new velocity of the thermochemical wave $V_{T/C}$', but the new temperature drop due to the thermochemical wave ΔT_C' is constrained to the cold spot. $\overline{X}$ was found to be 18%. Using the equation (3.21) $V_{T/C}$ = 4.42 x 10^{-5} m/s was found and the temperature rise is lower than in the previous cases. The

lower the injected fluid temperature, lower the as shown in Figs. 6-5(b) and 6-6(b).

Table 6-3 also compares the wave model predictions to the measured values from the numerical simulation. In the exothermic case, the temperature keeps rising higher and higher because there is no limit on the maximum temperature reached for the reaction to occur. Once the reaction is above the ignition temperature, the temperature of the plateau will always be larger and the $T_{plateau}$ can be calculated accurately. In the endothermic case, the temperature drops lower and lower until the cold spot is reached.

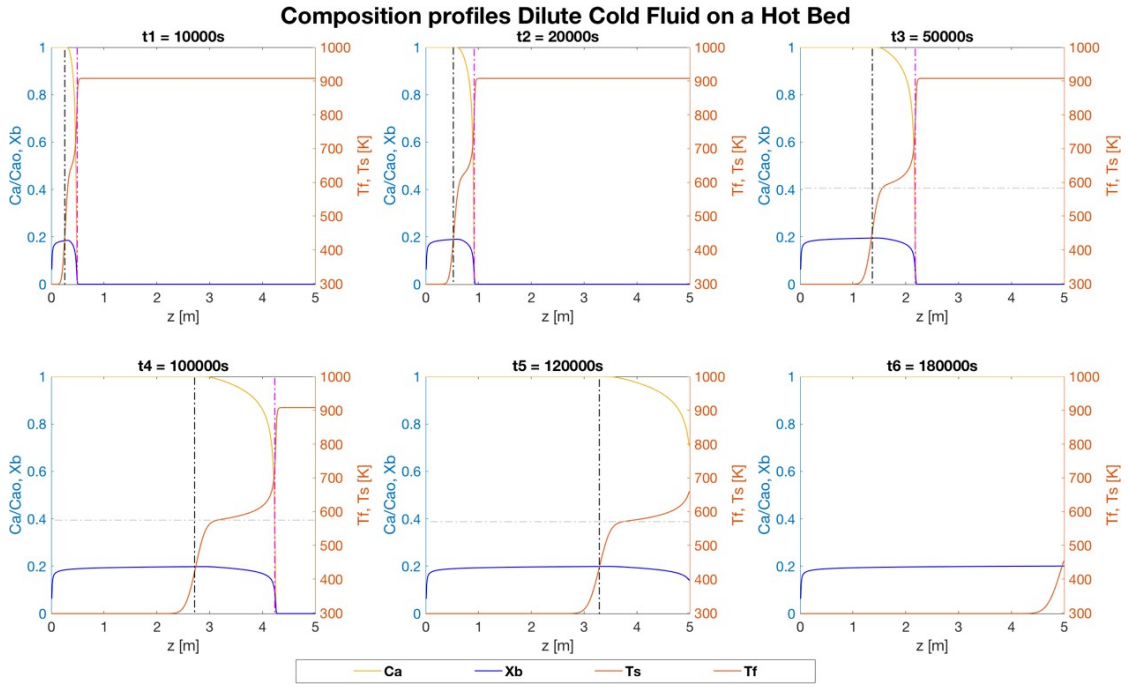

Figure 6-8: Composition profiles for cold fluid into a hot bed with Z_{T1} (black dashed), $Z_{T/C}$' (purple dashed), $T_{plateau}$' (grey dashed). T_o = 908K, T_{inj} = 298K

Time (s)	Wave Model			Simulation Results		
t	$Z_{T/C}$'	Z_{T1}	$T_{plateau}$ *(K)*	$Z_{T/C}$'	Z_{T1}	$T_{plateau}$' *(K)*
1.0 x 10^4	0.44	0.28	-	0.5	0.3	575
2.0 x 10^4	0.89	0.56	-	0.9	0.6	575
5.0 x 10^4	2.23	1.39	-	2.1	1.4	575
1.0 x 10^5	4.44	2.78	-	4.3	2.7	575
1.2 x 10^5	-	3.33	-	-	3.2	575
1.8 x 10^5	-	4.99	-	-	5.0	575

Table 6-3: Comparison of distance travelled by thermal, thermochemical waves & plateau temperature for dilute case cold fluid (298K) into a hot bed

wave trajectories for the dilute cases mentioned is the same except for partial conversion case. For the partial conversion case, the thermochemical wave travel at a correctly

predicted faster velocity and a new temperature plateau is reached, $T_{plateau}'$, where $T_{plateau}'$ is the cold spot temperature. Fig 6-9 illustrates this. For the other cases, the velocities of the thermal and thermochemical waves are the same as there is no change in any parameter except temperature, which does not affect the velocities of the wave model.

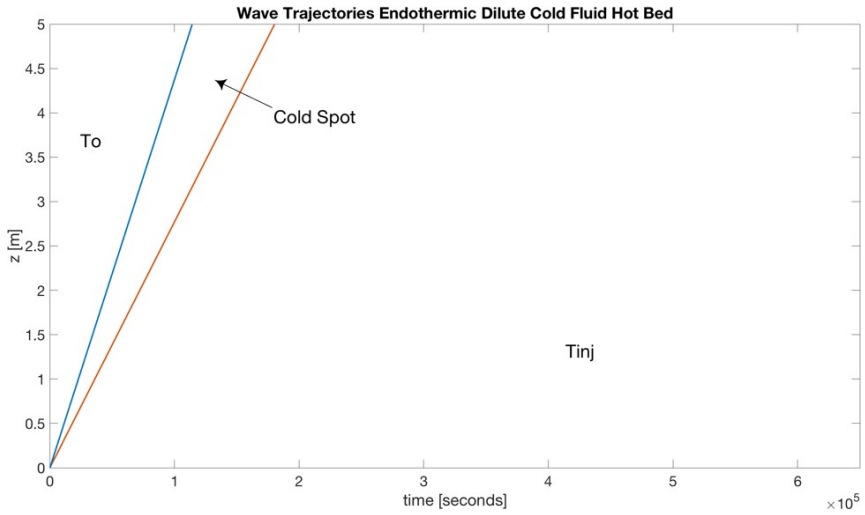

Figure 6-9: Distance-time diagram for cold fluid (298K) into a hot bed with thermochemical wave (blue), thermal wave (red) (dilute)

6.3.4 Reduced heat Strategy

As explained in Section 5.3.4, the reduced heat strategy involves delaying the cold dilute fluid long enough, so the trailing thermal wave meets the thermochemical wave at the end of the reactor bed. The trailing thermal wave will meet the thermochemical wave at the reactor exit. The wave model was used to calculate the time it takes a pure thermal wave to travel through the reactor (t_T) and time it takes a thermochemical wave to travel through the reactor ($t_{T/C}$) the cold thermal wave is therefore delayed at

$$t_{delayed} = t_T - t_{T/C} \tag{6.1}$$

where $t_T = 180000s$ and $t_{T/C} = 625000s$. Therefore, the time to inject cold dilute fluid, $t_{inj,fluid} = t_{delayed} = 445000s$. The diagram below can explain the reaction simply:

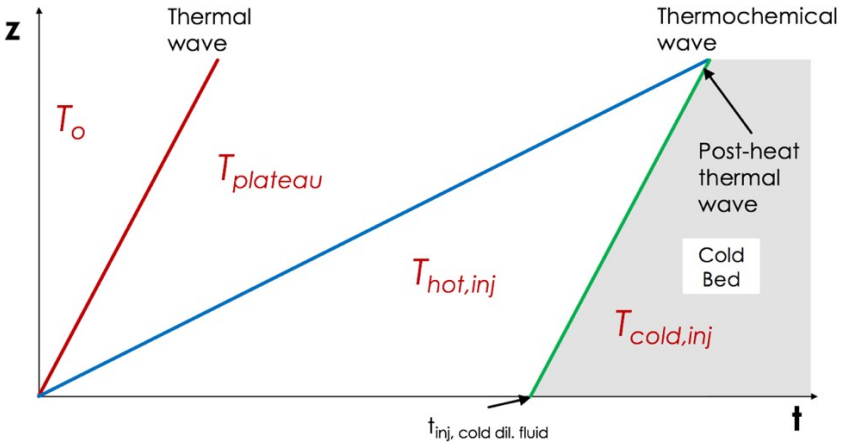

Figure 6-10: Distance-time diagram for reduced heat strategy (dilute)

The cold fluid is injected at 298K and it produces a thermal wave. This is represented as a post-heat thermal wave above. The gradient of the post-heat thermal wave is the same as the leading thermal wave because both waves travel at a velocity V_T. The post-heat thermal wave leaves a cold bed behind. This leads to 29% less heating than in any of the previous heating strategies whilst reducing the pyrite completely. The numerical simulation confirms the reduced heat strategy introduces a cold thermal wave as seen in t_4, meeting the thermochemical wave at the end of the reactor at time t_6. The wave trajectories prediction in Fig. 6-10 is identical to the wave trajectories form the numerical simulation.

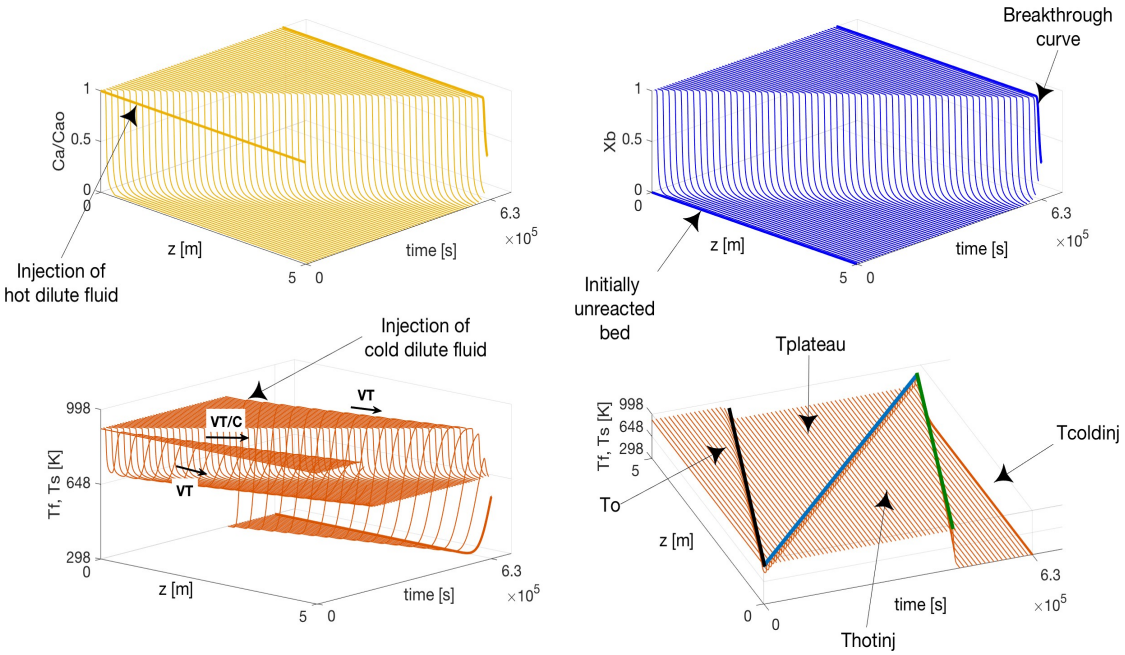

Figure 6-11: 3D plot of dependent variables with independent variables (dilute reduced heat strategy)

The bottom right graph in Fig. 6-10 shows the wave trajectories are indeed accurate and

describe the temperature variation in the system accurately. We are relying on the numerical solution to give a reasonably good representation of the reality.

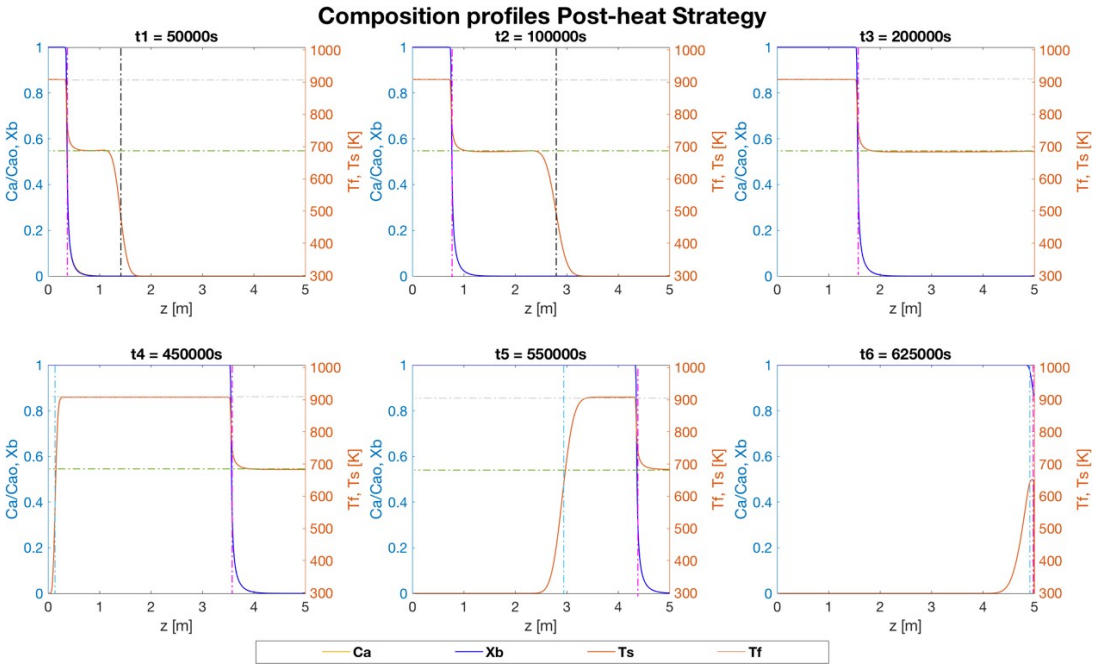

Figure 6-12: Composition profiles for dilute reduced heat strategy with Z_{T1} (black dashed), Z_{T2} (blue dashed), $Z_{T/C}$ (purple dashed), $T_{plateau}$ (green dashed), T_{fo} (grey dashed).

Time (s)	Wave Model				Simulation Results			
t	$Z_{T/C}$	Z_{T1}	Z_{T2}	$T_{plateau}$ *(K)*	$Z_{T/C}$	Z_{T1}	Z_{T2}	$T_{plateau}$ *(K)*
5.0 x 10^4	0.38	1.39	-	683.3	0.3	1.3	-	686
1.0 x 10^5	0.76	2.78	-	683.3	0.8	2.8	-	686
2.0 x 10^5	1.52	-	-	683.3	1.6	-	-	686
4.5 x 10^5	3.59	-	0.14	683.3	3.6	-	0.2	686
5.5 x 10^5	4.39	-	2.92	683.3	4.3	-	2.9	686
6.25 x 10^5	5.0	-	4.91	-	5.0	-	4.8	-

Table 6-4: Comparison of distance travelled by thermal, thermochemical waves & plateau temperature for dilute reduced heat strategy

A wave model has been developed that can predict the key elements of the simulation output for the dilute cases. The concentrated hydrogen case shall now be tackled.

6.4 Results for Concentrated Hydrogen case

The concentration of hydrogen is raised to 0.1 mol/dm^3. As shown in Fig. 6-12, the wave

model predicts a temperature drop of ~600K. The thermochemical wave is expected to be faster than the thermal wave. The temperature of the bed is the temperature which needs to be above the ignition temperature. Due to a cold spot around 550K, the thermochemical temperature drop will be lower than the cold spot temperature where no reaction is expected to occur. The temperature of the bed and the hydrogen are set at 1208K, which would guarantee a stable reaction and clear separation of waves. This would be the basis of validation of the concentrated case.

The wave model tells us that the thermochemical wave will be faster than the thermal wave in this case, $\boldsymbol{V_{T/C}}$ = 3.994 x 10^{-4} m/s, $\boldsymbol{V_T}$ = 2.778 x 10^{-5} m/s, $\boldsymbol{\Delta T_C}$ = -597.1K. The temperature increase is much larger in this case, as there is more concentrated oxygen injected into the reactor. An interesting point to be discussed is the critical concentration where the denominator of the temperature drop equation tends to give very high values. The approach to a cold spot causes splitting of waves when the temperature drop is below the critical temperature. The same injection strategies simulated in the dilute case will now be carried out for the concentrated case.

6.4.1 Hot fluid into a Pre-heated bed

Due to large temperature drop, the initial temperatures of the injected hydrogen and the bed were raised to 1208K to avoid the cold spot. It should be noted that the change in the initial temperature has no effect on ΔT_C. As the starting temperatures are much higher than the ignition temperature, the concentration profiles for the concentrated case show the thermochemical waves are sharper than in the dilute case. This means the system is closer to equilibrium. The thermal wave is unchanged and travels at the same speed as in the dilute cases. The thermal wave shows self-sharpening wave behaviour. The thermochemical wave approaches a fixed width as it is bounded by the chemical reaction. A coherent thermochemical wave is achieved.

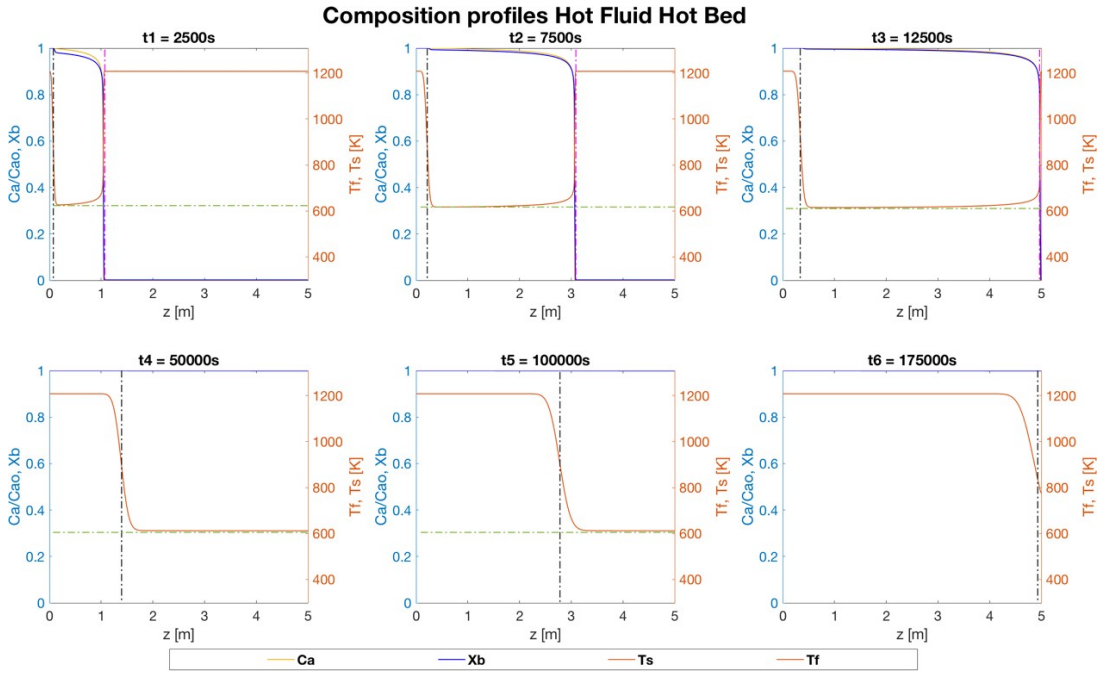

Figure 6-13: Composition profiles for hot fluid into a hot bed with Z_T (black dashed), $Z_{T/C}$ (purple dashed), $T_{plateau}$ (green dashed). T_o = 1208K, T_{inj} = 1208K

Fig. 6-14 describes the composition variables in space and time from the results of the numerical simulation. The figure shows the results as lines at specific intervals. The graph in the bottom left shows the thermal wave spreads as it travels across the reactor. The evolution of thermochemical waves shows a constant pattern without distortion. A comparison between Fig. 6-13 and Fig. 6-14 shows the wave trajectories are consistent.

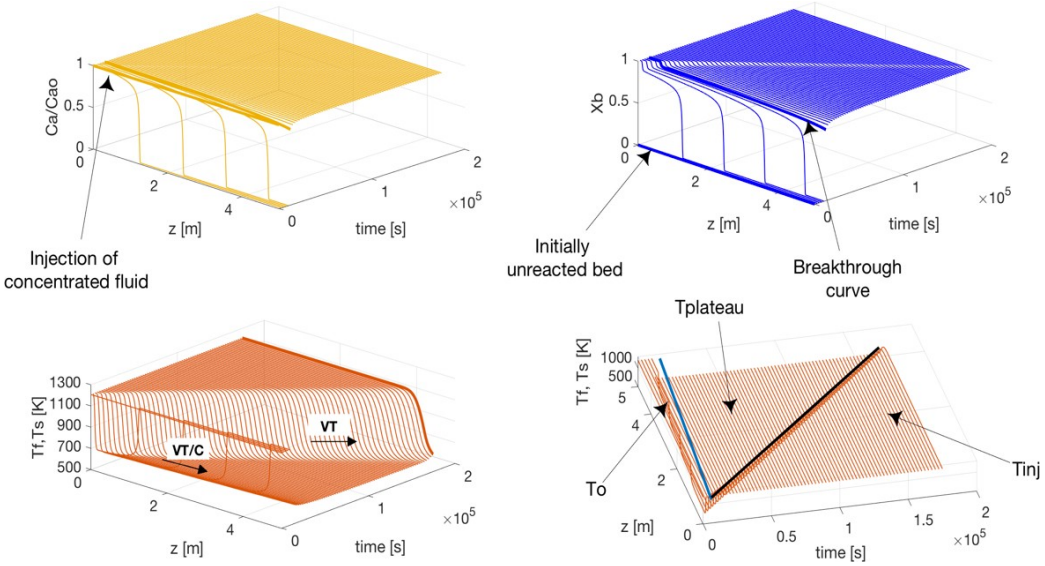

Figure 6-14: 3D plot of dependent variables with independent variables (concentrated)

6.4.2 Cold fluid into a hot bed

In this scenario, the thermochemical wave moves into a hot bed. The reaction is expected

to be stable. There is a sharp temperature rise from the plateau to the bed temperature. A trailing cold thermal wave is obtained by introducing a feed gas at low temperature. The thermal wave rises from the injected fluid temperature to the plateau temperature as a result of convective flow of cold hydrogen gas. Since the thermochemical wave is faster than the thermal wave, the thermochemical wave is unaffected by the temperature of the injected fluid. The numerical simulations are in good agreement with the wave model as shown in Fig. 6-15. There is a slight discrepancy with the predicted temperature drop. This is due to the slight curvature of the plateau which makes it difficult to pick out one value for the plateau. 99% of the bed completely reacted.

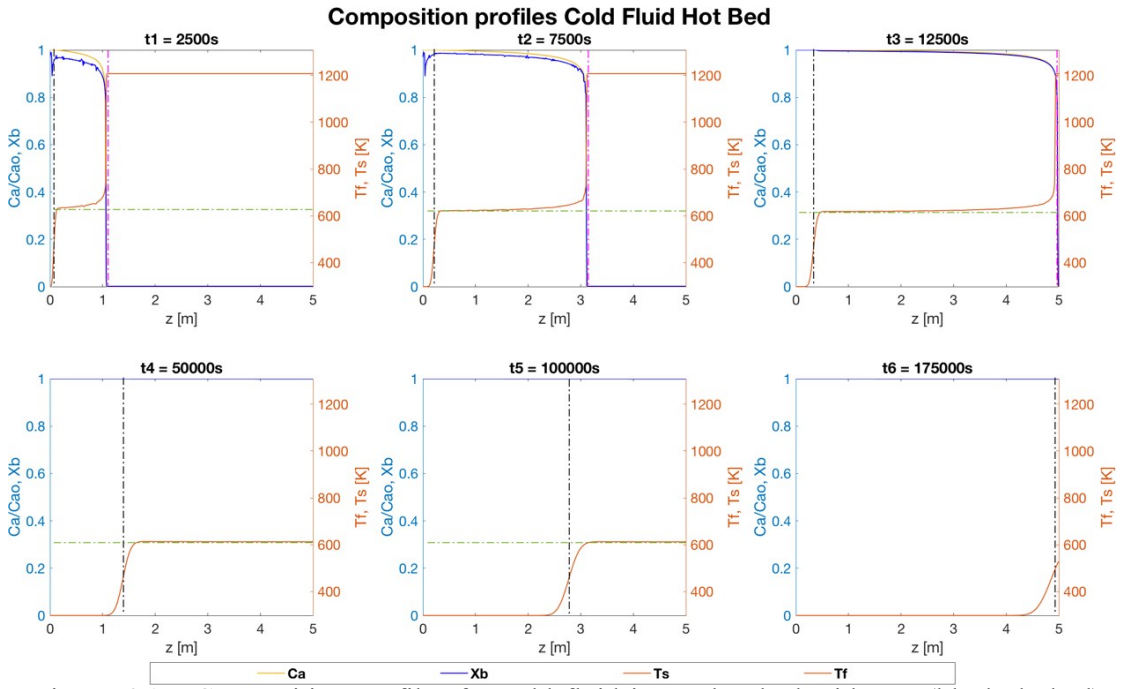

Figure 6-15: Composition profiles for cold fluid into a hot bed with Z_{T1} (black dashed), $Z_{T/C}$ (purple dashed), $T_{plateau}$ (green dashed). T_o = 1208K, T_{inj} = 298K

Time (s)	Wave Model			Simulation Results		
t	$Z_{T/C}$	Z_{T1}	$T_{plateau}$ **(K)**	$Z_{T/C}$	Z_{T1}	$T_{plateau}$ **(K)**
2.5 x 10^3	0.99	0.07	597.1	1.1	0.1	600
7.5 x 10^3	2.99	0.21	597.1	3.1	0.2	600
1.25 x 10^4	4.99	0.35	597.1	5	0.4	600
5.0 x 10^4	-	1.39	597.1	-	1.3	600
1.0 x 10^5	-	2.78	597.1	-	2.8	600
1.75 x 10^5	-	4.96	597.1	-	4.9	600

Table 6-5: Comparison of distance travelled by thermal, thermochemical waves & plateau temperature for concentrated case

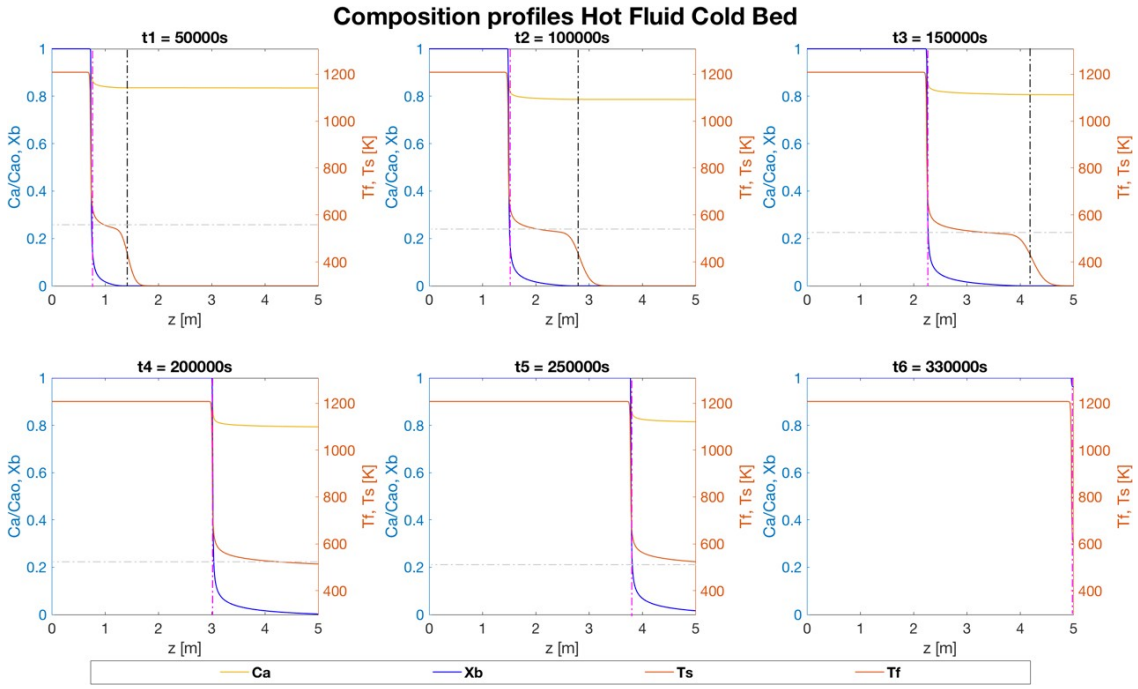

Figure 6-16: Distance-time diagram (concentrated) with thermochemical wave (blue), thermal wave (red)

6.4.3 Hot fluid into a cold bed

For this strategy, the thermochemical wave is moving into a cold region. As the temperature of the bed is too low, the thermochemical wave does not propagate ahead of the thermal wave. The thermochemical wave can only travel into a region above the cold spot. For this reason, the concentrated hydrogen only partially reacts with the reactor bed. This phenomenon is shown in Fig. 6-17. The partial concentration is approximately 21%. The wave model predicts a slower velocity when there is a partial concentration of fluid. This agrees with the retardation of the thermochemical wave. The temperature reduces monotonically from the injected fluid temperature to the plateau temperature to the bed temperature. The wave model cannot predict the numerical value of the partial concentration or the cold spot temperature. There is still a coherent thermochemical wave, so the wave model still has value in predicting the positions of the thermal and thermochemical waves.

Figure 6-17: Composition profiles for hot fluid into a cold bed with Z_{T1} (black dashed), $Z_{T/C}$ (purple dashed), $T_{plateau}$' (grey dashed). T_o = 298K, T_{inj} = 1208K

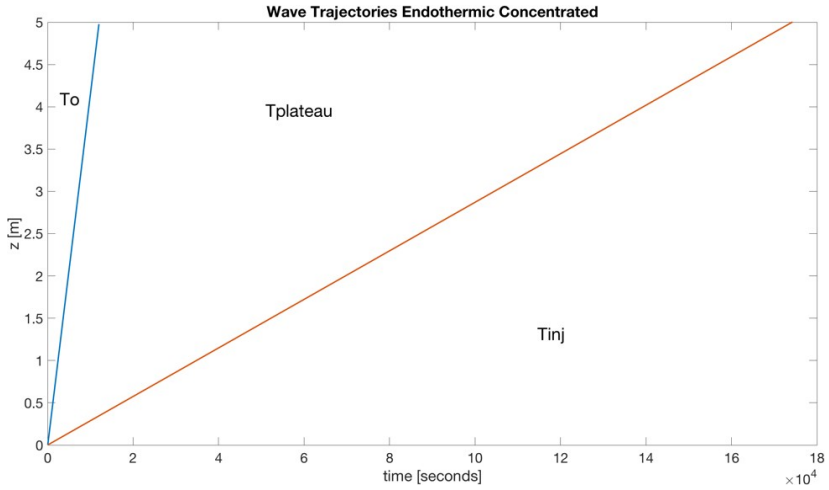

Time (s)	Wave Model			Simulation Results		
t	$Z_{T/C}$'	Z_{T1}	$T_{plateau}$' (K)	$Z_{T/C}$'	Z_{T1}	$T_{plateau}$' (K)
5.0 x 10^4	0.78	1.38	-	0.8	1.3	535
1.0 x 10^5	1.56	2.76	-	1.5	2.8	535
1.5 x 10^5	2.2	4.18	-	2.2	4.2	535
2.0 x 10^5	3.12	-	-	3.0	-	535
2.5 x 10^5	3.9	-	-	3.8	-	535
3.3 x 10^5	5.08	-	-	5.0	-	535

Table 6-6: Comparison of distance travelled by thermal, thermochemical waves & plateau temperature for concentrated case hot fluid into a cold bed (298K)

The distance-time diagram for the concentrated cases mentioned is shown in Fig. 6-18 is the same except for the cold fluid into a hot bed case ($V_{T/C} < V_T$), where there is a partial concentration. Fig. 6-18 shows a steep gradient for the thermal wave. A vertical cut from the point where the thermochemical wave reaches the reactor exit (z = 5m) shows the time when there is a pure thermal wave travelling across the reactor.. A horizontal cut at z = 3.1 m shows the time when the thermal and thermochemical waves cross the 3.1m mark in the reactor (t = 220000s). For the Hot fluid hot bed case, the positions of the thermal and thermochemical waves have switched, there is a faster thermal wave passing through the reactor shown in Fig. 6-18 and a less steep thermochemical wave. The temperature in the region in between the two waves is the cold spot. The diagram summarises in a succinct

way, the full development of the waves. The wave model accurately predicts the wave trajectories for the concentrated cases. The thermal wave velocity does not change and has the same gradient in all the concentrated cases.

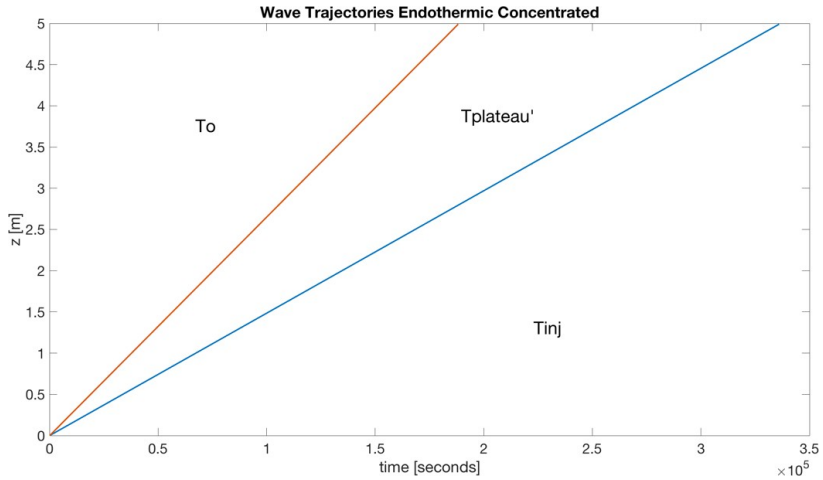

Figure 6-18: Distance-time diagram hot fluid into a cold bed (298K) (concentrated) with thermochemical wave (blue), thermal wave (red)

6.4.4 Pre-heat Strategy

The method of heating the reactor bed is with a nitrogen stream. It has been noted in the cold fluid hot bed case that hot hydrogen is not required to ensure a complete reaction. A continuous heating of the bed prior to injecting the cold fluid is not energy efficient. Pre-heat strategy involves injecting concentrated hydrogen whilst still heating the bed with nitrogen. The thermal wave is slower than the thermochemical wave. Therefore, the leading thermal wave associated with the pre-heat nitrogen stream is slow. Injection of concentrated fluid introduces a fast thermochemical wave at the right time, so the thermochemical wave meets the leading thermal wave at the reactor exit. The wave model was used to calculate the time to inject the concentrated cold fluid. Where $t_{T/C}$ is the time it takes a thermochemical wave to travel through the reactor ($t_{T/C}$):

$$t_{delayed} = t_T - t_{T/C} \tag{6.2}$$

where $t_T = 175000s$ and $t_{T/C} = 12600s$. Therefore, the time to inject cold dilute fluid is $162400s$. There is a trailing thermal wave associated with the injection of cold concentrated

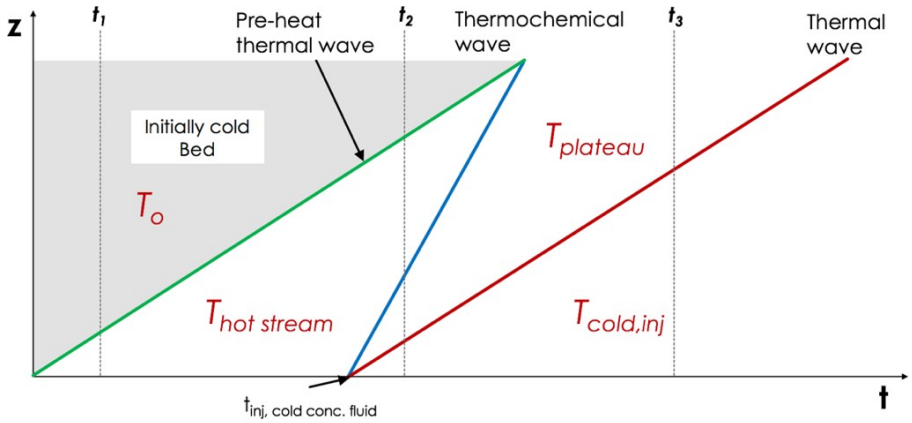

hydrogen cooling the reactor. The fluctuation of the temperature parameter in this system leads to 10% less heating than any of the previous cases. The numerical simulation is shown in Fig. 6-21 and compared with the wave model predictions in Table 6-6.

Figure 6-19: Distance-time diagram for pre-heat strategy (concentrated)

The nitrogen stream is represented as a pre-heat thermal wave. The gradient of the thermochemical wave is very steep and the wave model. Fig. 6-20 gives a simple picturesque description of the pre-heat strategy.

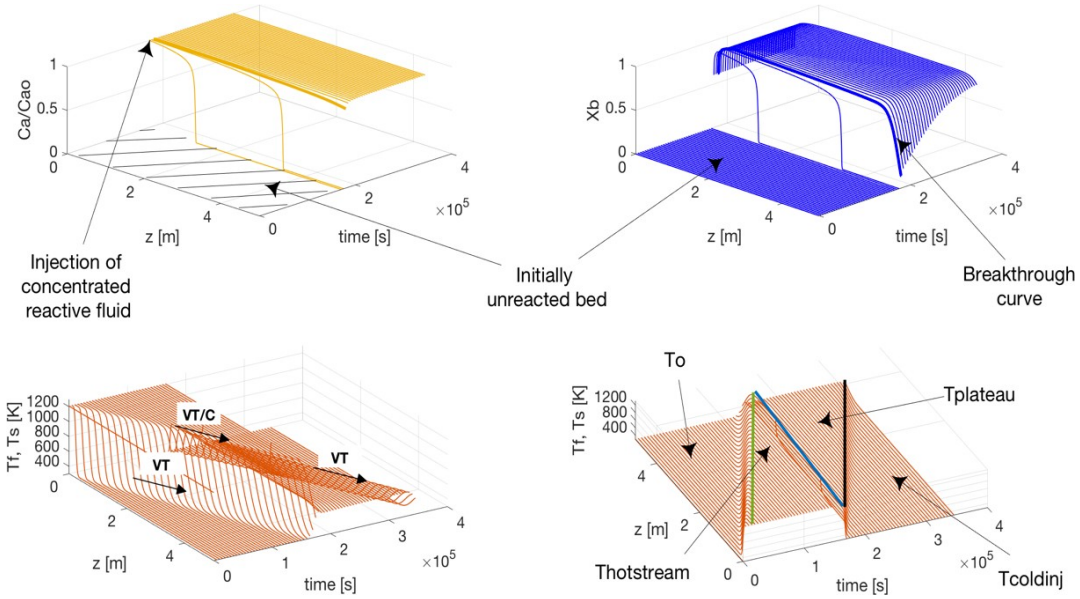

Figure 6-20: 3D plot of dependent variables with independent variables (concentrated pre-heat strategy)

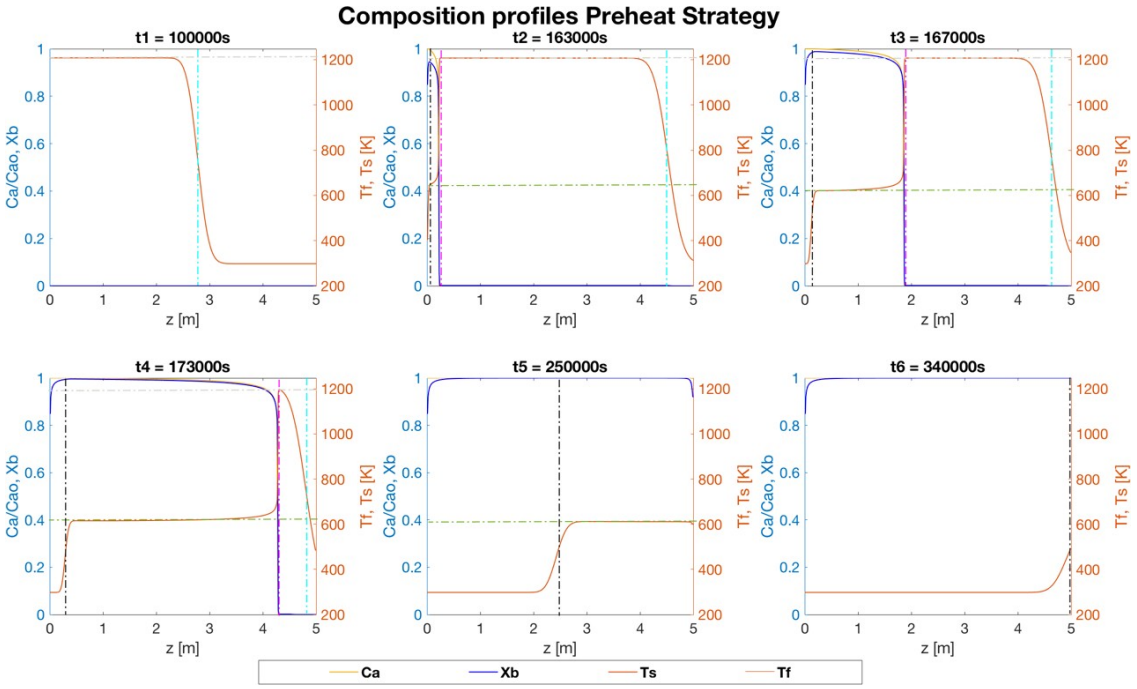

Figure 6-21: Composition profiles for concentrated pre-heat strategy with Z_{T1} (blue dashed), Z_{T2} (black dashed), $Z_{T/C}$ (purple dashed), $T_{plateau}$ (green dashed), T_{fo} (grey dashed)

Time (s)	Wave Model				Simulation Results			
t	$Z_{T/C}$	Z_{T1}	Z_{T2}	$T_{plateau}$ (K)	$Z_{T/C}$	Z_{T1}	Z_{T2}	$T_{plateau}$ (K)
1.0 x 10^5	-	2.78	-	-	-	2.8	-	-
1.63 x 10^5	0.20	4.53	0.02	597.1	0.2	4.5	0.02	610
1.67 x 10^5	1.80	4.64	0.13	597.1	1.9	4.6	0.1	602
1.73 x 10^5	4.19	4.81	0.29	597.1	4.2	4.8	0.3	602
2.5 x 10^5	-	-	2.43	597.1	-	-	2.4	602
3.4 x 10^5	-	-	4.93	-	-	-	5.0	-

Table 6-7: Comparison of distance travelled by thermal, thermochemical waves & plateau temperature for concentrated pre-heat strategy

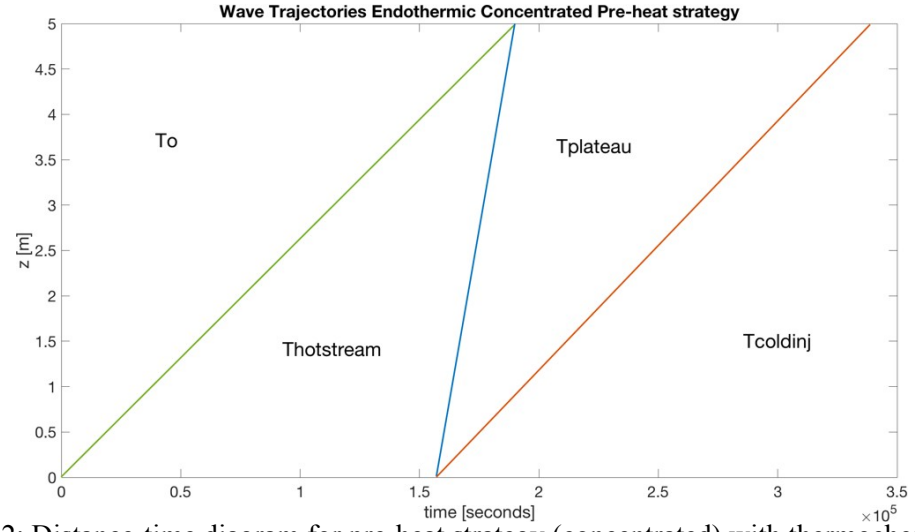

Figure 6-22: Distance-time diagram for pre-heat strategy (concentrated) with thermochemical wave (blue), thermal wave 1 (green) thermal wave 2 (red)

6.4.5 Cold Spot

The case where a critical value of inlet fluid concentration is injected. This concentration gives a theoretically infinite temperature drop. Intuitively, there is a limiting temperature, below which the reaction cannot occur. In this case, there is no pure thermal wave. There is instead a splitting of two thermochemical waves travelling at different velocities. In the pyrite case, C_{AO} = 0.00694 mol/dm^3 is the critical concentration where the temperature drop is maximum. The results for the case are shown in Fig. 6-23.

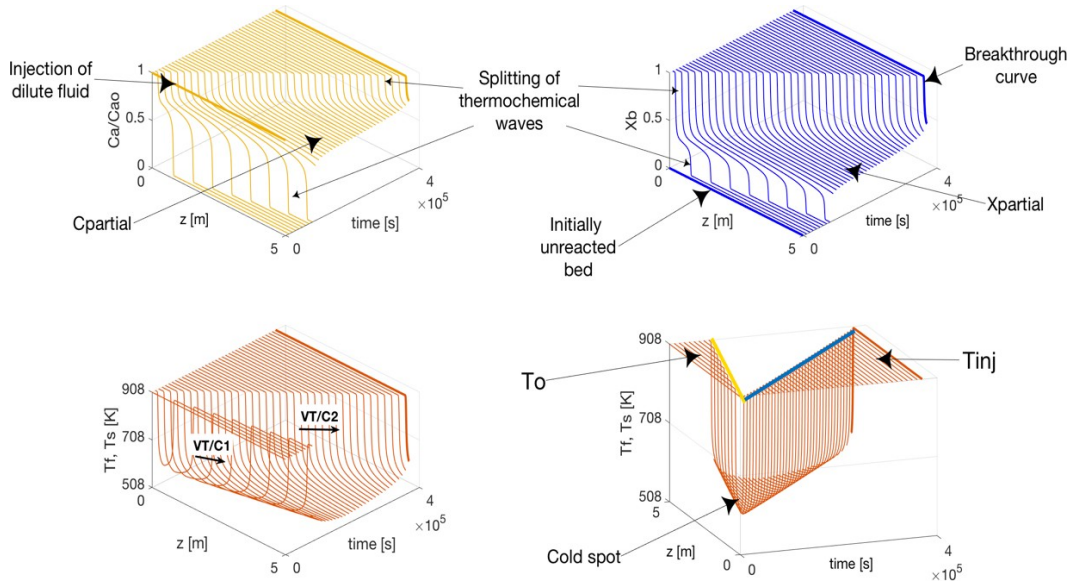

Figure 6-23: 3D plot of dependent variables with independent variables (cold spot)

A description in time and space above.

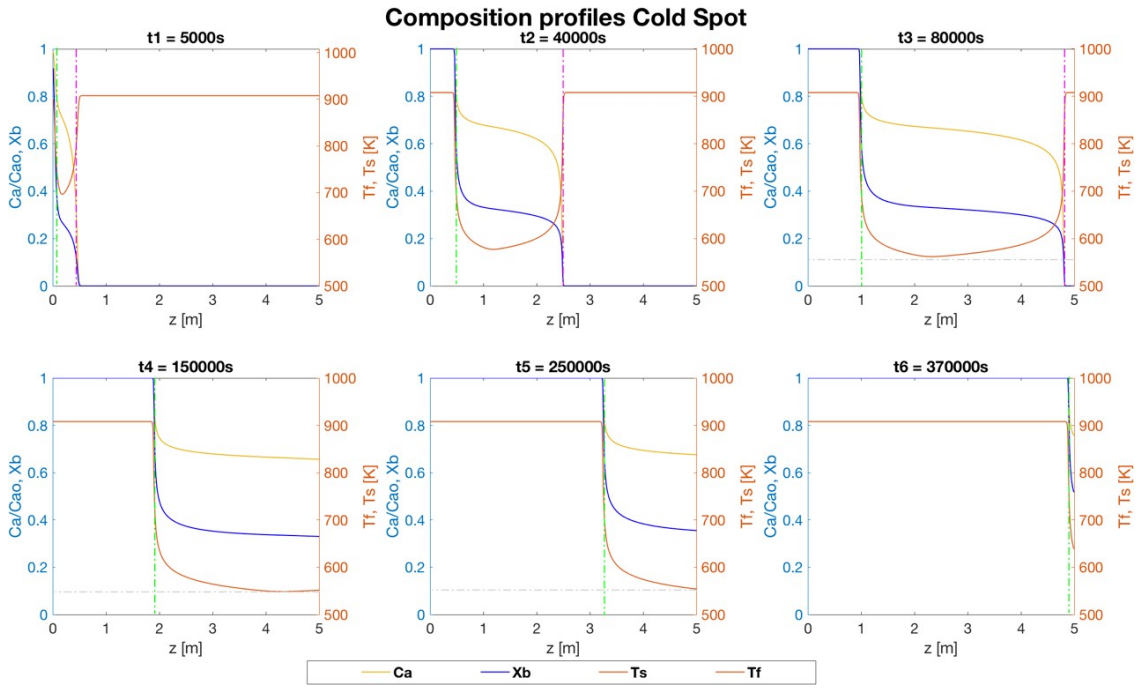

Figure 6-24: Composition profiles for cold spot with $Z_{T/C1}$ (purple dashed), $Z_{T/C2}$ (green dashed), $T'_{plateau}$ (grey dashed). T_o = 908K, T_{inj} = 908K

Time (s)	Wave Model			Simulation Results		
t	$Z_{T/C2}$	$Z_{T/C1}$	$T_{plateau}'$ (K)	$Z_{T/C2}$	$Z_{T/C1}$	$T_{plateau}'$ (K)
5.0 x 10^3	0.06	0.31	-	0.1	0.3	-
4.0 x 10^4	0.51	2.42	-	0.5	2.5	-
8.0 x 10^4	1.02	4.82	-	1.0	4.8	550
1.5 x 10^5	1.91	-	-	1.9	-	550

2.5 x 10^5	3.18	-	-	3.2	-	550
3.7 x 10^5	4.86	-	-	4.9	-	550

Table 6-8: Comparison of distance travelled by thermochemical waves & plateau temperature for cold spot case (908K)

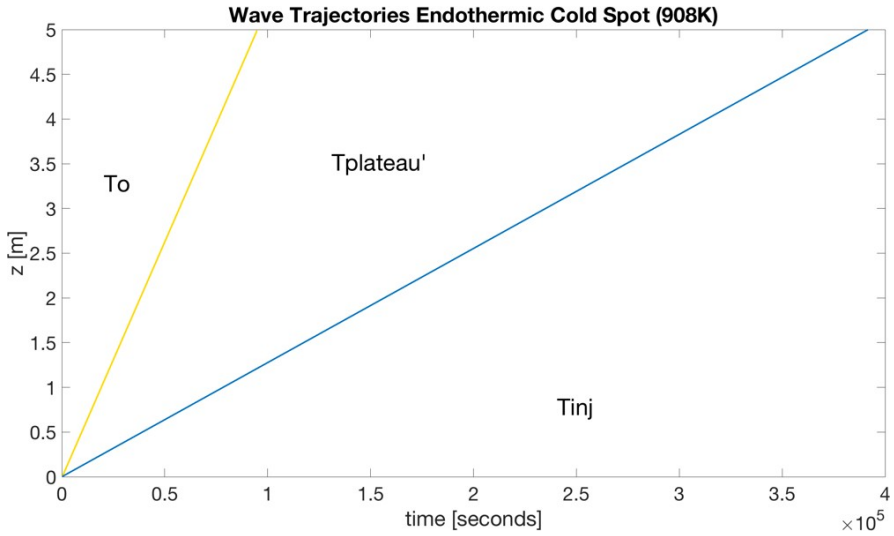

Figure 6-25: Distance-time diagram with thermochemical wave1 (blue) thermochemical wave 2 (yellow) for cold spot (908K)

The rate of reaction around the cold spot is very low as the temperature is too low to keep the reaction going. There is a reaction on either side of the plateau. This leads to both partial concentration of the fluid and partial conversion of the bed. The values of $C_{partial}$ and $X_{partial}$ are plugged into Eq. (3-23). The wave model accurately predicts the velocity of both thermochemical waves compared in Table 6-8. Calculation of the thermochemical wave velocity with the critical concentration value shows the position of the thermochemical wave to be in between the two thermochemical waves associated with partial reactions. This position is not indicated in the diagrams but verifies the numerical simulation.

To further verify this phenomenon. The injected fluid concentration was set to just below and just above the critical concentration (0.00694 mol/dm^3). The critical concentration was set to 0.00069 mol/dm^3 (dilute) and 0.0007 mol/dm^3 (concentrated). The wave model predicts these concentrations both lead to extremely large temperature drops. However, there will be a trailing thermochemical wave in the dilute case and a leading thermochemical wave

in the concentrated case. The initial temperatures need to be raised to such high temperature to ensure the cold spot is not reached and a single thermochemical wave is produced. Figs. 6-26 and 6-27 show the numerical simulations. The thermochemical wave and thermal wave travel are as predicted by the wave model. This shows the numerical simulation of the critical concentration is indeed correct and the splitting of thermochemical waves around the cold spot is not an artificial phenomenon. This is a major contribution to the research.

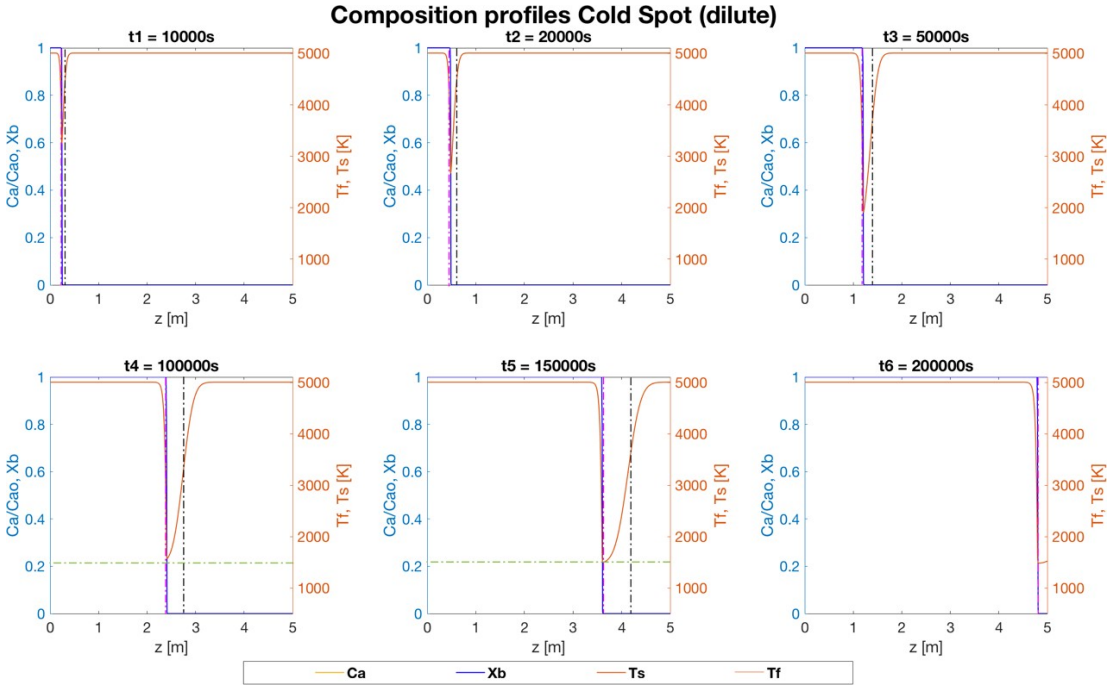

Figure 6-26: Composition profiles with Z_{T1} (black dashed), $Z_{T/C}$ (purple dashed), $T_{plateau}$ (green dashed) for dilute cold spot case (5008K)

Time (s)	Wave Model			Simulation Results		
t	$Z_{T/C}$	Z_T	$T_{plateau}$ **(K)**	$Z_{T/C}$	Z_T	$T_{plateau}$ **(K)**
1.0 x 10^4	0.24	0.28	1479	0.2	0.3	-
2.0 x 10^4	0.48	0.56	1479	0.4	0.6	-
5.0 x 10^4	1.20	1.39	1479	1.2	1.2	-
1.0 x 10^5	2.40	2.78	1479	2.3	2.8	1480
1.5 x 10^5	3.60	4.17	1479	3.6	4.2	1480
2.0 x 10^5	4.80	-	1479	4.8	-	1480

Table 6-9: Comparison of distance travelled by thermal, thermochemical waves & plateau temperature for dilute cold spot case

/

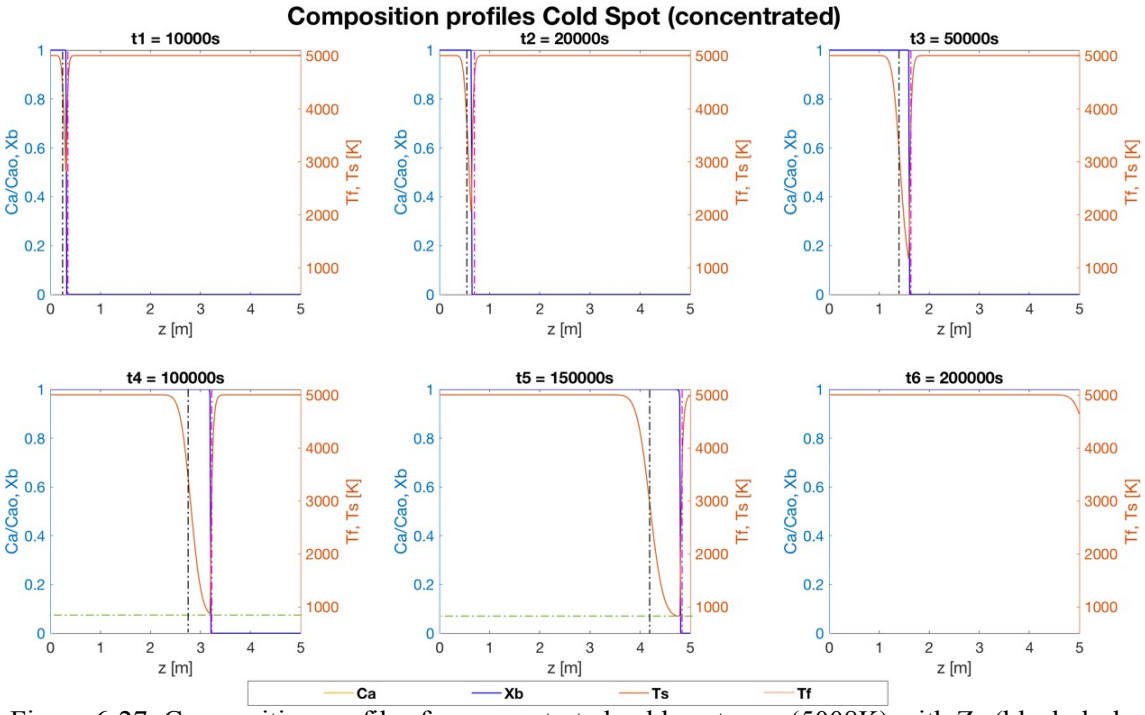

Figure 6-27: Composition profiles for concentrated cold spot case (5008K) with Z_T (black dashed), $Z_{T/C}$ (purple dashed), $T_{plateau}$ (green dashed)

Time (s)	Wave Model			Simulation Results		
t	$Z_{T/C}$	Z_T	$T_{plateau}$ (K)	$Z_{T/C}$	Z_T	$T_{plateau}$ (K)
1.0 x 10^4	0.32	0.28	797.4	0.3	0.3	-
2.0 x 10^4	0.64	0.56	797.4	0.7	0.6	-
5.0 x 10^4	1.59	1.39	797.4	1.6	1.2	-
1.0 x 10^5	3.20	2.78	797.4	3.2	2.8	798
1.5 x 10^5	4.80	4.17	797.4	4.8	4.2	798
2.0 x 10^5	-	-	797.4	-	-	798

Table 6-10: Comparison of distance travelled by thermal, thermochemical waves & plateau temperature for concentrated cold spot case

6.4.6 *Effect of variation in h_w*

Heat flux is interesting to analyse for two reasons. Firstly, it is important to analyse in terms of heat addition for endothermic reactions and secondly, as heat losses in exothermic reactions. A constant wall temperature is assumed. Heat addition have a significant influence on the temperature profiles. In endothermic reactions, this is a key method when designing fixed bed reactors. Beyond a certain heat transfer coefficient, reaction halts and the temperature variation form a bell-shape and remains that way till the wave passes

through the bed. The value of h_w = 10 W/mK increases the peak temperature from 400K to 560K. The leading thermal wave is retarded due to the effect of h_w. The wave model would not accurately predict the position of the thermal or plateau temperature.

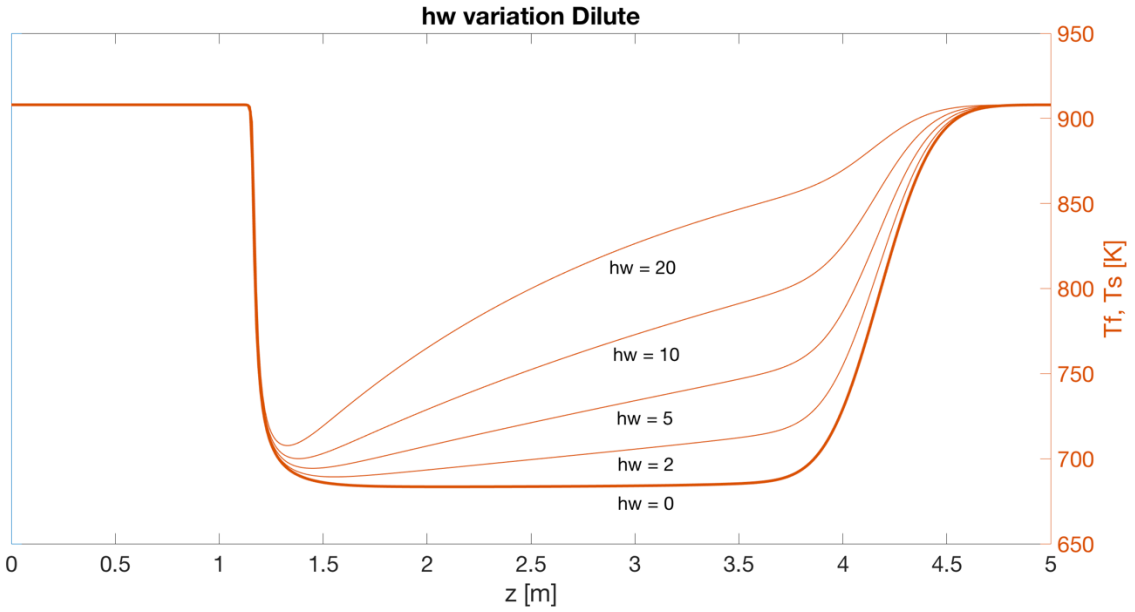

Figure 6-28: Influence of wall heat transfer coefficient on the temperature profiles Dilute. Range h_w= (**0**, 2, 5, 10, 20) W/mK.

	h_w (W/mK)	V_T (m/s)	$V_{T/C}$ (m/s)	ΔT_c (K)
Wave Model	0	2.67 x 10^{-4}	7.03 x 10^{-6}	-212.7
Numerical Simulation		2.8 x 10^{-5}	7.0 x 10^{-6}	-213
Wave Model	2	2.59 x 10^{-4}	7.03 x 10^{-6}	-202.1
Numerical Simulation		2.6 x 10^{-5}	7.0 x 10^{-6}	-204
Wave Model	5	2.45 x 10^{-4}	7.03 x 10^{-6}	-192.2
Numerical Simulation		2.5 x 10^{-5}	7.0 x 10^{-6}	-192
Wave Model	10	2.32 x 10^{-4}	7.03 x 10^{-6}	-186.8
Numerical Simulation		2.3 x 10^{-5}	7.0 x 10^{-6}	-188
Wave Model	20	2.07 x 10^{-4}	7.03 x 10^{-6}	-177.3
Numerical Simulation		2.1 x 10^{-5}	7.0 x 10^{-6}	-178

Table 6-11: Comparison of distance travelled by thermal, thermochemical waves & plateau temperature for wall heating (dilute)

It should be noted that the temperature drop calculated in Table 6-11 is associated with the thermochemical wave not the thermal wave. The thermal wave has a larger width and

therefore a constant wall heating raises the temperature of the wave higher than that of a thermochemical wave. According to the wave model equations in Chapter 3, The thermochemical wave velocity speeds up in the dilute case. The width of the thermochemical wave is so sharp that it has little effect on the wave velocity but more of an effect of the plateau. This shows the wave model can accurately predict the temperature required to raise the plateau. A useful result in applying heat integrated systems in endothermic reactions.

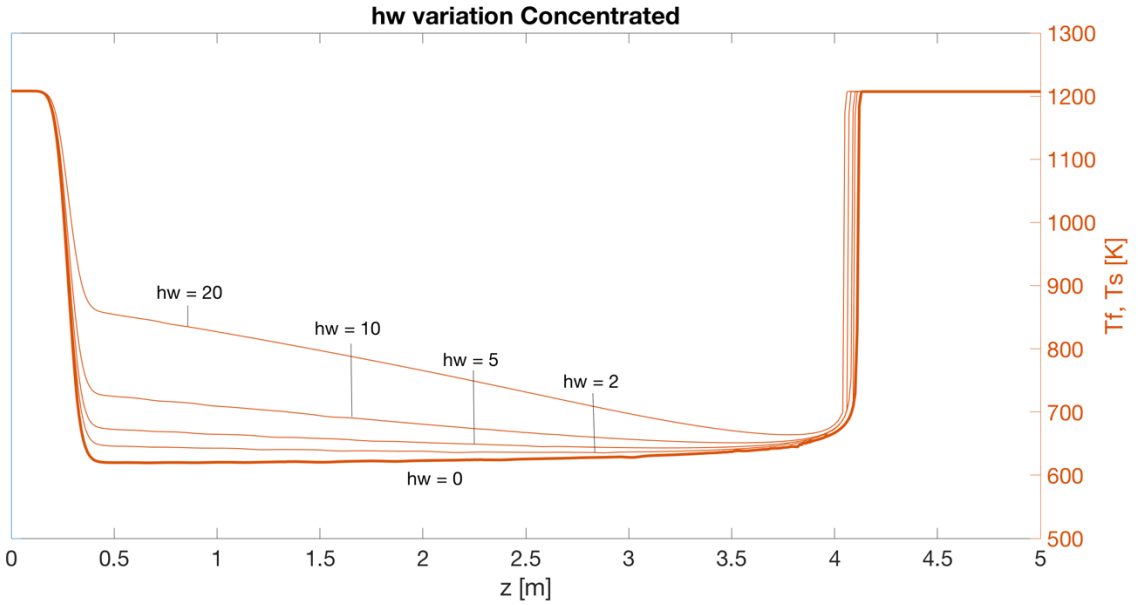

Figure 6-29: Influence of wall heat transfer coefficient on the temperature profiles Concentrated. Range h_w= (**0**, 2, 5, 10, 20) W/mK.

	h_w (W/mK)	V_T (m/s)	$V_{T/C}$ (m/s)	ΔT_c (K)
Wave Model	0	2.67×10^{-4}	2.13×10^{-3}	-212.7
Numerical Simulation		2.8×10^{-5}	2.1×10^{-3}	-213
Wave Model	2	2.59×10^{-4}	2.03×10^{-3}	-202.1
Numerical Simulation		2.6×10^{-5}	2.0×10^{-3}	-204
Wave Model	5	2.45×10^{-4}	2.0×10^{-3}	-192.2
Numerical Simulation		2.5×10^{-5}	1.9×10^{-3}	-192
Wave Model	10	2.32×10^{-4}	1.97×10^{-3}	-186.8
Numerical Simulation		2.3×10^{-5}	1.8×10^{-3}	-188
Wave Model	20	2.07×10^{-4}	1.93×10^{-3}	-177.3

Numerical Simulation	20	2.1×10^{-5}	1.8×10^{-3}	-178

Table 6-12: Comparison of distance travelled by thermal, thermochemical waves & plateau temperature for wall heating (conc.)

When a concentrated fluid is injected into the bed, the thermochemical wave velocity is predicted to slow down and the thermal wave to speed up. The thermochemical wave has a wider width and the effect is more pronounced than in the dilute case (Fig. 6-28). The realistic heat coefficient is 5 W/mK. The heating of the reactor all may not provide enough of a temperature rise but in this case the temperature of the wall should be raised to achieve the required temperature.

6.5 Summary and comparison with other works

This chapter involved looking at endothermic gas-solid reactions using pyrite reduction as an example. The endothermic case required an extension of the wave model to include adiabatic heating and its quantitative and qualitative effect on reactor dynamics. Mathematical expressions based on material and energy balances across the thermal and thermochemical waves and temperature of plateau included mass and heat transfer zones. This was essential in determining the amount of heat required to avoid cold spots in endothermic reactions. The developed wave model allowed the prediction of different injection strategies and comparison with the numerical simulations. The numerical simulations were in good agreement with the wave model. All the cases tested showed a constant pattern thermochemical wave travelling through the reactor, the speed of the thermochemical wave was limited by the temperature ahead of the wave. The pre-heat and reduced heat strategies were shown to also be energy saving in the endothermic system.

Vaccaro (2010) studied the supply of energy for endothermic removing carbon dioxide in water gas shift reactions. The results were prone to the formation of cold spots and

alternative solutions were needed to balance the heat flux generated and consumed, especially when high outlet conversions of CO are desired. These alternative solutions included the optimization of catalyst distribution in the combustion channel, and optimization of fuel distribution along the reactor. A simple application of the wave model presented here could be used as an optimisation tool. The results from the experimental results showed wave like behaviour similar to the numerical simulations in the current work. Of course, the wave model is an oversimplification of the process but is a valuable tool in terms of gaining insight into cause and effect. Glockler (2004) worked on auto thermal endothermic reactions Experimental verification of design concepts was presented showing a stable reactor performance during methanol steam reforming. This is promising as it shows the numerical simulations are a good description of experimental results.

It was shown that with a sufficient feed concentration, high conversion can be achieved at 900°C. Starting from a uniformly preheated catalytic fixed-bed, a sharp, travelling reaction wave with total conversion was established during the reforming period. During the regeneration period the uniform temperature profile was established by introducing heat in specific locations in the catalyst bed. The effect of varied concentrations or temperatures were not investigated. Instead a novel system based on reversing flows were sought.

An interesting observation was made when the injected fluid was set to a critical concentration producing a cold spot. This cold spot causes caused splitting of the thermochemical waves across the cold spot region. Thereby having two different reaction zones travelling at different velocities. Further analysis into the rates of reaction during the simulation showed two peaks propagating through the reactor bed, which match up to the positions of the splitting thermochemical waves. The wave model showed its value here by accurately predicting the positions of the two thermochemical waves. A major contribution of this current work. Heating from the reactor wall was shown to avoid the cold spot whilst

not distorting the coherent thermochemical wave in both the dilute and concentrated cases within a range of wall temperatures and heat transfer coefficients.

With a cold spot region in between. The result from these experiments showed that the formation of a cold spot in endothermic fluid-solid reactions is encountered in practice.

The results of the numerical model and the experiments were in good agreement. The numerical model was used to investigate the required thermal input to ensure high conversion to H_2. The system showed coherent thermochemical waves travelling across the reactor. The wave model would be useful in the heat control system by estimating the required heating to ensure a high yield. Instead a solution based on raising the temperature in a control loop was employed. This is not cost effective and does not lend insight into cause and effect.

For the pyrite case, when dilute hydrogen is used, $t_{T/C}$ = 624700s and t_T = 180000s. Therefore, 27.8% of the energy required to heat the injected dilute hydrogen is saved. Due to the endothermic nature of the process, there is a possibility of a large temperature drop, which reduces the rate of reaction creating a zone where the hydrogen and pyrite do not react. In practice, a concentrated hydrogen feed is used as the reaction is much faster and saves heating cost ($t_{T/C}$ = 12600s). A plausible strategy is to inject concentrated hydrogen while preheating a fixed bed of pyrite solids. A continuous heating of the bed prior to injecting the cold fluid is not energy efficient. Pre-heat strategy involves injecting concentrated hydrogen whilst still pre-heating the bed with nitrogen. The fixed bed of pyrite particles is initially heated to the ignition temperature 908K before hydrogen is injected. In terms of propagation of waves, a thermal wave travels ahead heating the pyrite. Injecting hydrogen introduces to a thermochemical wave, which is faster than the leading thermal wave associated with the pre-heat nitrogen stream. Injection of concentrated hydrogen at the right time, so the thermochemical wave meets the leading thermal wave at

the reactor exit is the pre-heat strategy. In other words, there is no need to completely heat up the pyrite bed before hydrogen is injected. The wave model is used to calculate the time to inject the concentrated hydrogen. The time to inject cold hydrogen is stream is 12600s before the thermal wave reaches the end of the bed of pyrite.

$$t_{injection} = t_T - t_{T/C} = 162400s$$

Injecting the concentrated hydrogen at $t_{injection}$ saves 10.4% of the heating time of the pyrite bed. It should be noted that in this concentrated case, the thermochemical wave has reached constant pattern very quickly and therefore the application of the wave model is valid.

$$E = m.cp.\Delta T$$

$$\text{Where } m = \rho.u.A = 1.44kg/s$$

$$E = 0.95 \text{ MW}$$

Chapter 7

Reversible Exothermic Gas-Solid Reactions

It should be noted that this chapter is completely theoretical particularly the modelling. The properties of reversible reactions introduce a number of new elements into the discussion about non-isothermal reactors. A numerical model is presented and used to simulate the kinetic and thermal behaviour of a reactive system in which the reversible reaction between a fluid and solid takes place. The value of the approach consists in the fact that it can deal with reactions whether they are exothermic or endothermic, for a fluid and a solid particularly in a reversible reaction, leading to a solid product. A modified shrinking core model is implemented in the material balances with an alteration of the rate equation in the PDEs. Wave model predictions are made for the reversible reaction and are compared with the numerical simulations. The reaction which is considered here is the reversible exothermic reaction of pyrite with oxygen to form hematite.

The contribution in this chapter is the analysis of an exothermic gas-solid reaction system with even slower reacting non-equilibrium systems than in the irreversible case. Even when conditions favour the reverse reaction, true reversibility is unlikely to be achieved since the physical form of the reformed solid is unlikely to be identical with its form before the reaction. The reactor is in the form of a fixed bed. The fixed solids in the downstream points of reaction within the bed will be exposed to a mixture of products and reactant gas. Thus, the conditions exist for the reverse element of the reaction to occur in the upstream part of the bed where the rate of overall conversion is increased.

7.1. Physical Model for Reversible Gas-Solid Reaction

The models previously presented consider that the reaction at the core shell interface is irreversible, so it only depends on the concentration of the injection fluid. Now the case where an equilibrium reaction is involved is considered. Since the development of the basic Shrinking Core Model (SCM) (Levenspiel, 1979, 1999), kinetic models have become progressively more sophisticated, in order to more closely describe the complex simultaneous phenomena involved in gas-solid reactions, including the chemical reaction itself, diffusional transport on different scales in the porous solid, external mass transfer, heat transfer and so on. A good way of classifying the different models in the literature and of contextualising the present one is to distinguish them according to the necessary assumptions on which they are based. A modified shrinking core model for reversible reactions is developed and presented.

For a reversible fluid-solid reaction, the chemical balance may be written as:

$$a\,A(fluid) + b\,B(solid) \rightleftharpoons c\,C(solid) \tag{7.1}$$

$$\frac{1}{2}O_2 + 2Fe_3O_4 \rightleftharpoons 3Fe_2O_3$$

The oxidation of magnetite is a noncatalytic gas-solid reaction characterized by the formation of a solid product (hematite).

$$Oxygen + Magnetite \rightleftharpoons Hematite$$

Some of the classical assumptions discussed in the irreversible model are removed in the present model:

- The reaction located on a surface is the most important assumption of the model. This is not always physically correct. In particular, if the particle is initially porous, it doesn't behave like a shrinking core.
- the reaction can be reversible, non-equimolar, and exothermic or endothermic,

- allowance is made for the possible presence of two reacting solid species in the formed ash layer.
- various reaction kinetics can be considered.

Conversely, the following assumptions are maintained:

- the particle is spherical, and its diameter remains constant,
- the total gas pressure is constant,
- the porosity and the tortuosity are not modified by the progression of the reaction.
- The reactor is one dimensional in plug flow.
- Effective diffusivity, heat transfer coefficient, density and specific heat of both gas and solid phases remain invariant during the reaction.

The model is modular in conception and in future versions could be made more general by eliminating some of the previous assumptions. In particular, the last two assumptions are certainly the most restrictive.

The modelling of the reversible reaction with iron ore directly as the starting material is rather challenging. Silaban and Harrison, 1995 studied the kinetics of the reduction of magnetite concentrate particles by hydrogen in the temperature range of 1423-1673 K. Du et al., 2017 reduced pure cylindrical compacts of magnetite isothermally at 973 - 1273 K with pure H_2. This would make the study more practical and industrially important. Reduction at a lower temperature would be more economical and worth studying. The variables studied by Du et al., 2017 for this purpose were as follows: time (0 - 30 min), temperature (973 - 1273 K), hydrogen flow rate (0.1 - 0.5 L/min), hydrogen partial pressure (0.25 - 1 atm), sample bed height (0.25 - 0.75 cm), and particle size (75 - 180 mm). The bulk density values of the three chunks of the concentrate were obtained with an average of 3763 kg/m^3. The bed porosity was calculated as 27%. Isothermal reduction of magnetite ore fines was performed at five hydrogen flow rates, 0.1, 0.2, 0.3, 0.4, and 0.5 L/

min, at 1173 K and 1 atm pressure. Argon gas was employed for the purging and pre-heating purpose before and after the reduction. In addition, argon was mixed with hydrogen in different proportions to produce different partial pressures of hydrogen. The reversible reaction was modified for the term k_f which takes different values for different reduction steps. Another important point is their suggested adaptations, are typically valid for dense bed where the reaction front moves downward through the bed progressively. The maximum fractional reduction (X) achieved increases from 0.7 to 0.9 as the flow rate increases from 0.1 to 0.4 L/min. Wagner et al., 2006 reported when temperatures higher than 570°C are used, hematite (Fe_2O_3) is first transformed into magnetite (Fe_3O_4). The results of the experiments carried out at different temperatures show the reaction rates at 5 % and 80 % of conversion were reported on an Arrhenius diagram. The activation energies calculated were 14.7 kJ/mol and 14.3 kJ/mol. The effect of the flow rate is not much noticeable with the increase of flow rate above 0.4 L/min.

Shen and Smith, 1965 and Uhde and Hoffman, 1997 have also considered reversibility in gas-solid reactions. The latter using a grain model. The assumption of linear concentration profile within the reaction zone has restricted its application. It is necessary to include reversibility aspects for the design procedures adopted for the regeneration process in fixed bed reactors.

A physical model is presented and used to simulate the kinetic and thermal behaviour of a reactive system in which the reversible reaction between a fluid and solid takes place. The reduction of hematite (B: Fe_2O_3) to magnetite (C: Fe_3O_4) using hydrogen (A: H_2) is a noncatalytic reversible gas-solid reaction. Some of the assumptions discussed in the irreversible model are removed in the present model:

- The particle is initially porous and does not behave like a shrinking core.
- Fluid to mass transfer is ignored

- The reaction in the ash layer is similar to a 'stirred-tank' where A & B are mixed in the porous layer.
- Reversible reaction is first order with respect to the reacting solid C.

Conversely, the following assumptions are maintained:

- The particle is spherical, and its diameter remains constant,
- The total gas pressure is constant,
- The porosity and the tortuosity are not modified by the progression of the reaction.
- The reactor is one dimensional in plug flow.
- Effective diffusivity, heat transfer coefficient, density and specific heat of both gas and solid phases remain invariant during the reaction.

When A reacts with B to form C, the reaction is in the porous layer (assuming the distribution of B is uniform i.e. a stirred tank). C is formed on the surface of the particle. In the reverse direction, C is not reacting with A but reversibly forming B in the ash layer. The overall rate of reaction per particle rate equation:

$$r'_A = -k' C_A N_{BO}(1 - X_B) + k" N_C \tag{7.2}$$

The forward rate constant (k') deals with the reaction in the ash layer between A and B. is the initial number of moles of B. is the number of moles of C as a function of the amount of B left ($1-X_B$).

$$N_C = \frac{c}{b} X_B N_{BO} \; where \; N_{BO} = \frac{4}{3}\pi r^3 X_B \frac{\rho_B}{M_B} \tag{7.3}$$

The reverse rate constant (k") represents with the reversible reaction of C on the surface of the particle. is the overall reaction rate in kmol/s and is plugged in the governing mass and energy balances for a fixed bed of solids given in Zhao et al., 2015. The equation for k' is the simple Arrhenius relationship except there is no k_T whereas k" has no k_T and D_E.

7.1.1 Rate equations for reversible reaction

Definitions of necessary terms used in the rate equations are introduced. n_C is the mole fraction of the solid C, n_B is the mole fraction of the solid B, n_{BO} is the initial mole fraction of solid B.

From our previous definition of conversion X_B;

$$X_B = \frac{n_{BO} - n_B}{n_{BO}} \tag{7.4}$$

the initial number of moles of the solid B can be written as

$$n_{BO} = \frac{4}{3}\pi {R_s}^3 \frac{\rho_B}{M_B} \tag{7.5}$$

For the amount of total solid to be conserved at the start of the reaction.

$$n_C + n_{CO} = \frac{c}{b}(n_{BO} - n_B) \tag{7.6}$$

The model assumes that there is no solid C at the start of the reaction. Therefore, the mole fraction of the solid C is the stoichiometric equivalent of the amount of B reacted, which can be expressed as

$$n_C = \frac{c}{b} n_{BO} X_B \tag{7.7}$$

In the simulations shown in Fig. 7-3. C_c is defined to represent n_c as the concentration of solid C.

Therefore, the mole fraction of the solid C can be expressed as

$$n_C = \frac{4}{3}\pi {R_s}^3 \frac{c}{b} \frac{\rho_B}{M_B} X_B \tag{7.8}$$

This equation means the amount of solid product C formed is the amount of solid reactant B. The amount of each solid present is dependent on the equilibrium kinetics of the system. If equilibrium is involved, the concentration balance for the product solid C must be coupled with the system of material and energy balance equations.

7.1.2 Material and Energy Balance for Reversible Gas-Solid Reaction

The idea of a reversible reaction occurring at the core shell interface is that, depending on the relative amount of gas and product present at that interface, the interface can shift towards the particle centre or towards the external surface depending on the value of the reaction rate (negative or positive respectively).

The rate of reaction per particle (r_a') at the core surface may be rewritten per particle as

$$r_a' = -k' 4\pi r_c^2 C_A\left(1 - X_B\right) + k'' n_c \tag{7.9}$$

The first term represents the forward reaction, the second represents the reverse reaction and n_c represents the number of moles of C in the ash layer per particle. Note the latter term is not strictly a 'shrinking core' term, as the reverse reaction may occur throughout the ash layer.

The stoichiometry of the chemical balance gives:

$$\frac{-r_a'}{a} = \frac{-r_b'}{b} = \frac{r_c'}{c} \tag{7.10}$$

Molar amount of C = $\frac{c}{b}$ x number of moles of B consumed. C is now the ash layer and is porous as shown in Fig. 7-1.

The shrinking core model initially used was based on uncertain grounds, but this was replaced it with a 'stirred tank' model and similar results were produced. The stirred-tank model assumes a single resistance controls throughout the reaction. A constant size particle where the gas-film resistance remains unchanged. There is no ash-layer instead a region where the fluid and solid are completely mixed where there is a reversible reaction. Strictly speaking, there is no shrinking particle but instead a completely mixed ash layer and a surface reaction.

To the level of detail that the thesis is concerned about, which is the propagation of moving fronts, the fluid to mass transfer does not affect the results significantly. Comparing the

results from the previously assumed reversible shrinking core model to a stirred tank model for a gas-solid reversible reaction. The results are similar, this is indicative of the fact that the reaction is completely controlled by the kinetics, and the fluid to mass transfer effects are negligible in this case. Therefore, fluid to mass transfer is ignored in the current development of reversible gas-solid reactions and the more complex problem shall be deferred to future work.

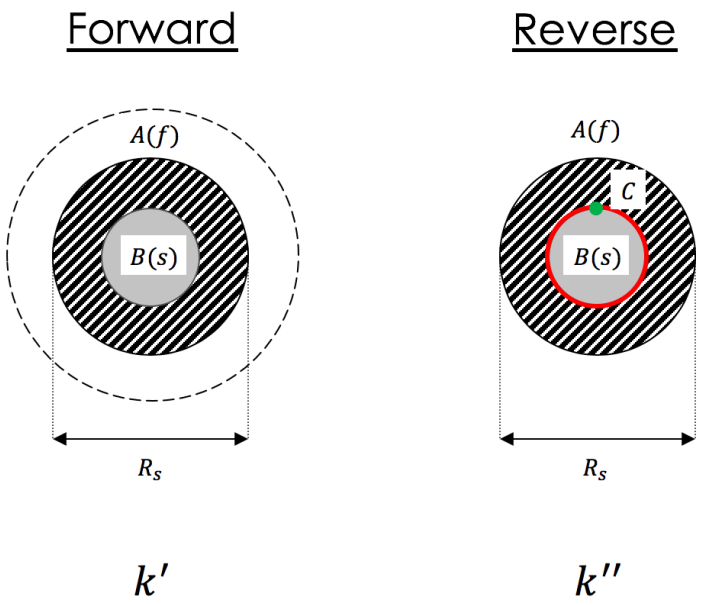

Figure 7-1: Shrinking core particle model for reversible reaction

The component mass balance for $A(fluid)$:

$$r_a' n_P = \varepsilon \left(\frac{\partial C_A}{\partial t} \right)_z + u \left(\frac{\partial C_A}{\partial z} \right)_t \tag{7.11}$$

The solid mass balance for $B(solid)$ per particle:

$$r_b' = - \frac{4\pi {R_s}^3 \rho_B}{3 M_B} \left(\frac{\partial X_B}{\partial t} \right)_z \tag{7.12}$$

r_b' varies with r_a' and r_c' in stoichiometric ratios. The reversible reaction of C is implicit in the rate of reaction at the core surface. This means that the material and energy balance of the irreversible case and be used whilst the rates of reactions are replaced by the rate

equations in 7.11.

It follows that the system of equations to be solved for the single reversible reaction in the $A + B \rightleftharpoons C$ are:

$$\varepsilon \frac{\partial C_A}{\partial t} + u \frac{\partial C_A}{\partial z} = r'_a n_P \tag{7.13}$$

$$\frac{\partial X_B}{\partial t} = - \frac{bM_B}{a\rho_B(1-\varepsilon)} r'_a n_P \tag{7.14}$$

$$\varepsilon \frac{\partial T_f}{\partial t} + u \frac{\partial T_f}{\partial z} = \frac{3h\left(T_s - T_f\right)(1-\varepsilon)}{R_s c_f} \tag{7.15}$$

$$\frac{\partial T_s}{\partial t} = - \frac{3h\left(T_s - T_f\right)}{R_s c_s} + \frac{r'_a n_P \Delta H}{c_s(1-\varepsilon)} \tag{7.16}$$

Where the rate constants for the forward and the reverse reaction are given as:

$$k' = \frac{\left(1 - X_B\right)^{\frac{2}{3}}}{\frac{1}{k_{TO}} e^{\frac{E_R}{RT_f}} + \frac{R_s}{D_{EO}} e^{\frac{E_{de}}{RT_f}} \left(\left(1 - X_B\right)^{-\frac{1}{3}} - 1\right) + \frac{1}{k_{FO}} e^{\frac{E_{AF}}{RT_s}} \left(1 - X_B\right)^{-\frac{2}{3}}} \quad and \quad k'' = \frac{1}{\frac{1}{k_{RO}} e^{\frac{E_{AR}}{RT_s}}} \tag{7.17}$$

7.1.3 Equilibrium of Reversible Gas-Solid Reaction

To run the numerical simulation of the equations presented, the parameters must first be explained. The equilibrium constant for this reaction is defined as

$$K_{eq} = \frac{k'}{k''} \tag{7.18}$$

With reversible exothermic reactions, the combination of thermodynamic and kinetic parameters means that increasing temperatures give rise to decreasing net forward reaction rates. This may seem a little counter- intuitive. Fig. 7-2 below explains the activation energies for the exothermic reaction considered here.

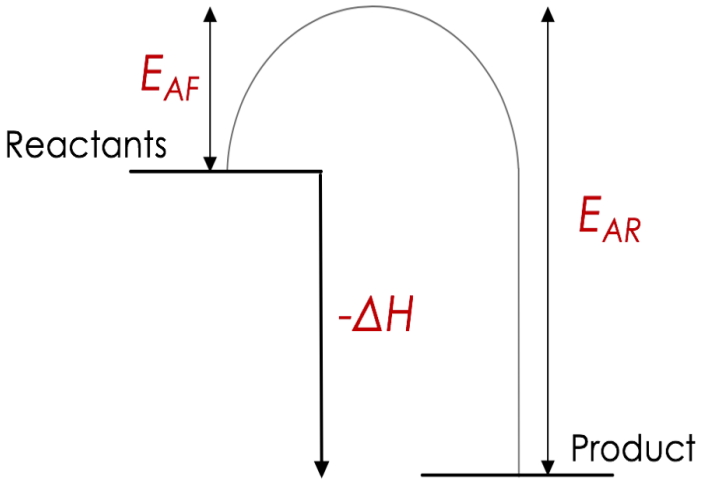

Figure 7-2: Activation Energies for reversible reaction

$$\therefore E_{AR} > E_{AF}$$

For exothermic reactions, this means that E_{AR} is greater than E_{AF}. $E_{AR} = E_{AF} - \Delta H$, where ΔH is negative for an exothermic reaction. Thus, as the temperature rises, the term "$e^{-\frac{E_{AR}}{RT_s}}$" increases in magnitude faster that the term "$e^{-\frac{E_{AF}}{RT_s}}$". Clearly both rate constants increase with increasing temperature. What this means is that for increasing temperatures, when $\Delta H < 0$, k'' increases faster, relative to k'. This is why the ratio $\frac{k'}{k''}$ $(= K_{eq})$ diminishes with rising temperature. This is examined in the hot spot case.

7.1.4 Evaluation of Physical Model

The modified shrinking core model that the solid product diffuses through the solid reactant ash layer, without reacting and the reversible reaction only occurs at the core. If this is certainly true for the solid product, this reaction is not a completely accurate description of a reversible reaction. Despite these limitations, the shrinking core model is still widely used also for the reversible cases considered, and several works with reversible and multi-step reactions can be found in the literature chapter. It is still possible to make

use of it, because of its simplicity and easy applicability to complex reactor problems. Other models such as Finite-Element method and Diffusion-Interface model (Khan (2011)) for reversible reactions have assumed that conditions at the interface between the reaction zone and the unreacted core correspond to equilibrium at the prevailing temperature. The gaseous concentrations were assumed to permeate the core at the interfacial values so that no reaction occurred in the core. These models have been applied successfully to the data of the reduction of hematite at different temperatures Khan (2011). The contribution of different forms of resistance, diffusion in product layer, chemical reaction and diffusion in the reactant core, is assessed as function of time (start to the end of reaction). The thickness of the reaction zones remain almost constant as the reaction progresses.

7.1.5 Parameters of Reversible Exothermic Gas-Solid simulated system

Parameters for this chapter are gathered from literature review and cited in Chapter 2. Philinis (1957) provided a description of the kinetic and thermodynamic data below. These parameters are assumed to be the same as in Chapter 6 with the exclusion of oxygen fluid properties instead of hyrdogen.

7.2 Prediction of Wave Behaviour for Reversible reactions

The common practice is to use diluted oxygen as demonstrated by Philinis, 1957. The reversible reaction is predicted by the wave model for concentrated and dilute oxygen. In each case, the effect of the reversibility, initial and injected temperature conditions are discussed.

Injection strategies

The behaviour of a reversible exothermic reaction under non-isothermal conditions can

be pieced together. This will be derived for a reactor bed initially free of solid C (only solid B is present) and at a temperature above ignition temperature receiving a constant composition of reactive fluid A. Two cases can be distinguished as before; a dilute and a concentrated fluid case.

7.2.1 Dilute Fluid case

In the dilute case, the wave model predicts the thermochemical wave to be slower than the thermal wave as the value of C_{AO} is larger. If the thermal wave is faster, the heat released by the thermochemical wave travels faster than the thermochemical wave, leaving the wave behind. Fig. 7-3 shows the predicted wave behaviour. All of the heat released is contained in a zone bounded by the two waves as shown in Fig. 7-3. The front of the zone (where the thermal wave is) entails no reaction with a velocity, V_T in equation (3-21). There can be no reaction ahead of the thermochemical wave. The rear of the zone (coincides with the thermochemical wave). This wave thus entails both a reaction and a temperature variation. The slow thermochemical wave relative to fluid flow, caused by the reaction of the reactor bed remains unaffected behind the thermochemical wave where the temperature is equal to that of the injected fluid.

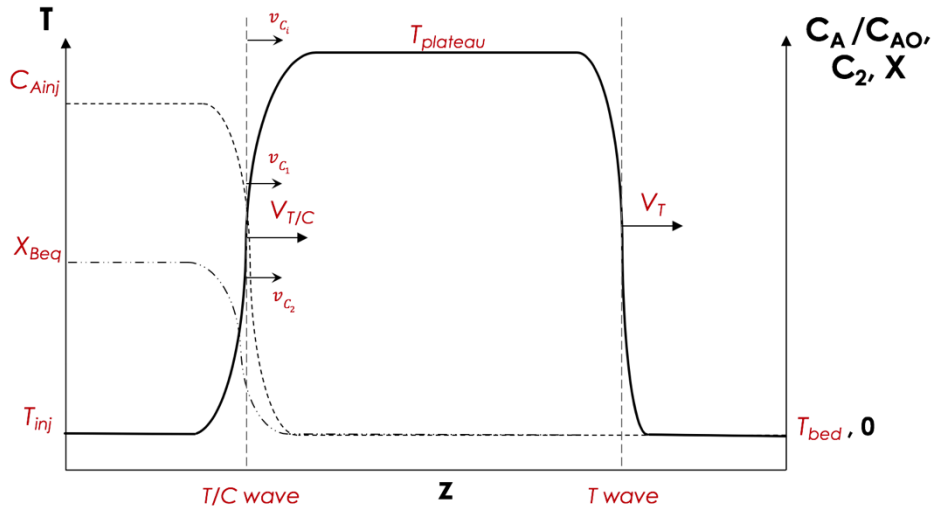

Figure 7-3: Temperature profile for hot fluid into a hot bed (dilute)

Typically, two distinct waves propagate along the fixed-bed reactor, a thermal wave with a velocity V_T and a thermochemical wave with a velocity $V_{T/C}$ as in Figure 7-3. When the heat of reaction is negative (exothermic), the wave model predicts a temperature rise. The thermochemical wave is moving into a heated region. If the temperature of the injected fluid and the bed temperature are high enough, the reaction is stable.

7.2.2 Concentrated Fluid case

In the concentrated case, the wave model predicts interestingly a leading the thermochemical wave and a trailing thermal wave which also has a reaction associated with it. In essence, there are two thermochemical waves travelling at different velocities with a plateau zone in between them as shown in Fig. 7-4.

If the thermal wave is slower, the released heat of reaction is left behind the thermochemical wave as the reaction progresses. The reactive fluid and a partially reacted reactor bed behind the leading thermochemical wave are now at a higher temperature. If the heat of reaction is negative, as presumed, a decrease in temperature increases the rate of reaction. In the rear of the plateau zone, a pure thermal wave might be expected as in the irreversible case. However, since the temperature drops back from the plateau to the injected fluid temperature, an additional shift in equilibrium occurs and there is more conversion of solid behind the wave at T_{inj}. Therefore, the trailing wave is also a thermochemical wave. In face the plateau zone can be thought of as having two sections, one section between the trailing thermochemical wave and a plane travelling at pure thermal wave V_T, which contains heat released by the trailing thermochemical wave. The second section between the plane and the leading thermochemical wave contains heat

released by the leading thermochemical wave.

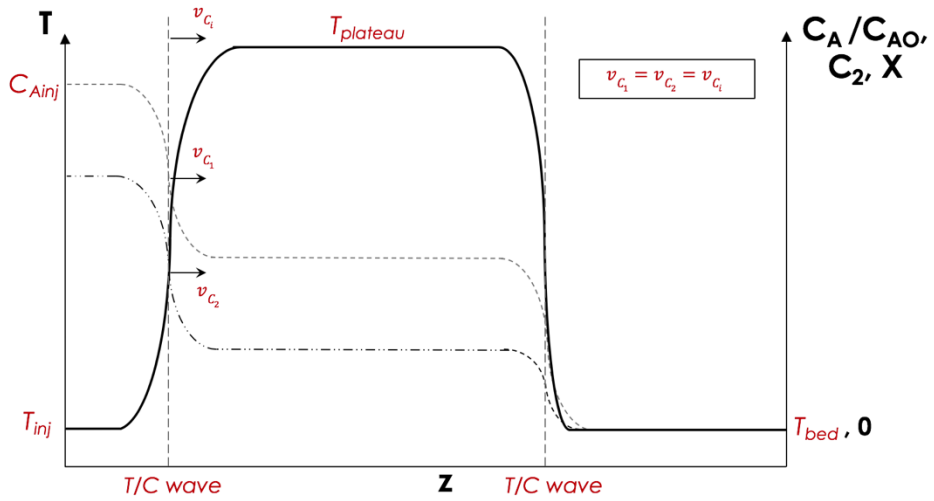

Figure 7-4: Temperature profile for hot fluid into a hot bed (concentrated)

The reaction will occur above the ignition temperature and be stable. The amount of A, B or C reacting depends on the kinetics of the system which can be employed in the wave model equations. A high injected fluid temperature and bed temperature is required to observe the propagation of waves as in Figure 7-4.

7.2.3 Hot Spot

A comparison of the dilute and concentrated injected fluid case brings out a significant difference. In the dilute case, with a faster thermal wave, the variation of temperature has no effect on the reaction (the waves are less sharp). In the concentrated case, the reaction is profoundly affected. There are two positions where the reaction occurs, each associated with a temperature drop with a plateau zone in between. The temperature of the plateau depends on the size of the plateau. The narrower the zone when the heat is released, the greater the temperature rise. However, in the exothermic reversible case, the higher the temperature, the lower the conversion of the reactor bed. There is no increasing temperature peak like in the irreversible case but instead a finite temperature peak is reached limited by the reversibility of the system.

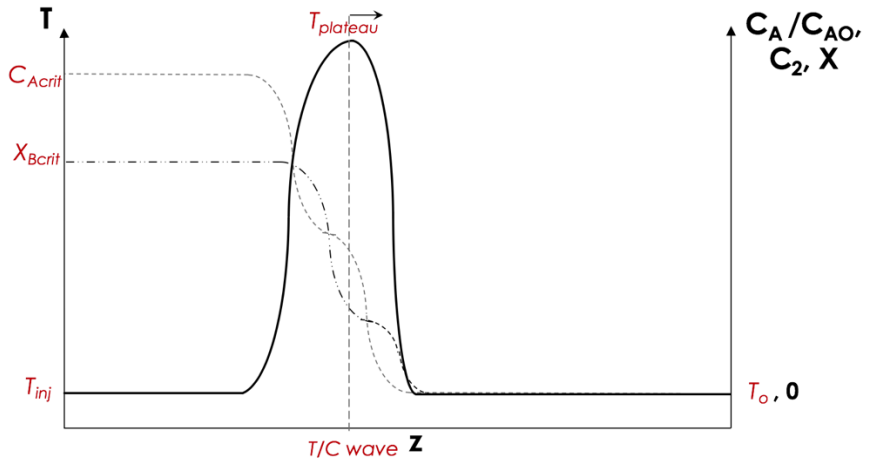

Figure 7-5: Temperature profile for hot fluid into a hot bed (hot spot)

7.3 Wave Model Simultaneous Equations

The wave model discussed in the earlier chapters were derived for dilute and concentrated cases with a distinct pure thermal wave and thermochemical wave. In the reversible case, there are two thermochemical waves travelling at different velocities. At the inlet, the injected fluid and solids reacting are at equilibrium. The plateau zone is a region where the reaction rate is also zero. Due to this fact, the concentration profiles are flat in this zone. Ahead of the plateau zone, the concentrations drop to zero and the temperature down to the bed a shown in Fig. 7-6.

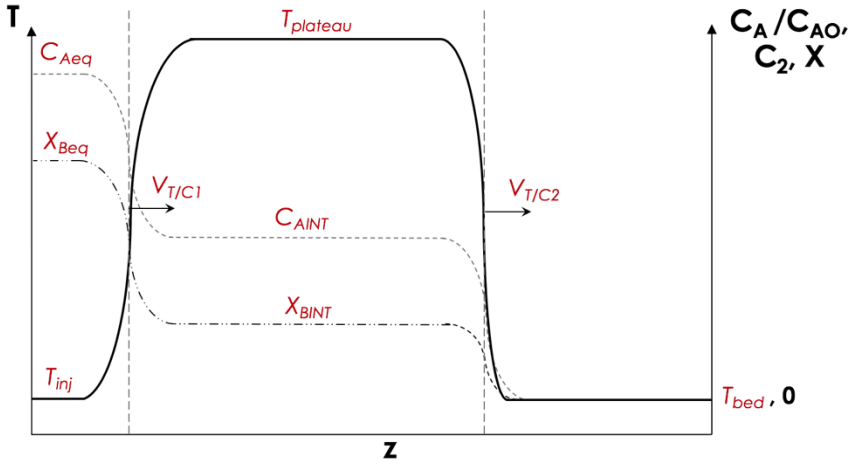

Figure 7-6: Temperature profile for hot fluid into a hot bed (concentrated)

The wave model can be solved by constructing equations based on no rate of reaction in

the inlet and the plateau zones giving

$$C_{Aeq} = \frac{k'' n_c}{k' 4\pi r_c^2 \left(1 - X_B\right)} \tag{7.19}$$

$$C_{Aeq} = \frac{R_s}{3} \frac{c}{b} \frac{\rho_B}{M_B} \frac{k''}{k'} \frac{X_{Beq}}{\left(1 - X_{Beq}\right)^{2/3}} \tag{7.20}$$

$$C_{Aeq} = f\left(X_{Beq}\right) \tag{7.21}$$

It then follows from the equations (3.22), (3.21) and (7.4), the following set of simultaneous equations can be used to find the unknowns: C_{AINT}, X_{Beq}, X_{BINT}, $V_{T/C1}$, $V_{T/C2}$ and $T_{plateau}$. $C_{Aeq}$is equal to the injected fluid concentration.

$$C_{Aeq} = \frac{R_s}{3} \frac{c}{b} \frac{\rho_B}{M_B} \frac{k''}{k'} \frac{X_{Beq}}{\left(1 - X_{Beq}\right)^{2/3}} \tag{7.22}$$

$$C_{AINT} = \frac{R_s}{3} \frac{c}{b} \frac{\rho_B}{M_B} \frac{k''}{k'} \frac{X_{BINT}}{\left(1 - X_{BINT}\right)^{\frac{2}{3}}} \tag{7.23}$$

$$V_{T/C1} = \frac{u/\varepsilon}{1 + \frac{(1-\varepsilon)}{\varepsilon} \frac{X_{Beq} - X_{BINT}}{C_{Aeq} - C_{AINT}}} \tag{7.24}$$

$$V_{T/C2} = \frac{u/\varepsilon}{1 + \frac{(1-\varepsilon)}{\varepsilon} \frac{X_{BINT}}{C_{AINT}}} \tag{7.25}$$

$$T_{plateau} - T_{inj} = \frac{(-\Delta H)}{\left(\frac{c_f}{C_{Aeq} - C_{AINT}} - \frac{c_s}{X_{Beq} - X_{BINT}}\right)} \tag{7.26}$$

$$T_{plateau} - T_O = \frac{(-\Delta H)}{\left(\frac{c_f}{C_{AINT}} - \frac{c_s}{X_{BINT}}\right)} \tag{7.27}$$

$$Note\ C_{Aeq} = C_{AO}, in\ (1)\ X_B = X_{Beq} for\ k' and\ (2)\ X_B = X_{BINT} for\ k''$$

These sets of simultaneous equations are solved using an iterative scheme outlined in the Appendix. The solution to these equations based on the wave model is used to predict the

C_{AINT}, X_{Beq}, X_{BINT}, $V_{T/C1}$, $V_{T/C2}$ and $T_{plateau}$ values of for the concentrated case. This extension of the wave model to include kinetic parameters for a reversible gas-solid reaction is a major contribution of his chapter.

7.4 Comparison between Wave Model Predictions and Numerical Simulations

The values of the thermochemical and thermal wave velocities, and the temperature of the plateau, are calculated from the wave model equations described in the previous section. Using the derived wave model equations, predictions were made for different strategies of reducing pyrite with hydrogen. These predictions are now compared with those obtained by numerical integration of the complete set of PDEs, which represent energy and material balances of the system. The wave model is compared with the numerical simulations by analysing snapshots of the chemical process for different values of the reversible rate.

7.4.1 Results for Dilute Oxygen Case

The concentration of oxygen for the dilute cases is 2.03×10^{-4} mol/dm^3 (3 mol% O_2 in N_2 at STP). The temperature of the fluid and solid waves become completely coherent after approximately 200s. Hence, the two temperature waves are superimposed on each other in the bed profiles. The reversible rate was measured and simulated at three different values: k'' = 0.1k', k', 10k'. As expected the higher the reversible rate, the lower the conversion of B and consequently less of solid C. The rise in temperature is moderate as the reaction is weakly exothermic. Highest temperatures are reached with lower conversion at k'' = 10k'.

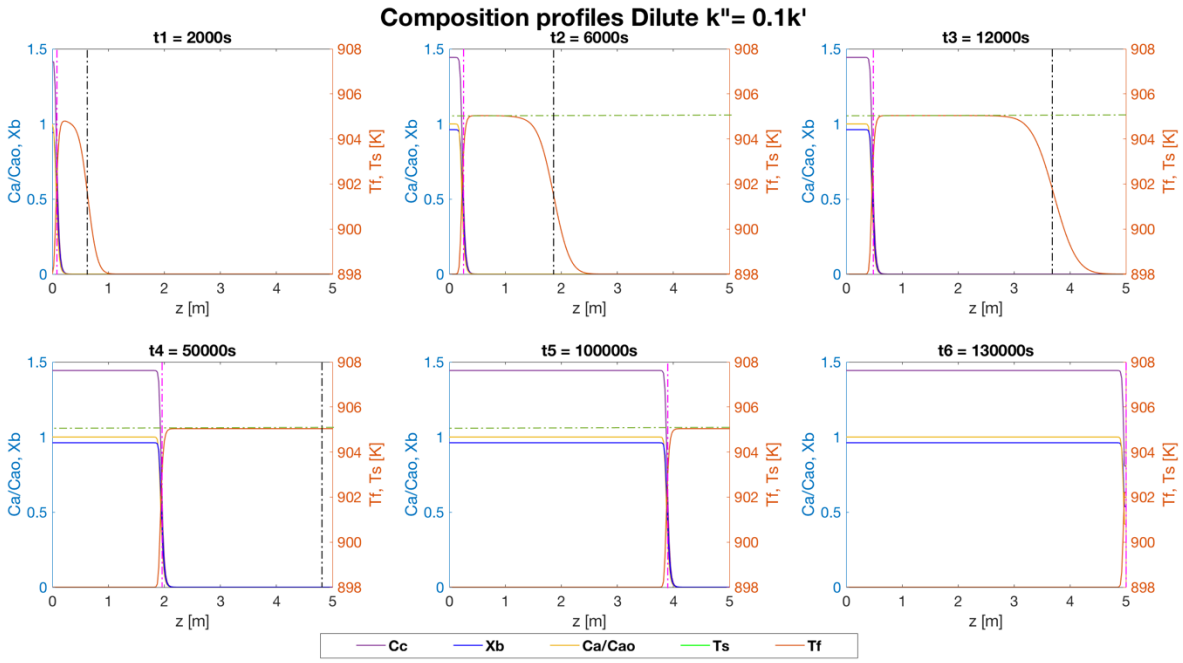

Figure 7-7: Composition profile for hot fluid into a hot bed (dilute k'' = 0.1k') Z_{T1} (black dashed), $Z_{T/C}$ (purple dashed), $T_{plateau}$ (green dashed).

The calculated gaseous and solid reactants and product mole fractions versus the axial coordinate of the reactor bed at specific times are shown in Figs. 7-7, 7-8 and 7-9. The reversible reaction of hematite and magnetite has a stoichiometric ratio of Fe_2O_3/Fe_3O_4 = 3/2, which is shown with a constant ratio from these results. It should be noted that the conversion of solid represents the amount of reacted B (magnetite) but n_c represents the amount of C (hematite) being formed. From the results in Fig. 7-7, the magnetite is 91% converted. The reversible rate of reaction in this case is a small fraction (0.1) of the forward reaction. Therefore, it is expected that the forward reaction dominates, the magnetite reacting almost completely. As seen in the rate equation for the equilibrium constant, equating the reversible rate to zero will not give the equivalent irreversible forward case. However, the irreversible forward case is less dominating with increasing k'' as shown in Figs. 7-7, 7-8.

	$V_{T/C}$ (m/s)	V_T (m/s)	ΔT_c (K)
Wave Model	3.92 x 10^{-5}	3.13 x 10^{-5}	7.1
Numerical Simulation	3.9 x 10^{-5}	3.0 x 10^{-5}	7.0

Table 7-2: Comparison of distance travelled by thermal, thermochemical waves & plateau temperature for dilute case k'' = 0.1k'

The profiles of all three reacting components travel jointly through the reactor bed. A comparison of wave velocities is shown in Table. 7-6. The wave model equations used in these predictions are from Chapter 3. Since the formation of hematite (n_C) is controlled stoichiometrically by magnetite (X_B). The value of the conversion can be used to calculate the velocity of the trailing thermochemical wave. The leading thermal wave is unaffected in this case.

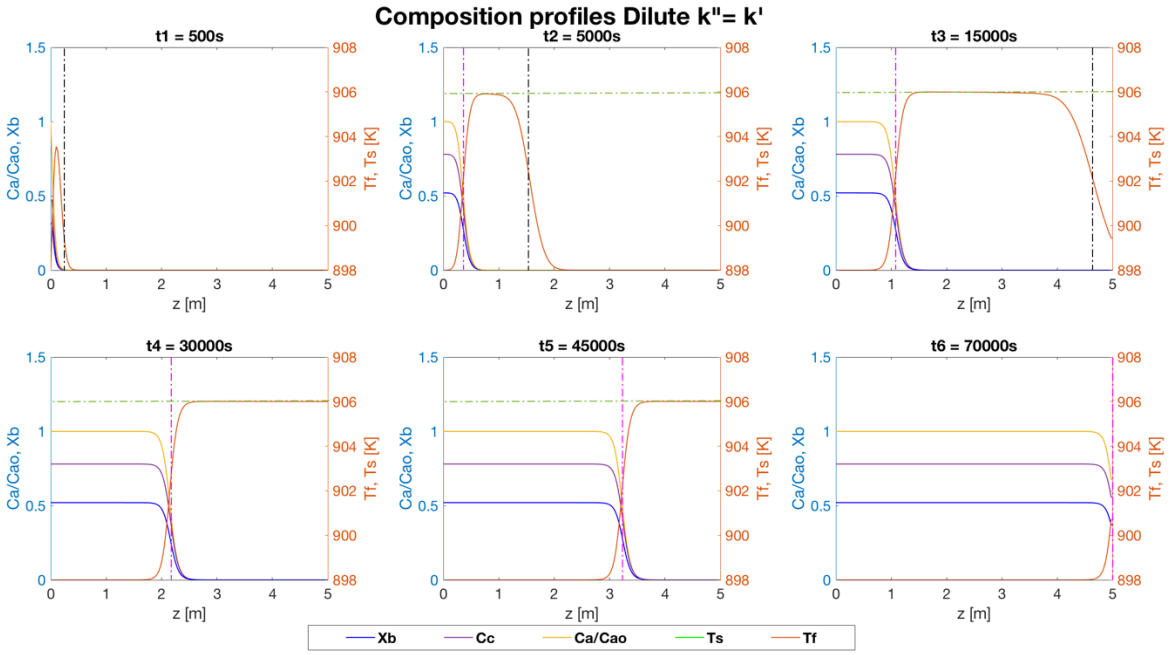

Figure 7-8: Composition profile for hot fluid into a hot bed (dilute k'' = k') Z_{T1} (black dashed), $Z_{T/C}$ (purple dashed), $T_{plateau}$ (green dashed)

The flow rate for the gaseous reactant through the bed in an equal forward and reverse reaction (k'' = k') results in partial conversion of the reacting solid in a short distance through the bed. In this case, a finite reaction zone through the bed is also formed as time passes, it moves towards the end of the reactor bed, leaving behind a reacted zone of 52% magnetite and 76% mol fraction of hematite formed. This means only 52% of each reacting solid particle is being converted while the rest of the particle remains unaffected in the ash layer. In Fig. 7-8 the progress of the reaction front with time in the bed is depicted. In this

figure the wavelike behaviour of the concentration profiles reveals the small effect of dispersion.

	$V_{T/C}$ (m/s)	V_T (m/s)	ΔT_c (K)
Wave Model	7.33 x 10^{-5}	3.13 x 10^{-5}	8.1
Numerical Simulation	7.2 x 10^{-5}	3.0 x 10^{-5}	8.0

Table 7-3: Comparison of distance travelled by thermal, thermochemical waves & plateau temperature for dilute case k'' = k'

As an illustration, in Fig. 7-8, at t_2 = 5000s and t_3 = 10000s. A flat temperature plateau is observed. It can be seen from a comparison of velocities between Table 7-1 and 7-2, the velocity of the thermal wave is unchanged. As seen in the incomplete reaction in the irreversible exothermic cases. This leads to an increase in temperature rise to the plateau. This was measure quantitatively by the wave model equations and shown to be a good fit for the reversible exothermic case as well. In the reversible case, it is incorrect to tag this as an incomplete reaction but rather the equilibrium conversion at a set reversible rate.

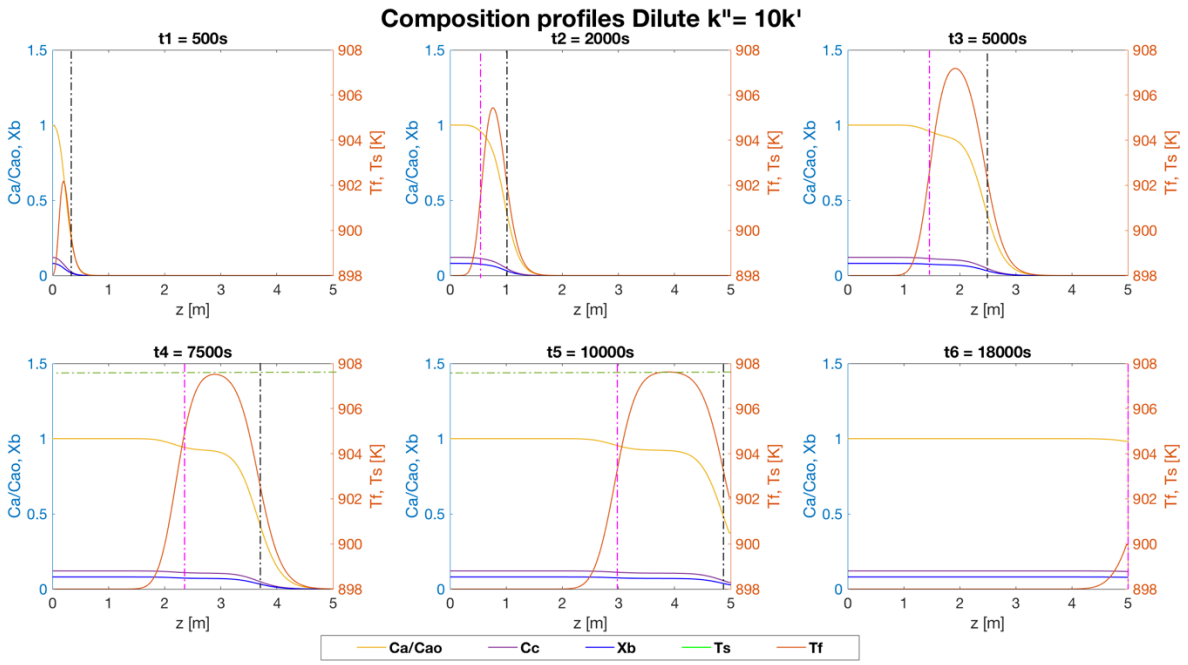

Figure 7-9: Composition profile for hot fluid into a hot bed (dilute k'' = 10k')
Z_{T1} (black dashed), $Z_{T/C}$ (purple dashed), $T_{plateau}$ (green dashed).

Fig. 7-9 shows profiles of temperature and concentration of the reactants and products

when the reversible rate is much larger than the forward case. It is seen that in this case, a separation of two distinct waves (thermal and thermochemical waves) with a flat plateau zone is not formed. A reduction in conversion consequently increases the velocity of the trailing thermochemical wave and the thermochemical temperature rise. The thermochemical wave is so fast that it interferes with the leading thermal wave. As the two waves are so close together, there is also a reaction associated with the leading thermal wave. The velocities of both reaction zones are given in Table 7-3 as two thermochemical waves. The results show discrepancies due to the difficulty of measure accurately the equilibrium conversions at the inlet. The wave model still gives good predictions in comparison with the numerical simulation.

	$V_{T/C1}$ (m/s)	$V_{T/C2}$ (m/s)	ΔT_c (K)
Wave Model	2.8 1x 10^{-5}	5.03 x 10^{-5}	9.7
Numerical Simulation	3.0 x 10^{-5}	4.8 x 10^{-5}	9.7

Table 7-4: Comparison of distance travelled by thermal, thermochemical waves & plateau temperature for dilute case k'' = 10k'

The numerical simulation of the dilute reversible exothermic cases shows a trailing reaction front characterized with its main parameters (propagation velocity, temperature and concentration profiles along the bed length, thermochemical temperature rise) remaining constant until the reaction is completed. Coherence is indeed achieved. The wave model is used to calculate the numerical values of the aforementioned parameters and is shown to be valuable in quantitative and qualitative description. Comparison with the results shown in this section agrees with the predictions in 7.2.1.

7.4.2 Results for Concentrated Oxygen Case

The concentration of oxygen for the dilute cases is 4.12×10^{-3} mol/dm^3 (61 mol% O_2 in N_2 at STP). The same reversible rates were simulated at k'' = 0.1k', k', 10k'. The interesting result here is the formation of two reaction zones irrespective of the value of the

reversible rate of reaction. This was expected as predicted by 7.2.2. The rise in temperature is higher in the concentrated case. The wave model predicts highest temperatures achieved with the highest conversion. This may seem counter-intuitive as it has been demonstrated in the previous chapters that an incomplete reaction leads to higher temperature rises, with the highest temperatures reached when conversion of the reactant solid is at the lowest possible value. The difference in the wave model prediction for the reversible case is the presence of two reaction zones with equilibrium at the inlet and in between the two reaction fronts formed as shown in Fig. 7-4. It is then proper to speak in the reversible cases about the velocities of the two reaction fronts. The closer the fronts are, the larger the temperature rise as shown in Fig. 7-9.

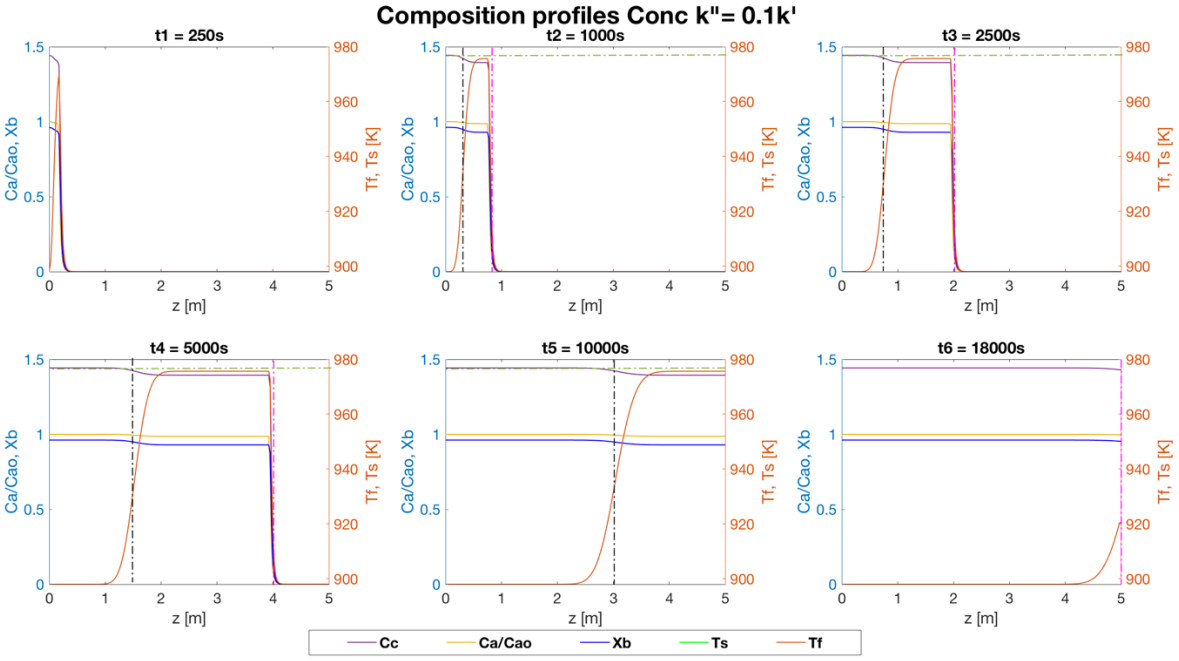

Figure 7-10: Composition profile for hot fluid into a hot bed (concentrated k'' = k')

	$V_{T/C1}$ (m/s)	$V_{T/C2}$ (m/s)	C_{AINT}	X_{BINT}	X_{Beq}	$T_{plateau}$ (K)
Wave Model	2.81 x 10^{-5}	1.13 x 10^{-5}	0.97	0.88	0.94	77.8
Numerical Simulation	3.0 x 10^{-5}	1.8 x 10^{-5}	0.98	0.9	0.95	75

Table 7-5: Comparison of distance travelled by thermal, thermochemical waves & plateau temperature for conc. case k'' = 0.1k'

Fig 7-9 shows good agreement with the wave model predictions in 7.2.2. The trailing thermal wave releases a heat of reaction. There is also a reaction front ahead the trailing wave as the reaction progresses. The reaction in this case is dominant in the forward reaction to convert the magnetite. The reaction associated with the trailing thermochemical wave has a small difference in concentration change of oxygen (C_A) and magnetite conversion (X_B). Therefore, the leading thermochemical wave travels fast as there is only a slight reaction to retard the wave.

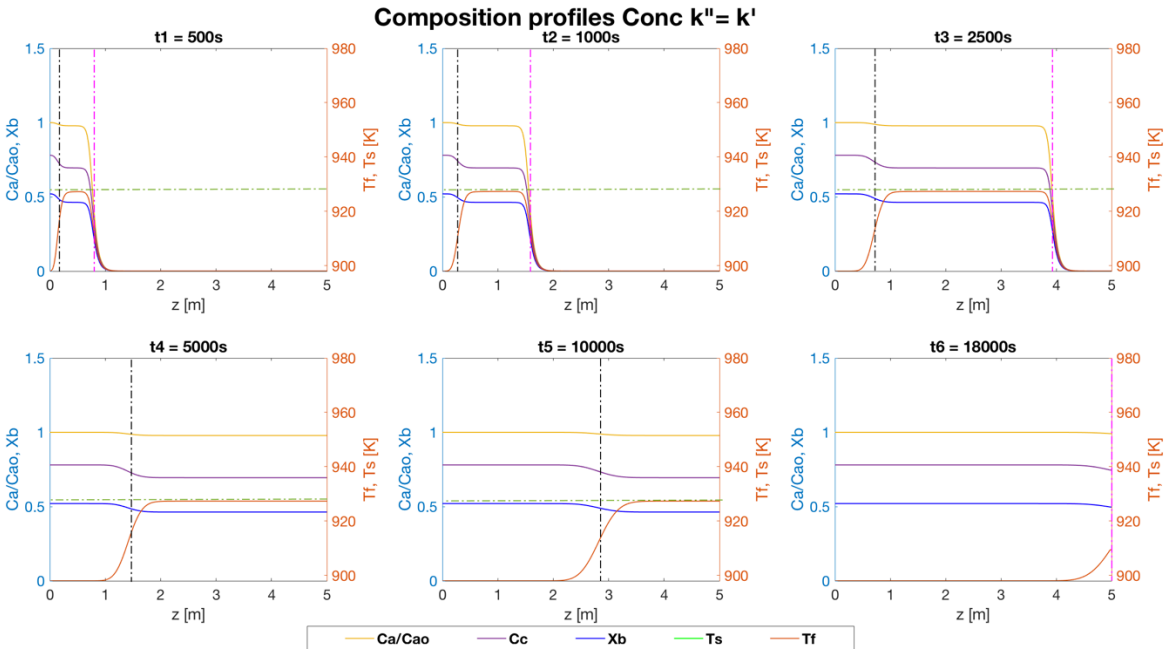

Figure 7-11: Composition profile for hot fluid into a hot bed (concentrated k'' = k')

Fig. 7-11 shows the simulation the reversible rate of reaction is equal to the forward reaction. At the inlet, there is an equilibrium conversion of 54% magnetite and 79% mol fraction of hematite is formed. The heat of reaction is negative, a decrease in temperature increases the rate of reaction. In the rear of the plateau zone, the temperature drops back from the plateau to the injected fluid temperature, an additional shift in equilibrium occurs and there is more conversion of solid behind the trailing thermochemical wave at T_{inj}. The leading thermochemical wave contains a zone behind it where heat is released by the wave.

Solution to the wave model simultaneous equations (7.22) – (7.28) is shown in Table 7-4.

	$V_{T/C1}$ (m/s)	$V_{T/C2}$ (m/s)	C_{AINT}	X_{BINT}	X_{Beq}	$T_{plateau}$ (K)
Wave Model	2.81 x 10^{-4}	1.56 x 10^{-3}	0.92	0.48	0.54	24.8
Numerical Simulation	3.0 x 10^{-4}	1.6 x 10^{-3}	0.90	0.47	0.55	24

Table 7-6: Comparison of distance travelled by thermal, thermochemical waves & plateau temperature for conc. case k'' = k'

If the temperature of a system is increased, according to Le Chatelier's principle the equilibrium acts to reduce the temperature. A reduction in temperature favours the exothermic forward reaction and an increase in temperature favours the reverse endothermic reaction. In the case of the reversible magnetite reduction, a reduction in temperature favours the exothermic forward reaction, so more magnetite is converted. This is shown clearly in the numerical simulation with an increase in X_B from 44% to 56% with a reduction in temperature from the plateau temperature to the injected fluid temperature. The wave model prediction is in good agreement with the results. To show the simulations are not as a result of numerical error. The rate of reaction was measured and plotted against reactor bed length.

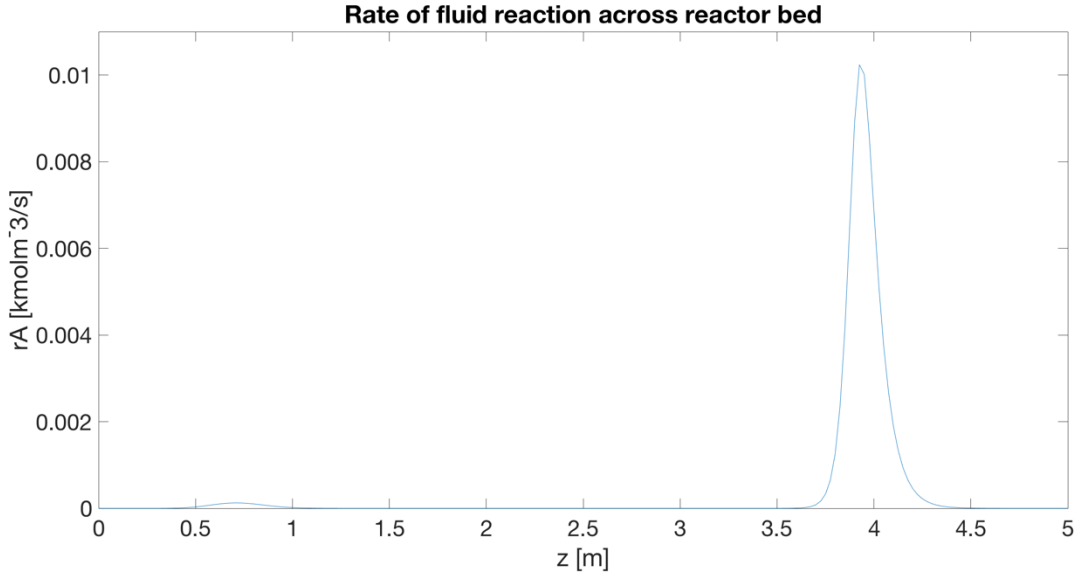

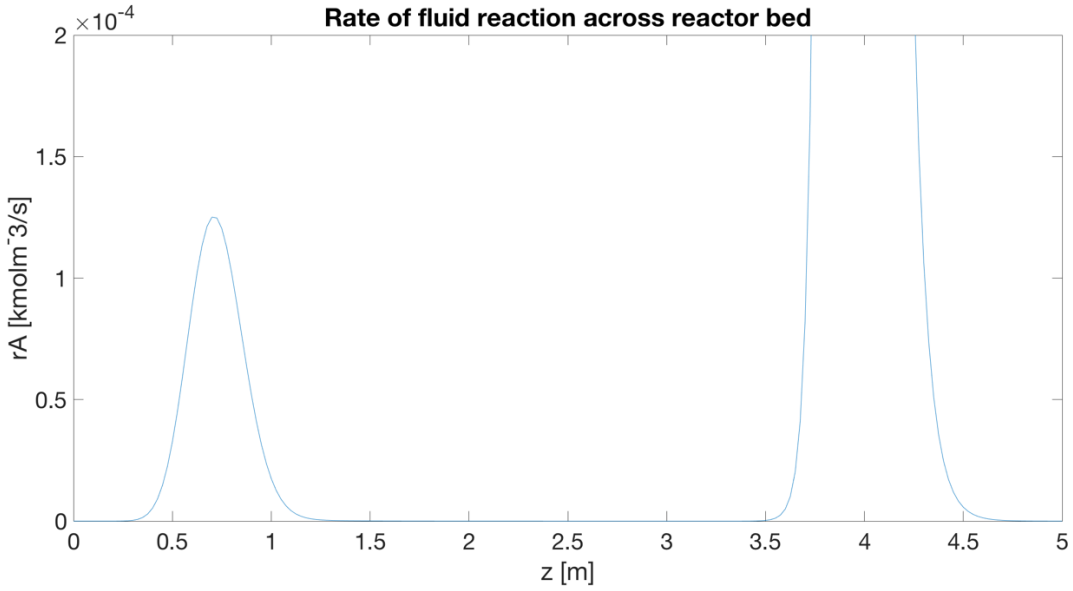

Figure 7-12: Rate of reaction for concentrated case k'' = k'

if k'' is too high, the maximum temperature reached in the reactor bed is much lower. The two thermochemical waves travel separately far apart from each other. There is a slight rise in conversion of the magnetite but too small to cause a noticeable temperature rise across the wave.

Fig. 7-13 presents the temperature profile in the bed at different instances during the dominant reversible reaction. The heat front ahead propagates through the bed but 10% conversion of magnetite (X_B). As only a small fraction of magnetite is reacting and hence only a small amount of hematite (C_c is formed). There is a very moderate temperature rise. The trailing reaction front is not clearly visible in the modelling results.

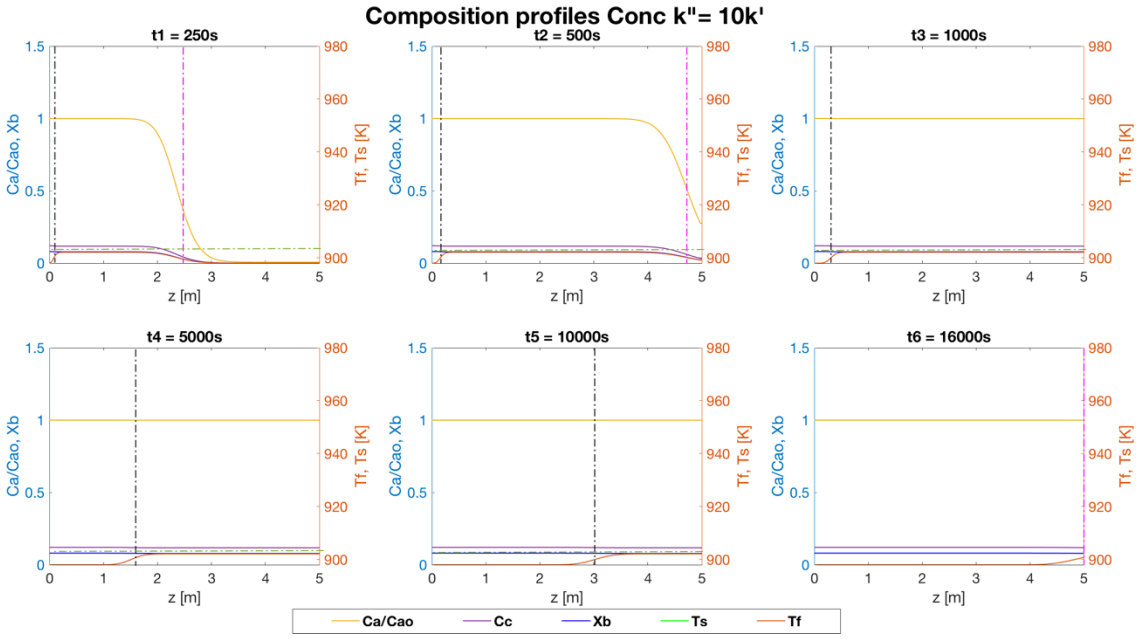

Figure 7-13: Composition profile for hot fluid into a hot bed (concentrated k'' = 10k')

7.5 Summary and Conclusions

The noncatalytic reactions between gases and solids in the previous chapters have been irreversible because the products are eventually swept away by the flow of the reactant gas and do not take part in the reaction. Reversibility slows down the overall rate of reaction. The properties of reversible reactions introduced the interaction of another reacting component solid C. The formation of solid C is bounded by the conversion of reactant solid B. A numerical model is presented, to simulate the dynamic behaviour of the reversible reaction of magnetite with oxygen. A modified shrinking core model was adopted to represent non-equimolar exothermic fluid-solid reactions. The model is implemented in the material and energy balances and compared to the wave model predictions for dilute and concentrated cases. This involved varying the reversible rate and measuring the equilibrium concentrations of the reaction.

The reactions in the previous chapters have not involved the products in the reaction.

The contribution in this chapter is in even slower non-equilibrium reactions with finite rates of reactions where there are reactions at either side of the temperature of the plateau. This was noted by Philinis, 1956. It should be noted that the reversibility is not realistically to be achieved since the form of the reformed solid is not in the same form before the reaction. It was shown that the results from the wave model prediction and the numerical simulations are in good agreement with each other and Le Chatelier's principle. Thus, varied temperature conditions existed for the reverse element of the reaction to occur in the upstream part of the bed where the rate of overall conversion is increased.

Chapter 8

Conclusions

8.1 Summary of conclusions

The variations of fluid reactant concentration, solid reactant conversion and temperature which propagate within fixed-bed, solid-fluid reactors may be considered as waves. To do so is appealing, as it allows us to picture and more readily comprehend their behaviour in terms of cause and effect. A numerical model for irreversible exothermic and endothermic, and reversible exothermic fluid-solid reactions has been developed and applied to decoking of fixed bed reactors, reduction of pyrite and oxidation of magnetite. The solution to the numerical model showed a coherent constant pattern reaction profile with a fixed width travelling across the reactor bed. This result shows that the wave model is applicable in slowly reacting non-equilibrium systems. The use of the wave model and coherence theory in these systems is the major contribution of the thesis. The wave model was extended to incorporate the fixed mass and heat transfer zones in the equations for the wave velocities and thermochemical temperature rise. Another contribution of the thesis. The calculation of the width of the heat transfer zones was used to show the effect of wall heating on wave propagation and plateau temperature. Dilute and concentrated cases with varying initial temperature conditions were tested and showed good agreement with the wave model predictions. In certain cases, i.e incomplete reactions, splitting of thermochemical waves, hot spots, cold spots, formation of two reaction zones in reversible reactions. The wave model showed its value by explaining quantitatively and qualitatively the observations from the numerical simulations. A modified shrinking core model was developed to account for exothermic reversible fluid-solid reactions by assuming the reverse reaction occurs in the ash layer. The solution to the partial differential equations derived was shown

to agree with Le Chetalier's principle with the effect of temperature change, resulting in two thermochemical waves with no reaction between in the zone between the two waves.

In the first part of the thesis, it is shown that if the injected fluid is dilute and above ignition temperature, the thermochemical wave where the reaction takes place moves into a hot enough region and the reaction profile propagates in a stable manner. The wave model was used to develop a reduced-heat injection strategy, reducing the requirement of constant heating of the injected fluid. We show that if the injected fluid is concentrated, the thermochemical wave travels ahead of the thermal wave and can only propagate if the thermochemical wave is moving to a bed set above ignition temperature. The critical concentration where the temperature becomes a delta function was examined resulting in a hot spot. The wave model predicts no separation of the thermal and thermochemical waves in the absence of dispersion. This was confirmed by running a numerical simulation at the critical concentration. When the thermochemical wave ran into a cold region of the reactor bed, there is an incomplete reaction of the reactive solid or injected fluid. The wave model showed its use here by accurately predicting the velocities of the thermal and thermochemical waves during incomplete reactions and gave an explanation to the unexpected temperature rise encountered in fixed beds as noted by a variety of researchers in both theoretical and experimental results.

In the second part of the thesis, a simple non-linear wave model has been developed to different injection strategies and heating mechanisms for reduction of iron pyrite by hydrogen. The results show the wave model accurately describes the behaviour of thermal and thermochemical waves under varied initial conditions. One of the contributions of this work is the expansion of the wave model to include heat and reaction zones. The interesting effect of a critical concentration was investigated showing a splitting of thermochemical waves at either side of the cold spot. The splitting of thermochemical

waves is a description of the two reaction fronts moving at different velocities. Such an outcome shows the wave model holds significant promise in the development of real time control algorithm and heuristic design problems. The effect of wall heating on the propagation of thermal and thermochemical waves was investigating under realistic kinetic parameters. Radial eating from the wall was shown to raise the temperature and reduce the zone in between the thermal and thermochemical waves. The wave model proves to be an efficient and simple tool in heat integrated concepts where a limiting temperature is to be avoided during a reaction.

In the third part of the thesis, a numerical model is presented to simulate the dynamic behaviour of the reversible reaction of magnetite with oxygen. The wave model predicted two reaction zones travelling across the reactor. Each associated with a temperature drop from the plateau temperature to the injected fluid temperature, which favours the conversion of magnetite (the forward reaction). Varied temperature conditions existed for the reverse element of the reaction to occur in the upstream part of the bed where the rate of overall conversion is increased. A novel system involving multiple reactors was designed using wave model predictions. This showed the simplicity of the wave model and the usefulness in applying the model in heuristic designs. This gives an insight into cause and effect.

Although it is unlikely that the wave model approach here could accommodate the complexities for an industrial fixed bed reactor, the wave model has a strong potential for use in screening and testing operating schemes.

8.2 Future Work

Varying density in wave model

The main deficiency in the analysis is the variation of fluid density during the reaction which will have some effect in both the physical and wave model. This is particularly important when high temperatures are reached during the reaction. A simple way to del with this is to incorporate a velocity profile which is a function of density and the reactor bed. The transient time before coherence is reached will also be greatly affected. To incorporate density into the equation for the gas velocity, there needs to be a function of density ($\varrho(T)$ which is a function of temperature) across the reactor bed. Preliminary studies were done to vary the gas velocity as $u = u^*(1 + \varrho(T)/\varrho_A)$. The temperature reached in the bed and the time it takes for the reaction to occur is affected. More so, for highly concentrated gas feed.

Calculating transient time using the wave model

The wave model in ints current form cannot calculate the transient time directly but instead uses the material and energy balances to reduce the PDEs into simpler simultaneous equations. The transient time is dependent on the rate expression. To include that rate expression into the wave model is beyond the scope of this thesis. Including this in future research will increase the power of application of the wave model.

Inclusion of Radiating effects

Radiative effects were not included in the analysis. The thesis focused on convection-diffusion. When temperatures are reached for both the gas and solid reacting, the temperature rise could cause forward and backward radiative effects which could have an

effect on the wave behaviour of the reacting system.

Extension of Wave Model and Numerical Model into Multiple reactions

An extension of the thesis will be to apply the wave model to the study of non-isothermal liquid-solid reactions, as an example well stimulation, in which there will be two or more coupled and reversible reactions. The numerical model simply would increase from four PDEs to proportionately more equations depending on the number of reacting species. From a programming point of view, this should be solvable using MOL explained in the thesis. The wave would be able to predict the changes in composition and temperature of the solid and fluid reacting species. The key assumption is that the conversion will be related to the porosity of the mud rock. There will be more than one solid in the system but only one or two of the solids are going to react. Once the change in conversion of the reacting solid is known, the change in the overall porosity of the rock can be calculated. Both the numerical and wave model need to account for dissolving solids and forming precipitates. Those precipitates will be deposited where they form, which is similar to what we have in our current numerical model with a fixed bed of solids. Ultimately, the wave model can be applied to a well stimulation study to predict the change in porosity of the mud rock. Hankins and Harwell (2007) concluded the theory was applicable to a wider range of applications such as well stimulation.

If there are multiple species reacting then there are multiple equilibria, then more dependent variables but the wave model simplicity remains, and the theory of coherence still predict a constant pattern thermochemical wave arising. The model may breakdown due to the high complexity of the proposed system but will still be valuable as an initial design tool to gain insight into the dynamics of the multiple reacting species. Successful simulation of multiple reactions shows the predictive power of a robust wave model.

References

Ahn, Hyungjun, and Sangmin Choi. "A comparison of the shrinking core model and the grain model for the iron ore pellet indurator simulation." *Computers & Chemical Engineering* 97 (2017): 13-26.

Amiri, A., K. Vafai, and T. M. Kuzay. "Effects of boundary conditions on non-Darcian heat transfer through porous media and experimental comparisons." *Numerical Heat Transfer, Part A: Applications* 27.6 (1995): 651-664.

Antos, George J., and Abdullah M. Aitani. *Catalytic naphtha reforming revised and expanded*. CRC Press, 2004.

Araque-Martinez, Aura N. *Modeling the effects of geochemistry on well impairment*. Diss. 2001.

Araque-Martinez, Aura, and Larry W. Lake. "Some frequently overlooked aspects of reactive flow through permeable media." *Industrial & engineering chemistry research* 39.8 (2000): 2717-2724.

Aris, Rutherford, and Neal Russell Amundson. *Mathematical Methods in Chemical Engineering: First-order Partial Differential Equations with Applications*. Prentice-Hall, 1973.

Bahr, Jean M., and Jacob Rubin. "Direct comparison of kinetic and local equilibrium formulations for solute transport affected by surface reactions." *Water Resources Research* 23.3 (1987): 438-452.

Bandai, Toshiyuki, et al. "The effect of particle size on thermal and solute dispersion in saturated porous media." *International Journal of Thermal Sciences* 122 (2017): 74-84.

Basu, Prabir. Biomass gasification and pyrolysis: practical design and theory. Academic press, 2010.

Behroozi, A., A. Rahimi, and Mohammad S. Hatamipour. "Simple correlation for reaction rate of coke-burning in a hydrocracker reactor using the mathematical modeling technique." *Special Topics & Reviews in Porous Media: An International Journal* 1.3 (2010).

Behroozi, A., M. S. Hatamipour, and Amir Rahimi. "Mathematical modeling and parametric study of coke-burning process in a hydrocracker reactor." *Computers & Chemical Engineering* 38 (2012): 44-51.

Bhusarapu, S., et al. "Measurement of overall solids mass flux in a gas–solid circulating fluidized bed." *Powder technology* 148.2 (2004): 158-171.

Binning, Philip John, et al. "Advective and diffusive contributions to reactive gas transport during pyrite oxidation in the unsaturated zone." *Water Resources Research* 43.2 (2007).

Bischoff, K. B. "Accuracy of the pseudo steady state approximation for moving boundary diffusion problems." *Chemical Engineering Science* 18.11 (1963): 711-713.

Bischoff, K. B. "Further comments on the pseudo steady state approximation for moving boundary diffusion problems." *Chem. Eng. Sci.* 20 (1965): 783-784.

Boyabat, N., et al. "Thermal decomposition of pyrite in the nitrogen atmosphere." *Fuel processing technology* 85.2-3 (2004): 179-188.

Bryant, S. L., R. S. Schechter, and L. W Lake. "Interactions of precipitation/dissolution waves and ion exchange in flow through permeable media." *AIChE journal* 32.5 (1986): 751-764.

Bryant, S. L., R. S. Schechter, and L.W. Lake. "Mineral sequences in precipitation/dissolution waves." *AIChE journal*33.8 (1987): 1271-1287.

Bryant, Steven L., and Karsten E. Thompson. "Theory, modeling and experiment in reactive transport in porous media." *Current opinion in colloid & interface science* 6.3 (2001): 217-222.

Butler, Ian B., and David Rickard. "Framboidal pyrite formation via the oxidation of iron (II) monosulfide by hydrogen sulphide." *Geochimica et Cosmochimica Acta* 64.15 (2000): 2665-2672.

Cahill, C. L., et al. "In situ time-resolved X-ray diffraction of iron sulfides during hydrothermal pyrite growth." *Chemical Geology* 167.1-2 (2000): 53-63.

Chang, Jong-San, et al. "Thermogravimetric analyses and catalytic behaviors of zirconia-supported nickel catalysts for carbon dioxide reforming of methane." *Catalysis today* 115.1-4 (2006): 186-190.

Cussler, Edward Lansing. Diffusion: mass transfer in fluid systems. Cambridge university press, 2009.

Cyprès, René, Mehdi Ghodsi, and Robert Stocq. "Behaviour of pyrite during hydrogenation of graphite at atmospheric pressure." *Fuel* 60.3 (1981): 247-250.

Davis, Mark E., and Robert J. Davis. *Fundamentals of chemical reaction engineering*. Courier Corporation, 2012.

De Moura, Carlos A., and Carlos S. Kubrusly. "The Courant-Friedrichs-Lewy (CFL) Condition." *Commun. Pure Appl. Math*10.2 (2013): 363-371.

Dehghani, O., et al. "A new configuration for decoking process in series reactors." *Chemical engineering journal* 215 (2013): 418-431.

Dria, Myra Ann, R. S. Schechter, and Larry W. Lake. "Behavior of thermochemical waves during reactive flow through permeable media." *Industrial & engineering chemistry research* 34.8 (1995): 2889-2897.

Du, Wenguang, et al. "Hydrogen Reduction of Hematite Ore Fines to Magnetite Ore Fines at Low Temperatures." *Journal of Chemistry* 2017 (2017).

Fitzgerald, J. *"A Word about Damkohler Numbers, MIT, 14 Sept.* 2001.

Fletcher, R. C., and A.W. Hofmann. "Simple models of diffusion and combined diffusion-infiltration metasomatism." *Geochemical transport and kinetics* 634 (1974): 243-259.

Glöckler, B., et al. "Autothermal reactor concepts for endothermic fixed-bed reactions." *Chemical Engineering Research and Design* 82.2 (2004): 148-159.

Goetz, V., and A. Marty. "A model for reversible solid-gas reactions submitted to temperature and pressure constraints: simulation of the rate of reaction in solid-gas reactor used as chemical heat pump." *Chemical Engineering Science* 47.17-18 (1992): 4445-4454.

Gómez-Barea, Alberto, and Pedro Ollero. "An approximate method for solving gas–solid non-catalytic reactions." *Chemical Engineering Science* 61.11 (2006): 3725-3735.

Graham, U. M., and Hiroshi Ohmoto. "Experimental study of formation mechanisms of hydrothermal pyrite." *Geochimica et Cosmochimica Acta* 58.10 (1994): 2187-2202.

Grüner, S., and A. Kienle. "Equilibrium theory and nonlinear waves for reactive distillation columns and chromatographic reactors." *Chemical Engineering Science* 59.4 (2004): 901-918.

Grüner, S., et al. "Nonlinear control of a reactive distillation column." *Control Engineering Practice* 11.8 (2003): 915-925.

Hankins, N. P. "A non-linear wave model with variable molar flows for dynamic behaviour and disturbance propagation in distillation columns." *Chemical Engineering Research and Design* 85.1 (2007): 65-73.

Hankins, Nicholas P., and Friedrich G. Helfferich. "On the concept and application of ‘partial coherence’ in non-linear wave propagation." *Chemical engineering science* 54.6 (1999): 741-764.

Hankins, Nicholas P., and Harwell, Jeffrey W. "Application of coherence theory to a reservoir enhanced oil recovery simulator." *Journal of Petroleum Science and Engineering* 42.1 (2004): 29-55.

Hansen, Jens Peter, et al. "Decomposition and oxidation of pyrite in a fixed-bed reactor." *Industrial & engineering chemistry research* 42.19 (2003): 4290-4295.

Helfferich, F. "Chromatographic behavior of interfering solutes: conceptual basis and outline of a general theory." *Adv. Chem. Ser* 79 (1968): 30-43.

Helfferich, F. G. "Multicomponent ion exchange in fixed beds. Generalized equilibrium theory for systems with constant separation factors." *Industrial & Engineering Chemistry Fundamentals* 6.3 (1967): 362-364.

Helfferich, F. G., and Barbara J. Bennett. "Weak electrolytes, polybasic acids, and buffers in anion exchange columns I. Sodium acetate and sodium carbonate systems." *Reactive Polymers, Ion Exchangers, Sorbents* 3.1 (1984): 51-66.

Helfferich, Frederick, and D. L. Peterson. "Accurate chromatographic method for sorption isotherms and phase equilibria." *Science* 142.3593 (1963): 661-662.

Helfferich, Friedrich G. "The theory of precipitation/dissolution waves." *AIChE journal* 35.1 (1989): 75-87.

Helfferich, Friedrich G. "Theory of multicomponent, multiphase displacement in porous media." *Society of Petroleum Engineers Journal* 21.01 (1981): 51-62.

Helfferich, Friedrich G., and Gerhard Klein. "Multicomponent chromatography." (1970).

Hill, W. J., et al. "Cation exchange and chemical flooding." *Journal of Petroleum Technology* 29.10 (1977): 1-336.

Hong, Y., and B. Fegley Jr. "The kinetics and mechanism of pyrite thermal decomposition." *Berichte der Bunsengesellschaft für physikalische Chemie* 101.12 (1997): 1870-1881.

Iordanidis, Arthouros Aristotelis. *Mathematical modeling of catalytic fixed bed reactors*. Enschede, The Netherlands: Twente University Press, 2002.

Jambor, Boris, and Elena Hájeková. "Formation of coke deposits and coke inhibition methods during steam cracking." *Petroleum & Coal* 57.2 (2015).

Janzen, Michael P., Ronald V. Nicholson, and Jeno M. Scharer. "Pyrrhotite reaction kinetics: reaction rates for oxidation by oxygen, ferric iron, and for nonoxidative dissolution." *Geochimica et Cosmochimica Acta* 64.9 (2000): 1511-1522.

Jaree, Attasak, et al. "Temperature response to reactant concentration perturbations in a packed−bed reactor." *The Canadian Journal of Chemical Engineering* 79.5 (2001): 823-827.

Jeffrey, Alan. "Quasilinear hyperbolic systems and waves." *London, Pitman Publishing, Ltd. (Research Notes in Mathematics, No. 5), 1976. 230 p.* 5 (1976).

Jennings, Aaron A., and David J. Kirkner. "Instantaneous equilibrium approximation analysis." *Journal of Hydraulic Engineering* 110.12 (1984): 1700-1717.

Jiang, Pei-Xue, et al. "Fluid flow and convective heat transfer in a vertical porous annulus." *Numerical Heat Transfer, Part A Applications* 30.3 (1996): 305-320.

Jiang, Pei-Xue. "Numerical simulation of forced convection heat transfer in porous plate channels using thermal equilibrium and nonthermal equilibrium models." *Numerical Heat Transfer: Part A: Applications* 35.1 (1999): 99-113.

Kern, Christoph, and Andreas Jess. "Regeneration of coked catalysts—modelling and verification of coke burn-off in single particles and fixed bed reactors." *Chemical engineering science* 60.15 (2005): 4249-4264.

Khan, A. R., and J. H. Bowen. "Analysis of fixed bed reactors using a diffuse interface single pellet model." *Chemical Engineering Research and Design* 1.77 (1999): 47-54.

Khan, Abdul Rehman. "Non−catalytic, gas−solid reversible reaction mechanism implementing diffuse interface model." *International journal of chemical kinetics* 31.8 (1999): 559-570.

Kim, Bo-kyung, et al. "Design and control of a reactive distillation column based on a nonlinear wave propagation theory: production of terephthalic acid." *Industrial & Engineering Chemistry Research* 49.9 (2010): 4297-4307.

Kolios, G., J. Frauhammer, and G. Eigenberger. "Autothermal fixed-bed reactor concepts." *Chemical Engineering Science*55.24 (2000): 5945-5967.

Kolios, Grigorios, et al. "Heat-integrated reactor concepts for catalytic reforming and automotive exhaust purification." *Applied Catalysis B: Environmental* 70.1-4 (2007): 16-30.

Kolios, Grigorios, Jörg Frauhammer, and Gerhart Eigenberger. "Efficient reactor concepts for coupling of endothermic and exothermic reactions." *Chemical Engineering Science* 57.9 (2002): 1505-1510.

Kuila, Saikat Kumar, Ritayan Chatterjee, and Dinabandhu Ghosh. "Kinetics of hydrogen reduction of magnetite ore fines." *international journal of hydrogen energy* 41.22 (2016): 9256-9266.

Kuntz, David, and Peter Grathwohl. "Comparison of steady-state and transient flow conditions on reactive transport of contaminants in the vadose soil zone." *Journal of hydrology* 369.3 (2009): 225-233.

Kutsovskaya, Marina L., Malcolm T. Hepworth, and John R. McGaa. "Recovery of lime, sulfur, and iron from gypsum and pyrite wastes." *Industrial & engineering chemistry research*35.5 (1996): 1736-1746.

Lake, L.W., et al. "Isothermal, multiphase, multicomponent fluid flow in permeable media." *In Situ;(United States)* 8.1 (1984).

Lake, L.W., et al. *Geochemistry and fluid flow*. Vol. 7. Gulf Professional Publishing, 2002.

Lambert, J. M., G. Simkovich, and P. L. Walker. "The kinetics and mechanism of the pyrite-to-pyrrhotite transformation." *Metallurgical and materials transactions B* 29.2 (1998): 385-396.

Lambert, J. M., G. Simkovich, and P. L. Walker. "The kinetics and mechanism of the pyrite-to-pyrrhotite transformation." *Metallurgical and Materials Transactions B* 29.2 (1998): 385-396.

Lee, Dae-Young, and Kambiz Vafai. "Analytical characterization and conceptual assessment of solid and fluid temperature differentials in porous media." *International Journal of Heat and Mass Transfer* 42.3 (1999): 423-435.

Leea, W. S., et al. "A MATLAB Method of Lines Template for Evolution Equations." (2003).

Leet, William A., and Santi Kulprathipanja. *Reactive separation processes*. Taylor & Francis: New York, 2002.

Levenspiel, Octave. "Chemical reaction engineering." *Industrial & engineering chemistry research* 38.11 (1999): 4140-4143.

Lu, Hui-Bo, Nathalie Mazet, and Bernard Spinner. "Modelling of gas-solid reaction—Coupling of heat and mass transfer with chemical reaction." *Chemical Engineering Science* 51.15 (1996): 3829-3845.

Lund, Kasper, and W. Scott Fogler. "Acidization--V: The prediction of the movement of acid and permeability fronts in sandstone." (1976).

Luss, Dan. "Temperature fronts and patterns in catalytic systems." *Industrial & engineering chemistry research* 36.8 (1997): 2931-2944.

Lv, Weizhi, et al. "The chemical role of CO2 in pyrite thermal decomposition." *Proceedings of the Combustion Institute* 35.3 (2015): 3637-3644.

Machat, Hela, and Jérôme Carrayrou. "Comparison of linear solvers for equilibrium geochemistry computations." *Computational Geosciences* 21.1 (2017): 131-150.

Matthews, Alan. "Magnetite formation by the reduction of hematite with iron under hydrothermal conditions." *American Mineralogist* 6 (1976): 927-932.

Mayer, K. Ulrich, Emil O. Frind, and David W. Blowes. "Multicomponent reactive transport modelling in variably saturated porous media using a generalized formulation for kinetically controlled reactions." *Water Resources Research* 38.9 (2002).

Mehraban, Majid, and Bahram Hashemi Shahraki. "A mathematical model for decoking process of the catalyst in catalytic naphtha reforming radial flow reactor." *Fuel Processing Technology* 188 (2019): 172-178.

Molson, J. W., et al. "Numerical simulations of pyrite oxidation and acid mine drainage in unsaturated waste rock piles." *Journal of Contaminant Hydrology* 78.4 (2005): 343-371.

Monteiro, J. L. F. "Thermal decomposition of pyrite in a fluidized bed." *The Canadian Journal of Chemical Engineering* 59.4 (1981): 511-516.

Müller, Norbert, Ralf Moos, and Andreas Jess. "In situ Monitoring of Coke Deposits during Coking and Regeneration of Solid Catalysts by Electrical Impedance-based Sensors." *Chemical Engineering & Technology: Industrial Chemistry-Plant Equipment-Process Engineering- Biotechnology* 33.1 (2010): 103-112.

Mutasher, E. I., A. R. Khan, and J. H. Bowen. "Reversible, noncatalytic reactions between gases and solids in fixed beds." *Industrial & engineering chemistry research* 28.10 (1989): 1550-1553.

Nandakumar, K., and R. P. Andres. "Minimum reflux conditions, part I: Theory." *AIChE Journal* 27.3 (1981): 450-460.

Novak, Craig Francis. "Metasomatic patterns produced by infiltration or diffusion in permeable media." (1991): 2779-2779.

Ozgumus, Turkuler, and Moghtada Mobedi. "Effect of pore to throat size ratio on interfacial heat transfer coefficient of porous media." *Journal of Heat Transfer* 137.1 (2015): 012602.

Özgümüş, Türküler, et al. "Thermal Dispersion in Porous Media—A Review on the Experimental Studies for Packed Beds." *Applied Mechanics Reviews* 65.3 (2013): 031001.

Partopour, Behnam, and Anthony G. Dixon. "Integrated multiscale modelling of fixed bed reactors: Studying the reactor under dynamic reaction conditions." *Chemical Engineering Journal* (2018).

Pinjala, V. C. Chen, and D. Luss. "Wrong-way behaviour of packed-bed reactors: II. Impact of thermal dispersion." *AIChE journal* 34.10 (1988): 1663-1672.

Quinn, M. A., L. W. Lake, and R. S. Schechter. *Designing Effective Sandstone Acidizing Treatments Through Geochemical Modelling. SPE Prod & Oper 15 (1): 33-41*. SPE-60846-PA. http://dx. doi. org/10.2118/60846-PA, 2000.

Rahimpour, M. R., et al. "A novel configuration for Pd/Ag/α-Al2O3 catalyst regeneration in the acetylene hydrogenation reactor of a multi feed cracker." *Chemical engineering journal*198 (2012): 491-502.

Rhee, Hyun-Ku, Rutherford Aris, and Neal Russell Amundson. *Theory and application of hyperbolic systems of quasilinear equations*. Vol. 2. Courier Corporation, 2001.

Saucez, Philippe, W.E. Schiesser, and Alain Van de Wouwer. "Upwinding in the method of lines." *Mathematics and computers in simulation* 56.2 (2001): 171-185.

Schiesser, W.E. "The numerical methods of lines." *Integration of partial differential equations Academic Press San Diego* (1991).

Schiesser, William E. *Computational mathematics in engineering and applied science: ODEs, DAEs, and PDEs*. CRC press, 2014.

Schiesser, William E., and Graham W. Griffiths. A compendium of partial differential equation models: method of lines analysis with Matlab. Cambridge University Press, (2009).

Schwab, George-Maria, and John Philinis. "Reactions of iron pyrite: its thermal decomposition, reduction by hydrogen and air oxidation." *Journal of the American Chemical Society* 69.11 (1947): 2588-2596.

Schwab, George-Maria, and John Philinis. "Reactions of iron pyrite: Its thermal decomposition, reduction by hydrogen and air oxidation." *Journal of the American Chemical Society* 69.11 (1947): 2588-2596.

Sevougian, S. David, Robert S. Schechter and Larry W. Lake. "A new geochemical simulator to design more effective sandstone acidizing treatments." *SPE Production & Facilities*10.01 (1995): 13-19.

Sevougian, S. David, Robert S. Schechter, and Larry W. Lake. "Effect of partial local equilibrium on the propagation of precipitation/dissolution waves." *Industrial & engineering chemistry research* 32.10 (1993): 2281-2304.

Shen, John, and J. M. Smith. "Diffusional effects in gas-solid reactions." *Industrial & Engineering Chemistry Fundamentals* 4.3 (1965): 293-301.

Silaban, A., and D. P. Harrison. "High temperature capture of carbon dioxide: characteristics of the reversible reaction between CaO (s) and CO2 (g)." *Chemical Engineering Communications* 137.1 (1995): 177-190.

Smith, Joseph Mauk. Chemical engineering kinetics. (1981) No. TP149 S58.

Sohn, H. Y., and J. Szekely. "A structural model for gas-solid reactions with a moving boundary—III: A general dimensionless representation of the irreversible reaction between a porous solid and a reactant gas." *Chemical Engineering Science* 27.4 (1972): 763-778.

Spallina, V., et al. "Chemical looping reforming in packed-bed reactors: modelling, experimental validation and large-scale reactor design." *Fuel Processing Technology* 156 (2017): 156-170.

Speight, James G. Perry's standard tables and formulas for chemical engineers. New York: McGraw-Hill, 2003.

Steyer, Frank, Zhiwen Qi, and Kai Sundmacher. "Synthesis of cylohexanol by three-phase reactive distillation: influence of kinetics on phase equilibria." *Chemical Engineering Science* 57.9 (2002): 1511-1520.

Stohs, Miriam. *A study of metal ion migration in soils from drilling mud pit discharges*. Diss.

Szekely, Julian. Gas-solid reactions. Elsevier, 2012.

Tang, Dahai, Christoph Kern, and Andreas Jess. "Influence of chemical reaction rate, diffusion and pore structure on the regeneration of a coked Al2O3-catalyst." *Applied Catalysis A: General* 272.1-2 (2004): 187-199.

Tartakovsky, Alexandre M., et al. "Simulations of reactive transport and precipitation with smoothed particle hydrodynamics." *Journal of Computational Physics* 222.2 (2007): 654-672.

Toghyani, Mahboubeh, Amir Rahimi, and Javad Mirmohammadi. "Mathematical modeling and parametric study of a dehydrogenation catalyst decoking process." *Applied Catalysis A: General* 489 (2015): 226-234.

Truche, Laurent, et al. "Kinetics of pyrite to pyrrhotite reduction by hydrogen in calcite buffered solutions between 90 and 180 C: Implications for nuclear waste disposal." *Geochimica et Cosmochimica Acta* 74.10 (2010): 2894-2914.

Truche, Laurent, et al. "Sulphide mineral reactions in clay-rich rock induced by high hydrogen pressure. Application to disturbed or natural settings up to 250 C and 30 bar." *Chemical Geology* 351 (2013): 217-228.

Uhde, Gerd, and Ulrich Hoffmann. "Noncatalytic gas-solid reactions: modelling of simultaneous reaction and formation of surface with a nonisothermal crackling core model." *Chemical engineering science* 52.6 (1997): 1045-1054.

University of Texas at Austin, 1986.

Vaccaro, S., and L. Malangone. "Catalytic combustion for supplying energy for endothermic reaction." *J. Adv. Chem. Eng* 4.2 (2014).

van Doesburg, Hans, and W.A. De Jong. "Transient behaviour of an adiabatic fixed-bed methanator—I: experiments with binary feeds of CO or CO2 in hydrogen." *Chemical Engineering Science* 31.1 (1976): 45-51.

Wagner, Damien, et al. "A laboratory study of the reduction of iron oxides by hydrogen." *arXiv preprint arXiv:0803.2831*(2008).

Walsh, M. P., et al. "Precipitation and dissolution of solids attending flow through porous media." *AIChE Journal* 30.2 (1984): 317-328.

Walsh, Mark P. *Geochemical flow modeling*. Diss. University of Texas at Austin, 1983.

Walsh, Mark P., and Larry W. Lake. "Applying fractional flow theory to solvent flooding and chase fluids." *Journal of Petroleum Science and Engineering* 2.4 (1989): 281-303.

Walsh, Mark P., Larry W. Lake, and Robert S. Schechter. "A description of chemical precipitation mechanisms and their role in formation damage during stimulation by hydrofluoric acid." *Journal of Petroleum Technology* 34.09 (1982): 2-097.

Wen, Dongsheng, and Yulong Ding. "Formulation of nanofluids for natural convective heat transfer applications." *International Journal of Heat and Fluid Flow* 26.6 (2005): 855-864.

Wesseling, Pieter, and Cornelis W. Oosterlee. "Geometric multigrid with applications to computational fluid dynamics." *Partial Differential Equations*. 2001. 311-334.

Westerterp, K. Roel, W. Jan Fontein, and Frits PH van Beckum. "Decoking of fixed-bed catalytic reactors." *Chemical engineering & technology* 11.1 (1988): 367-375.

Wiltowski, T., et al. "Kinetics and mechanisms of iron sulfide reductions in hydrogen and in carbon monoxide." *Journal of Solid-State Chemistry* 71.1 (1987): 95-102.

Yagi, Sakae, and Daizo Kunii. "Studies on combustion of carbon particles in flames and fluidized beds." *Symposium (international) on Combustion*. Vol. 5. No. 1. Elsevier, 1955.

Yagi, Sakae, and Daizo Kunii. "Studies on effective thermal conductivities in packed beds." *AIChE Journal* 3.3 (1957): 373-381.

Yagi, Sakae, and Daizo Kunii. "Studies on heat transfer near wall surface in packed beds." *AIChE Journal* 6.1 (1960): 97-104.

Yamazaki, S., Z. Asaki, and W. Kondo. "Thermal decomposition of pyrite in a fluidized bed." *TRANS MET SOC AIME* 242.5 (1968): 896-902.

Yan, Jinding, Long Xu, and Jianli Yang. "A study on the thermal decomposition of coal-derived pyrite." *Journal of Analytical and Applied pyrolysis* 82.2 (2008): 229-234.

Zanganeh, Maryam Namdar, et al. "The method of characteristics applied to oil displacement by foam." *SPE journal* 16.01 (2011): 8-23.

Zhang, Xinping, et al. "Modeling and simulation of coke combustion regeneration for coked Cr_2O_3/Al_2O_3 propane dehydrogenation catalyst." *Chinese Journal of Chemical Engineering* 18.4 (2010): 618-625.

Zhang, Yuegang, et al. "Thermal interface apparatus, systems, and methods." U.S. Patent No. 7,168,484. 30 Jan. 2007.

Appendices

A Prediction of wave behaviour for Exothermic reactions

A.1. Dilute Fluid Case

Typically, two distinct waves propagate along the fixed-bed reactor, a leading thermal wave and a trailing thermochemical wave.

A.1.1 Hot Fluid into a Preheated Bed

The wave model predicts that, in this case a thermal wave moving ahead of a thermochemical wave because the concentration of the fluid is low. The thermochemical wave is then moving into a heated region. The bed starts off at a high temperature and gets even hotter with a temperature rise (ΔT_C) across the thermochemical wave due to the heat generated during the reaction. If the temperature of the fluid rises above the ignition temperature, the reaction is very stable and should propagate. The figure below shows the predicted wave behaviour.

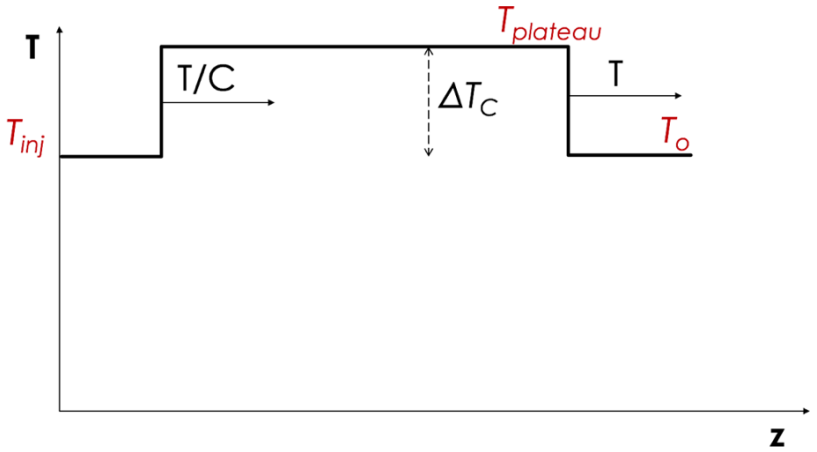

Figure A-1: Temperature profile for hot fluid into a preheated bed (dilute)

A.1.2 Hot Fluid into a Cold Bed

If the initial bed temperature is cooled down to T_O, the positions of the thermochemical wave and the thermal wave do not change, as none of the parameters in the equations for

the waves are changed. However, the thermal wave is moving into a region of cold solid and there is a large temperature drop at the front. If the plateau temperature is hot enough, ideally above the ignition temperature, the reaction will sustain itself. The thermochemical temperature rise is the same in both cases and the plateau temperature is the same.

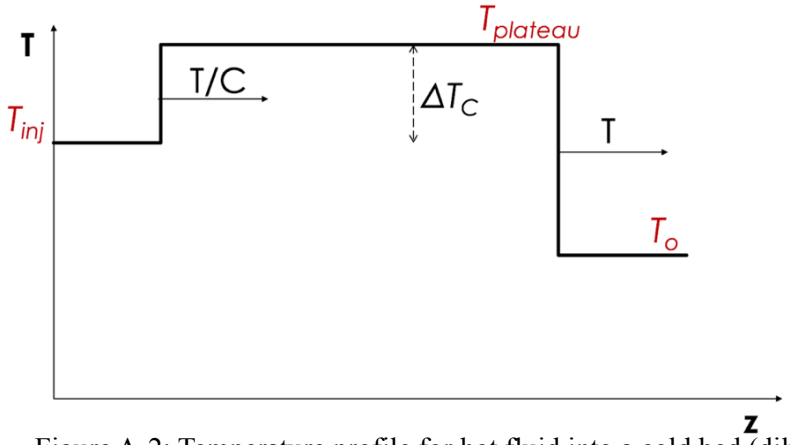

Figure A-2: Temperature profile for hot fluid into a cold bed (dilute)

A.1.3 Cold Fluid injected into a Preheated Bed

There is a cold fluid injection in this case. The thermal wave exhibits a smaller temperature drop because the thermal wave is moving into a preheated bed. If T_{inj} is higher than the ignition temperature, a complete reaction is expected, the waves will travel as predicted in Fig. A-4.

But if the fluid being pumped into a hot bed, is below the ignition temperature, the reaction is expected to be incomplete and not give a full conversion of the reactor bed. The velocity of the thermochemical wave will increase due to the partial conversion of the bed and a larger temperature rise associated with the wave. The wave model cannot directly predict the conversion of solid but can accurately predict the positions of the wave if conversion of solid across the reactor bed is known. The latter requires kinetic considerations, which are not part of the current wave model.

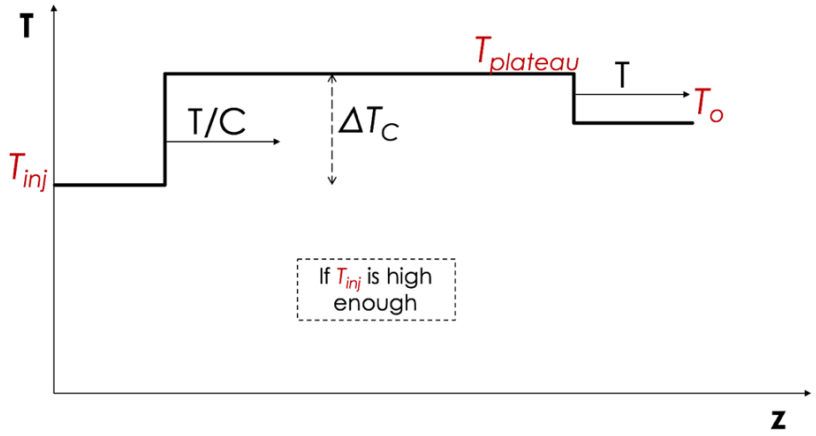

Figure A-3: Temperature profile for cold fluid into a hot bed (high T_{inj}) (dilute)

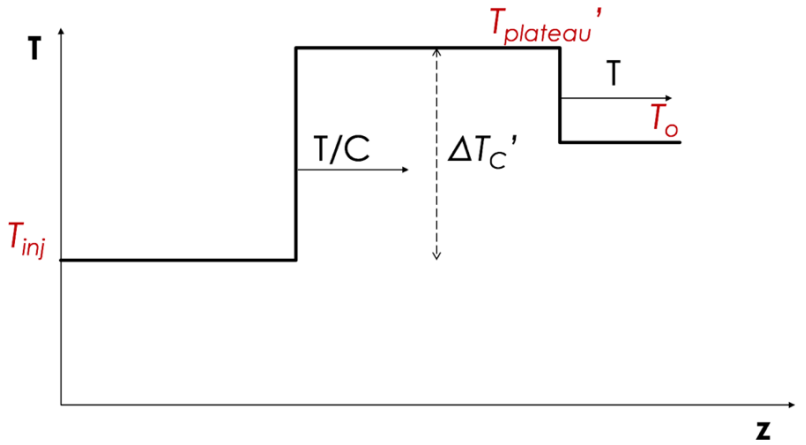

Figure A-4: Temperature profile for cold fluid into a hot bed (low T_{inj}) (dilute)

A.1.4 Cold Fluid pulse injected into a Preheated Bed

A strategy to save energy is to raise and then reduce the injected temperature of the fluid, after a period of time. This shall be known as a pulse. The injection of cold dilute fluid introduces a second trailing thermal wave (Fig. A-5). In principle, the leading and trailing thermal waves are travelling with the same velocity.

ΔT_T is the temperature drop due to the incoming injected cold fluid. The trailing thermal wave lags behind the leading thermal wave according to the size of the original pulse. The trailing thermal wave will then interfere with the tail end of the thermochemical wave. When the cold fluid starts being injected, the injected temperature drops down to $T_{cold,\,inj}$. Ahead of the trailing thermal wave is the initial temperature of the injected fluid (T_{inj}). The trailing

thermal wave overtakes the thermochemical wave; it is travelling at the same velocity (V_T) but never catches up with the leading thermal wave, as both thermal waves have the same velocity. The thermochemical wave is accelerated due to the partial conversion if the injected temperature is below ignition temperature, overheating the reactor. In Figure A-5, the wave model prediction is shown, the velocities after the introduction of a cold injection wave are also shown in the diagram. If the cold fluid is delayed enough, the trailing cold thermal wave only catches up with the thermochemical wave at the reactor exit to avoid the switchover shown in the figure below.

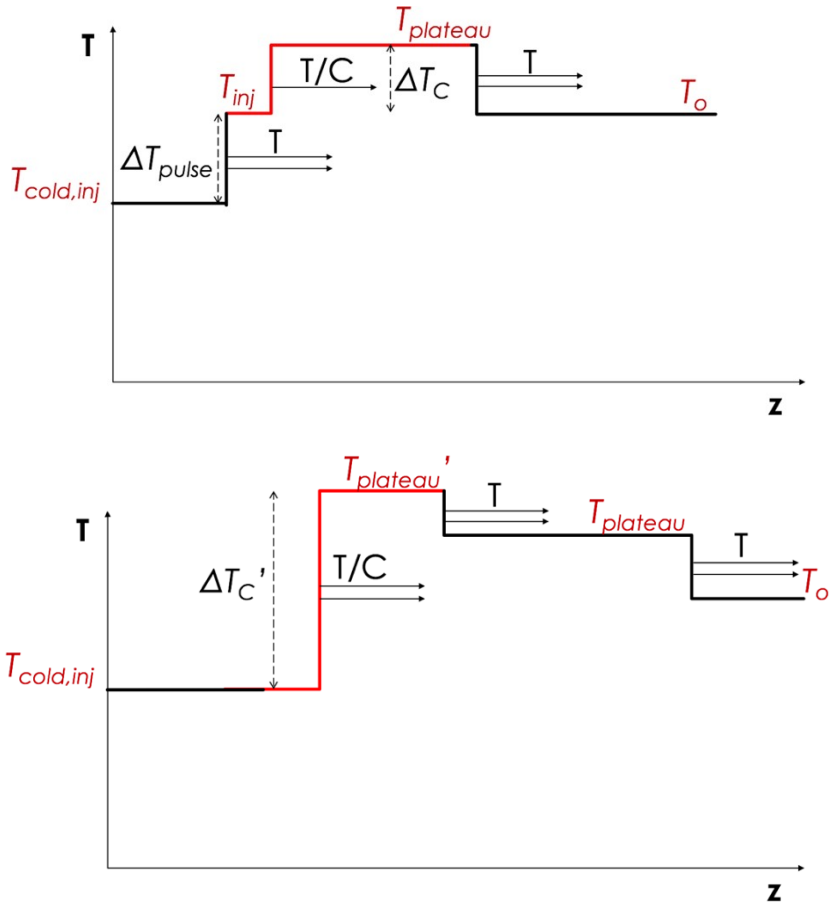

Figure A-5: Temperature profile for hot fluid pulse into a cold bed (dilute) with thermochemical wave (red)

A.1.5 Wave trajectories dilute case

Whether tracing the position of steps or fixed values of a composition variable, the resulting distance-time diagrams are known show the wave trajectories. As mentioned

earlier, the representation of the wave propagation is more convenient using distance-time diagrams. The time axis ($z = 0$) represents the injected conditions; the distance axis ($t = 0$) represents the initial conditions. The gradient of curves on these diagrams represent the velocity of waves.

(a) Constant injection temperature dilute case

In the first three cases of the dilute injected fluid, except when there is a partial reaction, there is a faster thermal wave and a slower thermochemical wave. The wave model prediction of the distance-diagram is two straight lines; the faster thermal wave has a steep gradient, V_T and the slower reactive wave has a less steep gradient, $V_{T/C}$.

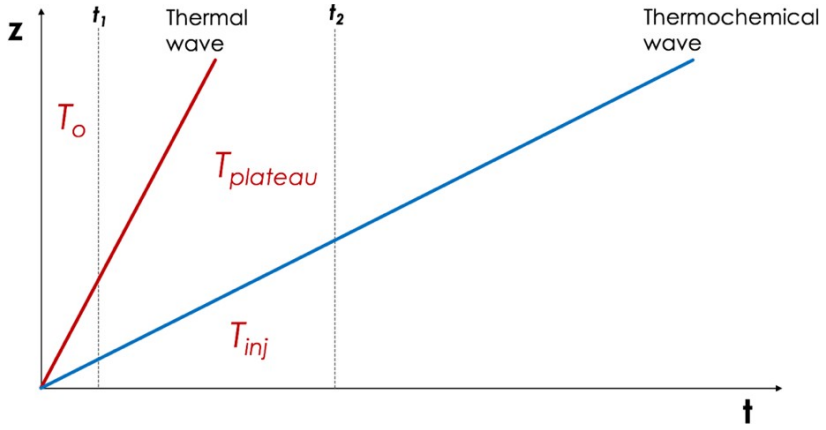

Figure A-6: Distance-time diagram for constant temperature (dilute)

Vertical cuts through the distance-time diagram are loci of constant time and horizontal cuts are loci of constant distance from the inlet. Variations of composition variables along horizontal and vertical cuts constitute wave histories and profiles, respectively. The diagram showing wave trajectories is a concise way of describing fully the wave response of a system and is a valuable tool for the wave model.

At cut t_1, as z increases the temperature of the fluid starts at the injected fluid temperature (Fig. A-6), there is then a temperature rise associated with the thermochemical wave into a region of maximum temperature. That temperature is maintained up to the thermal wave; the temperature then drops to the initial bed temperature. This description describes the

temperature profiles in the first three dilute cases, as seen in Figs. A-1, A-2 and A-3. At a later time, t_2 the faster thermal wave has already passed through and exited the reactor; the temperature of the fluid starts at the injected fluid temperature, with a thermochemical temperature rise into a region of constant maximum temperature (the temperature plateau) through the rest of the bed.

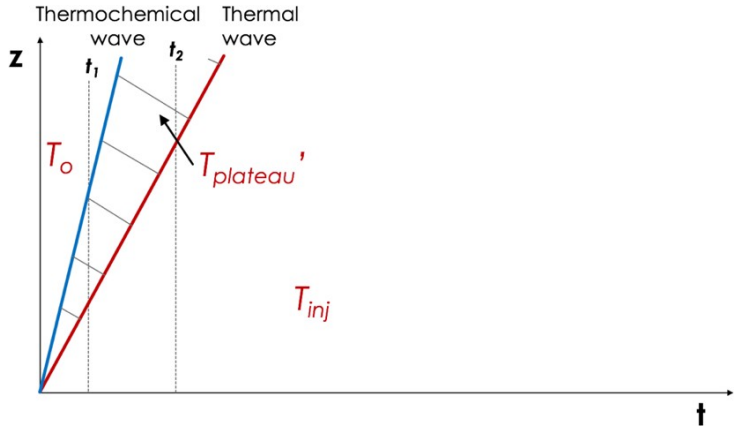

Figure A-7: Distance-time diagram for constant temperature dilute case with incomplete reaction

At t_1, there is a small distance between the two wave which increases with time. The temperature rises from $T_{cold,\,inj}$ to $T_{plateau}'$ ($T_{inj} + \Delta T_C'$) and then drops to the initial bed temperature. At a later time t_2, the thermochemical wave has passed through the reactor leaving a pure thermal wave travelling with an unchanged velocity $V_{T/C}$.

(b) Varied injection temperature dilute case

The introduction of a cold dilute fluid adds another wave into the distance-time diagram. The wave model predicts another thermal wave with the same velocity as the leading thermal wave (the same gradient in the distance-time diagram). The wave is introduced after a specific period of time; the cold thermal pulse wave is represented as a wave shifted to the right, as shown in green in the figure below.

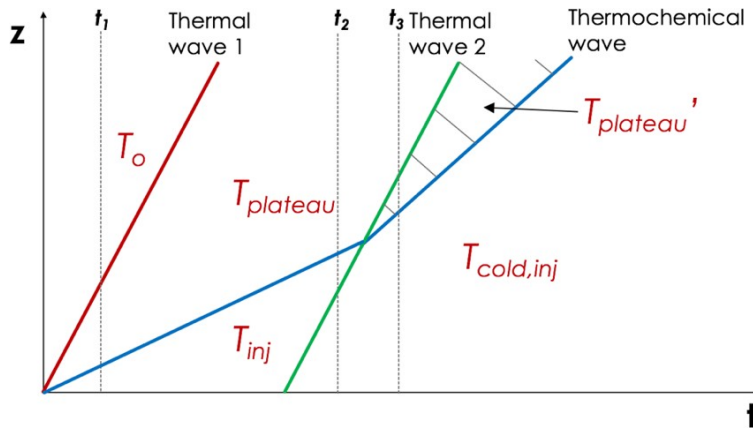

Figure A-8: Distance-time diagram for hot fluid pulse into a hot bed (dilute)

Initially at t_1, there is a leading thermal wave and a slower thermochemical wave. At t_2, the cold fluid has already been injected. The temperature of the fluid is now $T_{cold,\,inj}$ at the inlet, there is a temperature rise to the hot injected fluid temperature ahead. The temperature then rises from the hot injected fluid temperature to the plateau temperature $T_{plateau}$. The faster thermal wave (thermal wave 1) has already passed through the reactor. At t_3, the cold thermal wave (thermal wave 2) travelling at the same velocity V_T has overtaken the thermochemical wave, giving rise to a new temperature plateau $T'_{plateau} = T_{plateau} + \Delta T_{T/C'}$. The thermochemical wave speeds up as the bed is now cold, therefore the reaction rate is low. As a consequence, conversion of solid is greatly reduced and the thermochemical wave therefore travels faster across the reactor bed. A reduction in feed temperature mimics a cold fluid into a hot reactor bed after a certain period of time. As a result of this, a partial conversion may be found in this case.

A.2 Concentrated Fluid case

In the concentrated case, the wave model predicts the thermochemical wave to be faster than the thermal wave as the value of C_{AO} is larger. The thermochemical temperature rise is also greater. The thermal wave velocity is unchanged, but a faster thermochemical wave would give a smaller reaction time.

The increase in concentration of reactive fluid above a critical point switches the order of the thermal and thermochemical waves. The critical concentration itself gives rise to a hot spot; an intense travelling temperature rise.

A.2.1 Hot Fluid into a Preheated bed

The thermochemical wave moves into a hot bed with a slower thermal wave trailing it. The reaction will occur above the ignition temperature and be stable. The reaction occurs faster in this case compared to the dilute case.. The larger the inlet concentration of fluid, the faster the thermochemical wave and a larger temperature rise is expected. The diagram below represents a snapshot of the temperature profile in the fixed bed. It is important to note that the $T_{plateau}$ in the concentrated cases differ from the $T_{plateau}$ in the dilute cases.

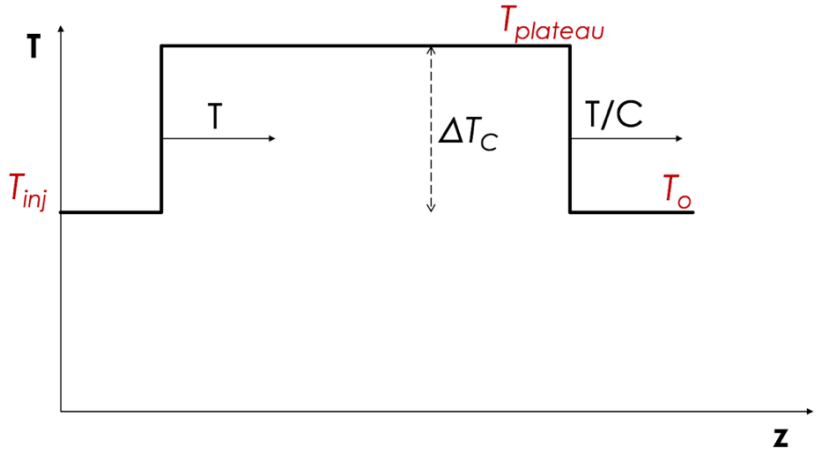

Figure A-9: Temperature profile for hot fluid into a hot bed (concentrated)

A.2.2 Hot Fluid into a Cold Bed

The leading thermochemical wave travels into a cold bed. The thermal wave trails behind the thermochemical wave and will not heat the bed ahead of the thermochemical wave. If T_{ign} is below the ignition temperature only, a partial removal of the fluid (to $C_{partial}$) is expected because the reaction occurs too slowly.

Initially, the fluid is hot and starts to react, but there is not enough heat retained in the bed for the solid and fluid to maintain the reaction at a high temperature. The reaction front is moving into a cold region. The reaction is not expected to be stable if T_o is very low.

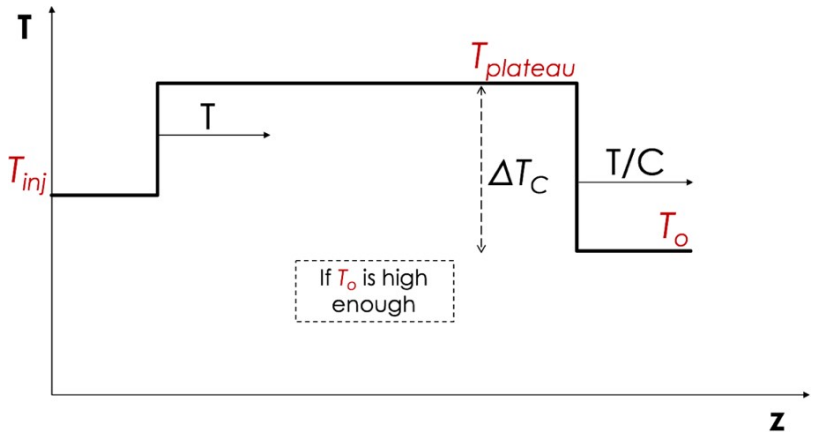

Figure A-10: Temperature profile for hot fluid into a cold bed (high T_o) (concentrated)

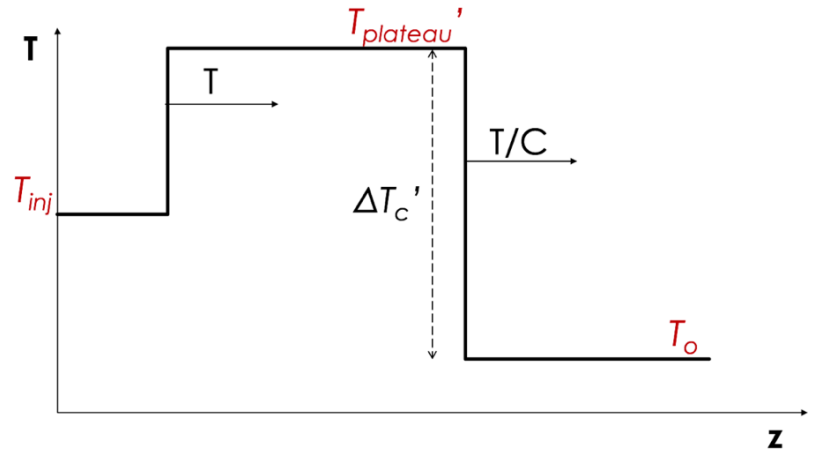

Figure A-11: Temperature profile for hot fluid into a cold bed (low T_o) (concentrated)

A.2.3 Cold Fluid into a Hot Bed

The cold thermal wave has a much bigger temperature rise because the fluid has to go from a low injected temperature to the plateau temperature. The bed is hot ahead of the thermochemical wave, so the reaction should be stable. This may then seem like a favourable strategy because the reaction time would be faster than in the dilute case. However, due to high temperatures reached in the concentrated case, a dilute fluid is preferred in decoking processes.

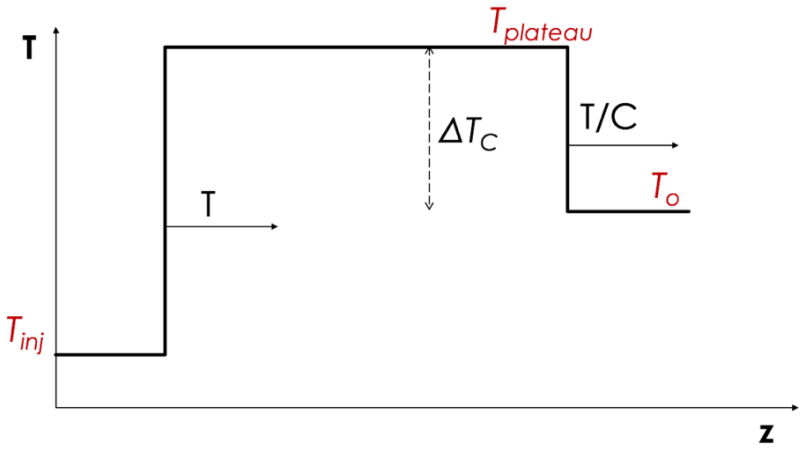

Figure A-12: Temperature profile for cold fluid into a hot bed (concentrated)

A.2.4 Hot Fluid Pulse into a Hot bed

The temperature of the injected fluid is initially hot and then reduced after a specific period of time a cold fluid is then introduced. The wave propagation is initially the same as shown in Figure A-10. The leading thermal and the cold trailing thermal waves have the same velocity. The trailing thermal wave would therefore never catch up with the leading thermal wave. The reaction of the hot fluid moving into the hot bed is expected to be completely stable as the injection of cold fluid cannot affect the reaction.

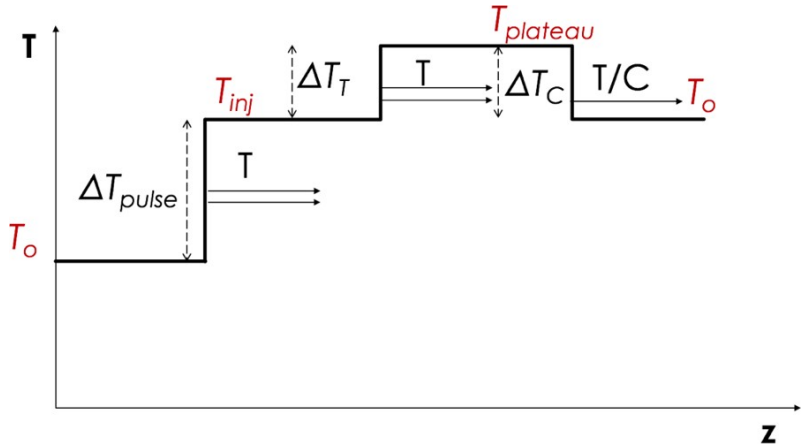

Figure A-13: Temperature profile for hot fluid pulse into a cold bed (concentrated)

A.2.5 Wave trajectories concentrated case

(a)Constant injection temperature concentrated case

For the concentrated case, a faster thermochemical wave and a slower thermal wave is predicted. Therefore, the distance-time diagram for the concentrated case shows a steep thermochemical wave and a less steep thermal wave (Fig. A-14).

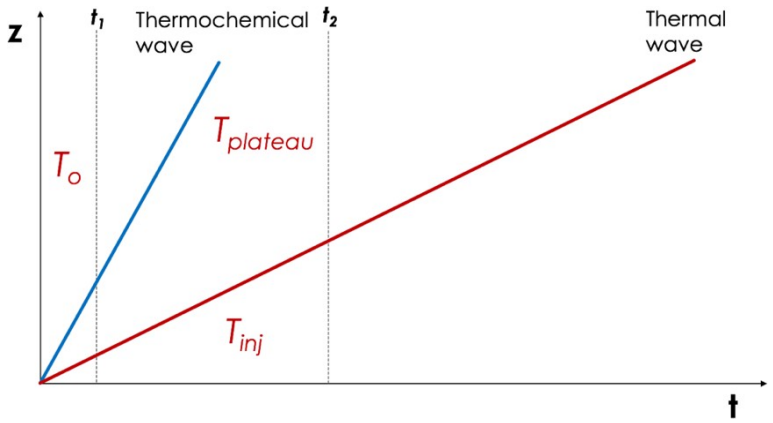

Figure A-14: Distance-time diagram for constant temperature (concentrated)

At t_1, the temperature of the fluid starts at the injected fluid temperature; and rises to the plateau temperature. That temperature is maintained until the thermochemical wave; the temperature then drops to the initial bed temperature. At a later time t_2, the faster thermochemical wave has passed through the reactor; the temperature of the fluid starts at the injected fluid temperature and rises into the region of plateau temperature for the rest of the bed.

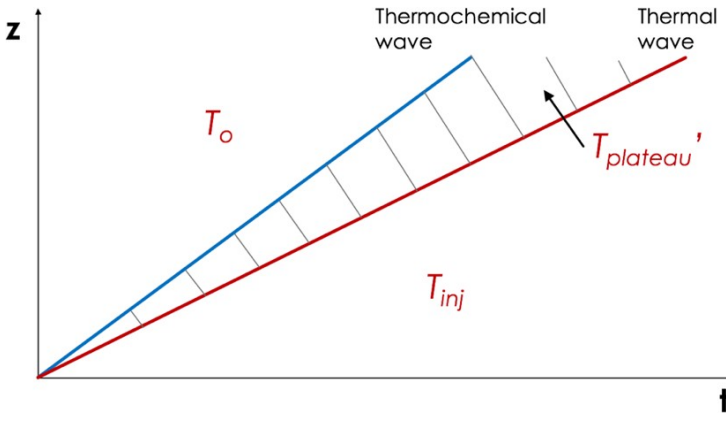

Figure A-15: Distance-time diagram for constant temperature incomplete reaction (dilute)

When there is a partial reaction, the thermochemical wave travels slower and a larger temperature rise is expected. When the thermochemical wave travels slower and closer to

the thermal wave travel, the thermochemical wave has a less steep gradient as shown in Fig. A-15. The proximity of the two waves, gives rise to a higher temperature plateau. The temperature is in the shaded region of Fig 5-15 is larger than the plateau temperature in Fig. A-14.

(b) Varied temperature concentrated case

The introduction of the cold trailing thermal wave would not have any effect on the waves ahead. The cold thermal wave is slower than the thermochemical wave. The trailing thermal wave travels at the same velocity as the leading thermal wave.

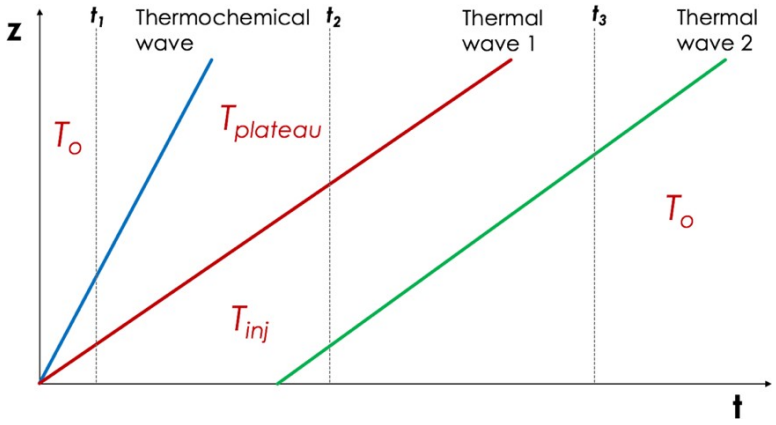

Figure A-16: Distance-time diagram for hot fluid pulse (concentrated)

B Prediction of wave behaviour for Endothermic reactions

The endothermic reaction to be considered is can be written as:

$$FeS_2 + H_2 \rightarrow H_2S + FeS$$

Injection strategies

B.1 Dilute Fluid case

Typically, two distinct waves propagate along the fixed-bed reactor, a thermal wave with a velocity V_T and a thermochemical wave with a velocity $V_{T/C}$ as in Figure B-1. The calculated velocities have the same mathematical expression as in the exothermic case.

When the heat of reaction is positive (endothermic), the calculated ΔT_c is negative. Therefore, the wave model predicts a temperature drop rather than a temperature rise.

B.1.1 Hot fluid injected into a preheated bed

The thermochemical wave is moving into an initially heated region. The bed starts hot and cools off between the thermochemical and thermal waves due to the heat absorbed during the reaction. If the temperature of the injected fluid is high enough, the reaction remains very stable. Figure B-1 shows the predicted wave behaviour.

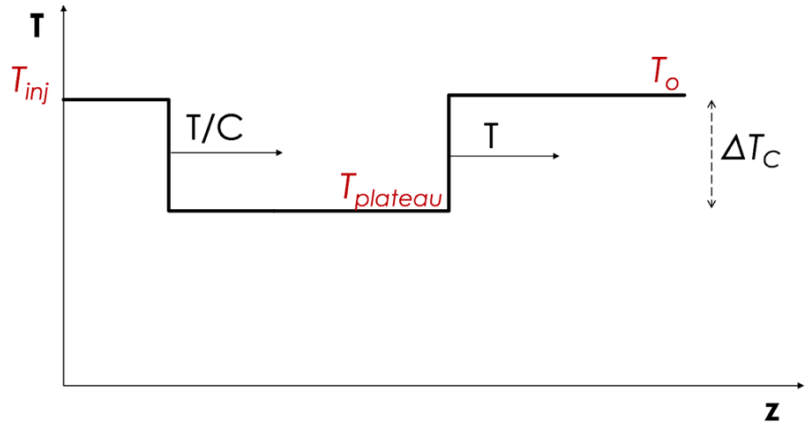

Figure B-1: Temperature profile for hot fluid into a hot bed (dilute)

B.1.2 Hot fluid injected into a cold bed

Initially the temperature of the bed is low. The positions of the waves do not change, there is a temperature drop due to the thermochemical wave (ΔT_c) down to the plateau temperature ($T_{plateau}$). Ahead of the thermochemical wave is the thermal wave which has an associated temperature drop due to the thermal wave down to the bed temperature (T_o). When a dilute hydrogen stream is used (C_{AO} is low), ΔT_C is moderate. $T_{plateau}$ is high enough for the reaction to propagate. The thermochemical wave is moving into a hot enough region.

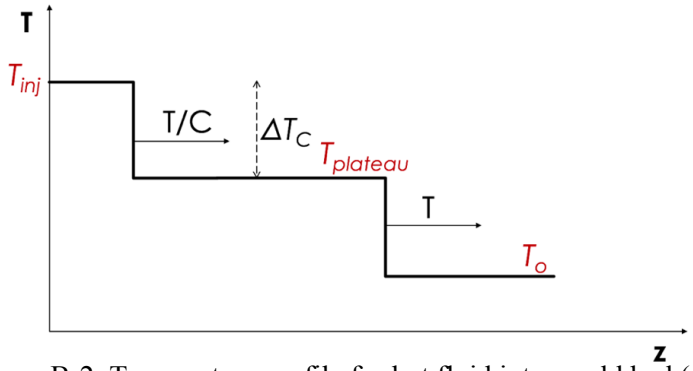

Figure B-2: Temperature profile for hot fluid into a cold bed (dilute)

B.1.3 Cold fluid into a preheated bed

We shall now discuss the case where a cold hydrogen is pumped into a hot bed. If the T_{inj} is high enough, then the reaction should propagate as in Figure B-3.

The thermal and thermochemical waves are expected to travel in a stable manner. When temperatures are higher, the system is closer to equilibrium and a complete reaction is expected. If T_{inj} is low, a partial reaction is expected because the fluid is too cold for the reaction to fully occur. The thermochemical wave is travelling into a cold region. The wave model cannot predict this partial conversion, but if the partial conversion is known, the wave model can accurately predict the velocity of the thermochemical wave.

The temperature drop in this case will be much larger. Since this is an endothermic reaction, there is a limit to where the reaction cannot drop below labelled as $T_{plateau}$' (cold spot) in Figure B-4. It is important to note the thermal wave is unaffected by this partial conversion because there is no reaction acrossthe thermal wave.

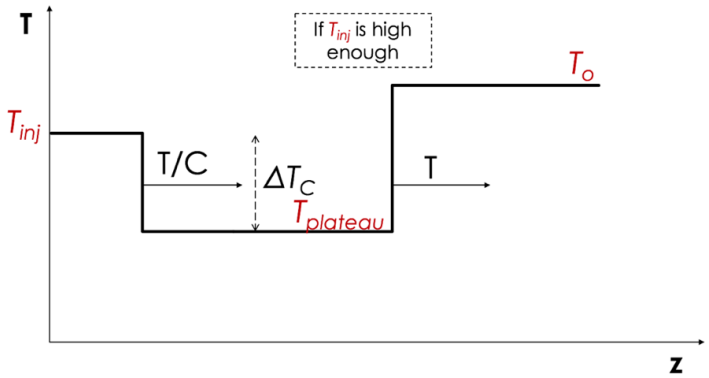

Figure B-3: Temperature profile for cold fluid into a hot bed (dilute)

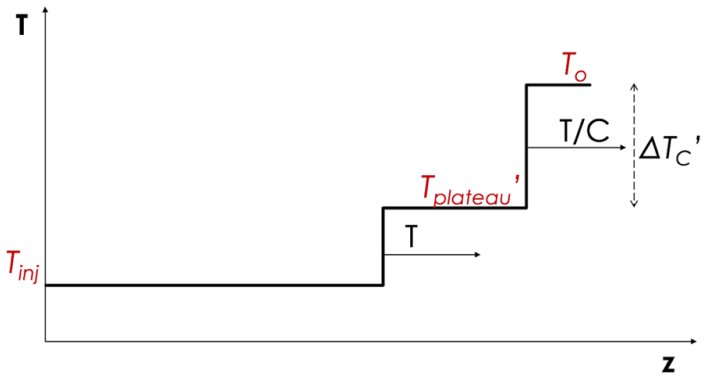

Figure B-4: Temperature profile for cold fluid into a hot bed (dilute)

B.1.4 Wave trajectories dilute case

In the first three cases of the dilute case, there is a fast thermal wave and a slower thermochemical wave. The wave model prediction of the distance-diagram is two straight lines; the faster thermal wave has a steep gradient, V_T and the slower reactive wave has a less steep gradient, $V_{T/C}$.

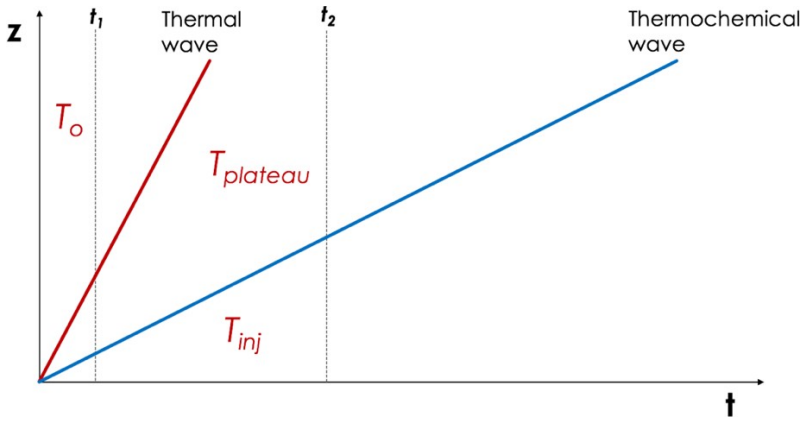

B-ure B-5: Distance-time diagram for constant temperature (dilute)

At cut t_1, the temperature of the fluid starts at the injected fluid temperature, there is then a temperature drop associated with the thermochemical wave into a region of minimum temperature ($T_{plateau}$). That temperature is maintained until the thermal wave; the temperature then rises to the initial bed temperature (T_o). This description describes the temperature profiles in the first three dilute cases. At a later time, t_2 the faster thermal wave has passed

out of the reactor; the temperature of the fluid starts at the injected fluid temperature, with a temperature drop into a region of the minimum temperature through the rest of the bed.

B.2 Concentrated Fluid case

In the concentrated case, the wave model predicts the thermochemical wave to be faster than the thermal wave as the value of C_{AO} is larger. There is also a larger temperature drop associated with the thermochemical wave. The thermal wave velocity is unchanged, but a larger concentration of fluid gives a faster thermochemical wave. Therefore, the increase in concentration of reactive fluid above a critical point switches the order of the thermal and thermochemical waves.

B.2.1 Hot fluid into a preheated bed

The thermochemical wave moves into a hot bed with the slower thermal wave trailing it. The reaction will occur above the ignition temperature and be stable. A high injected fluid temperature and bed temperature is required to observe the propagation of waves as in Figure B-6. If T_{inj} and T_o are set to the ignition temperature as in the dilute cases, $T_{plateau}$ will be limited to the cold spot temperature. The reaction will occur much faster in this case compared to the dilute case, because the thermochemical wave is so fast.

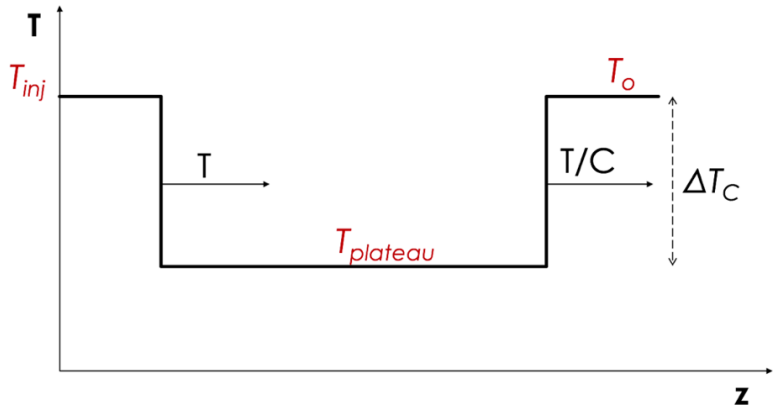

Figure B-6: Temperature profile for hot fluid into a hot bed (concentrated)

B.2.2 Cold fluid into a preheated bed

When a cold fluid is injected, the thermochemical wave will be travelling into a hot bed. Since, the bed is hot ahead of the thermochemical wave, the reaction is expected to be stable. If T_o is high enough to avoid the cold spot.

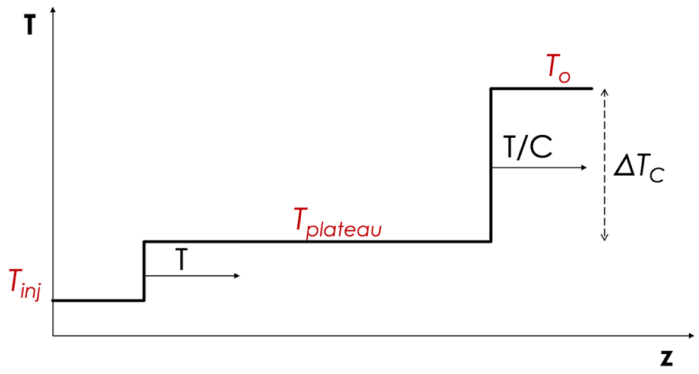

Figure B-7: Temperature profile for cold fluid into a hot bed (concentrated)

B.2.3 Hot fluid into a cold bed

When a hot fluid is pumped into a cold bed. The thermochemical wave cannot travel ahead because the temperature of the bed is too low. A partial concentration is expected because the fluid will pass through the reactor quickly and only some of the fluid will react. The thermochemical wave is delayed due to this partial concentration.

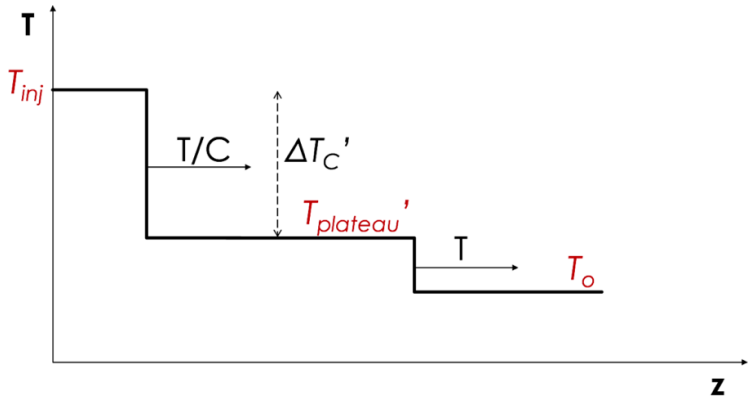

Figure B-8: Temperature profile for hot fluid into a cold bed (concentrated)

B.2.4 Wave trajectories concentrated case

The wave model predicts for the concentrated case a faster thermochemical wave and a

slower thermal wave. Therefore, the distance-time diagram for the concentrated case will have a steep thermochemical wave and a less sharp thermal wave.

In the first three cases of the concentrated case, the thermochemical wave is faster than the thermal wave.

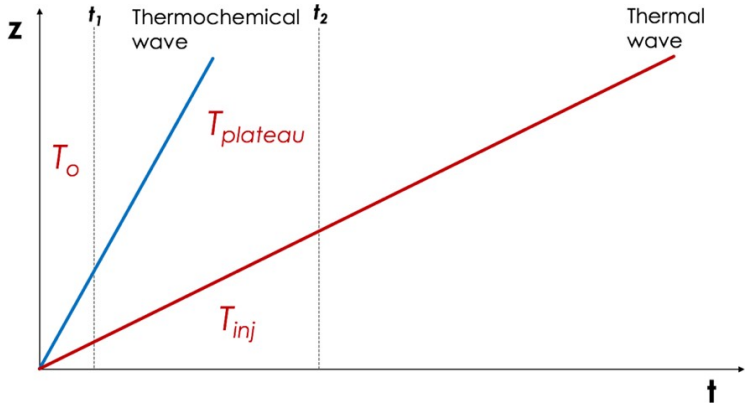

Figure B-9: Distance-time diagram for constant temperature (concentrated)

At t_1, the temperature of the fluid starts at the injected fluid temperature; there is then a temperature drop associated into a region of minimum temperature, the plateau temperature. That temperature is maintained at the thermochemical wave; the temperature then rises to the bed temperature. The wave propagation is similar to the dilute case, except the thermochemical wave and the thermal waves are switched. At a later time t_2, the faster thermochemical wave has passed through the reactor; the temperature of the fluid starts at the injected fluid temperature with a thermochemical temperature drop into the plateau temperature.

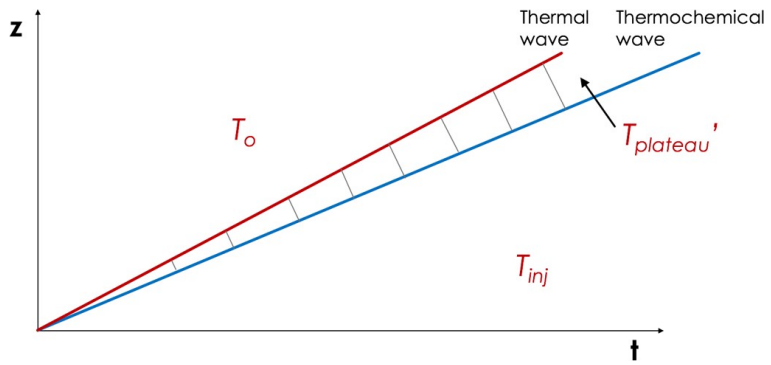

Figure B-10: Distance-time diagram for constant temperature with partial concentration (dilute)

When there is a partial concentration as in Figure B-10, the thermochemical wave travels slower than the thermal wave. The velocity of the thermochemical wave is:

(B.19)

The temperature drop is limited by the cold spot. It is important to notice the thermochemical wave will always travel behind the thermal wave when a cold bed is used.

B.2.5 Heat Addition case

In this method, radially uniform temperature change can be obtained by a jacketed vessel at the walls of the fixed bed reactor. The radial walls of the bed are insulated to decrease radial heat flux; thus, the axial heat flux becomes dominant.

If T_w is assumed to be equal to T_o, and the equations for the thermochemical and thermal wave velocities. The expected temperature profile is shown below, with increasing h_w.

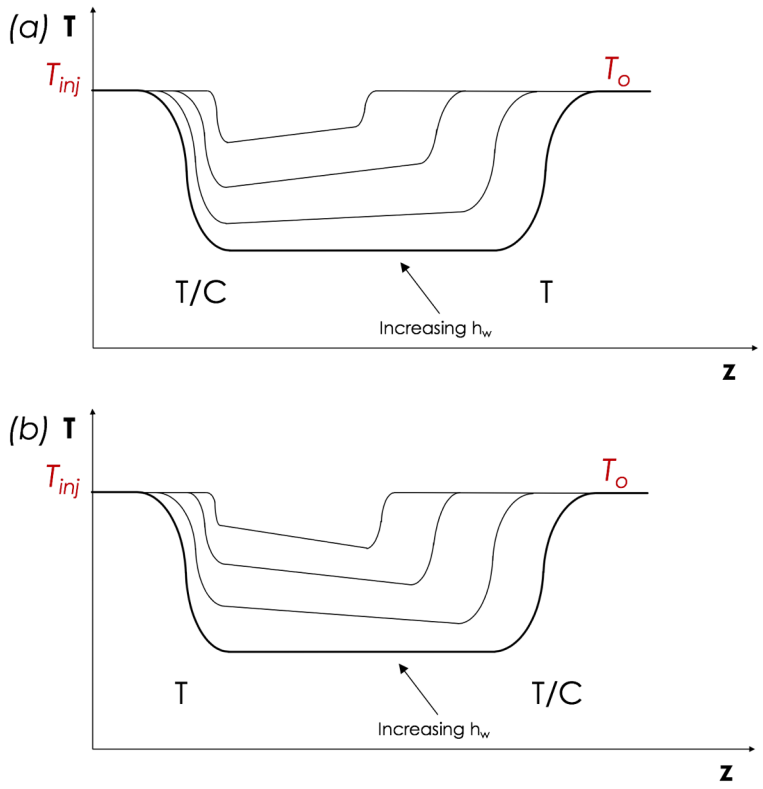

Figure B-11: Temperature profile for hot fluid into a hot bed with h_w (a) dilute (b) concentrated

C Flux Limiter

The MOL equipped with this slope and conventional limiters is second-order accurate in space for smooth problems. In fact, using $V_R' = \dfrac{u}{1 + \frac{(1-\varepsilon)}{\varepsilon}\frac{\Delta X}{\Delta C}\frac{1}{C_{partial}}}$ the piecewise linear limiters $\phi_{minimod}$, $\phi_{superbee}$ and ϕ_{MC}, the resulting method is exactly the same and the typical enhanced limiters for convection-advection equations. However, the two strategies are in general different if nonlinear limiters are used. In particular, using the conventional van Leer limiter leads to the loss of the TVD (Total Variation Diminishing) stability property. At t = 20000s, the exact solution is the wave model solution. Using 200 cells and r = 0.4 to mesh the domain. Three tests are used to solve the problem: (a) MOL using conventional limiters, (b) MOL using enhanced limiters, and (c) MOL using enhanced limiters and smaller spatial grid. Two sets of meshes generated by r = 0.2 and r = 0.3 are used to assess the convergence behaviours. For each r, four meshes with sizes ranging from 20^2 to 160^2 are used.

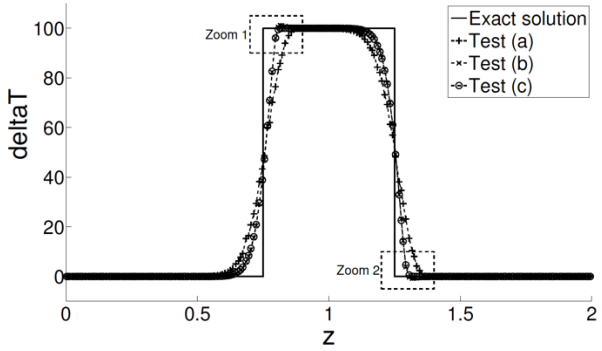

Figure C-1: Numerical solution at t = 2000s (Global view)

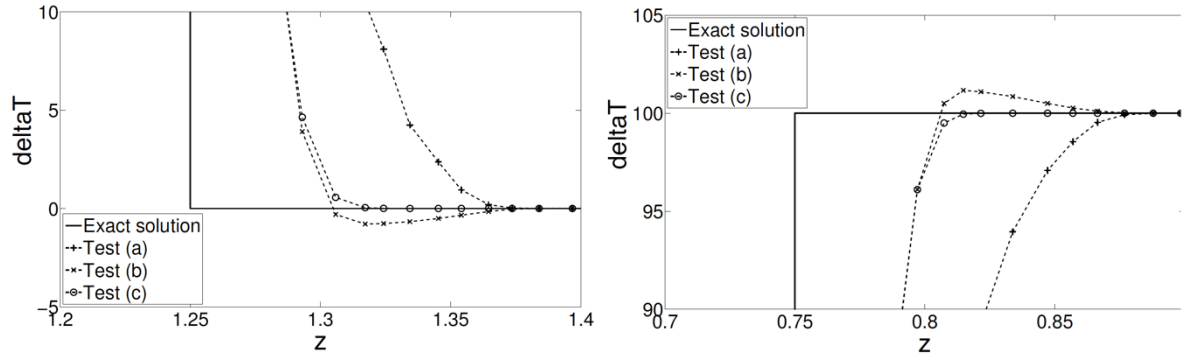

Figure C-2: Top and bottom of temperature plateau for Test (a), (b), (c) (Local view)

Three tests are used to solve the problem: (a) MOL using conventional limiters, (b) MOL using enhanced limiters, and (c) MOL using enhanced limiters and smaller spatial grid. Two sets of meshes generated by r = 0.2 and r = 0.3 are used to assess the convergence behaviours.

		Test (a)				Test (b)				Test (c)			
		$r = 0.2$		$r = 0.3$		$r = 0.2$		$r = 0.3$		$r = 0.2$		$r = 0.3$	
	Mesh	error	rate	error	rate	error	rate	error	rate	error	rate	error	rate
ΔT_C	20^2	1.89E-0		1.96E-0		1.89E-0		1.89E-0		1.72E-0		1.73E-0	
	40^2	8.96E-1	1.08	1.11E-0	0.82	7.44E-1	1.34	7.58E-1	1.32	6.30E-1	1.45	6.58E-1	1.39
	80^2	2.98E-1	1.59	4.82E-1	1.21	1.50E-1	2.31	1.55E-1	2.29	1.40E-1	2.17	1.57E-1	2.06
	160^2	1.15E-1	1.37	2.28E-1	1.08	3.21E-2	2.22	3.44E-2	2.17	3.59E-2	1.98	4.10E-2	1.94
X_B	20^2	4.13E-0		4.39E-0		4.08E-0		4.15E-0		3.80E-0		3.88E-0	
	40^2	1.67E-0	1.30	2.17E-0	1.02	1.39E-0	1.55	1.44E-0	1.52	1.26E-0	1.59	1.38E-0	1.49
	80^2	5.45E-1	1.60	8.43E-1	1.36	4.01E-1	1.79	4.25E-1	1.76	3.52E-1	1.84	4.03E-1	1.78
	160^2	1.95E-1	1.49	3.73E-1	1.18	1.08E-1	1.89	1.16E-1	1.88	9.36E-2	1.91	1.09E-1	1.88
C_A	20^2	4.15E-0		4.44E-0		4.11E-0		4.15E-0		3.76E-0		3.83E-0	
	40^2	1.60E-0	1.38	2.05E-0	1.11	1.32E-0	1.63	1.36E-0	1.61	1.19E-0	1.67	1.26E-0	1.60
	80^2	5.03E-1	1.67	8.35E-1	1.30	3.45E-1	1.94	3.64E-1	1.90	3.14E-1	1.92	3.53E-1	1.84
	160^2	1.95E-1	1.37	3.95E-1	1.08	8.90E-2	1.96	9.47E-2	1.95	7.96E-2	1.98	9.25E-2	1.93
ΔT_T	20^2	2.55E-0		2.64E-0		2.53E-0		2.55E-0		2.38E-0		2.40E-0	
	40^2	1.18E-0	1.11	1.49E-0	0.82	9.60E-1	1.40	9.79E-1	1.38	8.48E-1	1.49	8.93E-1	1.43
	80^2	3.83E-1	1.62	6.40E-1	1.22	1.91E-1	2.33	1.98E-1	2.31	1.87E-1	2.18	2.13E-1	2.07
	160^2	1.55E-1	1.31	3.12E-1	1.03	4.14E-2	2.21	4.45E-2	2.15	4.66E-2	2.01	5.55E-2	1.94

Table C-1: Errors and convergence rates and various meshes for Test (a), (b) and (c)

Clearly, the test (b) and test (c) show similar accuracy property, which are much better than the test (a). These results confirm that the enhanced limiter improves the accuracy of the MOL even on highly non-uniform grids; and the numerical errors are almost r-independent. On the one hand, the tests (b) and (c) show similar dispersion and dissipation properties, indicating that both are second-order accurate in space. On the other hand, the alternative strategy (test (b)) shows both overshoot and undershoot near the jumps, whereas tests (a) and (c) exhibit TVD (Total Variation Diminishing) property as expected. In fact, for a large class of possible alternative strategies, applying the conventional van Leer limiter leads to the loss of either second-order accuracy or TVD stability. For each r, four meshes with sizes ranging from 20^2 to 160^2 are used. The numerical errors at t = 2000s measured for C_A, X_B, ΔT_C as well as the

convergence rates computed using the conventional or enhanced van Leer limiters are summarized in Table 1.

		$r = 0.2$						$r = 0.3$					
		C_A		ΔT		X_B		C_A		ΔT		X_B	
	Mesh	error	rate	error	rate	error	rate	error	rate	error	rate	error	rate
$\phi^{\text{van Leer}}$	100	1.51E-3		1.64E-3		1.90E-3		1.99E-3		2.16E-3		2.52E-3	
	200	4.93E-4	1.62	5.32E-4	1.63	5.87E-4	1.70	7.20E-4	1.47	7.73E-4	1.48	8.51E-4	1.57
	400	1.83E-4	1.43	1.93E-4	1.46	2.18E-4	1.43	2.92E-4	1.30	3.01E-4	1.36	3.46E-4	1.30
	800	8.45E-5	1.12	8.86E-5	1.12	9.78E-5	1.16	1.39E-4	1.07	1.44E-4	1.06	1.61E-4	1.10
	1600	4.16E-5	1.02	4.21E-5	1.07	4.64E-5	1.08	7.01E-5	0.99	7.12E-5	1.02	7.89E-5	1.03
$\phi^{\text{van Albada}}$	100	2.18E-3		2.29E-3		2.75E-3		2.65E-3		2.83E-3		3.42E-3	
	200	6.44E-4	1.76	7.00E-4	1.71	7.86E-4	1.81	8.68E-4	1.61	9.52E-4	1.57	1.06E-3	1.69
	400	2.17E-4	1.57	2.32E-4	1.59	2.66E-4	1.57	3.29E-4	1.40	3.46E-4	1.46	3.97E-4	1.42
	800	9.19E-5	1.24	9.85E-5	1.24	1.10E-4	1.27	1.48E-4	1.15	1.57E-4	1.14	1.77E-4	1.17
	1600	4.39E-5	1.06	4.47E-5	1.14	4.96E-5	1.15	7.38E-5	1.01	7.54E-5	1.06	8.41E-5	1.07

Table C-2: Errors and convergence rates and various meshes for ϕ_{Albada} and $\phi_{van\ Leer}$

A comparison between van Leer and another flux limiter the conventional van Albada limiter show similar tendency to produce overshoots and undershoots on highly irregular grids. But the problem is much more severe than the enhanced van Leer limiter. In particular, the magnitude of undershoots is about 0.04 in absolute value by solving the same problem using this strategy on an extremely irregular mesh generated by r = 0.4195. Tables 2 summarise the errors and convergence rates obtained by the two methods, Albada and van Leer respectively. The results only show the effects of the van Leer and van Albada limiters; other limiter functions led to similar conclusion. Regarding the van Albada, as the mapping to z becomes less smooth by either increasing r or refining the mesh, the convergence rates decrease from near second-order to only first-order.